THE DEVELOPMENT OF A MONITORING AND CONTROL SYSTEM FOR A PULVERISED COAL-FIRE BURNER USING NEURAL NETWORK APPROACH

TAN OUI HONG

A thesis presented in partial fulfilment of the requirements of the University of Glamorgan/Prifysgol Morgannwg for the award of the degree of Doctor of Philosophy

April 2005

University of Glamorgan

Abstract

This thesis discusses the development of an Artificial Neural Network (ANN) based Flame Monitoring and Control System (FMCS) to optimise the combustion of a pulverised coal flame.

A series of experiments were conducted on a 150 kW pulverised fuel burner rig based at Casella CRE Ltd. in the United Kingdom. These experiments systematically varied the burner swirl number and the secondary airflow rate over a significant range for two different coals so that both "satisfactory" and "poor" combustion conditions were obtained. The infrared emissions from the flame, the combustion noise and the acoustic emission generated in the burner body were measured with appropriate sensors, as were the fuel and airflow rates and pollutant emissions. The signals from the sensors were analysed using signal processing techniques to yield a number of features. These in turn were employed to train a neural network to predict the gaseous emissions, such as NOx and CO, from the rig.

In a separate set of experiments, the combustion process was placed in a poor condition, and the sensors together with the neural models were incorporated into an intelligent control system, which was able to alter the excess air level to improve the combustion process. In this fashion simultaneous lower NOx and CO levels were achieved with both coal types. The technique uses relatively low cost sensors and artificial intelligence techniques to control the combustion of the pulverised fuel burner. It is envisaged that this technique will be particularly attractive for multiple burner installations that are often fed from a common air supply manifold, so that the individual burner performance is often not known and cannot be optimised.

Acknowledgements

First and foremost, I would like to take this opportunity to express my gratitude to those who enabled me to complete this research project. My heartfelt thanks go to Prof. Steven Wilcox (my director of studies) and Prof. John Ward, who gave me an opportunity to become one of their Ph.D students. Their extensive experience and knowledge have provided me with much valuable advice and comments that allowed me to pursue the research objectives. Their patience, constructive attitude, helpful and caring personalities inspired and motivated me throughout the period of my research.

My very special thanks to Dr. Chee Keong Tan. He has provided guidance and has supported me whenever needed. Also, I would like to mention Dr. Alex Chong, Dr. Kevin Monson and Mr. Shee Meng Thai for their companionship and constant encouragement.

I am also grateful to Mr. Mark Lewitt of Casella CRE Ltd. His efforts and co-operation and his courteous attitude were extremely helpful during the experimental aspects of the work.

Finally, I wish to take this opportunity to express my devotion and gratitude to my wife, Bei Bei Jiang, my family for their understanding, support and encouragements throughout my study.

Table of Contents

List of Figures

List of Tables

Chapter 1 Introduction

Coal continues to have the largest reserves of all the fossil fuels making it a viable fuel in many geographical areas of the world [Shimoda *et al.*, 1990]. The largest coal user is the power generation industry [Doherty *et al.*, 1994]. On a global scale, the demand for power is expected to double between now and 2030 and it is expected that coal will become cheaper than gas for power generation [IEA, 2002]. The scale of operation, costs, and the need for reliability in new power plant, will make it difficult to accommodate the large-scale introduction of new, unproven (e.g. biomass cofiring burner), and essentially small-scale energy technologies such as wind wave and solar power. In addition, biomass ash can be high in sulphur or halides [Ringe *et al.*, 1998], which can cause legal and other problems for its subsequent disposal. Therefore, it is clear that coal must continue to play a significant role if security and diversity of supply is to be met.

The EU has strict regulations covering the control of emissions from power generation plant, as set out in the Large Combustion Plant Directive (LCPD). Even more stringent emissions limits will come into force in 2008, and will fully apply to both new and existing plant from 2016 onwards. Thus from an environmental perspective, the development and deployment of advanced Clean Coal Technologies (CCTs), with higher efficiencies and better environmental performance, are seen as key enabling steps in achieving these limits in the medium to long-term development of lower emission power plant.

Europe is a leader in the development of advanced, clean power generation systems. Historically, the EU has supplied 50 % of the global market for power plant and has a reputation for innovation in the development of advanced systems and components due to previous investment in Research and Development (R&D) in CCTs [PowerClean, 2003]. This reputation represents a major market opportunity for EU industry to supply export markets. However if similar efforts are not continued, there is a risk of losing the international market share since both the USA and Japan have long-term strategic plans

to meet future domestic and export market requirements. Therefore, there is a need for the EU to continue the R&D programmes in coal utilisation for power generation.

Pulverised fuel (PF) plant is the most commonly used coal-fired technology for power generation. Fluidised bed combustion systems offer an alternative to PF plant but cannot provide the economy of scale provided by the larger plant. Coal gasification provides a route for producing large amounts of hydrogen and the use of Integrated Gasification Combined Cycles (IGCC)[1] with complete containment of undesirable pollutants within the system. However, it must be emphasised that IGCC is not yet a proven technology and much work remains to be done to resolve technical issues. In contrast, conventional coal-fired plant is inherently large scale and reliable in operation. Recent cycle improvement has led to increases in efficiency. Undoubtedly, research into CCTs has led to the development of environment-friendly coal utilisation technology for PF boilers.

Larger utility coal-fired boilers emit Nitrogen Oxides (NOx) and Sulphur Dioxide (SO_2) which contributes to acid rain. In addition, NOx may undergo photochemical oxidation and react with sunlight to form smog [Stanmore *et al.*, 2000; Singer, 1981]. For these reasons, the European Union has introduced more stringent legislation for the control of emissions for these pollutants. Unlike SO_2 emissions that are dependent on the sulphur content of the coal, there is no simple correlation between coal nitrogen and nitrogen oxide emissions. Good operating practice has played an important role in the abatement of NOx. However even when the overall stoichiometry of the boiler is maintained at the desired ratio in multi-burner installations, each individual burner may operate at a different excess air level as a result of air-fuel mal-distribution. This can lead to the inefficient use of fuel and the emission of high levels of NOx from individual burners. Moreover if uncorrected it can lead to burner operation under extreme reducing conditions which can in turn promote serious problems such as burner slagging and boiler tube corrosion. Although measurement of flue gas composition in the stack is

[1] Gasification or partial oxidation makes it possible to produce a fuel gas from solid or liquid carbonaceous feedstocks that can be cleaned and burned in a gas turbine. The resulting gas must be of such a quality that no damage (e.g. corrosion, erosion) is caused to the gas turbine whilst maintaining the high efficiency and low emissions of the combined cycle plant.

routine in modern boilers, this provides only the average values and so characterisation of individual burners is not readily achieved [Kay, 1994]. As a result, the present project is concerned with the development of a Flame Monitoring and Control System (FMCS) for individual burners. To maximise the boiler efficiency each burner should operate with the minimum excess air, which ensures virtually complete combustion. Moreover the NOx emissions from the burner should be within satisfactory levels. Consequently, the proposed monitoring system aims to provide carbon monoxide (CO) levels as a measure of the completeness of combustion together with the NOx concentration in the flame. These emission levels cannot be measured directly but are functions of combustion parameters such as the air-fuel ratio, the flame temperature, and the turbulence in the flame.

The objectives of the present project are therefore: -

1. To develop an effective and low cost flame-sensing system for the monitoring of individual burners.

2. To optimise a burner based on the information derived from monitoring the flame signature.

The project therefore employed (a) an infrared (IR) radiation detector, (b) a microphone (MIC) and (c) a probe, which measures Acoustic Emission (AE), for an individual burner since they are sensitive to the combustion parameters mentioned earlier. The intensity of radiation from a flame increases sharply as the flame temperature increases as well as being related to the air-fuel ratio. The electromagnetic radiation was measured at the root of the coal flame where the combustion is initiated [Clausen, 1995]. A broadband IR sensor was therefore used instead of measuring the UV radiation since this later component can be masked by un-burnt fuel [Jackson *et al.*, 1987]. Also, flame flickering effects are thought to be due to the fluctuation in the combustion rate of the coal as well as the turbulence in the flame. This makes it essential to study the temporal information in the flame signal [Khesin *et al.*, 1997]. Abugov (1980) measured sound emissions from

an open flame and claimed that the noise from the flame results from a direct coupling between the combustion and the sound created by the airflow. This occurs because the amplitude of the sound varies with the combustion rate, which is in turn, related to the air-fuel ratio and turbulent mixing. This sound amplitude can be measured by a broadband microphone [Gaydon, 1978]. Acoustic emission is a name given to stress waves that are generated within solids due generally to microcrystalline events, which can be detected by a sensor. Traditionally, AE has been applied on boilers to monitor events such as soot blowing, tube leaking and valve operations [Steven *et al.*, 1984; Kalyanasundaram *et al.*, 1992]. However, AE from a flame probably arises from inhomogeneity in the initial air-fuel mixture in the turbulent combustion zone causing fluctuations in the local rate of combustion even though the average combustion rate remains constant [Abugov, 1978]. Consequently, these fluctuations together with changes in flame turbulence can generate AE within the burner so that measurement of the stress waves at the rear of the burner was selected as a possible technique in this project.

It was decided to analyse the raw signals from the sensors in both the time domain (e.g., Mean value, Kurtosis and Skewness), and the frequency domain through an estimation of the Power Spectral Densities (PSD) via the Fast Fourier Transform (FFT) and also Wavelet Analysis. The average of these measurements over a short time period yielded features that were compared with the measured NOx, CO and O_2.

The relationships between these features and the gaseous emissions were complex and nonlinear so that Artificial Neural Networks (ANNs) were employed to learn the relationship. ANNs have the ability to analyse large classes of nonlinear relationships with acceptable accuracy and are particularly useful where analytical models are difficult to use. In control applications, ANNs offer the advantage of being able to handle a large class of nonlinear control problems with essentially the same algorithm, which can be customised, through minor code modifications [Jaques *et al.*, 1998]. In this project, the outputs of the ANNs can be considered as "software sensors" which predict the gaseous emissions, hence the proposed system is similar to a Predictive Emissions Monitor

(PEM) as defined by Sloss [IEA, 1997]. Recursive networks, which have ability to retain temporal information from the sensors [Jarmulak *et al.*, 1997; Gencay *et al.*, 1997] were employed since the use of "previous" values of the feature as well as current values were found to provide better predictions. The degree correlation of computed features with the combustion gases varies substantially from feature to feature. Consequently, selection of the most appropriate features was also undertaken prior to their use by the neural networks.

Low emissions of NOx can be achieved by regulating the excess air level [Rodriquez *et al.*, 2001; Grant, 1980]. The NOx and CO levels in the burner in the current project were controlled through identification of the burner condition by means of the sensors and neural network. The air supply was then adjusted by standard a set of rules, which were formulated to achieve appropriate NOx and CO levels.

Changes in the combustion conditions in the boiler can result from differences of coal properties, slag/soot deposits, and ageing of the plant [Booth *et al.*, 1998]. For these reasons, online retraining of the ANNs may be required. This retraining procedure can be achieved as long as sufficient plant data is available. However, it will be important to have a mechanism to detect when the response of the plant changes. As a result, this thesis discusses how a Self-Organising Map (SOM) neural network can be employed to detect when the original recursive network will require retraining.

The thesis is divided into 8 chapters. Chapter 2 reviews the literature relating to pulverised coal-fired systems and includes a discussion of the formation of various gaseous emission pollutants and low NOx technologies. Chapter 2 also discusses possible monitoring techniques and their limitations together with relevant ANN models and possible control schemes. Chapter 3 describes the combustion test facility, the sensor development, and the data acquisition system. Chapter 4 discusses the development of the monitoring system as well as the signal processing techniques, which employed. Finally compares individual features with gaseous emissions. Chapter 5 concentrates on methods for finding the best network for prediction of NOx and CO. Chapter 6 describes

the application of the Flame Monitoring and Control System (FMCA) and its testing on 150 kW combustion test facility. Chapter 7 discusses the use of Wavelet Signal Analysis (WA) and ANN *k*-steps model. Also, Chapter 7 discusses how SOM can be used to indicate when the burner characteristics have changed so that the original recursive network can be retrained. Finally, Chapter 8 draws conclusions corresponding to the work conducted and is followed by recommendation for future work.

Chapter 2 Literature Review

Chapter 2 reviews the basic operation of pulverised fuel (PF) boilers, combustion related emissions, and control techniques. The limitations of existing monitoring of coal-fired burners are highlighted and the application of Artificial Neural Networks for burner optimisation is discussed.

2.1 Coal & Pulverised Coal System

Coal is formed as a result of natural chemical processes in which plants absorb carbon dioxide from the atmosphere and convert it into a compound consisting of sugar, starch, cellulose, lignin and other complex substances. This compound is then converted into the different types of coals depending on the formation conditions.

2.1.1 The Formation of Coal

Organic matter such as woody fragments of stems, roots, and bark first changes to peat which when buried is cut-off from the oxygen in the air resulting in a slow bacterial action that prevents decay of the organic matter. The weight of more vegetation, rock, or water forming on top of the peat helps to compress and solidify the peat, which then changes into coal.

The term "coal" refers to a wide range of naturally occurring heterogeneous materials from brittle anthracites to brown fibrous lignites, which are closer to the original plant. These forms can be determined by their maceral information. The maceral is defined by their morphology and by the coals reflectance or colour when viewed under a microscope, and indicates the degree to which they have been metamorphosed [Singer, 1981]. Higher rank[1] coals are generally found in regions that have been under high pressure. Other factors such as time, heat, organic substances, and geological changes change (e.g., earth folding and mountain formation) have an important influence in this natural chemical evolution.

[1] The coal rank increases as the amount of fixed carbon increases and the amounts of moisture and volatile matter decrease.

2.1.2 Coal Analysis

Two types of coal analysis are generally used: the Proximate Analysis (PA) and the Ultimate Analysis (UA), in which the compositions are expressed as percentage by mass. The Proximate Analysis (ASTM Standard, D3172), by reference to four major constituents: (a) heating value, (b) mineral impurity, (c) volatile matter, and (d) moisture. The Ultimate Analysis (ASTM Standard, D3176), on the other hand, gives the chemical composition of the coal in terms of hydrogen, oxygen, carbon monoxide, methane and other hydrocarbons and that portion of moisture that is formed by chemical combination during thermal decomposition of the coal substance. Generally, the dry or wet and mineral-matter-free bases for analysis are used. [Singer, 1981]

Both Proximate and Ultimate Analyses are used to determine coal rank, which in descending order is as follows: -

1. Anthracite, which is hard, brittle, and shiny black with a homogeneous structure. It has a high percentage of fixed carbon and low volatile matter. It is ideal for domestic applications.

2. Bituminous, which is greyish black and distinctly granular in structure. When it is subjected to heat, it reduces to a cohesive binding, sticky mass. It has a higher calorific value and volatile matter but less carbon content as compared to Anthracite. Bituminous coals are further categorised into low, medium, and high-volatile bituminous coal according to their physical properties.

3. Sub-bituminous coal are brownish black and homogeneous with smooth surfaces. They have high moisture content and can produce an audible noise of disintegration ("crack") when exposed to air.

4. Lignite is brown and has a laminar structure in which the remnants of woody fibres can be seen under microscope. Its origin is mostly from plants rich in resin,

so it is high in volatile matter and has a low heating value. Lignite coals are hard but will loose moisture rapidly and disintegrate at room temperature.

5. Peat tends to be used only rarely as a commercial fuel. It contains high moisture content and has the lowest heating value. It is a heterogeneous material consisting of partially decomposed organic matter and inorganic materials.

2.1.3 Pulverised Coal System

In the process of steam generation in large boilers, the fuel burning system should provide a controlled, efficient conversion of the chemical energy of the fuel into heat energy and this in turn, is transferred to the heat absorption surfaces of the steam generator. Lump coal is pulverised and transported with the primary air stream, which directs it to the furnace where the fuel is consumed. Changes in the primary air stream and its velocity will affect the rapidity and stability of the ignition process. The fuel-burning system introduces the fuel and air for combustion into the boiler where they are ignited to produce a flame and the products of combustion. The rate and degree of completion of the chemical reactions are greatly influenced by the temperature, concentration, preparation, and distribution of the reactants, by catalysts, and by mechanical turbulence.

Figure 2.1 shows a low NOx pulverised fuel burner, in which coal and primary air are introduced tangentially to the coal nozzle, thus imparting a swirl within the nozzle, with adjustable inlet vanes also imparting swirl inside the wind box. The degree of swirl, coupled with the flow-shaping contour of the burner throat, establishes a recirculation pattern extending several throat diameters into the furnace. The hot products of combustion within the boiler chamber are directed back toward the nozzle to provide the ignition energy necessary to sustain stable self-ignition of the incoming coal.

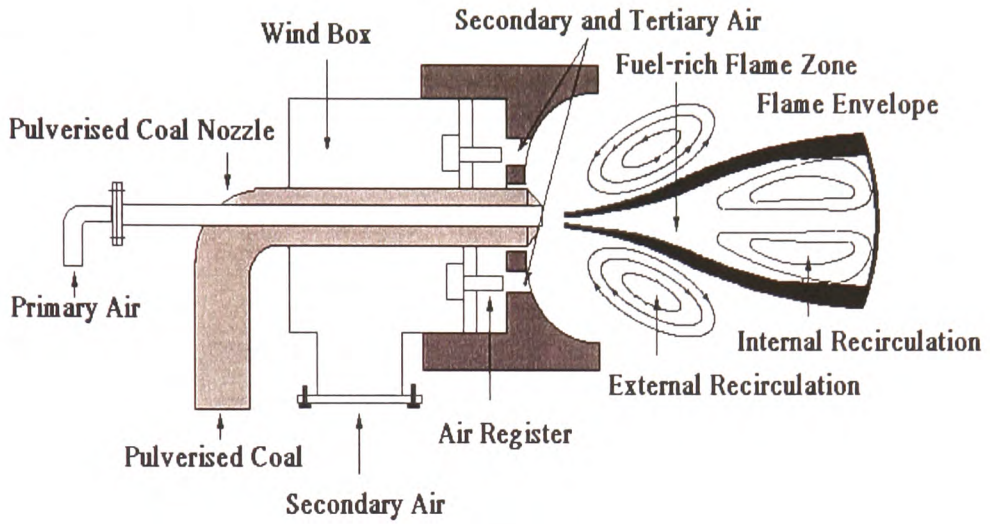

Figure 2.1 Pulverised Coal Burner

The velocity of the primary air and coal are generally held at approximately 25 m/s with a temperature of 75 °C (under preheat condition). The velocity of the primary air plus the pulverised coal stream of the nozzle must exceed the speed of flame propagation in order to avoid flashback. The optimum stoichiometry [2] (air-fuel ratio) in the fuel rich combustion zone has been found to be approximately 0.7 [IEA, 2000] and the mean particle size of the pulverised coal is about 25 μm. [Singer, 1981]

Utility boilers can generally be grouped into three major categories: (a) Horizontal firing (front wall), (b) Horizontal firing (opposed wall), and (c) Tangential firing boilers, as shown in Figure 2.2

[2] The theoretical amount of air required to burn a fuel completely to combustion products is defined as stoichiometric air.

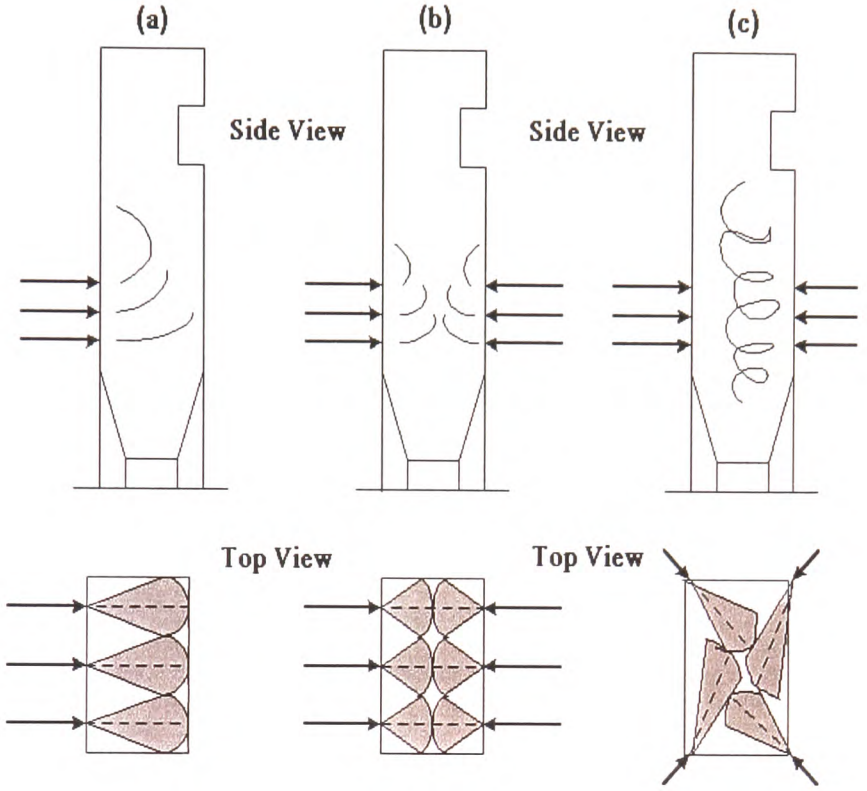

Figure 2.2 Burner Arrangement in PF-fired Boiler

(a) Front wall firing (b) Front and Opposed walls firing (c) Tangential firing

2.2 Pollutant Emissions in Pulverised Fuel Boilers

Legislation affecting coal-fired power stations has created a market opportunity for commercially viable technology aimed at the control of pollutant emissions. Nitrogen Oxides (NOx) and Sulphur Dioxide (SO_2) are the main agents contributing to the formations of acid rain and tropospheric ozone[3]. In the UK, the Environmental Protection Agency (EPA) has requested utility boilers to operate below 320 ppm of NOx from 1995 [IEA, 1997].

[3] Ozone is an important trace gas in the troposphere. It is not directly emitted into the troposphere, but chemically produced by NOx, CO, CH_4 and other hydrocarbons. These ozone precursors are emitted in large quantities due to human activities such as traffic and industry

2.2.1 The Mechanisms of NOx Formation

Nitrogen oxides from the combustion of coal comprise about 95 % nitric oxide (NO) and about 5 % nitrogen dioxide (NO_2), plus less than 1 % of nitrous oxide (N_2O). NOx is a by-product of coal combustion and originates from both the coal-bound nitrogen and nitrogen from air. There are three generally recognised formation mechanisms for NOx: -

1. Fuel NOx due to the oxidation of coal-bound nitrogen compounds at a temperature > 750 °C and these dependent on the nitrogen content of the coal.

2. Thermal NOx arising from reactions between oxygen and nitrogen in the combustion air at a temperature > 1300 °C in oxidizing atmosphere. This is largely dependent on flame temperature and residence time at high temperature.

3. Prompt NOx from the fixation of atmospheric (molecular) nitrogen by hydrocarbon fragments in a reducing atmosphere. This is formed in the early stages of all PF coal flames, i.e. in the ignition region.

The contribution of fuel and thermal NOx to the total NOx emission can be of the order of 80 % and 20 % respectively for a bituminous coal with high nitrogen content. The effect of prompt NOx is small and it is often neglected. Modelling of coal combustion is usually based on the assumption that the conversion of coal can be divided into two steps [IEA, 2000]: -

1. Pyrolysis of the raw coal and combustion of volatiles, and,

2. Char burnout.

The Visona and Stanmore model, which demonstrates the formation path for fuel NOx, can be seen in Figure 2.3. NOx is first liberated during the primary de-volatilisation as tars in the coal flame. Additional fuel nitrogen is released from the char as HCN and sometimes as NH_3 and NH, on time scales that are considerably longer than those for tar

formation are. At the same time, the volatiles undergo secondary reactions in the hot, fuel rich gaseous phase, which converts the nitrogen contained in the tar into HCN with some of the tar being subsequently converted into soot. The char and soot formed are then oxidised and these liberate additional nitrogen by chemical conversion to NO or by thermal dissociation induced at the high temperatures associated with char combustion. Numerous chemical reaction routes have been proposed which involve a series of intermediate species such as CN, CHO and NH radicals and compounds. These are produced from fuel nitrogen, which can then form gaseous nitrogen or NOx depending on oxygen availability. A detailed explanation of the chemical reactions is presented in Appendix A.

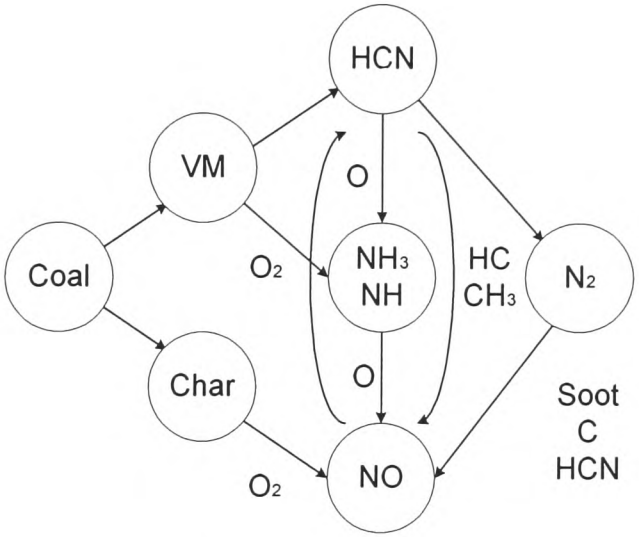

Figure 2.3 Reactions for Fuel NOx Formation [Visona and Stanmore, 1995]

2.2.2 Factors Affecting NOx Formation in a PF system

Having discussed the chemical paths of NOx formation, the overall physical and chemical characteristics governing the production of NOx can be summarised as: -

1. Coal properties such as, coal rank, volatiles, and moisture contents and coal particle size.

2. Burner parameters and the combustion parameters such as flame temperature, de-volatilisation rate, air-fuel ratio, swirl intensity, input air temperature, and firing load.

3. Furnace geometry and setup, for example, a tangential boiler tends to have lower NOx emissions. In addition, the coal and air distribution in the boiler will affect NOx.

The rate of emission of NOx generally increases as the coal nitrogen content increases [Mitchell *et al.,* 1982]. However, O'Connor (1999) showed that for given nitrogen content the NOx produced in low NOx burners decreased as the volatile matter content increased. O'Connor suggested that NOx decreased at low fuel ratio[4]and the reduction of NOx is due to the following reasons: -

1. The release of fuel nitrogen in a reducing environment generating N_2, as opposed to NO.

2. Lower retention of fuel nitrogen in the char inhibits the formation of NO from char oxidation.

Besides these, the boiler configuration, type, and geometry have remarkable influence on the formation of NOx. As such, the operational characteristics of two boilers will not be the same even with the same coal [O'Connor. 1999].

2.2.3 Low NOx Technology in PF Boilers

A variety of low NOx technologies, including, (a) Low NOx Burner (LNB), (b) the use of Overfire Air (OFA), (c) Reburn, (d) Flue Gas Recirculation (FGR), and (e) Burner Out of

[4] Fuel ratio is defined as the fixed carbon over the volatile matter in the coal.

Service (BOOS), are available on a commercial basis. One common feature amongst these techniques is that they are all based on staging of the combustion air, or fuel. Post combustion techniques such as catalytic conversion are also widely used. The working principle for these low NOx technologies as aforementioned in the above are summarised as follows: -

1. The design of a low NOx burner aims to reduce the flame temperature and to stage the oxygen distribution in the flame. Approximately 20 % of the combustion air is supplied as primary air [Borman *et al.,* 1998] with the rest split between secondary and tertiary supplies (Figure 2.1). The primary air is mixed with the fuel, producing a low temperature oxygen deficient fuel rich zone. This helps to reduce the formation of fuel NOx by promoting the conversion of the fuel nitrogen to molecular nitrogen. The use of a low NOx burner changes the flame temperature profile as well as the chemistry of the combustion. With "conventional" burners, the conversion of volatile nitrogen to NO is more efficient than the conversion of char nitrogen to NO. Consequently, an increase in the volatile and nitrogen content of the coal gives rise to higher emissions with un-staged conditions. [Smart *et al.,* 1993]

2. The use of overfire air burner achieves lower NOx levels in a similar way to that of a low NOx burner. The overfire air is injected above the primary combustion zone to achieve complete combustion using a special wind box with overfire nozzles mounted above the top level of the burners. Stowe *et al* (1996) reported a 50 % reducing in NOx by the combination of LNB and OFA. In a burner out of service system on the other hand, some of the burners are operated under sub-stoichiometric conditions with the supply of air for complete combustion provided through adjacent non-firing burners. Hence, the boilers effectively operated with air-staging [IEA, 2000].

3. Reburn operation involves the staged supply of fuel and combustion air in the furnace, to create three distinct combustion zones – primary, reburn and burnout.

In the primary zone, coal is fired with some excess air, producing NOx from both fuel-bound and combustion air nitrogen. A secondary fuel (reburn fuel), which can be natural gas, coal or oil, is injected above the primary zone to create the reburn zone. Hydrocarbon radicals released from the reburn fuel in this zone react with NOx formed in the primary zone to reduce it to molecular nitrogen. Finally, the remaining combustion air is injected above the reburn zone, i.e. in the burnout zone to complete combustion [DTI, 2000].

4. Flue Gas Recirculation is achieved by having part of the flue gas re-circulated in the furnace in order to modify the conditions in the combustion zone. The resultant reduction in oxygen concentration is the treatment in achieving low NOx emissions. FGR may also be used as a carrier to inject fuel into the reburn zone, thus promoting thorough mixing.

5. In the Selective Non-Catalytic Reduction (SNCR) process, an amine based chemical reagent, most commonly ammonia or urea is injected as a spray into the flue gas which is at 900-1100 °C, reducing NO_x to molecular nitrogen. NO_x reductions of between 40-50 % can be achieved with SNCR. SNCR needs proper control and operation to avoid the release of ammonia to the atmosphere. So far, it has been applied successfully only in small to medium scale plants (up to around 150 MW) because it is difficult to ensure proper mixing of the flue gas, the correct residence times and temperatures in larger boilers.

6. In the Selective Catalytic Reduction (SCR) system, vaporized ammonia is injected into the flue gas stream at about 300-400 °C. This is then passed over a catalyst, and the NO_x is reduced by ammonia to molecular nitrogen. The catalyst is usually based on the oxides of titanium, vanadium and tungsten, although its actual composition, including other active metals and support materials, is varied to meet the specific requirements of an installation. The capital cost of SCR systems is high due to the use of ammonia and the need to replace degraded catalysts at relatively short intervals. Therefore, it is generally not cost-effective.

2.3 Monitoring of PF burners

Determination of the emissions of the gaseous combustion products provides useful information on complex combustion processes taking place inside a boiler. All power stations monitor their stack emissions as well as other performance indices, such as heat rate, auxiliary consumption, pollution concerns and slagging [EPRI, 1986; Kay, 1994] as part of the economics and legislative commitments. Different plants will have their own way of carrying out monitoring, and often the information is used to undertake improvements to the boiler. Monitoring systems that accurately reflect the status of individual burners are also important for advanced boiler management. Accurate monitoring of individual burners is even more important for advanced low NO burners because these burners are typically more sensitive to changes in operating parameters and feed system variations than conventional burners [Timothy, 2003].

2.3.1 Limitations of Existing Monitoring Methods

Although there are a large number of commercially available instruments for monitoring combustion applications, the difficulties of obtaining detailed information in a large utility boiler due to problem related to inaccessibility have been reported [Rodriquez *et al.,* 2001]. Conventional intrusive probes (e.g., water-cooled probes, suction pyrometers and other thermocouples), which allow for direct measurements inside the furnace through boiler inspection ports, have limited application. This is because they are restricted to the limited areas where direct access is viable.

Measurements of gaseous and particulate flows (e.g., electrostatic and acoustic emission techniques) and temperatures prior to the burner (i.e. so-called pre-combustion measurements) can be used to determine the individual inputs of air and fuel. However, it is expensive to apply to individual burners in large utility boilers and measurements of the flow to groups of burners whilst limiting their usefulness. In addition, they are the indirect measurements of the real combustion process that tends not to be as reliable because the reading can be easily masked by the complexity of the process itself.

Post combustion analysis systems such as flue gas analysis and laboratory based thermal gravimetric analysis to measure sample carbon-in-ash contents, also have limitations. For example, flue gas analysis system is often located some distance from the region so that mixing of the products from individual flames prevents the characterisation of individual burners [Greaves, 1999; Kay, 1994]. In addition, extractive gas sample based post combustion analysis systems can be subjected to the effects of particulate stratification and air leakage, which may lead to significant errors. Gas analyses by wet chemical methods, for example, gas chromatography[5], are time consuming and demand high-level technical skills.

Alternative non-intrusive techniques use sensors mounted on the boiler walls to detect changes in burner operation. These so-called non-intrusive instruments can be of two classes as follows [Larrimore *et al.*, 1997]: -

1. Active systems, which consist of an emitter and a receiver. The signals generated by the emitters are modified during their transmission through the furnace and hence can yield information on boiler characteristics.

2. Passive systems, which determine the properties of the flame directly using flame detectors such as, IR pyrometers, cameras, or heat flow sensors.

With rapid increases in available computing power, the facility to build ever more "intelligent" control systems appears to be limited to some extent by the sensor technology [DTI, 2003]. Because of this, the current project emphasised in the development of effective flame monitor and control system for PF burners.

[5] Chromatography is a powerful separation process: it can separate components that have only slightly different properties. Therefore preparative chromatography is mainly used for difficult separations and for separation of sensitive products.

2.3.2 Some Techniques for the Diagnosis of Combustion

There is a growing interest in the study of flame radiation in PF systems. Pastor (2000) suggested that flame radiation monitoring is one of the most appropriate ways of examining the condition of the burner. This is because they are non-intrusive and due to the luminosity of the flame, any change in combustion process will be revealed in the flame itself. Kay (1994) acknowledged the importance of the flame information for burner diagnostics and improvements. Flame detectors are composed of a light receiver for detecting and converting light into an electrical signal. In the past, flame detectors were employed mainly as a safety feature to detect the presence of a flame. However, due to increased computational capacity and the development of advanced signal processing algorithms the pulsating frequency of the light emitted can be analysed to yield useful flame information [Willson *et al.*, 1985; Martin, 1993]. In another respect of flame monitoring, Lu *et al* (1999) demonstrated the possible use of vision-based optical devices to characterise flame in a gas-fired boiler and other similar combustion systems. Undoubtedly, the use of optical method for monitoring of industrial flame has become popular gradually. This is in fact influence by the evolution of low cost silicon based optoelectronics, which promises enhanced sensitivity to any industrial flame monitoring applications [Martin, 1993].

Industrial combustion consists of light contributions of continuum radiation from the dispersed phase following Planck's law[6] and of band emissions from the gas-phase chemiluminescence [Leipertz, 1996]. The intense chemical reactions close to the flame front release energy as Ultraviolet (UV), Visible (VIS) and Infrared (IR) electromagnetic radiation [Jackson *et al.*, 1987; Willson *et al.*, 1985]. The variation of the radiation intensity versus wavelength differs for the different fossil fuels [Singer, 1981]. See Figure 2.4.

[6] The Planck law gives the intensity radiated by a blackbody as a function of frequency (or wavelength). see http://scienceworld.wolfram.com/physics/PlanckLaw.html

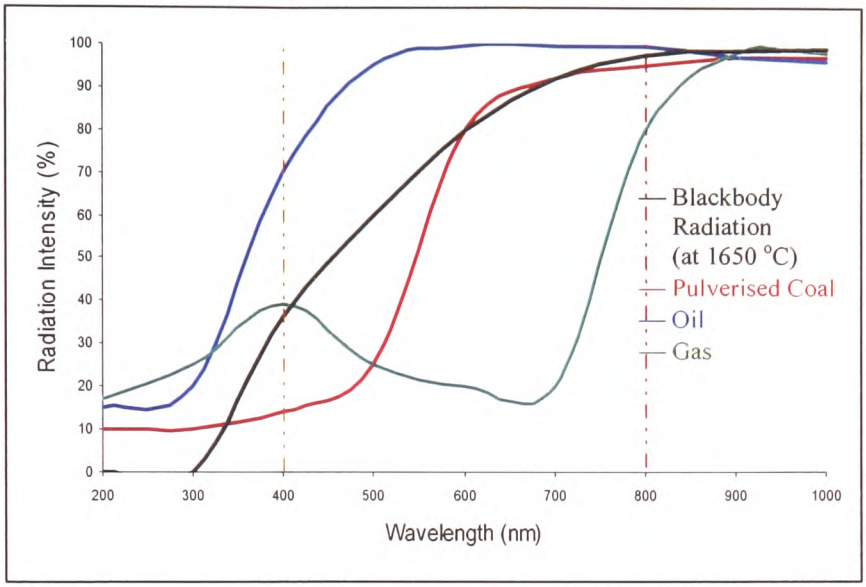

Figure 2.4 Spectral Distributions of Flame Radiations for Common Fossil Fuels [Bryant, 1980]

Refractory materials emit both UV and IR radiation with the radiation intensity increasing sharply with increasing temperature inside the furnace. Leipertz (1996) used a UV based spectroscopy[7] for the early detection of NOx generated flame radicals with the results suggested that OH, (H)CN, NH and CH can be identified as possible precursors and indicators to the NOx. Glasheen (1998) in his experiment used UV sensors to determine flame temperature and frequency information that corresponded to boiler parameters such as flame quality and emission concentrations.

Even though a UV photocell is capable of discriminating flame under supervision and its adjacent one, or the background radiations, they have been found not sensitive to the variations in the flame resulted from different burner settings. Apparently, UV tends to be blocked or absorbed by oil-mist, water vapour, carbon particles, and other combustion by-products. Consequently, this prevents a reliable measurement of the sensor signal being obtained [Ballard, 1984; Bryant, 1980].

[7] A spectroscope equipped with a photoelectric photometer to measure radiant intensities at various wavelengths

The emission of IR radiation takes place as molecules undergo transition from one vibration-rotation state to another [Kay, 1994]. IR resists absorption and contamination by the combustion by products and is preferred for the use in coal-fired system [Willson *et al.,* 1985; Jackson *et al.,* 1987]. Many successful applications, for example, Ballard (1984) and Daw (2002) assessed flame quality in the visible and IR parts of the spectrum. Once again, the attribute of low cost CMOS in the range of IR wavelengths improve the number of applications in monitoring of combustion flame [Bendisciol *et al.,* 1988, Martin, 1993]. Other advance flame monitors such as IR spectrometer, Fast Fourier Transform IR (FTIR), Multicolour pyrometer [Shepard *et al.,* 1993, Michel *et al.,* 2001; DTI, 2003], are currently available for different applications. Furthermore, both Jackson *et al* (1987) and Martin (1993) confirmed that specific wavelengths corresponding to CO, CO_2, NO, NO_2 and SO_2 can be found predominantly at the flame root.

Despite all advantages as aforementioned, the issue in relation to the discrimination between a flame and the glowing refractory remains a problem. The glowing refractory was found to emit radiation at the end of the UV wavelength region and is increasing smoothly to the maximum in the IR region. If IR sensor is to be used, some distinguishable features between the flame and glowing refractory or nearby flames have to be found [Ballard, 1984; Jackson *et al.,* 1987]. In principle, this can be achieved through identifying the flicker characteristics of the flames. The radiation emission of the flame is irregular due to the back flash behaviour hence manifesting itself through intensity fluctuation. In contrast, background radiation appears to be a largely steady component.

In general, the pulverised coal flames fluctuate more intensely in comparison to those of oil and gas flames [Willson *et al.,* 1985]. The frequency of these pulsations or flame flicker is dependent on a number of factors such as fuel type, burner configuration, firing load, viewing area and distance of viewing from the flame. These serve to be vital information for flame monitoring. According to Jackson *et al* (1987) and Hashimoto *et al*

(1992) the temporal change in the flame pulsation (i.e. the frequency of flame flicker) of IR radiation correlates with combustion intensity at different loads and swirl numbers.

Typically, an IR detector for measuring flame flicker should be located at the back of the burner, thus viewing along a line roughly parallel to the flame front [Jackson *et al.*, 1987]. This avoids error due to the sensor picking up emissions radiating from the refractory at the burner mouth. However, this position may not always be accessible in existing boilers. As such, Willson (1985) and Bendisciol (1988) proposed the use of a high pass filter (i.e. cut-off frequency of > 250 Hz) to eliminate the lower frequency signal emitted by the background radiation from the burner quarl arc. Alternatively, Booth *et al* (1998) suggested the use of two photocells looking at different regions (one at the flame and the other at the refractory) and both signals were then compared using cross-correlation technique. In conclusion, the study of the oscillations in the radiation intensity can indicate the combustion efficiency [Huang *et al.*, 1999].

Another area of flame monitoring that attracted much consideration in recent years relates to vision-based imaging technique. Lu (2000) and Yan (2002) assessed both gas and coal flames using CCD cameras. They concluded that flame images can provide both qualitatively and quantitatively information corresponding to combustion performance. The same approach was used by [Shimoda *et al.*, 1990], [Durbin *et al.*, 1996] and [Wang *et al.*, 2002] with agreement that flame images are well correlated to the flame parameters such as temperature, radiant energy, flame velocity and flame geometry. Tomographic[8] is another imaging technique designed for estimating flame temperature that involves Planck's law was proposed by Leipertz (1996). The experimental result shows that the estimated temperature was somewhat close to the readout from a suction thermocouple. Evident enough, the vision-based system has been found feasible for flame monitoring. Nevertheless, one must bear in mind that the process of digital imaging demands considerable computational power and storage. Besides, the CCD camera is more

[8] A number of optical modalities (i.e. physical processes that can be experimentally quantified by measurements of optical radiation) based on various interactions between matter and the electromagnetic field, have been identified, assessed, and utilized. Among these, optical absorption has emerged as a simple, well-studied, chemically selective (by optical wavelength) and comparatively easy to interpret modality

expensive to setup and tends to undergo degradation under high temperature condition. In addition, CCD requires large aperture in order to sustain a sufficiently large view into the furnace and consequently boiler modification. One way to get pass the installation problem is to made use of fibre optic. Jackson (1987) suggested that a fibre optic image sensing system could provide good accessibility to the flame. The output images could transmit meters away thus lowering the temperature the sensor is exposure to.

It is evident from the previous paragraphs that installing an optical sensor was highly recommended in this project. Examples for the commercial flame monitor and burner diagnostic systems are as follows: -

1. FLAMANCO is a flame monitor developed by MK Engineering Incorporation, USA. The idea is based on the flame flicker information for determining important burner parameters. [Khesin *et al.*, 1997].

2. OPTICOM operates in a similar way to an optical pyrometer. It is mostly use for measuring flame temperature and gaseous emissions. OPTICOM is developed under a joint research programme between Ingeniería Energética y de Contaminación, Spain. (INERCO) and University of Seville, Spain (AICIA). [INERCO (2003) – *http://www.inerco.com/en/products/opticom.html;* Last Accessed 10 March 05; Rodriguez *et al.*, 2002].

3. Flame Doctor is known as flame scanner designed for discriminating flame patterns with has in-built software that can autonomously determining mathematical functions between the emissions and combustion settings [Timothy *et al.*, 2003; Daw *et al.*, 2002; Flame Doctor (1996) – *http://www.babcock.com /pgg/ps/flame/doctor.html*; Last Accessed 10 March 05]

Industrial flames generate audible sound from a range of sources and overall, this can be observed as "combustion noise" [Smith, 1963; Giammar, 1970]. The pulsation frequency associated with combustion instability affects combustion chamber pressure, due to irregular heat release, and is well correlated to the combustion noise [Warren, 1978]. Combustion noise occurs when fuel and air enter a flame pocket where the mixture becomes flammable and burning continues, increasing the volume of the pocket that displaces the air and fuel streams, forming a non-flammable pocket again. This cycle continues the on-off nature of the combustion can be seen as pressure fluctuations. In conclusion, the turbulence of the combustion gases produces sound pressure related noise [Pinder *et al.*, 2004].

Combustion noise has been identified as an important source of information for industrial furnaces. In general, the total noise is making up of two main sources: (a) direct combustion noise, which arises due to unsteady combustion process, and (b) indirect combustion noise that generated by increased air velocity at a density that differs from the bulk density of its surroundings under highly turbulence and swirl conditions [Xu *et al,* 1997]. Abugov (1978) claimed that the noise generated by the flow of cold jets is dependent on the turbulence characteristics, which greatly amplified as the turbulence intensity increases. As such, this is also known as turbulence-combustion interaction noise [Warren, 1978].

The characteristic acoustic frequencies in an enclosed combustion chamber are related to its dimensions and the velocity of sound through the burning gases [Abugov, 1980]. Gaydon (1978) observed experimentally that the sound pressure signal follows the radiant intensity of the flame with a delay. This delay was thought to be due to the time taken for the sound to reach the microphone. Gaydon concluded that the sound pressure, the variation in light intensity, and the combustion rate are interrelated. In addition, Abugov (1978) suggested that the noise generated in a turbulent flame can be viewed as arising from a collection of burning elements in the combustion gases and is equivalent to a collection of monopole sound sources. Abugov claimed that pulses from monopole source tend to interfere with each other and the total noise intensity (dipole) will fluctuate

in the flame due to fluctuation in the combustion process. Based on his explanation the existence of spatial and temporal inhomogeneity in the state of the initial fuel mixture in the turbulent combustion zone ultimately causes fluctuations leading to the generation of noise even though the average combustion rate remains constant. This indicates a direct coupling between combustion process and the emission of sound.

There is also evidence of the measurement of noise of industrial systems with microphone sensors. In combustion, Zukowski (1999) and Xu (1997) both used a microphone to measure sound intensity in Fluidised Bed Combustor (FBC). The generated noise was found to be related to fluidisation of the solids by a gas and was connected with the movement of solid particles and the formation and movement of bubbles or slugging in the bed. Even though the noise from other equipment such as air pumps and the sound generated while the fluid flowed through the pipeline and the coal feeder are potential contributors to the measured noise, the change of phase (i.e. formation of vapour from liquid and solid fuels, which occurs during combustion) effectively produces many monopole sources. These noises can dominate the overall sound effects. Consequently, qualitative and quantitative changes in the acoustic signals emitted from a FBC can be used to obtain information about the combustion process.

Michel (2001) reported the possible use of acoustic method in measuring flue gas flow rate in a boiler. Tretnikov (1987) suggested the need for making a definitive identification of a source of noise using a microphone, for instance, to determine the noise level (interdependent spectrum) of each boiler and characteristics of boilers when the boiler house and the machines hall are link acoustically to within the overall noise level of the boiler house. In addition, Kidin (1984) established the link between noise intensity (sound spectrum) and burning rate using a microphone and concluded that they were in proportion.

Even though the task of recognising combustion noise of an individual burner within a burner bank can be hardly achieved, a cylindrical pipe can be installed as waveguide to attenuate any unwanted noise arising from unrelated sources [Willson *et al.*, 1985]. In

addition, the microphone should also be placed close to the burner because maximum noise level occurs near the area where combustion takes place [Tretnikov, 1987]. Because the combustion noises changes under different working conditions due to changes in the instantaneous combustion rate, pressure, and mean temperature, a microphone sensor has been installed to measure the combustion generated noise in a burner.

Overall this literature review regarding the use of IR and microphone has indicated that these sensors can be used for combustion monitoring. Measurements of flame radiations appear to provide useful information on the flame characteristic and in addition "flame flicker" can be related to the rate of combustion and other factors, such as the swirl setting. The noise intensity during combustion arises from the collection of the sound emitted by different monopole sources within a boiler so that fluctuation in combustion noise can be relevant to flame characteristics. Finally, the literature review established that both IR detector and microphone are suitable sensors to monitor combustion process in the present project.

2.4 Acoustic Emission (AE)

Acoustic emission (AE) refers to the generation of elastic waves as a result of micro-sized releases of transient energy in a material. Monitoring these waves can provide fundamental information about the location and mechanism of the transient energy release as well as the time-stress history. Potential sources of acoustic emission include [Jiaa, 1990] : -

1. Crack nucleation and propagation.

2. Impulsive shock loading.

3. Micro vibration excited by stick-slip phenomena at the interface of moving parts.

2.4.1 Introduction to AE

AE energy is attenuated and dispersed as it travels through the material both in terms of frequency as a result of geometrical beam spreading, energy absorption by the material, and wave dispersion. In principle, any impulsive event occurring within a solid or on its surface is capable of generating AE. For example, the breaking of pencil lead producing audible "clicks" contains AE with frequencies of up to 50 MHz.

The most common transducer for detecting AE is constructed from a piezoelectric ceramic element, composed of Lead Zirconate Titanate (PZT). The detected signals are often amplified, filtered and transmitted to a data logging system that stores the incoming signals. Figure 2.5 shows a schematic of an Acoustic Emission monitoring system.

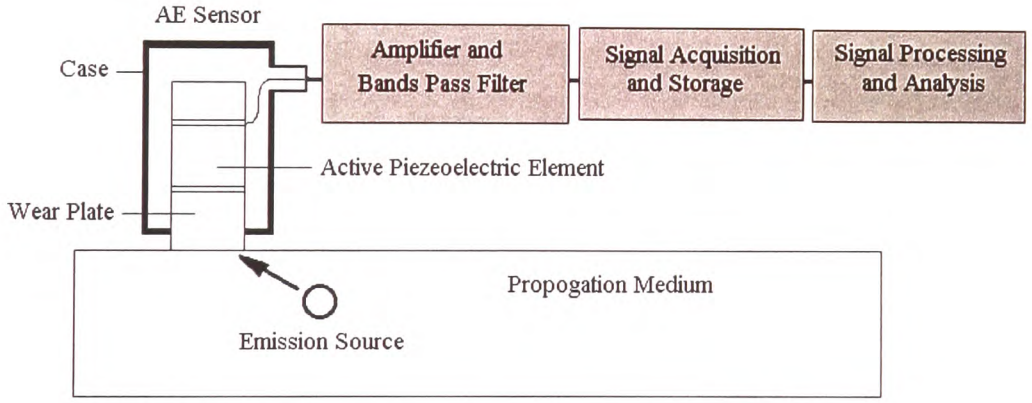

Figure 2.5 Schematic of the Acoustic Emission Scheme

AE waves have ultrasonic frequencies and have sufficient power to make it possible to undertake measurements away from the AE source. Because of the high frequency, AE signals are free from contamination from low frequency background noise. This further enhances the application of AE to condition monitoring [Reuben, 1998]. The majority of AE signals are between 0.1 to 1 MHz, once generated AE waves can travel both as longitudinal, and transverse (shear) waves depending on the geometry of the structure. They can also suffer reflection and refraction. One of the advantages of using AE is that

there are a wide range of mechanisms that can generate these elastic waves including plastic deformation, cracking, abrasion, bubble collapse, fluid flow effects and impacts. Therefore, AE has a great potential in condition monitoring [Fog, 1999].

Consequently, it has been widely employed in applications such as structural integrity monitoring and machinery monitoring. Fog (1999) used AE to monitor the exhaust valves of marine diesel engines over a broad range of engine operating conditions with the aim of allowing maintenance to be carried out before a fault occurs. Reuben (1998) reviewed the use of AE not only to detect process degradation but also to trace process abnormality. He also explained that machinery such as gas turbines or reciprocating compressors have a multitude of AE sources from bearings, fluid flow, sliding contacts and mechanical impacts. Dimla *et al* (1996) reported the use of an AE sensor for tool condition monitoring in metal cutting and suggested that AE arises in this case as the work piece undergoes considerable plastic deformation as the tool removes material. This results in the generation and movement of a large number of dislocations. Elghamry (1998) demonstrated that detection of AE (the root-mean-square, *rms*, of the AE signal) can be used to provide an appropriate air-fuel ratio to prevent "knock" in gas engine. Elghamry also suggested that those acoustic signals were harmonics of the engine cycle, which made them useful for sensing mechanical and combustion processes.

Disturbances in fluid flows also generate AE so that Neill *et al* (1997) used AE to detect the onset of incipient cavitation in centrifugal pumps. Neill established that the AE signals were statistically different both in the time and frequency domains for the pump running under normal and cavitating conditions. Cavitation induces bubbles in the flow that cause stress waves that can be transmitted to adjacent structures such as the pump casing and pipe-work. In addition, the hydrodynamic pressure fluctuations in solid liquid two-phase flows can be a source of AE, which can be detected at the surface of the containment structure. Hou *et al* (1998) used AE with a bandwidth of 0-190 kHz to diagnose changes in the operating conditions of a laboratory-scale hydro-cyclone that was used to separate fine silica flour from water. This investigation focused on the effect of the turbulent flow intensity in the cyclone and spectral characteristics of the generated

AE signals. It was found that the AE signals could be closely correlated with several important operating parameters such as the solids concentration, feed pressure, and mass flow rate. Also, chemical processes, particularly those associated with reactions and phase transformations have been identified to be acoustically active. For example, the reactions of metals in acidic solutions are often accompanied by "hissing" sounds. These can be detected as high frequency AE on the surfaces of the container in which the reaction is taking place [Cao *et al.,* 1998].

2.4.2 Possible Use of AE to Monitor a PF Burner

The previous discussion has indicated that the measurement of AE can provide information on flow and chemical processes so that it has the potential to be applied in combustion system. However, it appears that the use of these sensors in combustion is limited. In fact, there is no direct evidence of using AE sensor for measuring combustion parameters except for detecting coal acoustic waves generated by the coal flow [Zadiraka,1996].

Kondakov (1992) developed a theory linking AE to the ignition and combustion of fuels in an enclosed compartment and claimed that AE signals can be related indirectly to the characteristic of the combustion process. Kondakov explained that AE can be transformed through micro structural deformation in the burner arising from fluctuation in the intensity of the combustion process of the fuel. In addition, Abugov *et al* (1982) demonstrated, in his research that there is interaction between a gas-fired combustion process and acoustic vibration. These authors discovered that the pressure fluctuations, which are a source of AE, are related to the intensity of combustion. The pressure fluctuations can be propagated as acoustic waves through the burner quarl and other sections of the chamber. Abugov concluded that the interaction between the combustion process and the acoustic vibrations is influenced by: -

1. The magnitude of the standing wave[9] factors in the chamber.

2. The attenuation velocities of the pressure fluctuations.

3. The ionisation current fluctuation in the chemical zone.

Therefore, from this previous work it appears that installing an AE sensor in contact with the burner structure may detect AE information that can be related to the combustion processes.

In summary, installing an AE sensor in contact with the structure outside the combustor may detect AE information related to characterise of the combustion processes. As a result, an AE sensor was chosen to be used in monitoring of combustion processes.

2.5 Mathematical Modelling of PF Process

Mathematical models are regularly developed for different purposes and applications, for example, for stress analysis, heat transfer and in aerodynamics. However, rigorous modelling of combustion plant is difficult because of the complexity of the process and the difficulty of obtaining plant performance data. Nevertheless, modelling is regarded as a valuable tool for validating plant design changes over a wide range of plant operating conditions without involving costly full-scale plant trials [IEA, 2000]. Modelling can also provide a link between laboratory scale and full size plants. It is an important simulation tool for plant design and overall boiler optimisation.

There are two main types of models used for analysing utility boilers, namely, the theoretical models establish from physical principles, and so-called "black box" models developed using input-output data. The former involves detailed study of the physics of

[9] The standing wave (N), factor is ordinarily used to determine the wave reflection coefficients and is expressed in terms of the ratio between maximum and minimum pressure amplitudes. The greater the magnification of the flame fluctuations, the greater is the standing wave value.

the system whereas the latter is commonly used for control design where specific input-output relationship is of more concern. Modelling has been used typically to: -

1. To assess the changes to plant operating conditions.

2. To predict and control pollutant and ash formations.

3. To predict the influence of furnace conditions on NOx boilers emissions and of coal quality in existing combustion boilers.

Theoretical models are usually based on knowledge of the physical and chemical relationships such as reaction kinetics, material balances, and thermodynamics. These models require a significant amount of empirical data and knowledge to develop relationships that are valid over a wide range of operating conditions. To build a model, it is necessary to define the boundaries. The input design parameters for power plant are factors such as boiler geometry and operational parameters while the outputs are the performance parameters such as pollutant emissions, steam pressure, temperature and boiler efficiency [Lu *et al.,* 2000]. Although the models can be accurate, they are only applicable to the specific combustion unit for which they are developed. Besides, these models may fail when the dynamics of the combustion unit changes over time [IEA, 1997].

Computational fluid dynamics (CFD) is commercially available simulation software specifically developed for modelling or prediction of fluid flow and heat transfer. In the coal utility industry, CFD is used to predict boiler and burner performance by combining heat transfer modelling with chemical kinetics and the fluid dynamics of the system. These generations of sub-models can account for gaseous species mixing, chemical reaction, coal particle de-volatilisation, char oxidation, and heat transfer by radiation and have been used successfully to predict parameters such as ash deposition, NOx emissions, temperature distributions, gas composition, velocity, and heat transfer. However, this approach requires knowledge of the coal and air inputs to the burner so that it is not

appropriate in the current project, which aims to monitor the burner solely from output measurements.

An alternative, in full-scale boilers, is to model the combustion process as a "black box" [Rodriquez *et al.*, 2002]. Artificial Neural Networks (ANNs) are a way of producing such a model. ANNs have the ability to represent highly complex nonlinear data and so they are suited to process where it is difficult to make use of conventional mathematical and empirical based modelling techniques. As a result, this feature of ANNs would appear in principle to make them suitable for representing a coal combustion process. Lu (2000) compared a mathematical model of power plant parameters, to an ANN simulation of the system and concluded that the ANN outperformed the mathematical model. Lu stated that models based on first principles tend to require detailed specific plant data, which can be difficult or expensive to measure. Since it is difficult to make sure that the CFD model is representing well the system in a constantly changing environment and therefore the ANN, which can be easily updated, was found to be more convenient for combustion applications [Zhao *et al.*, 2004].

Alternatively, empirical models can use well-established regression techniques that can be employed to generate relatively simple mathematical relationships. However, a regression model oversimplifies the combustion process and so they tend to work poorly, particularly when they are required to extrapolate outside the range of application and therefore confidence limits must be applied [IEA, 1997; Lu *et al.*, 2000]. Also regression method is often restricted to using linear functions, for example, the Multiple-Linear-Regressor (MLR) model [Wildman *et al.*, 1994].

In summary, the use of an ANN appears to be a useful modelling tool for combustion processes, which exhibit nonlinear and complex behaviour. Consequently, they were used in the present work to represent the relationships between the sensor signals and the concentration of gaseous species in the combustion products. In addition, such a model that provides an input-output relationship will be appropriate for incorporation into a

control system. Since these networks are employed in this project, they are reviewed in the next section of the thesis.

2.6 Artificial Neural Networks (ANNs)

ANNs are a range of parallel processing systems that is useful in specific types of complex problems. ANNs are different from conventional Von Neuman computation in that they "mimic" some of the fundamental properties of a biological brain [Masri *et al.*, 1992]. ANNs consist of massively connected networks that can be trained to represent complex nonlinear functions to a high level of accuracy. As such, they can perform complex tasks under ill-defined conditions and have been found suitable of representing many physical processes such as in coal combustion and biological processes [Zhu *et al.*, 1999; Premier *et al.*, 1999]. The attributes of an ANN, such as the ability to learn from example, generalisation, redundancy, and fault tolerance, make these networks very suitable as an appropriate approach for "black box" modelling. In summary, neural networks have the following advantages: -

1. The ability to adapt and learn from the environment means that the neural network models can deal with imprecise data and ill-defined situations.

2. The ability to approximate nonlinear continuous function.

3. They are suitable for multivariate system.

Learning in an ANN can be either supervised or unsupervised. In a supervised neural network, the network is adjusted using the input and known output characteristics of the process to obtain a desired output from the ANN. Multilayer Perceptron (MLP) and Recursive networks are two examples of supervised learning schemes. In an unsupervised learning algorithm, the output characteristics are determined by the network itself without knowledge of the desired output data. The Self-Organization Map (SOM) is an unsupervised scheme. Both supervised and unsupervised networks will be discussed in the following sections.

2.6.1 Feedforward Multilayer Perceptron (MLP) Network

The MLP network is probably the most often used member of the neural network family [Pacheco-Vega *et al.*, 2000]. Other back-propagation neural networks such as the Radial Basis Function (RBF) and Hopfield networks have their use for different applications. Figure 2.6 illustrates a simple three-layer (input, hidden and output layers) network structural that can provide accurate estimation of general nonlinear function [Neural Network Toolbox - Matlab™, 1998].

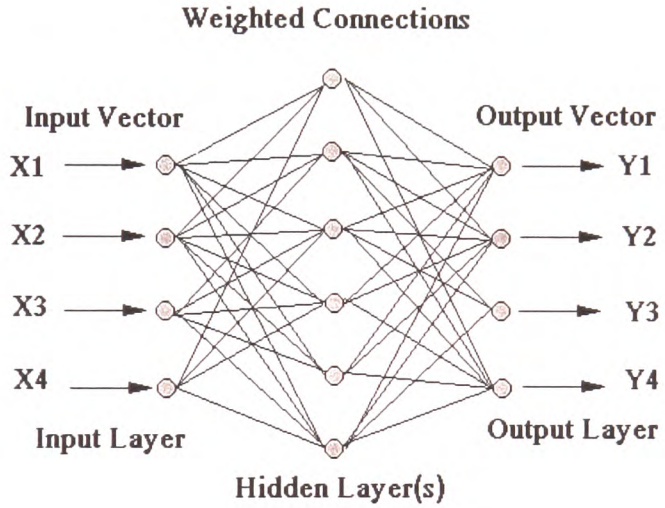

Figure 2.6 Multilayer Perceptron Network

The input neurons that together form the input layer carry out no calculations, their only task is to store and propagate normalised data forward into the network. The task of each hidden and output neuron is determined by the activity of the preceding neurons and the weights of the respective connections. Two calculations are performed: First, a weighted sum of all inputs from the neurons in the preceding layer is formed. Then, this weighted sum is passed through a nonlinear transfer function for which a hyperbolic tangent relationship (Figure 2.7) is generally used [Linko *et al.*, 1996] because it responds to neuron's net input that goes from negative to positive infinity [Matlab™ Neural Network Toolbox, 1998]. The next layer then repeats this set of calculations before giving an

output from each of the output neurons. Other transfer functions include the radial basis function (RBF), hard limit or log-arithmetic.

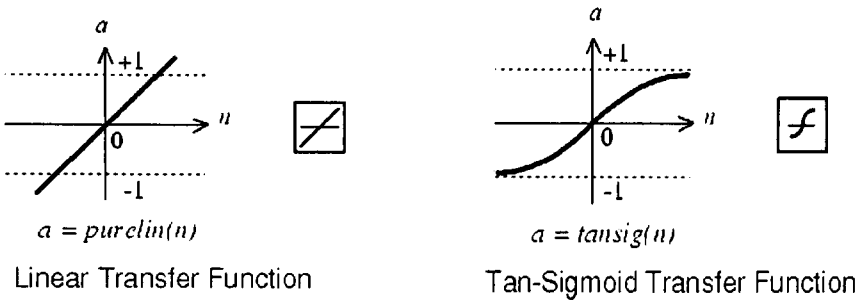

Figure 2.7 Neuron Transfer Functions

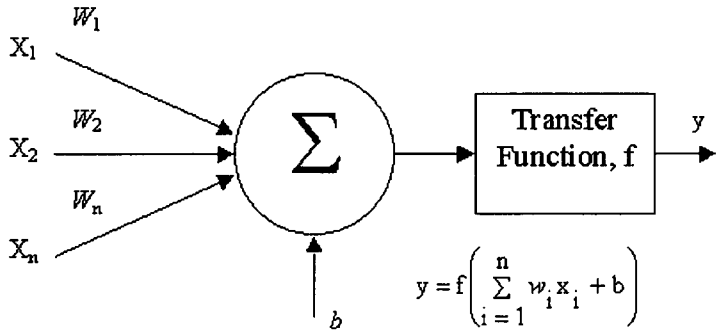

Figure 2.8 Computational Model of a Hidden Neuron

Mathematically, a single hidden layer network with only hyperbolic tangent and linear activation functions (f, F), as illustrated in Figure 2.8, can be expressed as: -

$$\hat{y}_i(b,W) = F_i\left[\sum_{j=1}^{q} W_{ij} f_j\left[\sum_{l=\theta}^{m} w_{il} x_l + b_{j\theta}\right] + b_{i\theta}\right] \qquad [2.1]$$

where b and W are the bias and weight (in matrices), F and f are the neuron activation transfer functions, x is the input vector, i and j represents 1st and 2nd layers of the network respectively.

The weights (specified by the vector θ, or alternatively by the matrices w and W) are adjustable parameters in the network, and are determined by comparing the network output predictions with the known outputs. The objective of training is to adjust the weights of the model connection to achieve a satisfactory representation of the training data so that the network will produce predictions $\hat{y}(t)$, which are "close" to the actual training outputs $y(t)$.

The ability of the network to represent the training data can be assessed by means of a prediction error, which uses the Mean-Square-Error (MSE) criterion. This MSE is defined as: -

$$MSE = \frac{1}{N}\left[\sum_{t=0}^{N}\left(\hat{y}(t) - y(t)\right)^2\right] \qquad [2.2]$$

Besides, the square root of the MSE (i.e. Mean Error (ME)) is also commonly used simply because they indicate true magnitude of the error.

The standard back-propagation algorithm, which is commonly used to modify the connection weights, is called Levenberg-Marquardt. Levenberg-Marquardt is one of the gradient descent [10](see Turner, 1996) types used for minimisation of the MSE criteria. The Bayesian framework developed by MacKay is recommended as a regularisation parameter that can be used to optimise neural network training in an automated fashion [Neural Network Toolbox - Matlab™, 1998]. The Bayesian measures the number of effective network parameters (weights and biases) used by the network and promises a better convergence property. In addition to regularisation as discussed, it is recommended to always train the network a couple of times by assuming different initial weights [Premier *et al.*, 1998].

[10]Gradient descent methods are the most popular method for training networks not only because of the rapid convergence which can be obtained but also, more importantly, due to the simplicity with which they can be implemented.

Other factors that affect ANN predictions include the number of hidden layers, types of transfer functions, and the number of neurons in each layer. Essentially increasing the number of neurons and hidden layers increases network complexity thus yielding more accurate results. However, an excessive number of assigned neurons will lead to a problem called data "over-fitting" as shown in Figure 2.9. This means that the learned function fits very closely the training data however it does not generalise well, that is it cannot model sufficiently well unseen data from the same task [Linko *et al.*, 1996]. Regrettably, there are only loose guidelines for selecting network parameters so that a neural network can only be trained on a "trial-and-error" basis. [Krishnapura *et al.*, 2000].

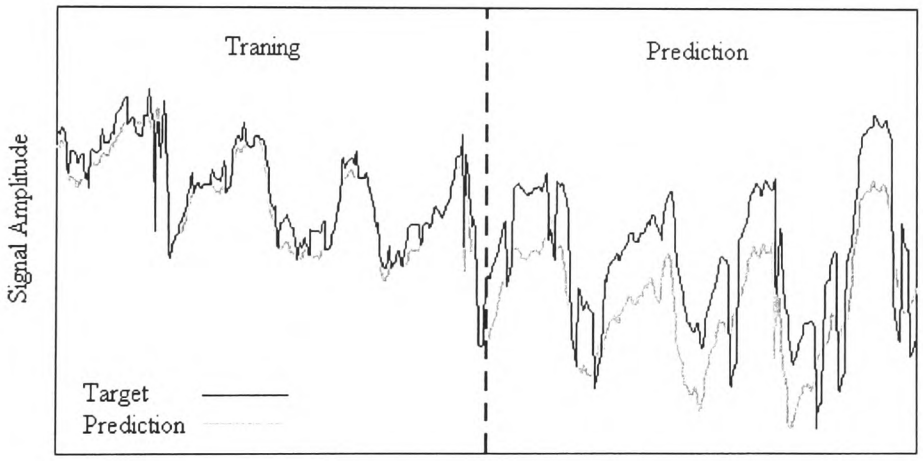

Figure 2.9 Over-fitting of Training data

2.6.2 Recursive Network

ANN which contains feedback connections is a recursive network (an example of which is an Elman network). The idea of a recursive network is that while a set of topologies of a feedforward networks is fairly constrained, the recursive network topology can take on any arbitrary topology as any node in the network may be linked with any other node (including itself). The output is dependent upon both the input to and the predicted output from the network. It is this feature, which enables a recursive network to describe time varying and temporal behaviour in addition to mapping spatial patterns [Swanston *et al.*,

1995]. However, one must bear in mind that unlike a feedforward model, the predictions of the two recursive networks with the same weights, biases as well as the data input for training, their outputs cannot be the same due to different feedback states.

In spite of the internal feedback of a recursive model, the static nature of feedforward network prediction can also be improved to cope with a dynamic system by presenting past output of the system as input to the network by means of a set of regressor vectors (e.g., Auto-Regressive with Exogenous Input), in which the past output and input values as well as a number of delays are organised accordingly before being fed into the network for training and validation [Van *et al.*, 1995]. By this way, the predictor employs past measurements of the process output, and past as well as future values of the manipulated input, to forecast the future output of the process [Tan *et al.*, 1999], which will be dicussesd in the following section.

2.6.3 Artificial Neural Network with Regressor of Exogeneous Structure (NNARX)

System Identification (SI) is concerned with creating good mathematical models of dynamic systems based on time and frequency domain input-output data. One effective way to achieve this is to employ Neural Network based System Identification (NNSI) as generic structure for the identification of nonlinear dynamic systems. Noørgard (2000) suggested that improved model predictions can be achieved through incorporating a set of regressor externally to an MLP network. Noørgard suggested that the basic identification of dynamical systems should consist of the following steps as illustrated in Figure 2.10.

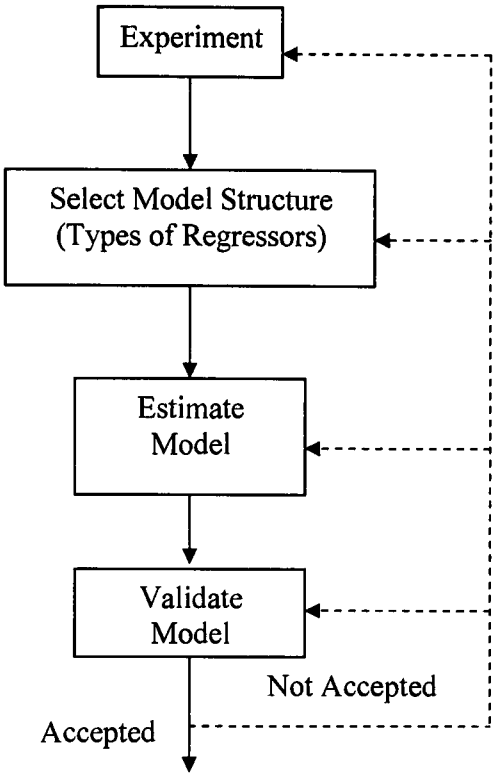

Figure 2.10 Structure of System Identification [Noørgard, 2000]

The commonly used Auto Regressive with Exogeneous input (ARX) regressor structure is defined as: -

$$\varpi(t) = [y(t-1)....y(t-n_a), u(t-n_k).....u(t-n_a-n_k+1)]^T \qquad [2.3]$$

Where y and u are the output and input vectors. The number of past inputs, past output and delays of the data are denoted as n_a, n_b and n_k respectively. The predictor then becomes: -

$$\hat{y}(t|\theta) = \hat{y}(t|t-1,\theta) = g(\varpi(t),\theta) \qquad [2.4]$$

where $\varpi(t)$ is a vector containing the regressor, θ is a vector containing the weight and g is the function realised by the neural network. The entire structure of NNARX model is shown in Figure 2.10 where P_n and P_{output} represent input and output vectors, t being the sample number and *-1*, or *-2* indicates the number past inputs and delays.

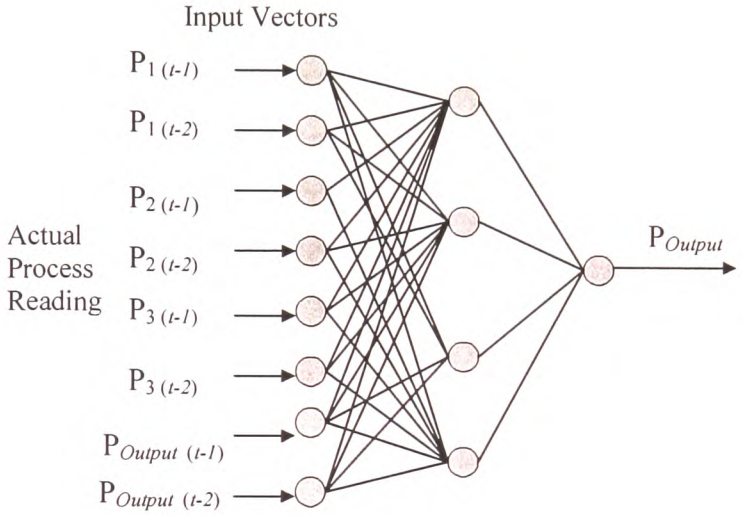

Figure 2.10 Neural Network of the Auto Regressor with Exogeneous Function Model

Some understanding of the process dynamics may be required in order to correctly define the number of past inputs, outputs, and delays of the regressor. The Levenberg-Marquardt nonlinear least squares is benchmark. Also, apart from ARX regressor as in equation [2.3], there are other regressor forms, such as NNARXM and NNOE (see Neural Network Based System Identification Tool Box) that will lead to different model structures. Nevertheless, the ARX regressor is always preferred because it provides predictions without considering the feedback. Other regressor vectors may experience inadequate predictions in certain regimes of the network operating range [Noørgard, 2000].

2.6.4 Self-Organising Map (SOM) Neural Network

The SOM network has been successful applied in various engineering applications covering, for example, areas such as pattern recognition, image analysis, process monitoring and control, and fault diagnosis. It is a valuable tool in data analysis, mining and knowledge discovery [Simula *et al.*, 1996; Vesanto, 1999]. The prototype vectors are positioned on a regular low dimension grid in an ordered fashion, making the SOM a powerful visualisation tool. [Vesanto *et al.*, 2000].

Unlike supervised learning methods, the SOM can be used for clustering data without knowing the class memberships of the input data. The SOM algorithm performs topology-preserving mapping from the high dimensional input space onto map units so that relative distances between data points are preserved. Data points lying near each other in the input space will be mapped onto nearby map units. The SOM can thus serve as a clustering tool for multi-point data. It also has the capability to generalise, i.e. the network can interpolate between previously encountered inputs.

In the same way to supervised networks, the SOM is trained iteratively. In each training step, one sample vector x from the input data set is chosen randomly and the distance between it and all the weight vectors of the SOM are calculated using some distance measure. The neuron whose weight vector is closest to the input vector x is called the Best Matching Unit (BMU). The distance between the BMU and newly presented data vectors become: -

$$\|x-m\|^2 = \sum_{k\in K} \omega_k (x_k - m_k)^2 \qquad [2.7]$$

where $\|\cdot\|$ is the distance measure, typically the Euclidian distance. k is the set variables of sample vector x. x_k and m_k are the k^{th} component of the sample and weight vectors. ω_k is the k^{th} mask value.

The SOM learns on a "winner-take-all" basis. The neuron in the competitive layer (Figure 2.12) with weights most closely resembling the current input is the winner The unsupervised learning network transforms p-dimensional input patterns to a q-dimensional (usually q = 1 or 2) discrete map in a topological ordered fashion (e.g., hexagonal and rectangular). Input points that are close in the p-dimension are also mapped closer on the q-dimensional lattice. Each lattice node is represented by a neuron associated with p-dimensional adaptive weight vector. The best matching weight vector and some of its topological neighbours are then adjusted to better match the input points. Figure 2.13 shows the updated topology of the SOM, in which the BMU and its neighbour vectors have moved closer to the input vector. The use of SOM for time-series prediction was also documented in Simula (1996).

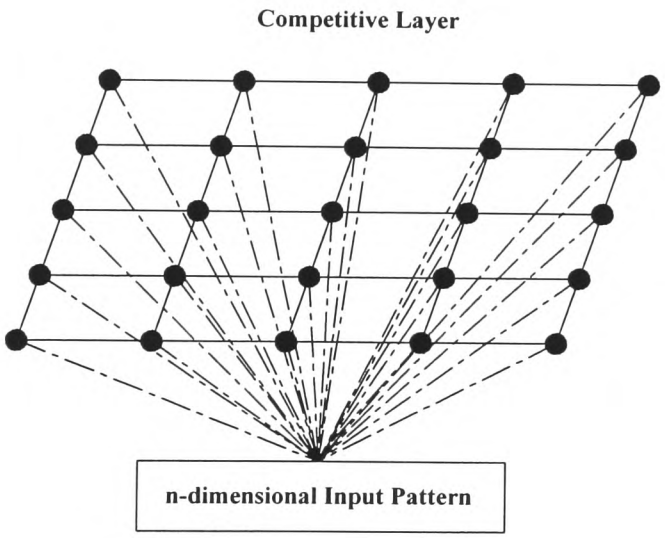

Figure 2.12 SOM with 25 Competitive Neurons on Rectangular Grid

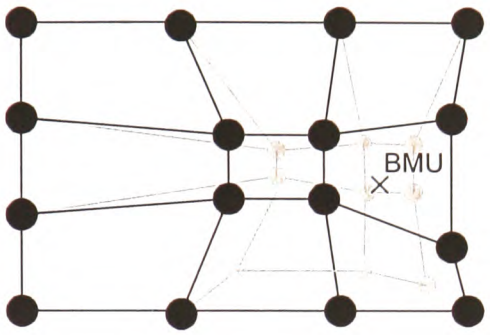

Figure 2.13 Updating the BMU and its neighbours towards an Input pattern x (the solid and dashed lines correspond to neurons position before and after updating respectively)

2.6.5 Neural Network Optimisation

Optimisation of an ANN is a prerequisite in order to achieve good prediction accuracy. Normalisation is a process of scaling the numbers in a data set to improve the accuracy of the subsequent numerical computations. For instance, if one variable has a value in the range of [0... 1000] and another in the range of [0... 1], the former will almost completely dominate the weight determining process because of its greater impact as a result of the magnitudes of these variables. For this reason, it is necessary to scale the training and simulation inputs and targets into the range -1 to 1, or zero mean and unity standard deviation.

Also, because the performance of the ANN is influenced by the model parameter settings, for example, the number of hidden layers and neurons used for training. Therefore, to select good model input requires considerable experience. The basic notion is to increase the number of neurons improves network predictions. However, the expectation can differ if too many neurons are added to a model structure. This is known as data "over-fitting" where the unseen situation is not well represented as shown in the right domain of Figure 2.9. In order to prevent this, two methods are recommended, namely, early stopping and the Optimal Brain Surgeon (OBS).

Early stopping is a technique based on dividing the data into two subsets. The first subset is the training set that is used for computing the gradient and updating the network weights and biases and the second subset is used as the validation set. The error in the validation set is monitored during the training process and training is stopped when the validation error starts to rise, as this is an indication that the network has started to be over-trained. If early stopping is used, the network should always be set to small random initial values, a slow learning rate, and a large number of neurons to avoid under fitting.

The advantages of early stopping are: -

1. It can be applied successfully to networks in which the number of 'weights' out numbers the sample size.

2. It requires a decision by the user.

The Optimal Brain Surgeon (OBS), on the other hand, prunes away any superfluous links and weights from the network thereby reducing computer run time, memory and cost for hardware implementation. Unlike early stopping, the execution of OBS entails long computational time and as a result, they are less popular [Lendasse *et al.*, 2001].

In addition to this, it is always possible to improve ANN prediction effectiveness and reduce PC run time by pre-processing data prior to training. Principal Component Analysis (PCA) can be used to reduce the number of input parameters for network training [IEA, 2000]. Essentially, PCA eliminates those inputs that have only a marginal effect on the output and as a result a significantly number of inputs to a neural network can be reduced [Bishop, 1995]. PCA takes account of three aspects for the given data, that is: -

programmers can create neural networks sophisticated enough to perform visual and audio recognition at the same time.

Today, there are a number of commercially developed neural network software, for example, NeuroSolutions [Neural Dimension – *http://www.nd.com/;* Last Accessed 07 March 05], Netlab [Netlab Neural Network Software – *http://www.ncrg.aston.ac.uk/ netlab;* Last Accessed: 07 March 05] and Neural Network for Microsoft Excel [Neuro Network Add-in for Microsoft Excel – *http://www.neuroxl.com/*; Last Accessed: 07 March 05]. If not, neural network can be programmed using Visual C++, Matlab and other programming platforms [Linko *et al.,* 1996] and as such this provides the user with the power and flexibility in the search for the best solution for a specific problem.

In combustion systems, ANN has the following advantages: -

1. They are particularly useful in system modelling and can represent a system with no priori knowledge [Bing, 1997].

2. The application of ANNs is data intensive and dependent upon multiple interacting parameters where the function to determine solutions is unknown or expensive to discover.

3. An ANN is able to handle noisy and incomplete data containing errors (i.e. it is fault tolerant), unlike the classical expert system, which is governed by a rigid rule-based reasoning framework.

4. The use of an ANN tool is relatively simple to implement and can be generalised to all kinds of functions. Therefore, it can be easily incorporated into control structure.

Both William (1992) and Reinschmidt *et al* (1994) demonstrated that an ANN can provide an adequate function to predict the NOx emissions from a boiler at all control settings based on a small number of measured data points. Wang *et al.* (2002) relates the NOx concentration to the flame signal using ANN and suggested that accurately estimations of NOx were obtained. Gabor *et al* (2000) reported the success of implementing an ANN model controller to maintain good NOx, SO_2 and CO in a PF boiler located at the Valley Power Plant, Wisconsin, USA. ANNs have also been used to predict the ash fusion temperature based on ash compositions for the coal instead of traditional techniques such as the ternary equilibrium phase diagrams and regression relationships [Yin *et al.,* 1998]. Zhu *et al.* (1999) demonstrated that the ANNs can be used to predict combustion rates of coal chars with good accuracy.

Wilson (2002) suggested that NOx reduction and increasing combustion efficiency are not contradictory goals. In his study, Wilson developed an ANNs based optimisation system to provide closed-loop control and a plant model depending on historical data. Wilson claimed a 10-20 % reduction in NOx emissions with no appreciable increase in carbon in ash could be achieved. Another successful implementation of an ANN based optimisation system to reduce NOx in a PF boiler was reported by Booth *et al* (1998). According to the investigators, the major challenges were the performance changes due to wear and maintenance activities, adjusting to fluctuations in fuel quality, and improving operating flexibility. Apart from the modelling of NOx and other gaseous emissions, ANNs have also been used to model ash deposition in which the pace of ash deposition is based on the coal chemical and physical characteristics, system operating conditions, and system design. Salehfar (1997) and Wildman (1994), on the other hand, developed an ANN model to determine the impurities and ash forming species in coal. The resultant model can be used to accurately select, blend, and forecast fuel quality for power plants. In other respects, ANNs are used for fault diagnosis. Sharkey (1996) reported the use of an ANN to monitor combustion in an diesel engine cylinder and established that the ANN was able to recognize faulty conditions which would normally require the intervention of experience engineers. Zhou *et al* (2004) demonstrated the use

of an ANN combined with a Generic Algorithm (GA) to search for the best burner setting in order to keep NOx emissions low.

2.6.7 Artificial Neural Networks as Software Sensors

Process monitoring and control relies heavily on accurate and reliable sensor information and many process parameters can be measured continuously using relatively simple and cheap physical sensors. However, the determination of certain quantities of interest requires costly laboratory analyses that cannot be performed online and so many monitoring approaches provide indirect measurement about the condition of a system. The required information may, however, sometimes be inferred from available measurements of observable quantities using a statistical model usually known as a software sensor.

Examples would include the use of an ANN to predict the nutrient dynamics using online sensor measurements in a wastewater treatment plant [Lee *et al.,* 1999]. The required process parameters were inferred from the given plant inputs based on historical data and the results were promising. The same approach was used by Valentin *et al* (2001) to predict the coagulation process in the water treatment plant based on physical sensor readings. In combustion, partly due to the complexity of the combustion process, it is difficult to formalise (mathematically) relationships between input settings and the gaseous emissions even though correlation analysis and least square based algorithms can be used. These statistical models were found to be relatively weak and furthermore it is difficult to create a good model based on only one input variable [Wojcik *et al.,* 2003, Valentin *et al.,* 2001]. In contrast, the ANN is good at capturing complex nonlinear relationships and suitable for description of phenomena where an exact law describing dependencies is unknown and was found to be more reliable than statically models [Cobourn *et al.,* 2000]. Wojcik (2003) used the processed signal from the optical sensors as inputs to the ANN model for predicting combustion gases such as NOx and CO. Lu and Yan (2000) developed an ANN based intelligent vision system for monitoring and control of PF coal combustion flames. Wang (2002) and Krytatos *et al* (1999) made use of the same approach by using flame images to predict NOx emissions using ANNs for a

coal-fired boiler and diesel engine of a containership respectively. Finally, Linko *et al* (1996) demonstrated that a well-trained ANN was able to estimate the production of enzyme by means of aerobic fermentations based on a few parameters such as CO and O_2 production/consumption rates.

2.7. Control of a Pulverised Coal-Fired boiler

The operation of a coal-fired boiler is largely influenced by its inputs such as the coal quality, air-fuel ratio, burner geometry, swirl intensity, and firing rate. The overall objective of this work was to minimise NOx whilst ensuring CO emission remained acceptable. As far as a complex system of coal-fired boilers, the control of the burner frequently entails multiple objectives.

The abatement of gaseous pollutants by the installation of a low NOx burner, or the use of a catalytic converter will not achieve the best performance without the burner being properly tuned. Typical common control systems employ process variables such as the air-fuel ratio to each burner. Simply by adjusting the settings on a few poorly operating burners can significantly improve overall unit emissions and energy efficiency [Michel, 2001]. High excess air levels mean additional energy losses, increased stack temperatures and reduced boiler efficiency and conversely, gradual supply of air to create reduction zones in a flame reduces the emission of gaseous pollutants [Wojcik *et al.*, 2003]. Control over the flow of air is achieved either by regulating individual fans or by varying the entry dampers on a common manifold [DTI, 2003]. Since, automatic oxygen trim systems are not generally found on older industrial boilers and therefore it is desirable to develop a boiler management system in order to meet the national legislation.

The extraction of the experimental correlation between burner settings and pollutant control is a formidable task that requires sophisticated modelling techniques as well as human intuition and experience. Since an ANN is an empirical modelling tool, the integrated ANN and expert system can provide a good solution for process control. The ideal control system for a coal-fired burner should have the following features: -

1. It should automatically determine the optimum plant set points.

2. It should be capable of adapting to dynamic changes by generating a set of new settings over time.

3. The system should require minimal a *priori* information and be capable of handling time delays.

4. The controller should be capable of handling multi-variable decisions.

Conventional control techniques are usually implemented by means of a good understanding of the dynamics of the process. These techniques fail however, to provide satisfactory results when applied to ill-defined processes such as coal-fired systems. For simple dynamic plants, a linear control theory was found appropriate [Krishnapura *et al.*, 1999]. However, a large class of industrial problems are nonlinear (or at least partially nonlinear) [Tan *et al.*, 1999] and for the linear or linearised model based prediction methods may fail if the nonlinearity of the process is severe [Ahmed, 1999; Tan *et al.*, 1999]. In addition to nonlinearity, a more serious problem is that of the time-varying patterns in coal-fired boiler hence preventing the use of mathematical control theories. In general, most existing control schemes fall within one of three classes as illustrated in Figure 2.14.

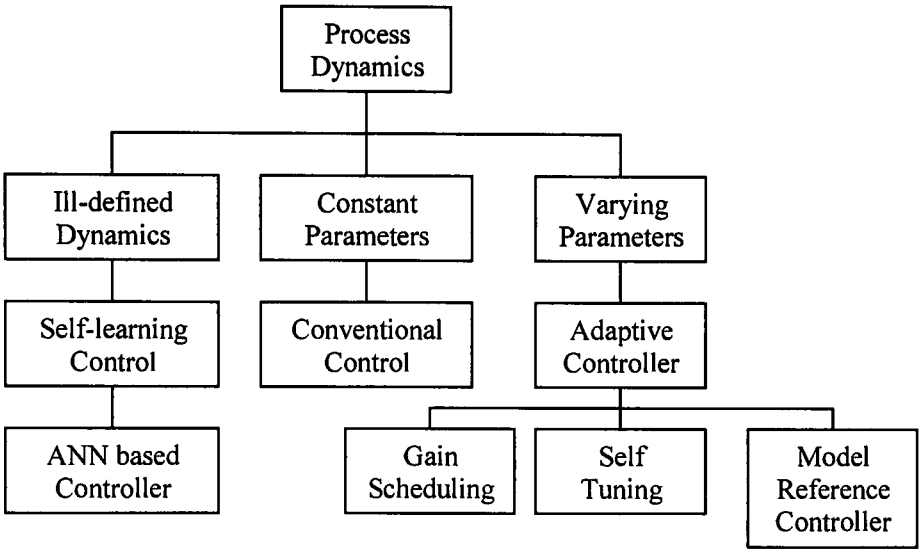

Figure 2.14 Classes Controller

2.7.1 The Adaptive, Model Reference and ANN based Controller

For an adaptive scheme, the controller parameters are adjusted in response to the operating conditions. This controller class is particularly useful when the variations of the process dynamics are predictable. An adaptive scheme requires an explicit model that accurately describes the system.

The Proportional-Integral-Derivative, PID, scheme is one of the popular schemes for industry. These types of controllers often require gain, reset-time, and dead-time adjustments according to the change of the process to provide satisfactory performance for new operating conditions. The design of the system gain, integral time and derivative time can be determined using the pole-placement[11] strategy, or through Ziegler-Nichols

[11] The ideas involved in the pole-placement approach are based on the root-locus method and allow the poles of a closed-loop system to be placed at defined locations in the s-plane (or the z-plane).This gives a wide choice in selecting satisfactory performance.

method, or other, when little is known about the dynamics of the system. Most adaptive controller schemes have shared common features that is: -

1. The plant must be tested in every different operating condition – this may not be practical for the economic and safety reasons.

2. It requires a well-defined model.

The PID, by its nature, is a Single-Input-Single-Output (SISO) controller; having more than one PID controller may result in a coupling effect if the control parameters are reversely co-dependent, and as a result, the PID scheme is unjustifiable because control of coal-fired burners involve multivariate decisions. In addition, it is not always possible to obtain a well-descriptive combustion model as opposed to other more predictable processes.

Model Reference Controllers (MRC), on the other hand, are claimed to be capable of handling processes with unpredictable changes. This type of application is often encountered in Multiple-Input-Multiple-Output (MIMO) cases. The idea is to create a mathematical model that process dynamic characteristic are considered acceptable. This model thus represents a precise definition of what the closed-loop behaviour should be with the fundamental assumption that the plant loop can actually be forced to behave in the manner specified by the model. However, because the representation model in MRC is "static" and so constant updating of the model and controller parameters to reconcile with unpredictable changes within a system, may be required. Consequently, this give rise to a requirement for a considerable amount of computational power, especially when a higher order discrete model is being used to represent the system as well as the convergence of the model is not always guaranteed [Krishnapura *et al.*, 1999]. Even thought adaptive and model reference theories are well established, their applicability to nonlinear problem has found to be restricted [Saha *et al.*, 1998].

One area in ANN research that has recently received a great attention is the inverse identification. This is because the use of inverse model of a system has an immediate utility for control. An example of a commercial application of an ANN controller to control of Pressure Support Ventilators (PSV) that assists patients who are unable to breathe on their own. The adaptive block makes use of online data collected during the operation for retraining of the model, and this is then used to update the existing controller weights (Figure 2.15) which modify themselves to the breath differences of patients [Neural Ventilator (Introduction to Adaptive Inverse Control) – *http://www.nd.com/ventilator/aic.htm*; Last Accessed 07 March 05].

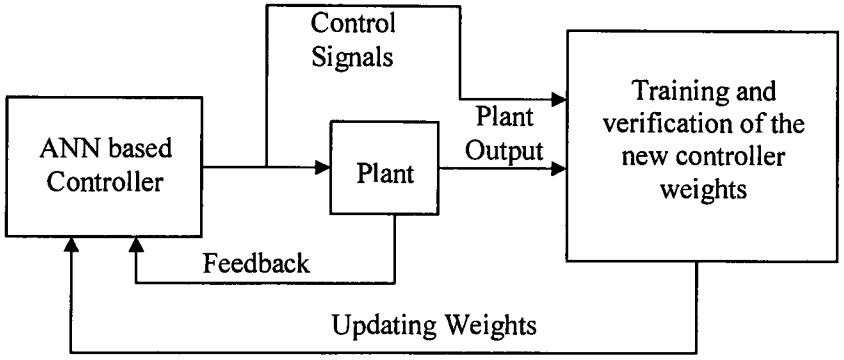

Figure 2.15 Pressure Support Ventilators (PSV)

In combustion, both Reinschmidt (1994) and Booth (1998) demonstrated the use of inverse dynamics of boilers as functions to decide good operating parameters. In a similar event, Saha *et al.* (1998) reported the development of inverse dynamics based model controller for optimising boiler settings. Other control applications that involve inverse dynamics model of the plant can be found in [Reifman *et al.*, 1998] and [William, 1992]. Essentially, the training of an inverse model required a good representation selection of the training set for the correct identification of the process inverse dynamics than it is for the estimation of the forward model [Bittanti *et al.*, 1997]. However, one downside of using inverse identification is that they lack robustness. This is due to an absence of feedback related to persistency of excitation, and the possibility that an incorrect or even unstable, inverse might be modelled [Luh *et al.*, 2000; Pham *et al.*, 1999]. Nevertheless,

the specialised learning approach used in the Internal Model Controller (IMC) was designed to overcome this problem of generalised inverse method [Irwin *et al.*, 1995]. A specialised scheme trains an inverse neural network controller using the error between the plant output and trained ANN model located in parallel with the plant. The training effectively learns the identity mapping across the inverse model and the feedforward model as shown in Figure 2.17. Because the use of IMC scheme involves both data collection and training of the controller consequently anticipated longer setup time.

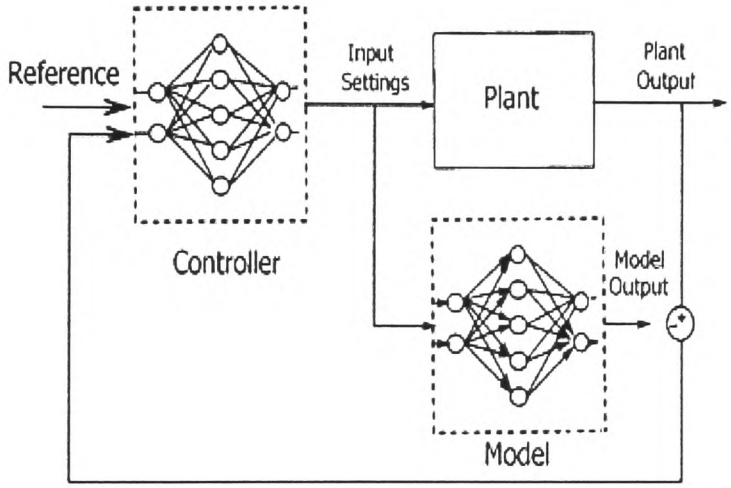

Figure 2.17 Specialised Inverse Model (Internal Model Controller)

2.7.2 ANN based Expert Scheme for Boiler Control

To optimise a coal-fired boiler requires MIMO scheme and as far as MIMO controller is concerned, the controller have complicated dynamic coupling behaviours and so the decoupling for controller design is frequently unachievable [Huang *et al.*, 2000]. Also, as boilers grew bigger in capacity, with correspondingly increased complexity, the single input single output (SISO) independent control schemes have become inadequate [Saha *et al.*, 1998]. Unlike in the assessment of boiler performance that may require consideration of multiple factors such as NOx and CO readings, the operation of a burner can be effectively controlled by the air input to the boiler. For this reason, to optimise a burner based on oxygen trimming can be largely achieved by formularising a sequence of rules and decisions.

To generate "rules for conditions" is fundamental to control, for example, a rule-based controller was designed to assess fouling in a heat exchanger where the rules were derived from the definition of plant data such as hot and cold stream flow rates corresponding to fouling thickness measurements [Afgan, *et al.,* 1995]. Also because an ANN is ideal for the generation of knowledge information and therefore to unite both ANN and rule-based schemes formed a new class of controller [Jain, 1999; Patino *et al.,* 2000]. As such, an expert system that uses neural network rules as the knowledge base is so-called a neural network based expert system [Wang, 1996]. In combustion, for example, a neural network based expert scheme known as Generic NOx Control Intelligent System (GNOCIS) was developed for targeting NOx and carbon-in-ash levels. GNOCIS uses previous plant data to train an initial plant model which is used to indicate the overall accuracy of the modelling and to highlight potential difficulties. Based on the predictive model obtained, a control strategy can be formed by taking combustion specialist, and plant engineer advice on what information should have been given to an operator to prompt any desired control action [Allison *et al.,* 1996]. With the same notion in mind, ANNs can be used to model gaseous emissions corresponding to individual burners using sensor readings, whereas rules and decisions command can be formularised as generic strategy to improve burner condition, were implemented. In addition, it is well informed that ANNs are relatively flexible for online retraining and so this allows updating of the model that corresponds to plant aging, changes in coal quality and/or slagging and fouling to be achieved. The implementation of dynamic optimisation, as integration to an online solution in control, offers the opportunity for greater emissions reduction, fuel savings, and the ability to respond rapidly and flexibly to changes in operating conditions, compliance regulations and the market environment [Eakle *et al.,* 1998].

2.8 Summary of Chapter 2

In summary, Chapter 2 has reviewed the topics relevant to the present project. These include the general features of coal, PF boiler operation, existing monitoring and emission control techniques, the adoption of ANNs in combustion processes, and the improvement of individual burners.

Coal properties, burner parameters and boiler types are factors affecting NOx emissions. Although system retrofit techniques, such as installing low NOx burners and over-fire air in existing plants can result in improvements, the boiler will never achieve its best performance without the burners being properly tuned. This implies there is a need to develop a monitoring and controller scheme to maintain good operation of burners within a full-scale boiler.

One obvious challenge in coal combustion plant is the lack of suitable monitoring devices. Partly, this is due to the poor deterministic and complex nature of combustion parameters. Other factors include limited accessibility of the sensor probes in measuring boiler parameters, gaseous stratification, and air leakage hence preventing emissions of individual burners to be identified. Slow response time and high operation cost are others reasons, particular in wet chemical analysis processes. For these reasons, IR, microphone, and AE sensors were proposed. The flame emits electromagnetic radiation at different wavelengths. This allows the light source of the flame to be measured. In addition, it was identified that the combustion noise is made up by a series of monopole sources that are generated during the combustion of the coal in the flame. Constant perturbations of combustion products and pressure fluctuations were the source of AE, which can be measured outside the burner body.

Modelling is regarded as a tool for validating plant design. System modelling can be achieved from either the first principles or empirical methods. First principal modelling demands specific knowledge and data that makes them unsuitable for modelling complex processes. CFD is a computational based modelling and although CFD can be applied to combustion, inaccurate predictions were reported because of unknown characteristics

such as the rate of coal de-volatilisation. Both least square based curve-fitting and Multiple Linear Regressor (MLR) models have their associate limitations, as most of them use linear functions as the "approximator" and therefore the deviation can be significant when undertaken nonlinear modelling. In distinction to these, ANNs have the capability to adapt and learn from their environment. In addition, they are able to deal with imprecise data and handle multivariate functions. ANNs can be useful in system control for the situation where input-output relationships are of more concern.

MLP is a simple feedforward network capable of approximating any continuous nonlinear functions. Recursive networks, on the other hand, take account of temporal information of a system and achieve better predictions. Self-Organising map (SOM) is an unsupervised ANN and is best known as a data classifying and visualisation tool. As a result, the possible idea to integrate the supervised and unsupervised schemes of ANNs can be seen as: (a) for gaseous predictions (b) to identify the change of the burner resulted from the reason such as ash deposition and fuel variation.

Good control design is usually accompanied by good understanding of process dynamics. PID is a popular adaptive scheme that proved to be able to deliver precision control only if a well-defined mathematical model is available. As combustion processes tend not to have a well-defined model and the control of combustion plants involve multiple objective decisions, these prevent the use of a SISO controller scheme. MRC, on the other hand, claims to be capable of handling unpredictable change. Nevertheless, constant updating of model weights and parameters require extreme computational power and as well convergence is not always guaranteed. Since ANNs can offer knowledge-based information and rule-based expert system was found suitable for handling imprecise data. The integration of both salient features generated a new class of controller, which is capable of handling ill-defined and complex problems more elegantly and naturally [Jain, 1999].

Chapter 3 Combustion Test Facility and Experimental Methodology

The experiments in this project were undertaken on a pilot-scale PF combustion test facility (CTF) located at Casella CRE, Stoke Orchard, Cheltenham, UK. This chapter therefore provides a description of the facility as well as of the existing instrumentation and the new sensors, which were installed, and finally, a description of the experimental work is provided.

3.1 The Combustion Test Facility

Figure 3.1 portrays the 150 kW experimental test facility, which was designed to represent a scaled down version of a single burner in a typical front-wall fired utility boiler. In broad overview, the whole system can be divided into three main sections (a) the coal handling system, (b) the burner, and (c) the combustion chamber.

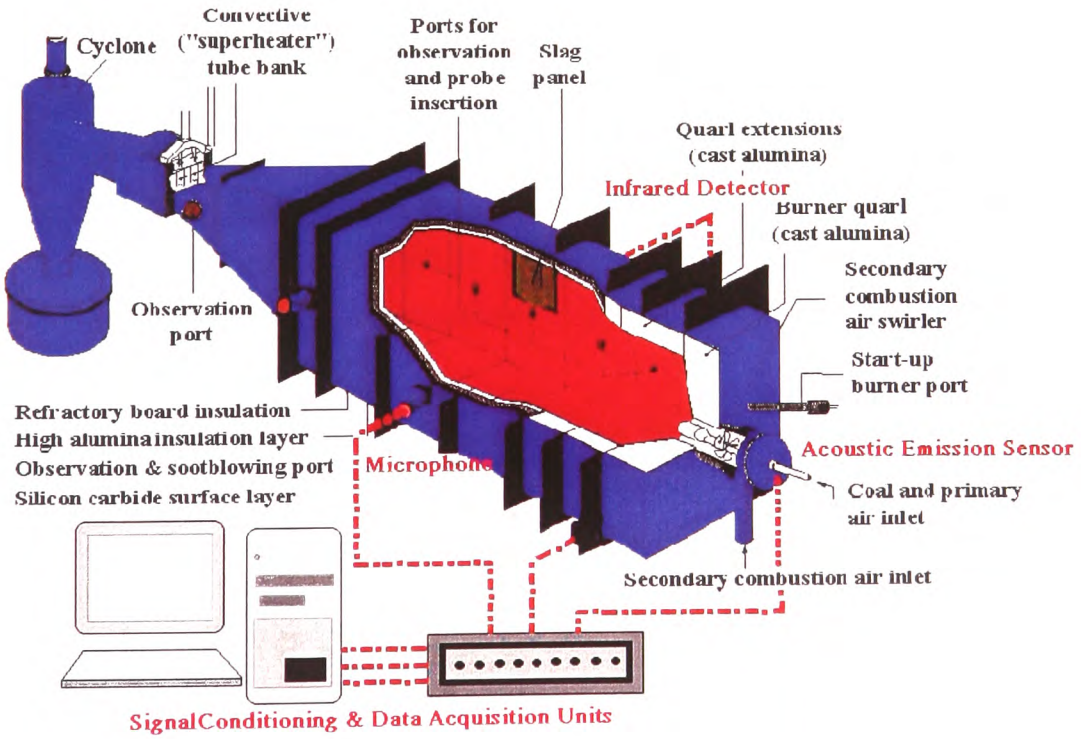

Figure 3.1 The 150 kW Combustion Test Facility

3.1.1 Coal Handling System

In any PF firing process, accurate fuel feed control is required to correctly maintain the air-fuel ratio and ensure complete combustion with the optimum level of excess air. Because coal is a blended mixture of coarse and fine particles and exhibits dramatic changes in flow density (i.e., the material bulk density under flowing conditions) with small changes in the surface moisture, gravimetric feeding by weight is more effective than the alternative volumetric method [Stock Equipment Company – Gravimetric Feeder Description, *http://www.stockequipment.com/about2.asp*, Last Accessed 03 March 05]. Figure 3.2 is a schematic of the test facility coal handling system, which used the gravimetric method. The pulverized coal was discharged into the upper hopper by a vacuum suction pump. The upper hopper acts as the main storage and can hold approximately 350 kg of coal. The coal was then transferred from the upper hopper to a bottom hopper where it was weighed and subsequently discharged into the feeder by the screw feed mechanism. The feeder delivered the coal at a pre-defined rate by progressively changing its rotational speed in accordance with the mass lost from the bottom hopper. The coal was then discarded onto a vibrating tray to smooth out any irregularity in the feed mechanism. Finally, the pulverised coal was carried away by the primary cold air stream via a flexible hose into the burner. Pulverised coal-fired systems have coal feeders which are generally gravimetric to measure the rate of coal fed to the pulveriser. The correct functioning of these coal feeders is essential to efficient and safe operation. Feeders are mechanical devices having a weighing system and a conveyor system, and they are required to be maintained for most efficient combustion [Wojcik *et al.*, 2003].

During normal operation, the bottom hopper nominally held 20 kg of coal. The hopper was refilled by activation of a rotary valve when the coal mass fell below 17 kg through an independent control system. The main controller continuously recorded the weight-loss from the bottom hopper and attempted to provide a constant coal feed rate. The controller compared the target feed rate with the rate of weight loss. The difference in these rates was used as a feedback signal in order to adjust the screw feed rotational speed. Unfortunately, the refilling of the hopper with coal and the regulation of the coal

feed rate could not be conducted simultaneously. When refilling was required, the screw feed mechanism was temporarily set to a constant speed. In addition, during the discharge of coal from the upper hopper, the dynamics led to an increase in the coal passed through to the screw feeder. The consequence of this was a small fluctuation of the coal fed to the burner, which was manifested by corresponding small fluctuations in the emissions and performance of the burner.

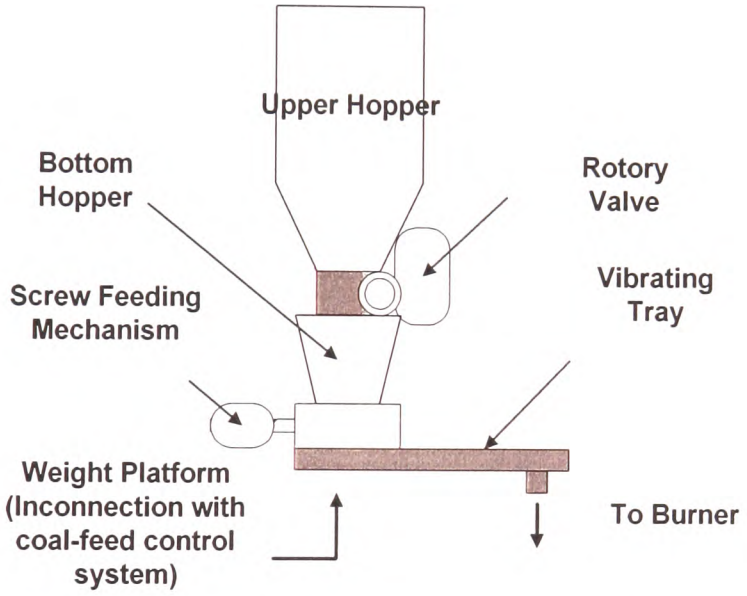

Figure 3.2 The Pulverized Coal Handling Unit

3.1.2 The Low NOx Burner

Figure 3.3 illustrates the low NOx burner installed in the test rig. It included a natural gas gun to provide primary ignition and once the ignition was achieved, the gas gun was retracted and switched off. The pulverised coal was carried by the primary air stream travelling at constant velocity. The wind box was cylindrical in shape and internally fitted with adjustable swirl vanes, which allowed the incoming air to be imparted with "swirl". Swirling assists in providing a homogenous air distribution for better mixing and hence the combustion efficiency can be improved.

The allowable swirl settings were from 0 (no swirl) to 10 (maximum swirl). The relationship between the swirl settings and the actual swirl number provided by the burner manufacture is presented in Figure 3.4. The secondary air could be preheated to a temperature up to 250 °C and was introduced tangentially to the coal/primary air stream with the facility to regulate the swirl according to the user's requirement. The contribution of the primary air to the overall flow rate is relatively small as compared to the secondary airflow. The secondary air therefore represented the main combustion airflow and was adjusted to maintain the desired flue gas oxygen concentration.

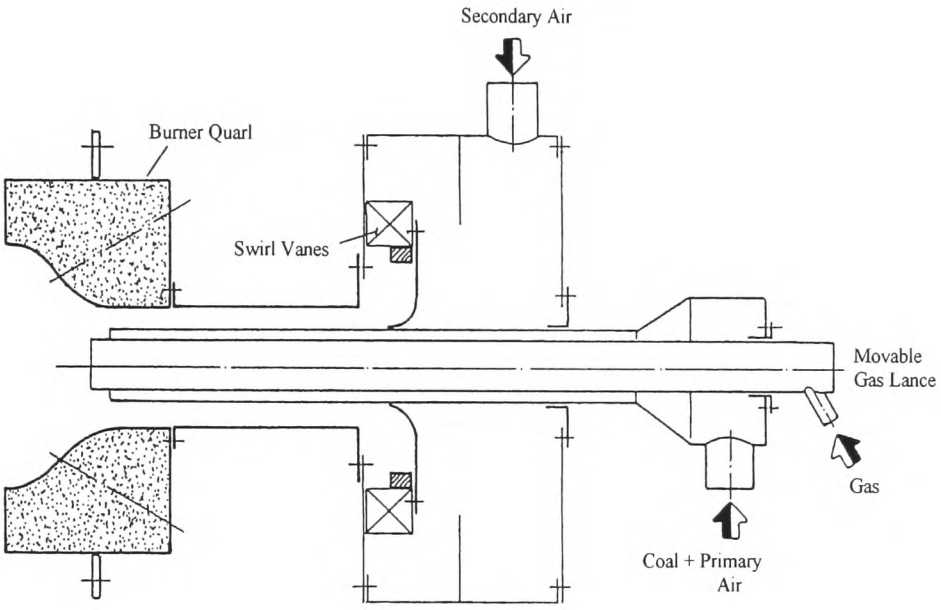

Figure 3.3 The Low-NOx burner of the Experimental Rig

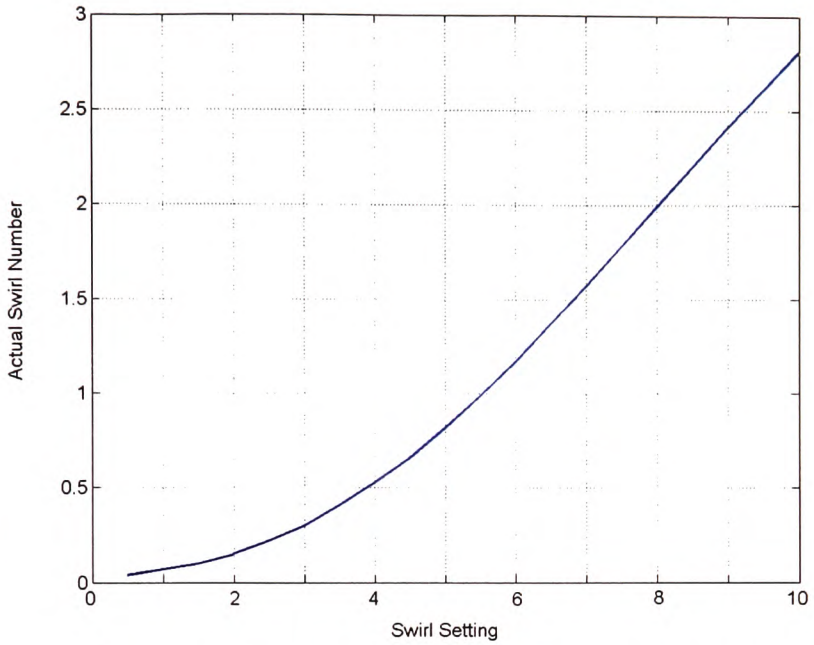

Figure 3.4 Swirl Setting vs. Swirl Number (IFRF Burner)

3.2 The Combustion Chamber

The burner fired horizontally into the combustion chamber that had a cross-section of 0.4 m^2. The chamber was 2 metres long and an array of observation ports were positioned along the sidewalls. These ports enabled any external instrumentation to be installed. At the exit of the combustion chamber, the velocity of combustion products was increased to a level typical to that found at the furnace exit in a full-scale boiler. The flue gas then passed through a cyclone where fly ash was collected before final discharge into the stack.

3.2.1 Burner Management System

The test facility had controlled by a burner management system, which aimed to ensure safe start-up, operation, and shutdown. The burner management system was located inside the test facility boiler house, to provide easy access to the operator. The system included two fail-safe IR flame detectors to detect the existence of a flame. Other input components included the control of the gas igniters and a low fuel alarm.

3.2.2 Existing Plant Instrumentation

The test facility has a permanent data logging system consisting of a Field-1000 Series DAQ board mounted in a Pentium II 233 MHz PC. The system has a total of 24 analogue input channels and the process measurements were acquired at an interval of 10 second.

The flue gas was sampled at the furnace exit and was extracted through a sintered steel filter. The gas then passed to a gas-conditioning unit (ADC TYPE WA-517) for the removal of water vapour and any remaining particulates by a heated filter with two parallel drying units. The heated filter operated in a condensation mode and was suitable for the sampling gases that are relatively insoluble in water such as the O_2, CO_2 and CO. Measurements of the concentration of other gases were based on the use of semi-permeable membrane capillaries operated in a partial vacuum and were best suited to water soluble gases such as SO_2. The sampled flue gases were transferred through a small diameter PTFE tube to a bank of 5 gas analysers for O_2, CO_2, CO, SO_2, and NOx. These analysers included: -

1. ADC RF Series infrared gas analysers for O_2 and CO in the range 0-25 % and 0-1000 ppm respectively.

2. ADC 7000 Series infrared gas analyser for CO_2 in the range 0-20 %.

3. 4000 Series (Signal Instrument Company Limited) NOx gas analyser in the range 0-1000 ppm.

4. URAS 10E Series (Mannesmann, Hartmann & Braun, NDIR-Industrial photometer) SO_2 gas analyser in the range 0-2000 ppm

In addition to measurement of the concentrations of the gases, the following burner input parameters were logged during the tests: -

1. Coal feed rate (kg/h) through direct measurement of the mass.

2. Secondary airflow rate (m^3/h) by mean of flow sensor.

3. Secondary air temperature (°C) by a thermocouple inserted in the supply ducting.

4. Primary air pressure at 65m bar (constant).

The following temperatures and pressures were also recorded throughout the test: -

1. Combustion products temperature (°C) at the convergent section of the rig using thermocouples.

2. Burner quarl temperatures (°C) at 8 equally spaced points around the burner using Type-K thermocouples inserted near the surface of the refractory (see Figure 3.5).

3. Heat flux through to the slag panel (kW/m^2) by measuring the flow rate and rise in temperature of the cooling water flowing though the panel.

4. Combustion chamber pressure (mbar) by mean of a pressure transducer.

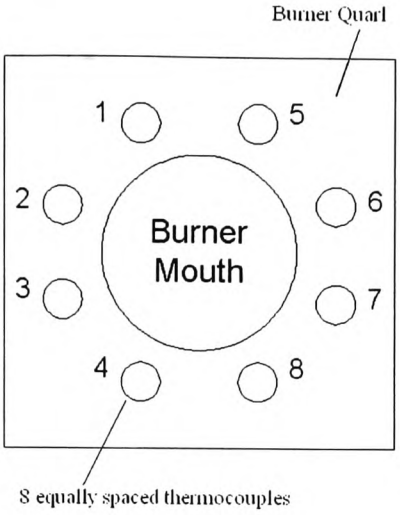

Figure 3.5 Burner Quarl Thermocouple Insets (Burner front View)

3.3 Additional Test Instrumentation

Given the overall objectives of this work, it was necessary to fit additional instrumentation to characterise the PF flame as discussed previously. An infrared (IR) sensor, a microphone to detect audible combustion noise and a high frequency sensor to measure acoustic emission were required. The details of this additional instrumentation are as follows: -

1. The IR Detector consisted of a lead sulphide photocell connected into a C7015A series IR flame detector mount (Honeywell Ltd.). The IR sensor operated on the principle that when the photocell was exposed to flame radiation, its resistance value decreased in proportion to the intensity of the radiation. The maximum operating temperature of this sensor was 71°C and it responded to radiation with wavelengths between 700 and 1000 nm.

2. The Microphone. This was a TCM100 Series omni-directional Electret-Condenser microphone with a maximum operating temperature of 43°C. The maximum frequency response of this microphone was 16000 Hz.

3. The Acoustic Emission (AE) sensor. The AE sensor was a MICRO-80S (Physical Acoustics Corporation) device, with a pre-amplifier, which had a selectable gain of 20, 40, or 60 dB and a frequency response in the range 100-1200 kHz.

Selection of a suitable location for the sensors to obtain reliable measurements was restricted by the availability of suitable access points. Both the IR and Microphone required a direct view of the flame. For this reason both these sensors were mounted at the end of straight cylindrical pipes that were in turn located in separate sight ports perpendicular to the flame. This not only resulted in attenuation of any unwanted surrounding noise which could arise from unrelated sources instead of the flame but also shielded the microphone from high temperature, or radiation. Moreover, it avoided contamination of the IR lens from particulate matter in the flame. The best position for mounting the AE sensor was identified to be on the back of the gas lance since the flow induced AE should be readily propagated from the tip of the coal nozzle to this surface. Also, to protect the AE sensor the interface material had a low heat conductivity and also ensured good contact with the gas lance. The position of the sensors is illustrated in Figure 3.1 and Figure 3.6 shows photographs of the sensors mounting.

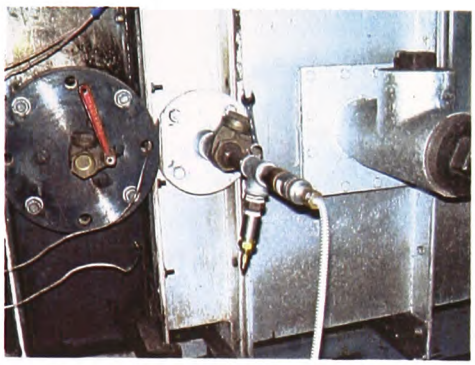

(a) IR Detector

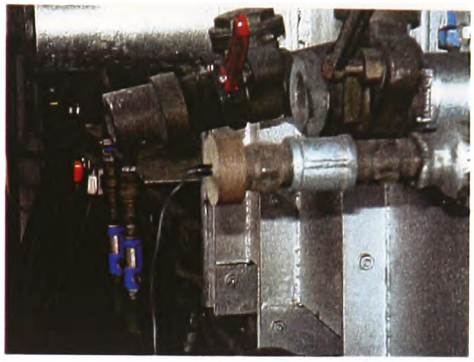

(b) Microphone

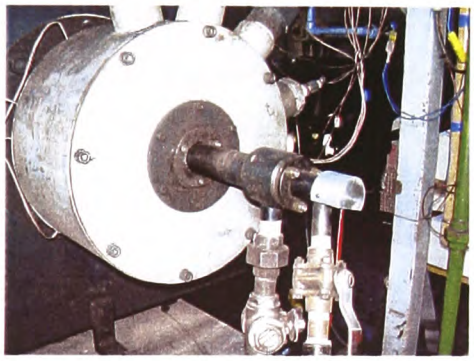

(c) AE sensor

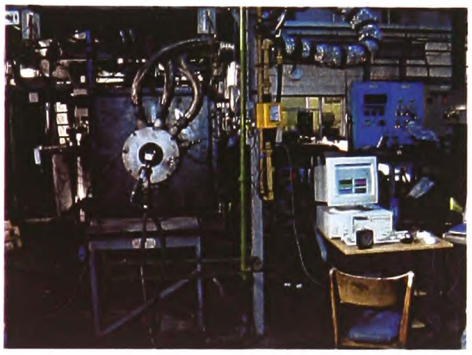

(d) Overview of the test facility and the data acquisition system

Figure 3.6 Mounting of the Sensors during the Tests

3.3.1 Signal Conditioning and Acquisition

Signal conditioning of the IR sensor involved the use of a resistance to electrical voltage converter and an amplifier, before the signal was fed into the DAQ board. The Microphone output was a voltage so that only amplification was necessary. Both of the amplifiers for the IR and Microphone sensors were ac-coupled with the intention of removing dc component in the signals, and had an adjustable gain factor from 1 to 11. The circuits for the resistance-to-voltage converter and the amplifiers are shown in Figure 3.7.

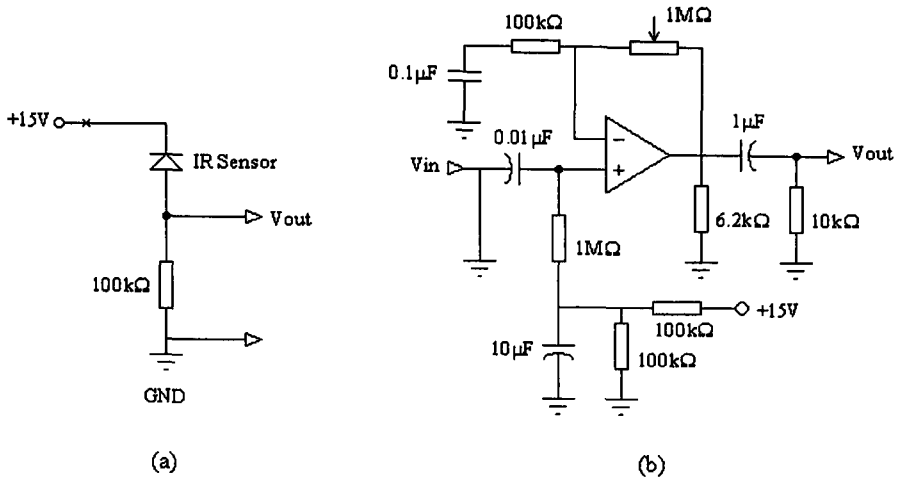

Figure 3.7 Electrical Circuits for Signal Conditioning
(a) Resistance-to-Voltage Converter (b) ac-couple Amplifier

Low-pass filters were used to limit the bandwidth of the sensor responses to reduce aliasing effects while still retaining most of the useful information contained in the signals. Several authors [Willson *et al.*, 1985; Timothy *et al.*, 1996; Hashimoto *et al.*, 1992] have suggested that the useful frequency range for the IR radiation from the flame is restricted to 1000 Hz. Also, Abugov *et al* (1978) have shown that the combustion pressure fluctuations can be correlated with the IR radiation signal. Consequently, it can be argued that the frequency range associated with useful information from the microphone signal would approximately coincide with the frequencies of the IR signal. Nevertheless, two higher frequency low-pass filters were implemented in this case to ensure adequate coverage so that all appropriate information was obtained. These 4^{th} order continuous time active Bessel filters had a cut-off frequency of 1800 Hz. The advantage of using a Bessel filter is that it provides minimum phase distortion. The actual response of the Bessel filter is given in Figure 3.8. For the AE sensor, the full frequency response of 100-1200 kHz was taken into consideration and as the result no additional filters were required.

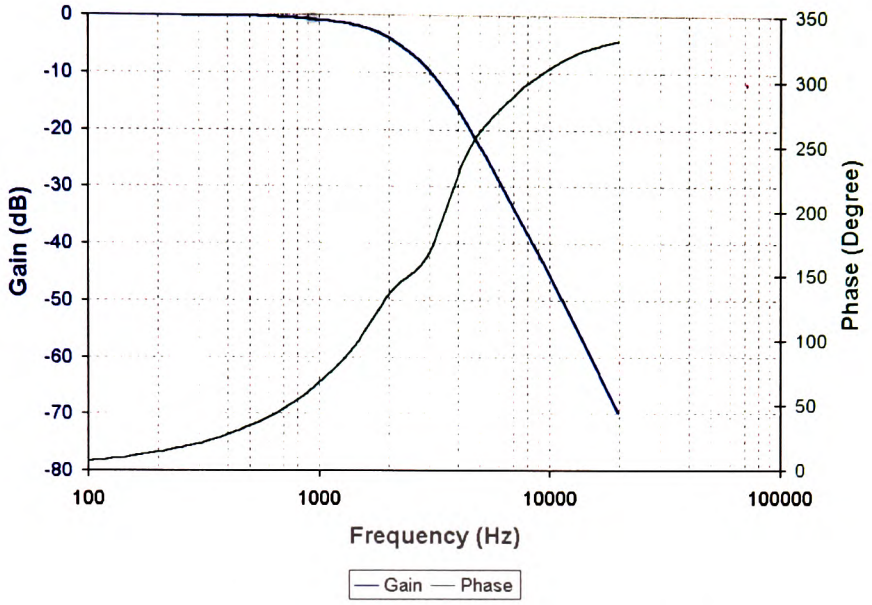

Figure 3.8 Actual Response of the 4th order Low Pass Bessel Filter

Two data acquisition boards, one for the IR and microphone signal and the other for the AE sensor, were installed in a stand-alone Pentium III 550MHz PC. Both boards were programmed with LabView™ Virtual Instruments Software (National Instruments Corporation) and were run within this environment. Details of the sampling rate and other parameters are presented for each sensor in Table 3.1 and technical information for the data acquisition boards can be seen in Table3.2

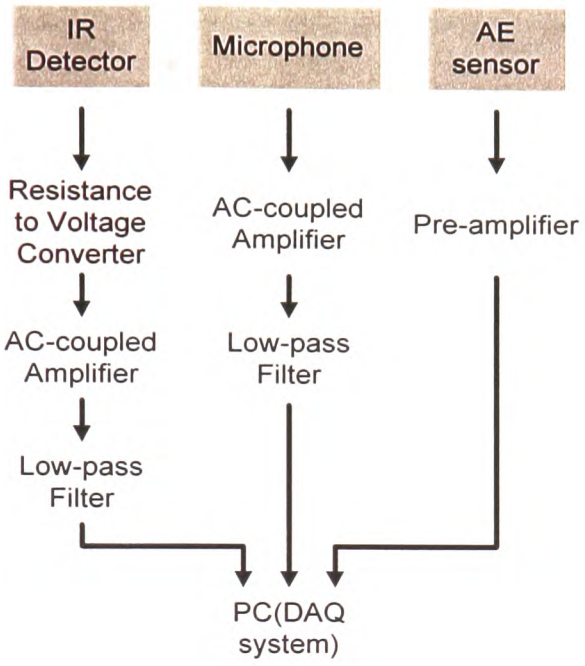

Figure 3.9 Schematic of the Signal Conditioning and Data Acquisition System

Table 3.1 Acquisition of the Sensors Signal from the Sensors

Sensors	**Signal Type**	**Sampling Rate**	**Number of Samples Acquired**	**Duration of the Signal**
IR	Analogue Waveform	8192Hz	32768	4 s
Microphone	Analogue Waveform	8192Hz	32768	4 s
AE	Analogue Waveform	5MHz	32768	6.55 ms

Table 3.2 Technical Information for the DAQ Boards

DAQ Boards	Number of Input Channels	Maximum Sampling Rate	ADC Resolution
AT-MIO-16L (National Instruments)	8 (Differential Mode)	100 kHz ÷ number of inputs	12-Bits
COMPUSCOPE 1250 (GaGe)	2	25, 10, 5MHz	12-Bits

3.4 Experimental Details

This section describes the overall experimental work undertaken on the test facility at Casella CRE. Two different coals, namely, Daw Mill coal from the U.K. and so-called Cerrejon Columbian coal were used in the tests. The ultimate analyses of these coals together with their stoichiometric combustion air requirement can be found in Appendix B (Table A1 and A2).

The test facility was operated at the maximum thermal input of 150 kW to ensure a more stable flame. This was maintained nominally constant by changing the feed rate of the coal to accommodate the differences in calorific value of the two coals, see Table 3.3.

Table 3.3 Calculation of Coal Feed-Rate

Coal Type	Calorific Value (MJ/kg)	Burner Load (kW)	Coal feed-rate (kg/h) = $\left(\frac{\text{Burner Load}}{\text{Calorific Value}}\right) \times 3600$
Cerrejon	27.98	150	19.3
Daw Mill	25.00	150	21.6

The primary air pressure was set to its maximum value of pressure of 65 mbar and maintained constant for the whole period of the experiments. The only two input variables, which were changed during the experiments, were the secondary air flow-rate and the burner swirl setting. The secondary air flow-rate dictates the amount of excess air

since the primary airflow rate is constant consequently variations in these parameters affect the concentration of NOx, CO, and O_2 in the flue gases. The flame characteristics combustion intensity and hence position of the flame front[5] can also depend on the degree of swirl supplied to the secondary air. The degree of swirl influences the flame stability and flue gas emissions particularly NOx and CO emissions.

Initial trials were used to determine the allowable operating range for the secondary airflow rate and the burner swirl setting. The operation of the test facility was governed by fail-safe devices, which detected the presence of a flame during the tests and the emission monitoring instrumentation for NOx and CO, which saturated at 1000 ppm. Consequently the upper and lower limits of the secondary air flow rate and burner swirl settings were selected to avoid a burner trip and to prevent saturation of the instrumentation.

The allowable secondary airflow rates were found to lie between 130 and 160 m^3/h corresponds to overall excess air levels varying from approximately 1 to 22 %. A step change of airflow of 10 m^3/h was performed as shown in Figure 3.10 every 20 minutes. The burner swirl settings were 3, 4, 5, and 6 which corresponded to swirl numbers of 0.3, 0.5, 0.8, and 1.2 (refer to Figure 3.4). The calculation of the excess air for each secondary air setting is presented in Appendix B (Table A3).

[5] The flame front refers to the location where the PF starts to ignite relative to the coal nozzle, and it is an important factor in the flame stability. A stable flame should have a flame front that is well rooted in the burner mouth.

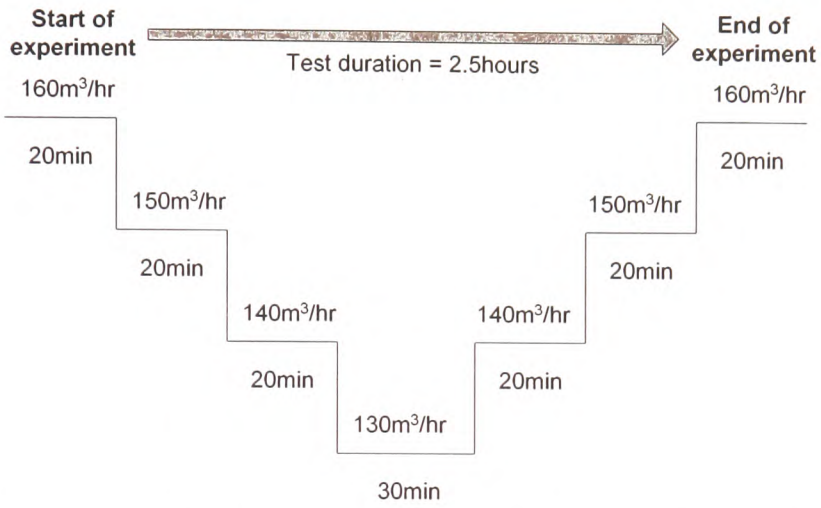

Figure 3.10 Operating Profile of the Secondary Airflow Rate for each Test

During the tests, the emissions, plant process parameters, and the sensors signals were monitored as discussed earlier in this chapter. Initially 8 tests were undertaken to gather representative data for a range of burner operating conditions. However the control experiments, which will be reported later in Chapter 6, were restricted to a single swirl number for each of the coals.

Table 3.4 Summary of the Combustion Tests

Experiment	Swirl Number	Coal Type
Test 1	0.3	Daw Mill
Test 2	0.5	Daw Mill
Test 3	0.8	Daw Mill
Test 4	1.2	Daw Mill
Test 5	0.3	Cerrejon
Test 6	0.5	Cerrejon
Test 7	0.8	Cerrejon
Test 8	1.2	Cerrejon

3.5 Summary of Chapter 3

This chapter provides an overview of the test facility at Casella CRE together with the novel sensors used in the experiments. The operating boundaries were governed by the fail-safe devices on the system and the saturation of emission analysers. The range of test conditions is presented and limitations in the test facility are discussed.

Chapter 4 Experimental Results and Analysis

This chapter presents the results gathered during the experiments conducted on the pilot scale 150 kW PF burner. Initially the discussion starts by showing the concentrations of the gases NOx, CO and O_2 at different secondary airflow rates and swirl numbers as defined in Chapter 3. This information is important as it allows an understanding of how the combustion test facility operation affects the combustion process. The discussion will then move to consider the signal processing of the "raw" IR, microphone, and AE sensor signals into a set of useful features that may be related to the combustion characteristics and gaseous emissions.

4.1 The Flue Gas Concentrations

The experiments were conducted by varying burner parameters such as the secondary airflow rate and the secondary air swirl setting, so that a workable range of burner operating conditions were studied. The experiments were arranged so as to enable the optimum settings to be identified, and provide the information required for the design of the controller as will be presented in Chapter 6.

To reduce NOx emissions whilst maintaining low CO concentrations has been an on-going requirement for the utility industry. Although NOx is the major concern, high CO emissions which are associated with a reduction in boiler efficiency should not be overlooked. One can reduce NOx by minimising the excess air but the consequences can include reduced thermal efficiency, boiler tube corrosion, and poor electrostatic precipitator performance. For these reasons, optimising a PF boiler requires skill, experience, and careful consideration. Under growing pressure from increasingly stringent legislation, significant efforts are underway in the search for advanced burner monitoring and control techniques. Ultimately, the research objective is to reduce NOx so as to comply with the relevant legislation without sacrificing boiler efficiency. It is envisaged that an adequate burner controller scheme will increasingly needed for existing and newly built boilers.

4.1.1 Gaseous Emissions for Daw Mill and Cerrejon Coal at different Swirl Settings

As outlined in Table 3.4, a series of experiments were conducted by operating the burner at different swirl settings (i.e., swirl numbers 0.3, 0.5, 0.8, and 1.2). Each of the individual tests was repeated using a standard secondary air profile as illustrated in Figure 3.11. These tests therefore covered a representative combination of the secondary airflow rate and swirl setting for the test burner. The same procedure was also repeated for the two coal types, namely, Daw Mill and the Cerrejon Coals.

Figure 4.1 shows the NOx, secondary airflow rate, CO, and O_2 for Test 1. The experiment fired Daw Mill coal with a swirl number of 0.3. The initial operating condition started with a secondary airflow rate of 160 m^3/h and resulted in high NOx (> 500 ppm) and low CO (< 75 ppm) concentrations. As the test proceeded, the NOx emissions reduced as the secondary airflow rate decreased while the CO remained low. However, once the secondary airflow rate reduced to 130 m^3/h, the concentration of CO rose rapidly. This suggests that insufficient O_2 was available to achieve complete combustion and hence the combustion efficiency was subsequently reduced and this would need to be corrected in practice.

One can notice in Figure 4.1 (b) that the secondary airflow rate and hence the oxygen concentration affects both NOx and CO levels. Oxygen is an indication of the amount of air present and was therefore considered as one of the significant monitoring parameters as presented as a blue line (Figure 4.1 (b)). It is clear in Test 1 that although the combustion airflow remained constant, all three gases (i.e., NOx, CO and O_2) showed "regular" periodic fluctuations. Similar behaviour was also observed in all the other tests and this itself, was associated with fluctuations in the coal feed rate of ± 2.5 kg/h around the set point. Consequently, this coal feed rate fluctuation resulted in periodic variations in the air-fuel ratio and hence in the flue gas emissions. A description of the coal feed mechanism can be found in Section 3.1.1

(a)

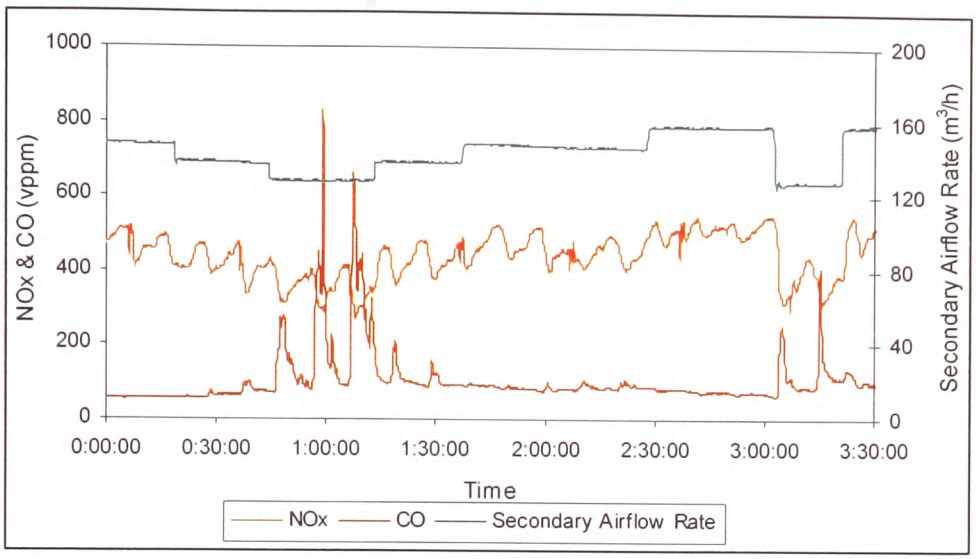

(b)

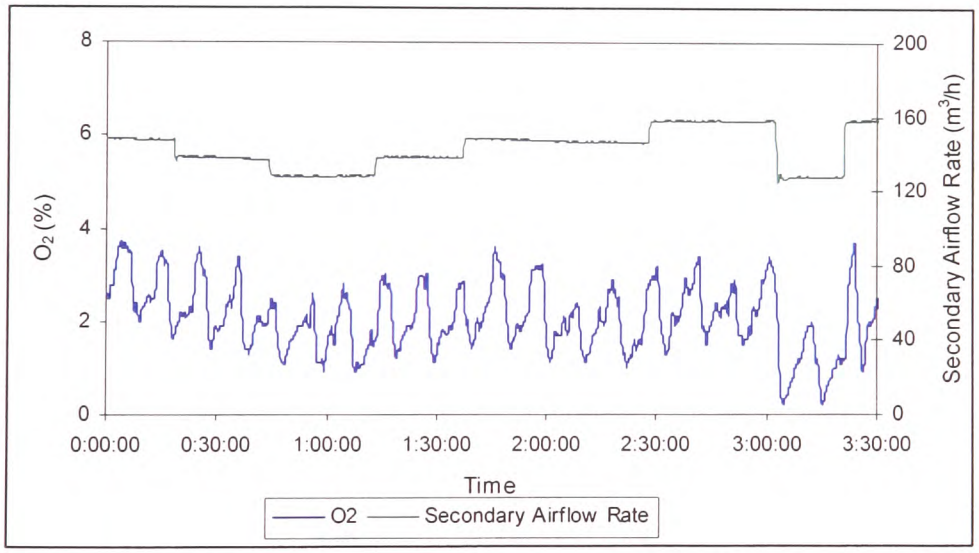

Figure 4.1 Measurements of (a) NOx, CO and Secondary Airflow Rate, (b) O_2 and Secondary Air flow rate, when firing Daw Mill Coal at a Swirl Number of 0.3 (Test 1)

In Test 2 (Figures 4.2 (a) and (b)), the burner was configured with a swirl number of 0.5. The NOx, CO and O_2 emissions behaved in a similar way to that observed in Test 1, with the NOx decreasing as the secondary airflow rate was reduced. A peak CO of 1000 ppm was observed for the lowest secondary airflow rate, which was approximately 200 ppm higher than in the previous Test 1.

(a)

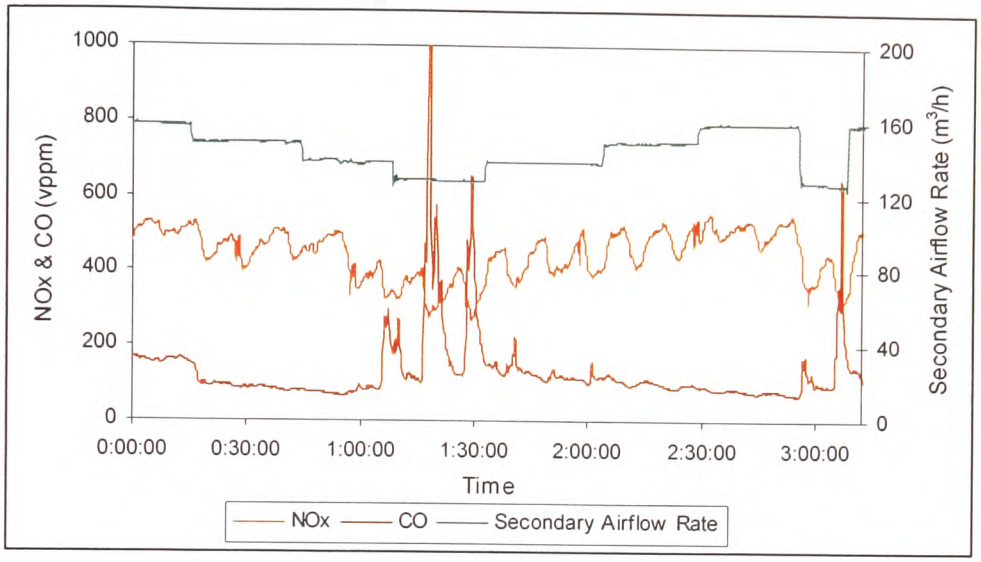

(b)

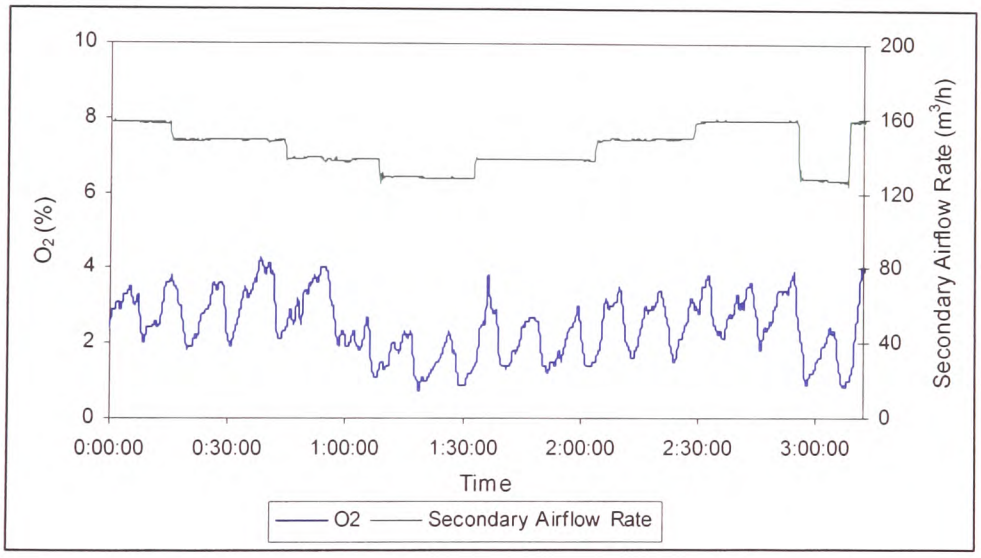

Figure 4.2 Measurements of (a) NOx, CO and Secondary Air Flow Rate, (b) O_2 and Secondary Airflow Rate, when firing Daw Mill Coal at a Swirl Number of 0.5 (Test 2)

The NOx in Test 3 (swirl number of 0.8) (Figure 4.3 (a)) varies relatively little as the secondary airflow rate reduces in contrast to the other tests. The CO remained relatively stable even at a secondary airflow rate of 130 m^3/h. This suggests that the swirl number of 0.8 provides the most stable combustion condition.

(a)

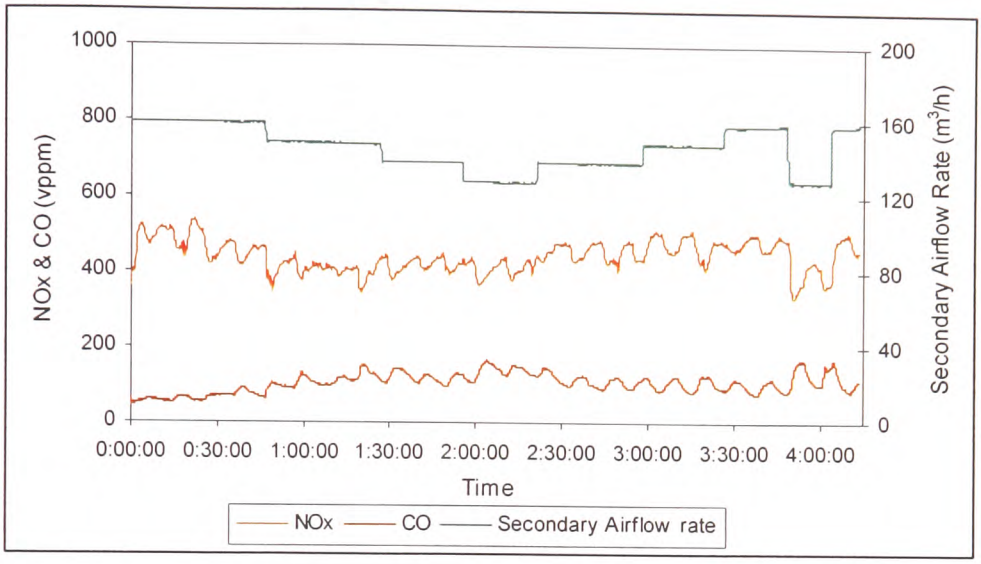

(b)

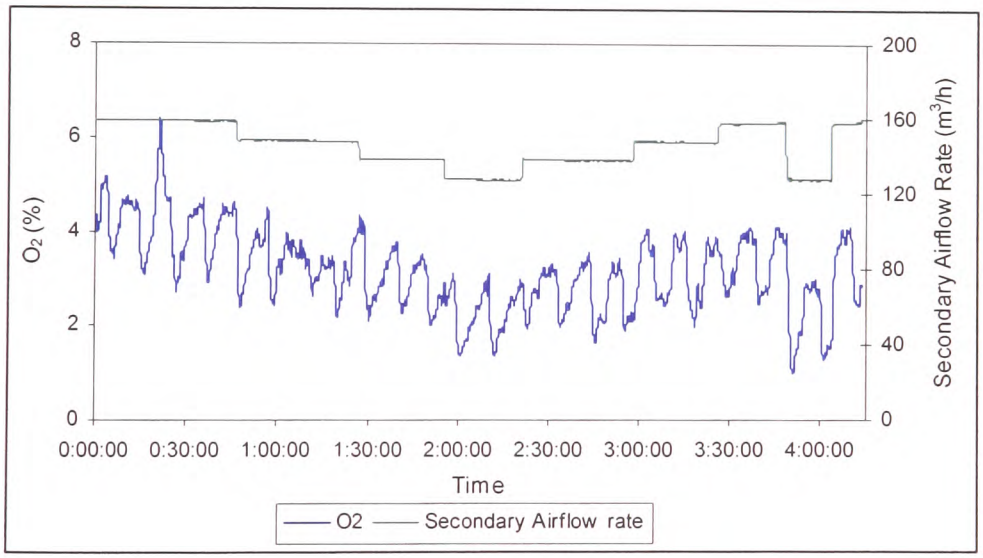

Figure 4.3 Measurements of (a) NOx, CO and Secondary Airflow Rate, (b) O_2 and Secondary Airflow Rate, when firing Daw Mill Coal at a Swirl Number of 0.8 (Test 3)

Figure 4.4 presents the gaseous emissions for Test 4 with a burner swirl number of 1.2. The average CO concentration is the highest observed throughout Tests 1 to 4 with the Daw Mill coal. In Test 4, the level of CO constantly "saturated" the gas analyser, particularly with the low secondary airflow rates of 130 and 140 m^3/h. Also, the O_2 level

under these conditions was the lowest observed throughout Tests 1 to 4. Hence, for example, at the lowest airflow rate the oxygen concentration was approximately 1.2 %. Red arrows are included in Figure 4.4 (a) and (b) to highlight when the combustion test facility was automatically shut down due to burner "tripping", when the safety sensors (consisting of two IR detectors) failed to detect the flame. It is known that the flame shifts towards the burner quarl (i.e., shorter flame is produced) as the swirl number is increased [Martin, 1993] and on occasion it appears that the visible flame may lie outside the field of view of the sensors at this high swirl number of 1.2.

(a)

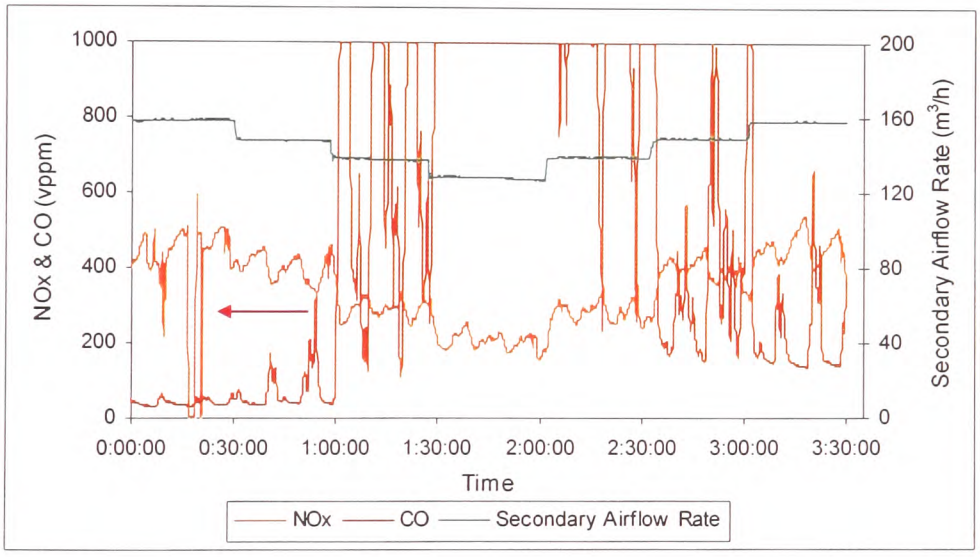

(b)

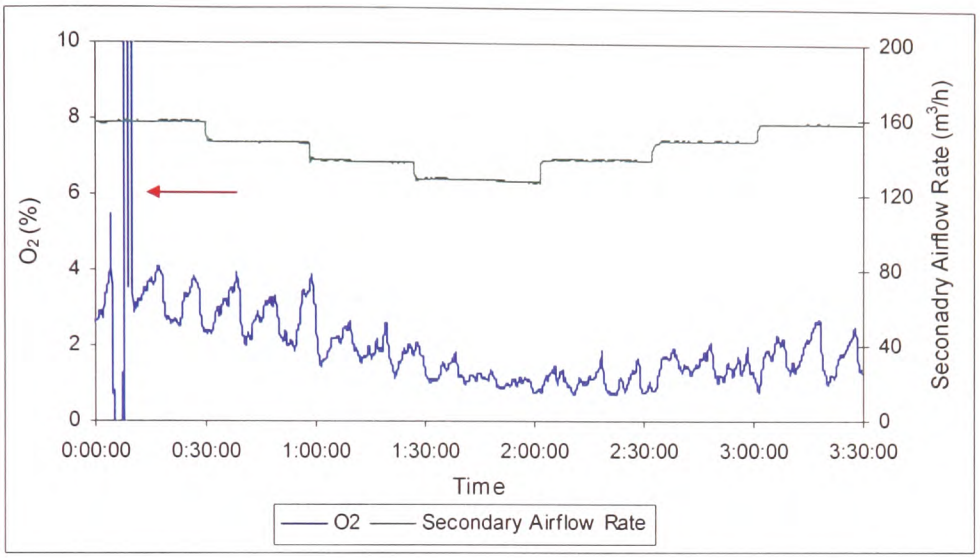

Figure 4.4 Measurements of (a) NOx, CO and Secondary Air Flow Rate, (b) O_2 and Secondary Airflow Rate, when firing Daw Mill Coal at a Swirl Number of 1.2 (Test 4)

Observation of Figures 4.1 to 4.4 indicates that at each secondary airflow rate, the average O_2 concentration varies as the swirl number was varied. This is illustrated more clearly in Figure 4.5 which presents the average concentrations of the flue gases for a secondary air flow rate of 130 m^3/h. The O_2 concentration varied from 1.2 % to 2.3 % and this suggests that the air-fuel ratio varied from test to test despite the nominal excess air remaining constant. This variation is probably due to variations in coal quality and moisture content, and as the airflow was controlled by appropriate setting of a butterfly valve there is likely to be variations due to change in the ambient temperature and humidity. Consequently, the variations in NOx and CO observed in Figure 4.5 are due to changes in the excess air level as well as changes in swirl number.

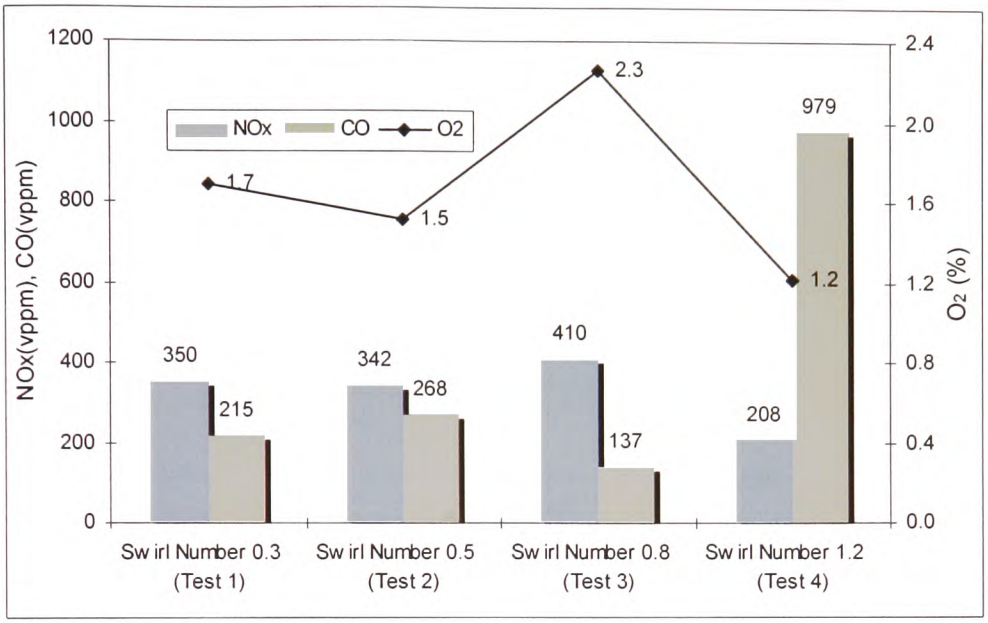

Figure 4.5 Average NOx, CO and O_2 correspond to the Secondary Airflow Rate of 130 m^3/h for Swirl Numbers of 0.3, 0.5, 0.8, and 1.2

For Tests 5 to 8, the combustion test facility was fired with Cerrejon coal and Figures 4.6 and 4.7 illustrate the concentrations of the combustion gases of NOx, CO and O_2 in the flue for Tests 5 (swirl number 0.3) and 6 (swirl number 0.5) respectively. The Cerrejon coal has a higher calorific value than the Daw Mill and hence required a lower coal feed rate for the same thermal input as indicated in Table 3.3. Therefore, the test facility could achieve a thermal input of 150 kW with a coal feed rate of 19.3 kg/h. Generally, these tests at the lower swirl numbers, with Cerrejon coal yielded lower NOx emissions than the corresponding Daw Mill tests. This is evident by comparing Test 1 (Daw Mill) and 5 (Cerrejon) for the same swirl number in which the highest NOx concentrations were 500 and 300 ppm respectively.

The flue gas emissions with the Cerrejon coal were different to that observed in Tests 1 to 4. In general, there were smaller changes in the magnitude for the gaseous concentrations when the combustion test facility was subject to the nominal air variations. Test 6 (Figure 4.7 (a)) shows a marginal improvement over the Test 5 (Figure

4.6 (a)) for the NOx and CO, which implies that the combustion process benefits from the higher swirl number.

(a)

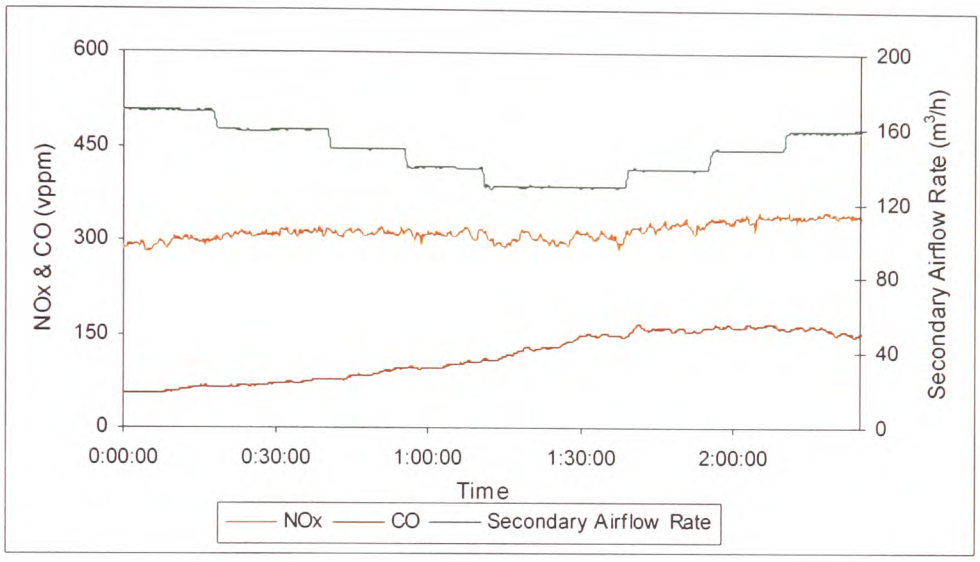

(b)

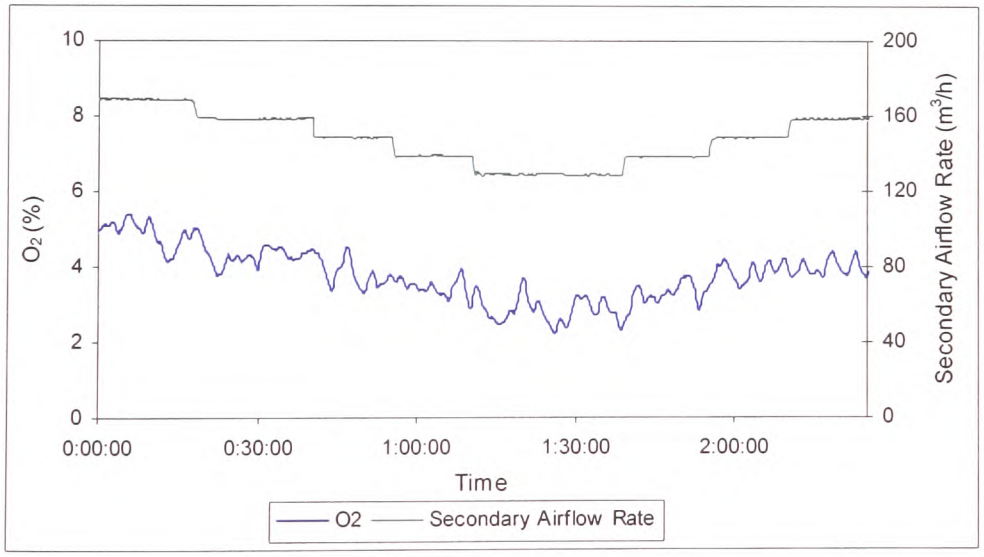

Figure 4.6 Measurements of (a) NOx, CO and Secondary Air Flow Rate, (b) O_2 and Secondary Airflow Rate, when firing Cerrejon Coal at a Swirl Number of 0.3 (Test 5)

(a)

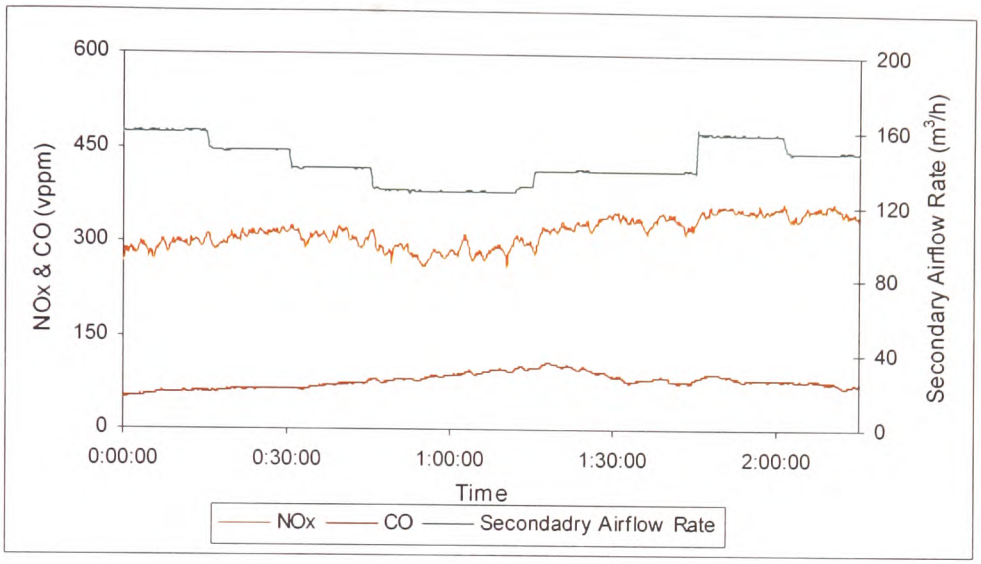

(b)

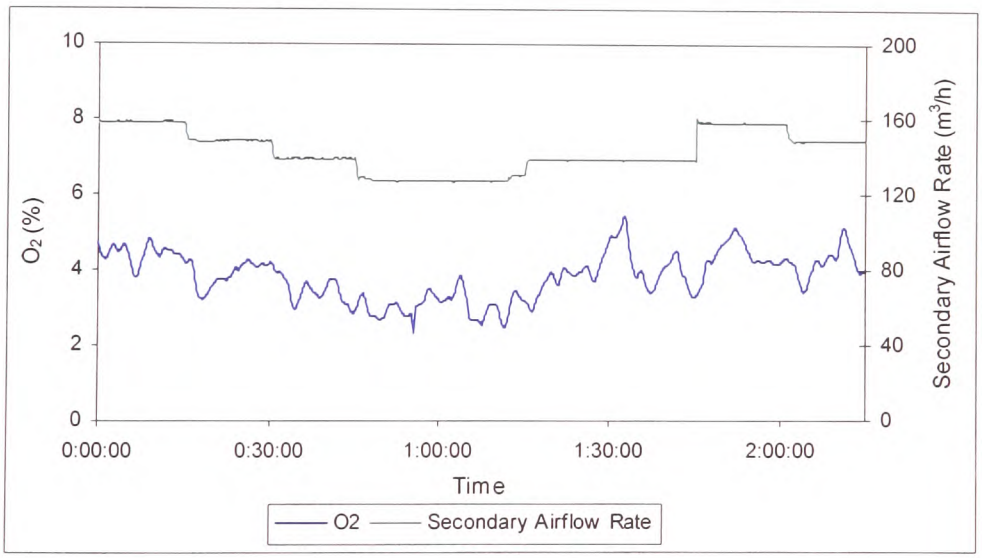

Figure 4.7 Measurements of (a) NOx, CO and Secondary Air Flow Rate, (b) O_2 and Secondary Airflow Rate, for Cerrejon Coal at a Swirl Number of 0.5 (Test 6)

Figure 4.8 presents the emissions of Test 7 where a swirl number of 0.8 was used. This was acknowledged to be the optimal setting for the Cerrejon coal. The burner achieved the lowest NOx (approximately 200 ppm for a secondary airflow rate of 130 m^3/h) with no excessive increase in CO throughout the test. Two red arrows are included in Figure

4.8 (b), at approximately 00:40 and 1:45 respectively of the test duration, to highlight either spurious reading made by the O_2 analyser.

(a)

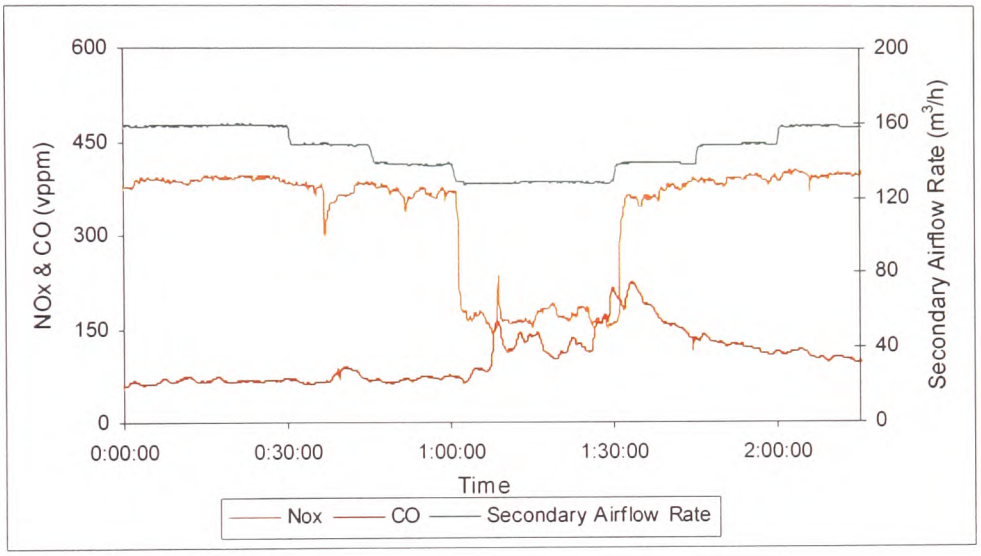

(b)

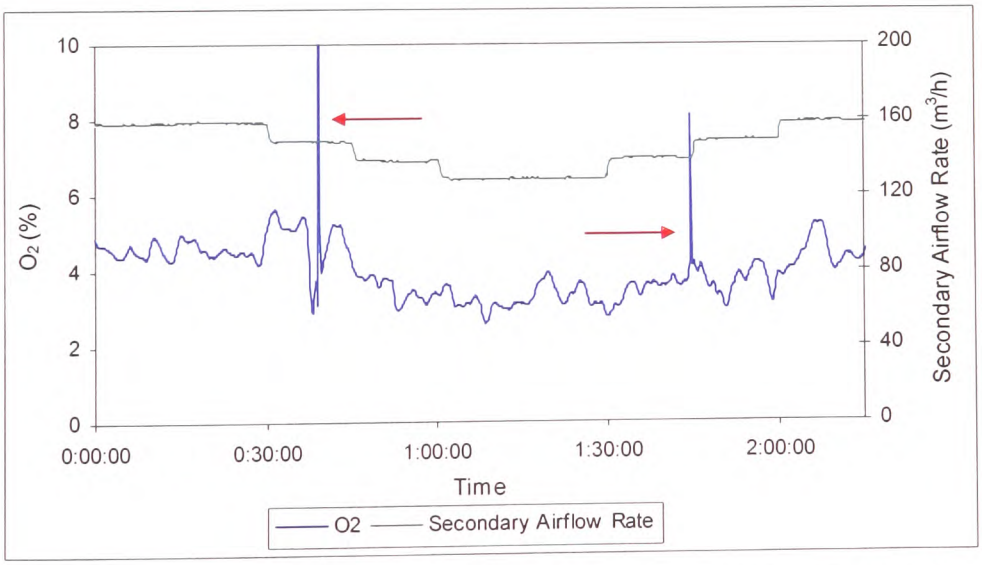

Figure 4.8 Measurements of (a) NOx, CO and Secondary Air Flow Rate, (b) O_2 and Secondary Airflow Rate, when firing Cerrejon Coal at a Swirl Number of 0.8 (Test 7)

A further increase in the swirl number to 1.2 resulted in the highest NOx values observed throughout Tests 5 to 8 with reasonable emissions of CO (Figure 4.9)

(a)

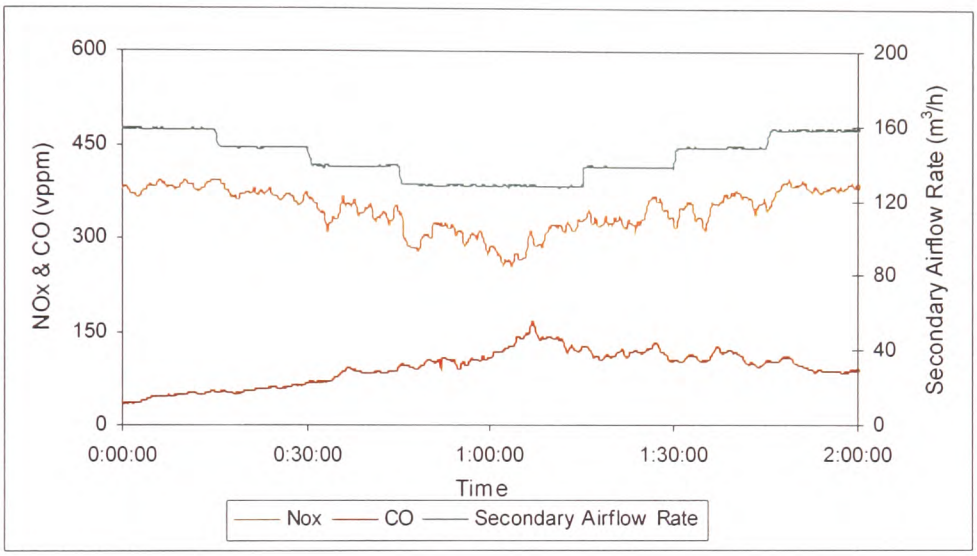

(b)

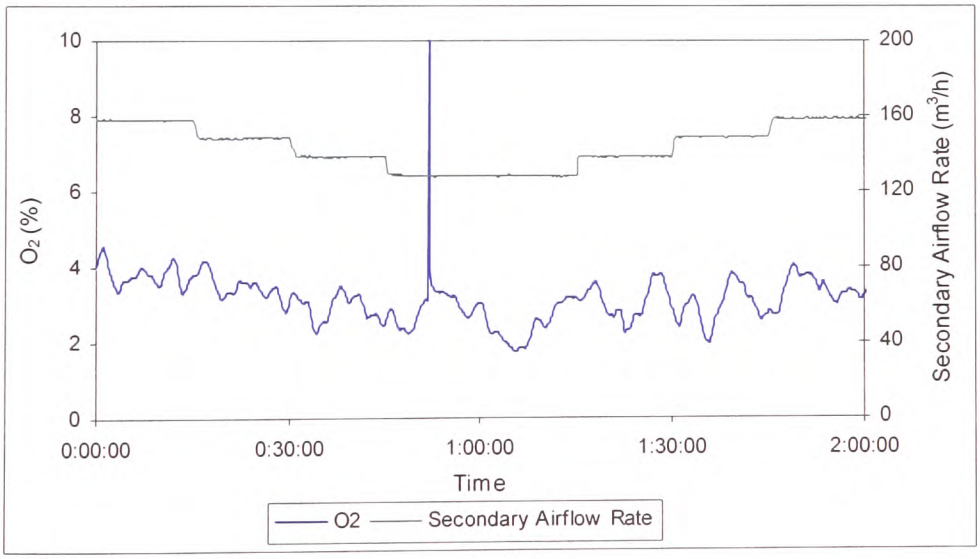

Figure 4.9 Measurements of (a) NOx, CO and Secondary Air Flow Rate, (b) O_2 and Secondary Airflow Rate, when firing Cerrejon Coal at Swirl Number 1.2 (Test 8)

The average concentrations of NOx, CO and O_2 for the Cerrejon tests at a secondary airflow rate of 130 m^3/h are presented in Figure 4.10. In general, the O_2 and hence excess air levels were higher than those for the Daw Mill tests and consequently the CO emissions were lower. Furthermore the NOx concentration tended to be lower with this coal despite its high nitrogen content. Again, the emissions are a function of both swirl number and excess air.

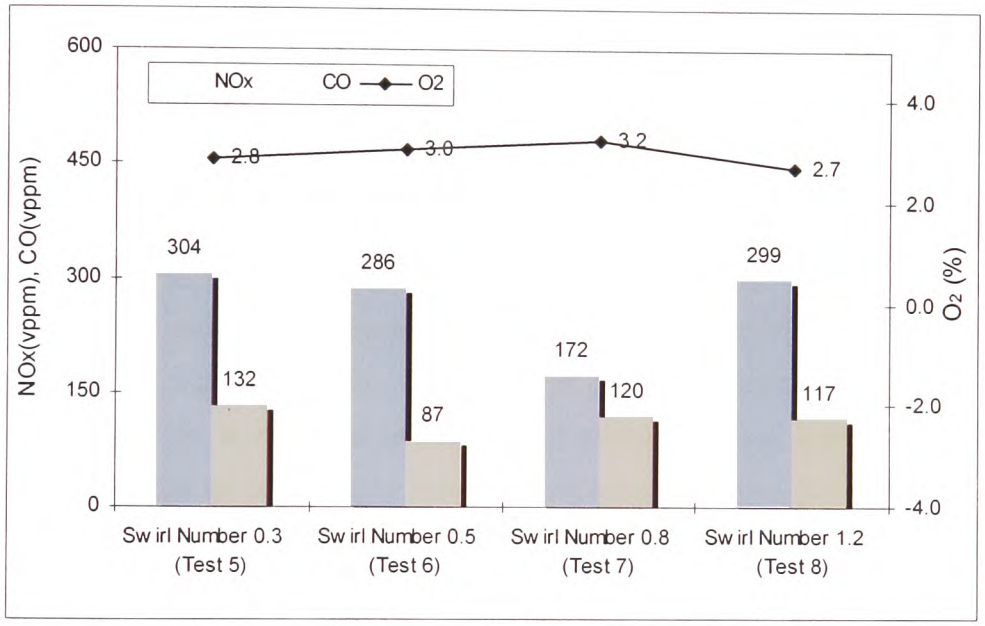

Figure 4.10 Average NOx, CO and O_2 corresponded to the Secondary Airflow Rate of 130 m^3/h for Swirl Numbers of 0.3, 0.5, 0.8, and 1.2

The purpose of these tests was to provide data so that the sensor signals can be compared with the flue gas concentrations. It can be observed that a suitable range of gaseous emissions were obtained for this purpose with significant "spread" so that the sensors can be tested over the range likely to occur in practice.

4.2 Signal Processing

Any physical variable representing a message in a communication system is termed a "signal". In this work, the physical properties which were monitored were the infrared intensity, combustion noise, and acoustic emissions (AE). Since these signals are a function of time and were sampled at high frequencies, large amounts of data were collected. One way to quantify these data is to represent them by a number of parameters known as "features" generated from both time and frequency domain signal analysis techniques [Lynn, 1989; Khesin *et al.*, 1997]. Consequently, this section reviews the signal processing techniques and discusses the use of these features for representing the concentrations of the combustion gases.

4.2.1 Complex Signals

A periodic signal is one which repeats itself exactly every T seconds, where T is called the period of the signal waveform. The treatment of periodic waveforms assumes that this exact repetition is extended throughout all time, both past and future. Simple periodic signals can be described by using mathematical notations, for example, a sine wave. However, the raw signals of the IR, Microphone and AE were considerably more complex (Figures 4.11 (a), (b) and (c)), with fluctuations possibly related to irregular air-fuel mixing and heat release in the flame [Abugov, 1978].

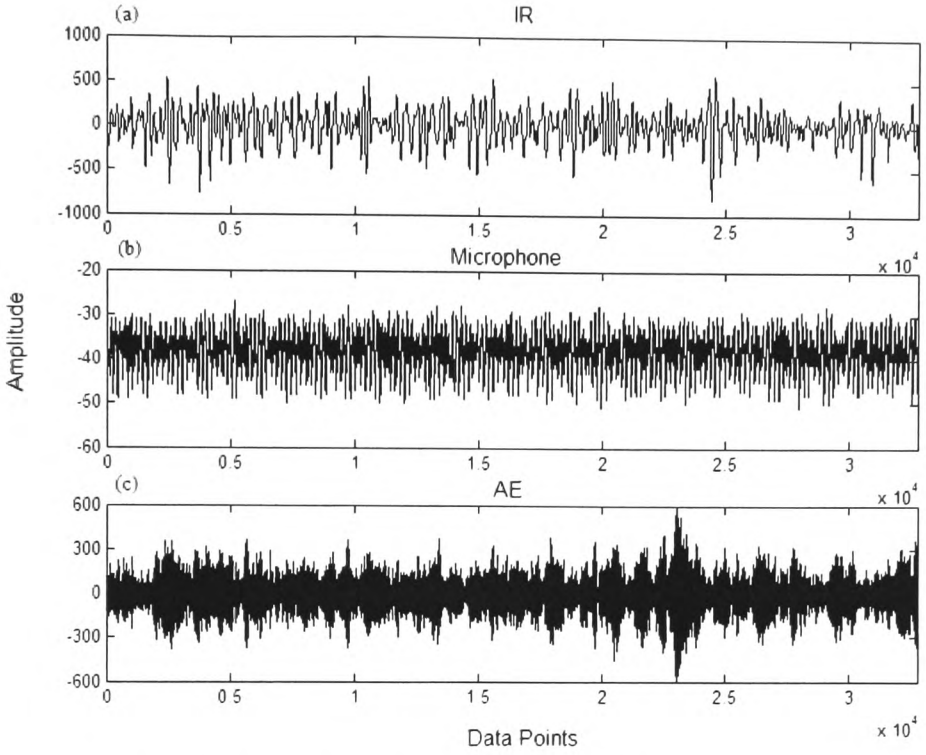

Figure 4.11 Raw (a) IR, (b) Microphone, and (c) AE, signals

4.2.2 Statistical Description of the Data

One way to describe complex signals is to calculate the statistical properties of the data. Some of the best known statistics are the Mean ($\overline{X}$), Median (X_{med}), variance (σ^2) and the standard deviation (σ). Higher moments can be used to help classify the actual shape of the distribution function. Higher moments require calculation of quantities like $\overline{X}^3$ and $\overline{X}^4$, resulting in a third central moment, and so on.

Skewness (*skew*), or third moment is a measure of the asymmetry of the distribution. A positive value for *skew* reflects a distribution that stretches out farther to the right (values greater than X) than to the left; the converse is true for a negative *skew*. It is defined as:

Skewness:

$$skew = \frac{1}{N}\sum_{i=1}^{N}\left[\frac{X_i - \overline{X}}{\sigma}\right]^3 \qquad [4.1]$$

The Kurtosis (*kurt*), or fourth moment is a measure of the "pointiness" of the distribution.

Kurtosis:

$$kurt = \frac{1}{N}\sum_{i=1}^{N}\left[\frac{X_i - \overline{X}}{\sigma}\right]^4 - 3 \qquad [4.2]$$

A large positive value of *kurt* suggests a very sharp, even cusplike, peak to the distribution. A large negative value represents a distribution with a broad, relatively flat, peak. A value of 3 is subtracted in the definition so that a Gaussian distribution[1] has a distribution of zero.

Although moments of higher order than the second are not often used, it is worth noting two things: firstly, if the probability distribution is symmetrical in form, the third and higher odd order central moments must be zero, and therefore such moments give an indication of asymmetry or "*skew*" in a distribution, and secondly, moments of higher order pay increasing attention to the extreme values of a signal (i.e., if a signal has outlier points, the validity of the using higher moments will seriously diminished).

In addition, it is also possible to describe the spread of the data by means of Root-Mean-Square (*rms*) of the signal. Physical scientists often use the term *rms* as a synonym for standard deviation when they refer to the square root of the mean squared deviation of a signal from a given baseline or fit. In addition, the *rms* is a measure of the "energy" of a signal. The *rms* is defined as: -

[1] As far as signal theory is concerned, any random signal, which is caused by a number of contributing processes is likely to have a Gaussian (normal) amplitude distribution.

Root-Mean-Square: $$rms = \sqrt{\frac{\sum_{i=1}^{N} [X_i - X]^2}{N}} \qquad [4.4]$$

The number of times the signal amplitude changes its sign, i.e., the number of zero crossings (zrcs) can be counted as a further statistic. Unlike the description of the amplitude distribution, this feature characterises the time structure of the signal, and is a measure of the frequency content of the signal. The *zrcs* is defined as: -

Number of zero crossings: $$zcrs = \sum_{i=1}^{N} 1 \text{ if sign } (X_{i+1} * X_i) \subset \text{negative} \qquad [4.5]$$

Most of the statistical descriptions of data discussed under this section need not take account of any time information (i.e., assuming that the data were equally spaced, and the sequence of the data). However, the number of zero crossing (*zrcs*) that requires time information must be performed without changing the order of the sequence.

4.2.3 Frequency Domain Analysis

Signals can also be quantified by frequency domain analysis. Spectral analysis seeks to describe the variation in properties of a signal at different frequencies. The basic concept of spectral analysis is that a waveform of any complexity may be considered as the sum of a number of sinusoidal waveforms of suitable amplitude, periodicity, and relative phase [Dwight, 1995; Lynn, 1998]. Therefore the Power Spectral Density (PSD) is concerned with the distribution of the signal power over an appropriate frequency range. It can be estimated by either parametric[2] or non-parametric techniques. Welch's method is a non-parametric Fast Fourier Transform (FFT) technique for estimating the PSD. The advantages of employing FFT are [Borse, 1997]: -

[2] Parametric modeling techniques find the parameters for a mathematical model describing a signal, a system, or process by finding the coefficients of a linear system that models the system.

1. It has the ability to filter data (i.e., to remove large portions of the noise or other undesirable data segments).

2. It is a fast accurate method to estimate the power spectrum of a signal.

Figure 4.12 shows examples of the calculated PSD for the IR, microphone and AE signals, for specific ranges of frequency.

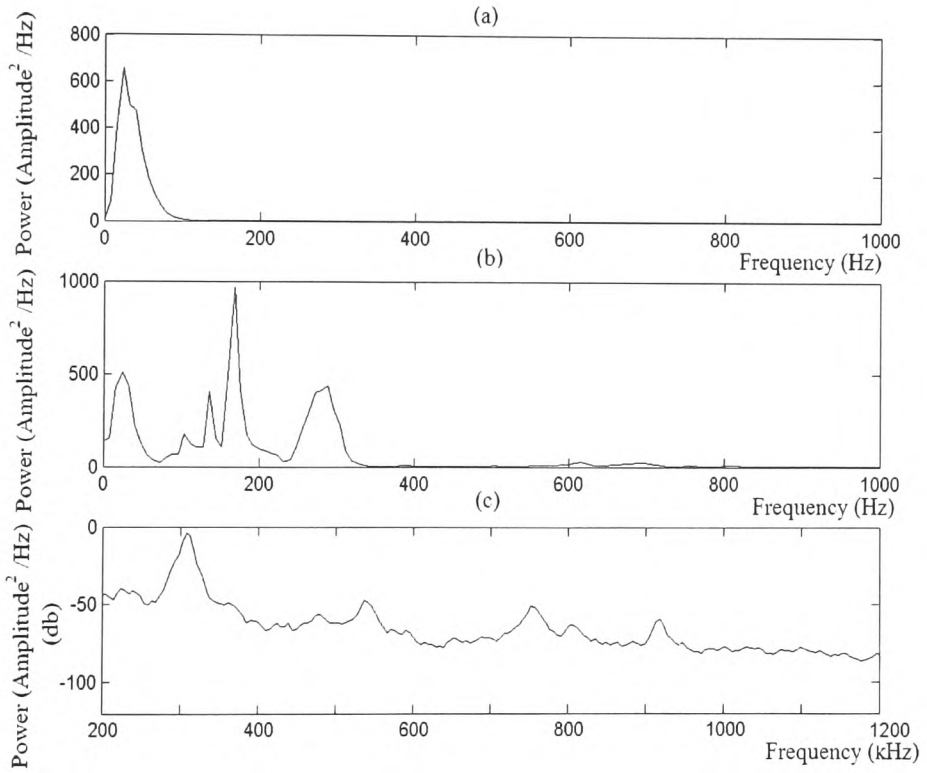

Figure 4.12 The Power Spectral Density of the Sensor Signals: (a) 0-1000 Hz of IR signal, (b) 0-1000 Hz of Microphone signal, and (c) 200-1200 kHz of AE signal

Both Willson (1985) and Timothy (1996) suggested that the information carried by the IR and Microphone signals is contained within frequencies less than 1000 Hz. These findings are supported by the data presented in Figures 4.12 (a) and (b). For AE signals, most of the information was presented in the range of 100-1200 kHz.

The PSD represents the Power, U versus the Frequency, f. It can also be defined in terms of the proportion (or probability) of total power occurring at a particular frequency. The treatment of the PSD in a probability context is analogous to the amplitude probability distribution in the time domain [Chung *et al.*, 2000]. The proportion or probability, P_i at a particular frequency can be defined as: -

$$P_i = \frac{U_i}{\sum_{i=1}^{N} U_i} \qquad [4.6]$$

where, $\sum_{i}^{N} P_i = 1$ satisfies the condition that any probability density function must have a unit area [Lynn, 1989]. This procedure normalises the data to the total power of the signal in order to ignore spurious trends such as the attenuation of the light signal by contamination by dust [Timothy, 1996]. It is also possible to calculate the proportion of the PSD in a particular frequency band. The probability or proportion of the PSD for the IR and Microphone signals was determined for frequency bands of (a) 0-200 Hz, (b) 200-400 Hz, (c) 400-600 Hz, (d) 600-800 Hz and (e) 800-1000 Hz. In addition, the PSD of the AE was divided into (a) 100-200 kHz, (b) 200-300 kHz .....up to 1100-1200 kHz, see Table 4.1.

The Entropy (S) of the signal is commonly used to indicate the relative similarity of the PSD for two signals [Dwight, 1995; Tzanakou, 1999]. In other words, it is a measure of the distribution pattern of the PSD, and is given by: -

Entropy: $$S = -\sum_{i=1}^{N} P_i \log P_i \qquad [4.7]$$

where P_i is the probability of the signal power as defined in Equation 4.6.

One way to compute the average frequency is to find the Centriod (*cga*), which is based on the first moment of the signal power. It is defined as the magnitude of the sum of the product of the power and the frequency over the whole spectrum PSD.

Centroid:
$$cga = \frac{\sum_{i=1}^{N} U_i \times f_i}{\sum_{i=1}^{N} U_i} \qquad [4.12]$$

The last feature which was used is known as the Shape Factor and can be defined as the standard deviation of the power normalised in terms of the mean power [Tang *et al.*, 1999], is given by: -

Shape Factor:
$$SF = \frac{\left[\frac{1}{N-1}\sum_{i=1}^{N}(U_i - \overline{U})^{\frac{1}{2}}\right]}{\overline{U}} \qquad [4.13]$$

Where, $\overline{U}$ = mean of the power

A summary of the signal processing algorithms which were used in this project is presented in Table 4.1.

Table 4.1 Signal Processing Algorithms

Sensors	Selected Features
IR detector	$\overline{X}, X_{med}, \sigma, \sigma^2, zrcs, rms, skew, kurt, S, SF, cga,$ $P_{[0-200Hz]}, P_{[200-400Hz]}, P_{[400-600Hz]}, P_{[600-800Hz]}, P_{[800-1000Hz]}, P_{[0-1000Hz]}$
Microphone	$\overline{X}, X_{med}, \sigma, \sigma^2, zrcs, rms, skew, kurt, S, SF, cga,$ $P_{[0-200Hz]}, P_{[200-400Hz]}, P_{[400-600Hz]}, P_{[600-800Hz]}, P_{[800-1000Hz]}, P_{[0-1000Hz]}$
AE sensor	$\overline{X}, X_{med}, \sigma, \sigma^2, zrcs, rms, skew, kurt, S, SF, cga,$ $P_{[100-200kHz]}, P_{[200-300kHZ]}, P_{[300-400kHz]}, P_{[400-500kHz]}, P_{[500-600kHz]}, P_{[600-700kHz]}$ $P_{[700-800kHz]}, P_{[800-900kHz]}, P_{[900-1000kHz]}, P_{[1000-1100kHz]}, P_{[1100-1200kHz]}, P_{[100-1200kHz]}$

4.3 The Effect of Ensemble Averaging

Due to the complex nature of combustion the underlying information of the acquired sensor signals were averaged so that more representative values could be found. The motivation behind ensemble averaging of the data was two fold:

1. The ensemble average helps to reduce signal noise.

2. The ensemble average helps to replace large data sets with a few representative points.

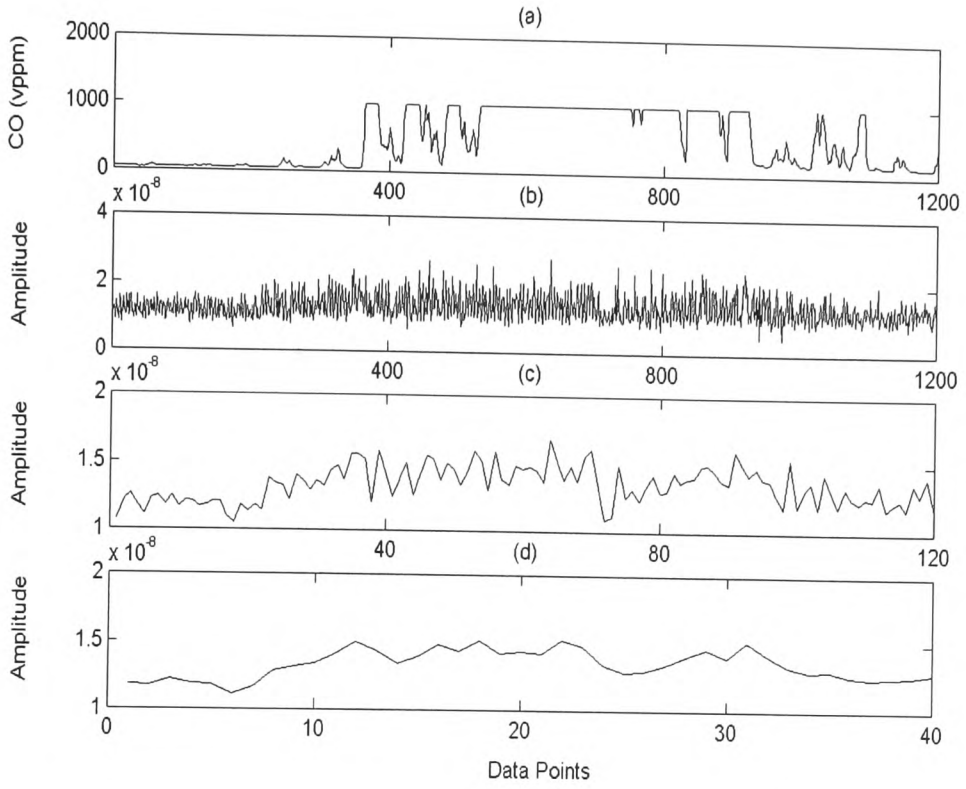

Figure 4.13 shows the signals of (a) gaseous CO, (b) AE feature, (c) 10 point ensemble average of the AE feature, and (d) after 30 point ensemble average of the AE feature

Figures 4.13 (a) and (b) show the CO concentrations and a typical AE feature. Figures 4.13 (c) and (d) demonstrate 10 and 30 point averaged results and it can be observed that as the number of averaging points increases, the signal becomes a slightly better representation of the CO concentrations.

4.4 Comparing the Signal Features with Flue Gas Emissions

During the data collection phase, the flame monitoring system was operated together with the gas analyser which measured the concentrations of the flue gases. The raw sensor signals were then processed to yield the features of Table 4.1, which were then compared with the gaseous emissions. The idea of the procedure was to evaluate the

relationship between the features and the gaseous concentrations. *Since a considerably large number of features were generated, only a selection of features from each sensor are compared with the swirl number, excess air level and gaseous emissions for each coal in this thesis.*

4.4.1 Comparison of Typical IR Features with the Flue Gas Concentrations and Secondary Airflow Rate

Figure 4.14 below compares the NOx concentrations with the *RMS* and *Kurtosis* of the IR sensor signals. It was found that the trends of the sensor features were in reasonable agreement with the trends in NOx emissions. However, there are "differences" in individual cases, see Figures 4.14 (c), (d) and (j), where large discrepancies are highlighted by the red arrows.

In Figure 4.15, NOx emissions are compared with the *Average Energy* in the bands of 400-600 and 600-800 Hz. Again the trends in the features are comparable with the trends in NOx. It was found that the sensor features were unable to cope with the large step change in NOx that are highlighted by the two red circles (Figures 4.15 (a) and (b)). Other poorly correlated examples can be seen in Figures 4.15 (f) and (j), and also Figure 4.14 (p) shows the feature progressively diverging from the NOx as the test proceeded.

It should be noted that some features are actually plotted on an inverse and/or a logarithmic scale as those features exhibited an inverse as well as a nonlinear relationship with the NOx readings. Overall, many of the other features analysed were found to be reasonably well related to the NOx in addition to these shown in both Figures 4.14 and 4.15. Nevertheless as can be seen from these figures, there is considerable scatter in the relationships for individual data points so that any single feature cannot be used to predict the flue gas concentration.

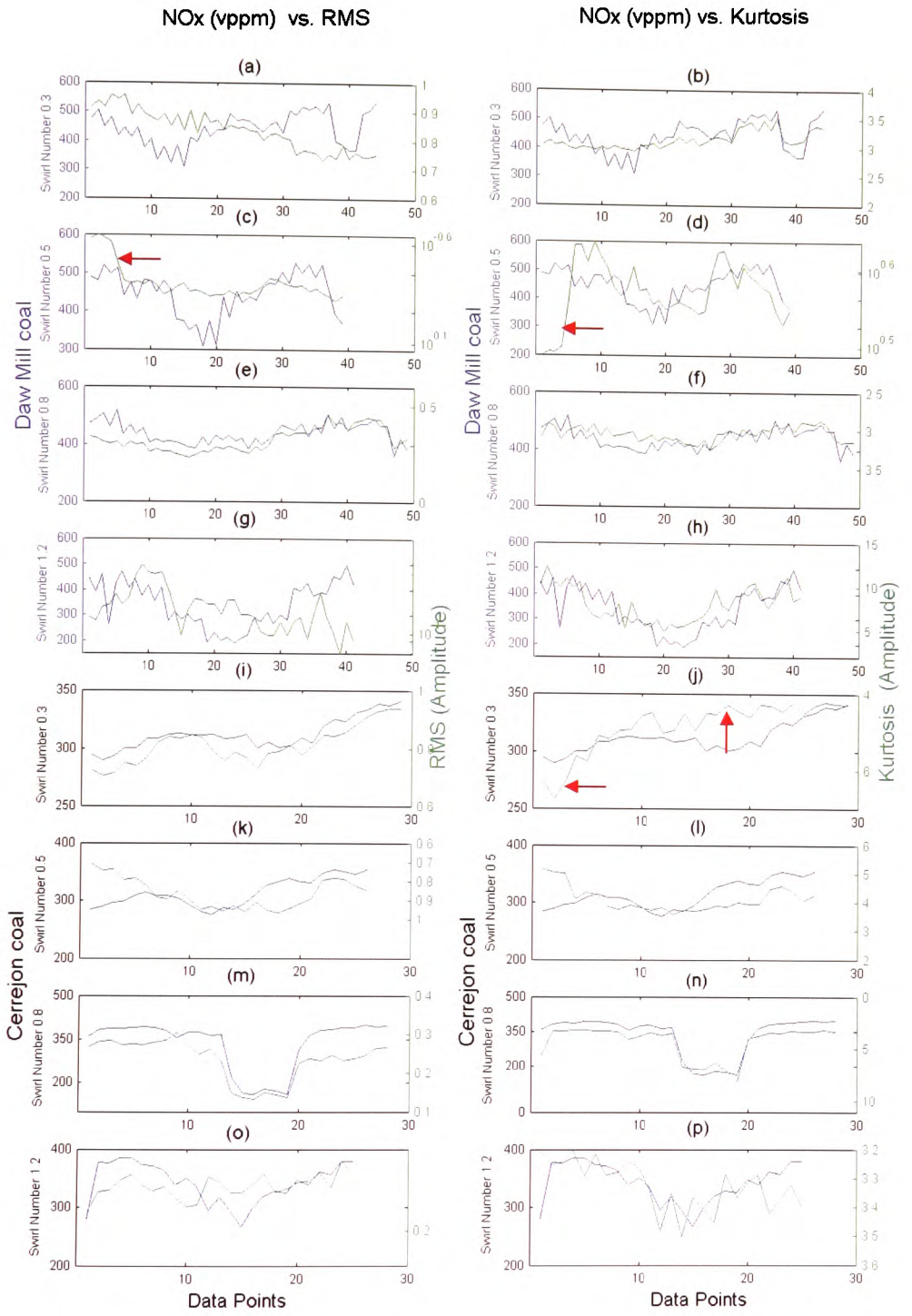

Figure 4.14 NOx and the *RMS* and *Kurtosis* for the IR sensor

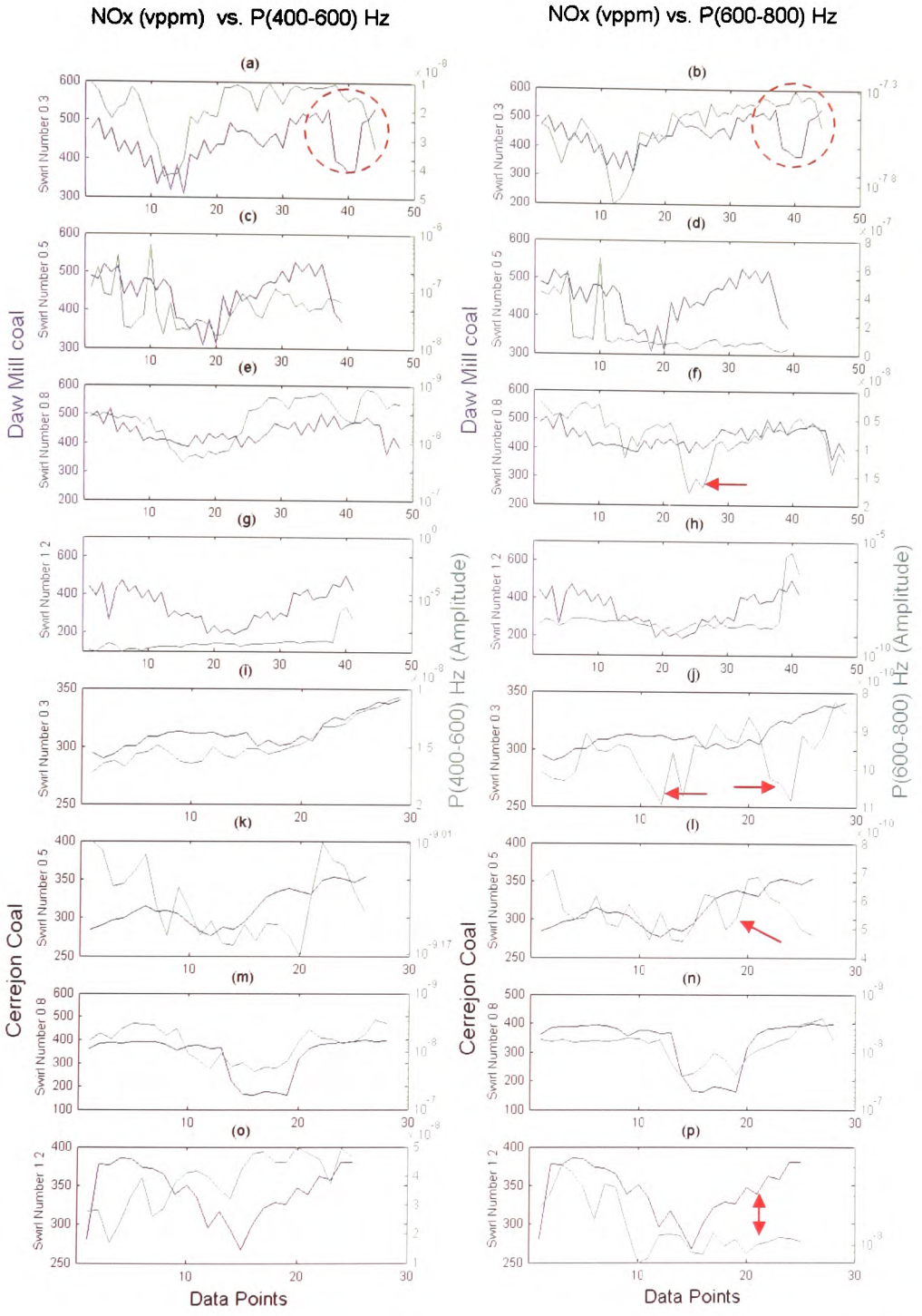

Figure 4.15 NOx and the *Average Energy* in the bands of 400-600 and 600-800 Hz for the IR sensor

The trends in the *RMS* and *Kurtosis* of the IR signals and the secondary airflow rate are similar, see Figure 4.16 below. Again, there is considerable scatter with the trends predicted better in particular tests, see Figure 4.16 (k) for example, which presents the data at a swirl number of 0.5 when burning the Columbian coal.

Similar relationships with a relatively high degree of scatter are observed using the *Average Energy* in the 400-600 and 600-800 Hz frequency range, see Figure 4.17. Once more these figures indicate that a combination of features may be required to predict the secondary airflow rate at particular burner conditions.

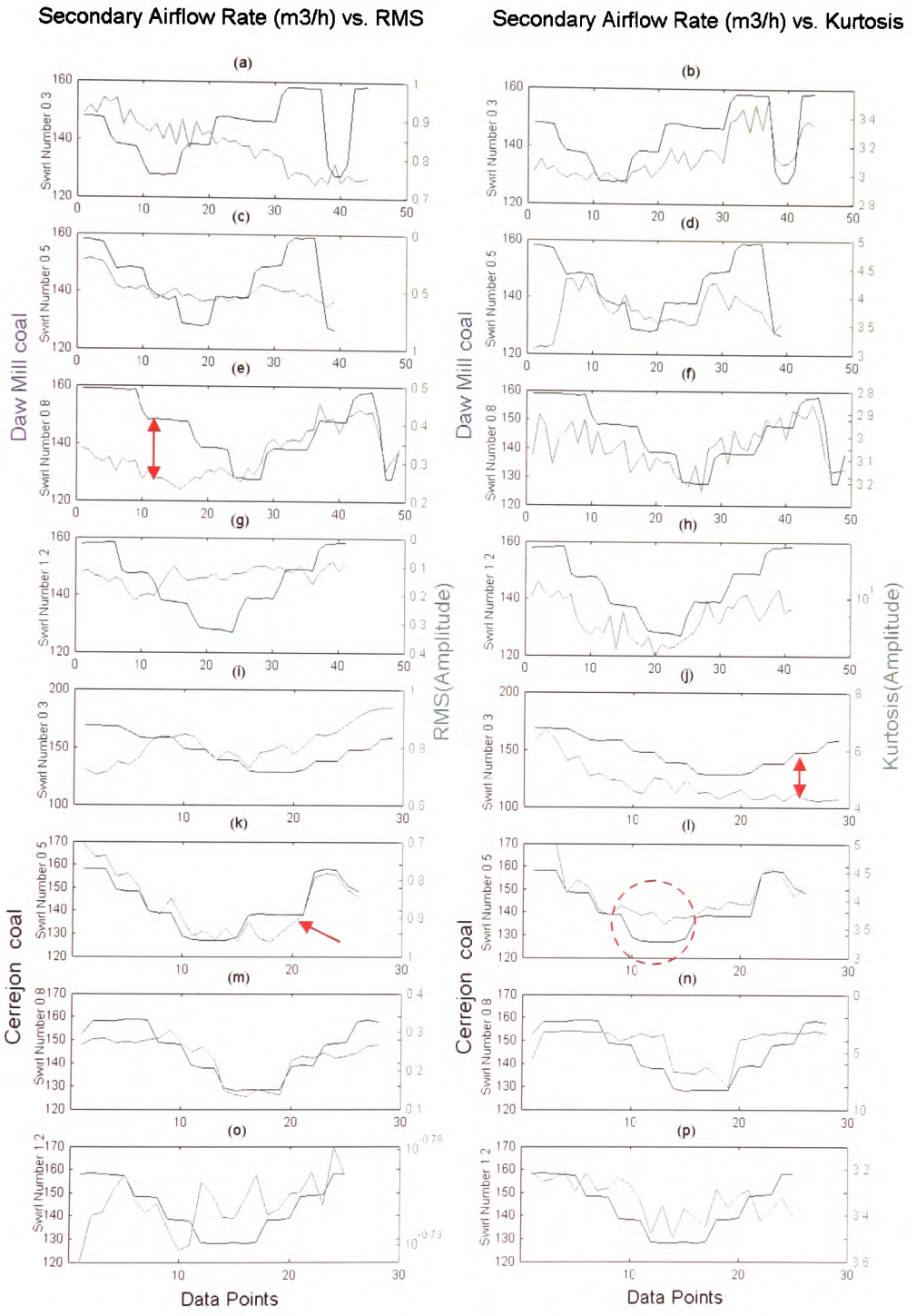

Figure 4.16 Secondary Airflow Rate and the *RMS* and *Kurtosis* for the IR sensor

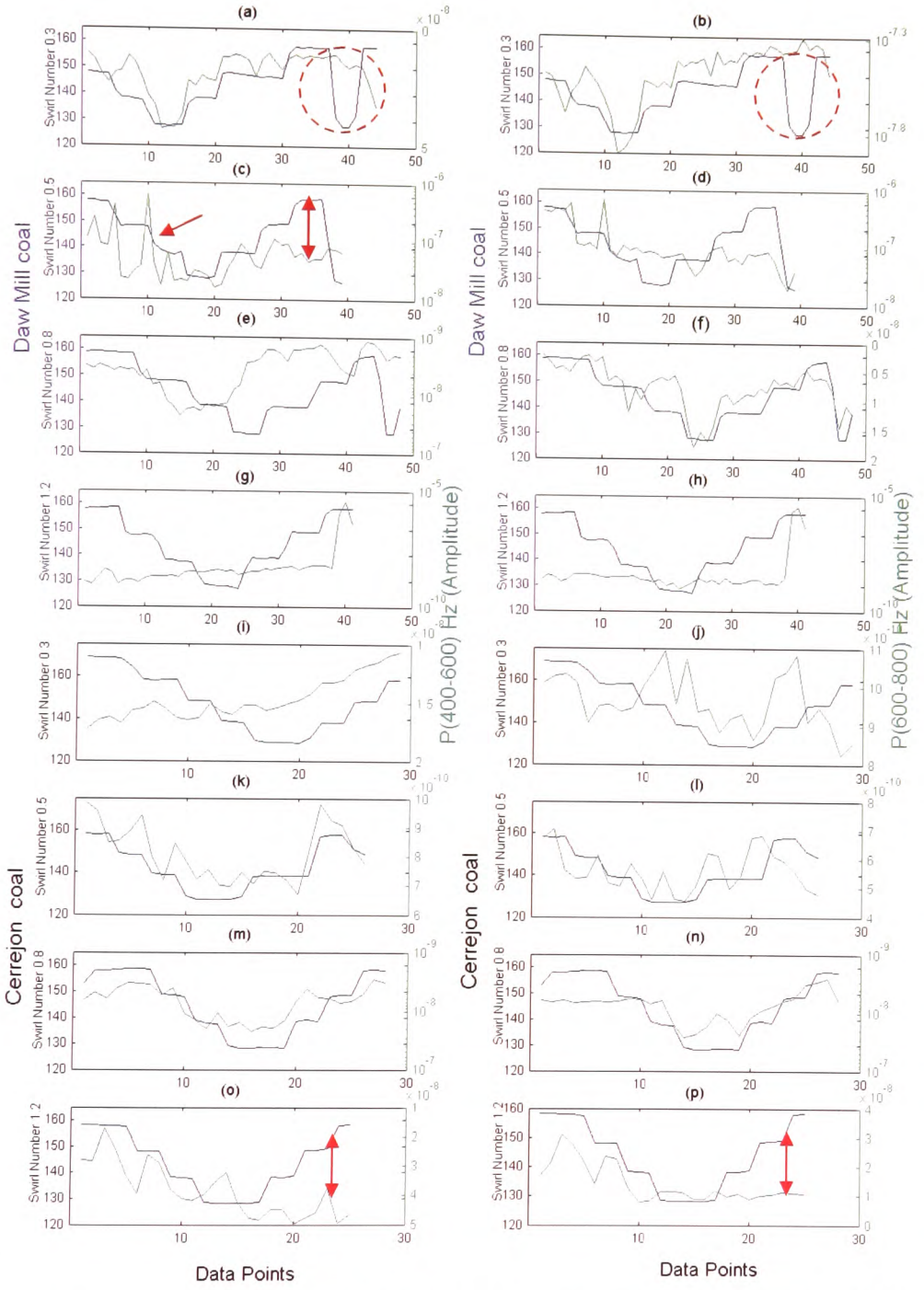

Figure 4.17 Secondary Airflow Rate and the *Average Energy* in the bands of 400-600 and 600-800 Hz for the IR sensor

The trends in the *RMS* and *Kurtosis* features of the IR are compared with the variations in CO concentration in Figure 4.18. CO has a very nonlinear relationship with excess air, and was found to be one of the most difficult gases to accurately monitor and therefore larger differences were anticipated. In order to overcome this, a longer averaging period would be required so that the process feature would that resemble the red curve in Figure 4.18 (p) which then provides a reasonable representation of the CO emissions.

The *Average Energy* in the bands of 400-600 and 600-800 Hz of IR sensor are compared to the CO with the mostly related being Figures 4.19. As usual, significant differences are highlighted, as shown in Figures 4.19 (e) and (j).

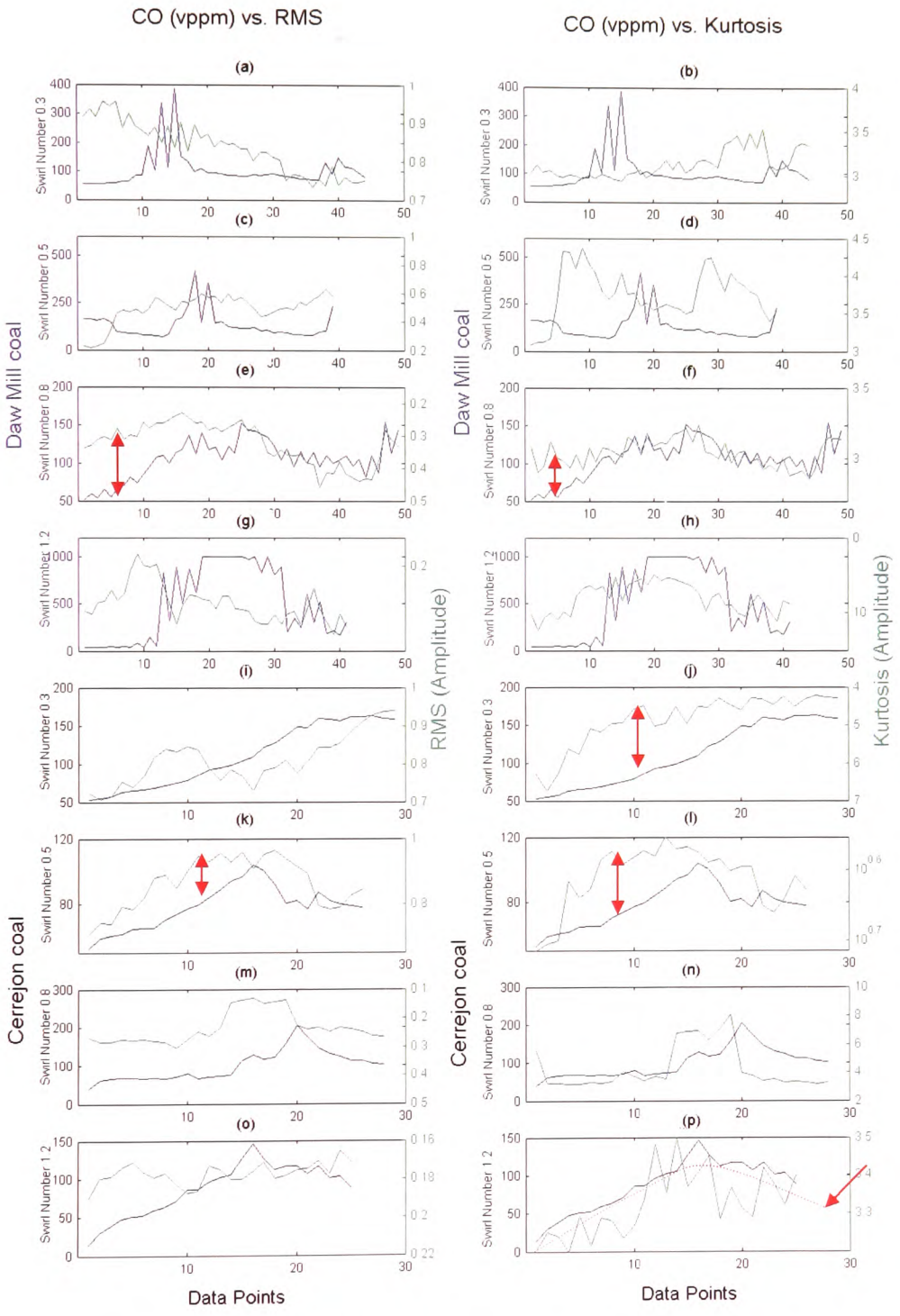

Figure 4.18 CO and the *RMS* and *Kurtosis* for the IR sensor

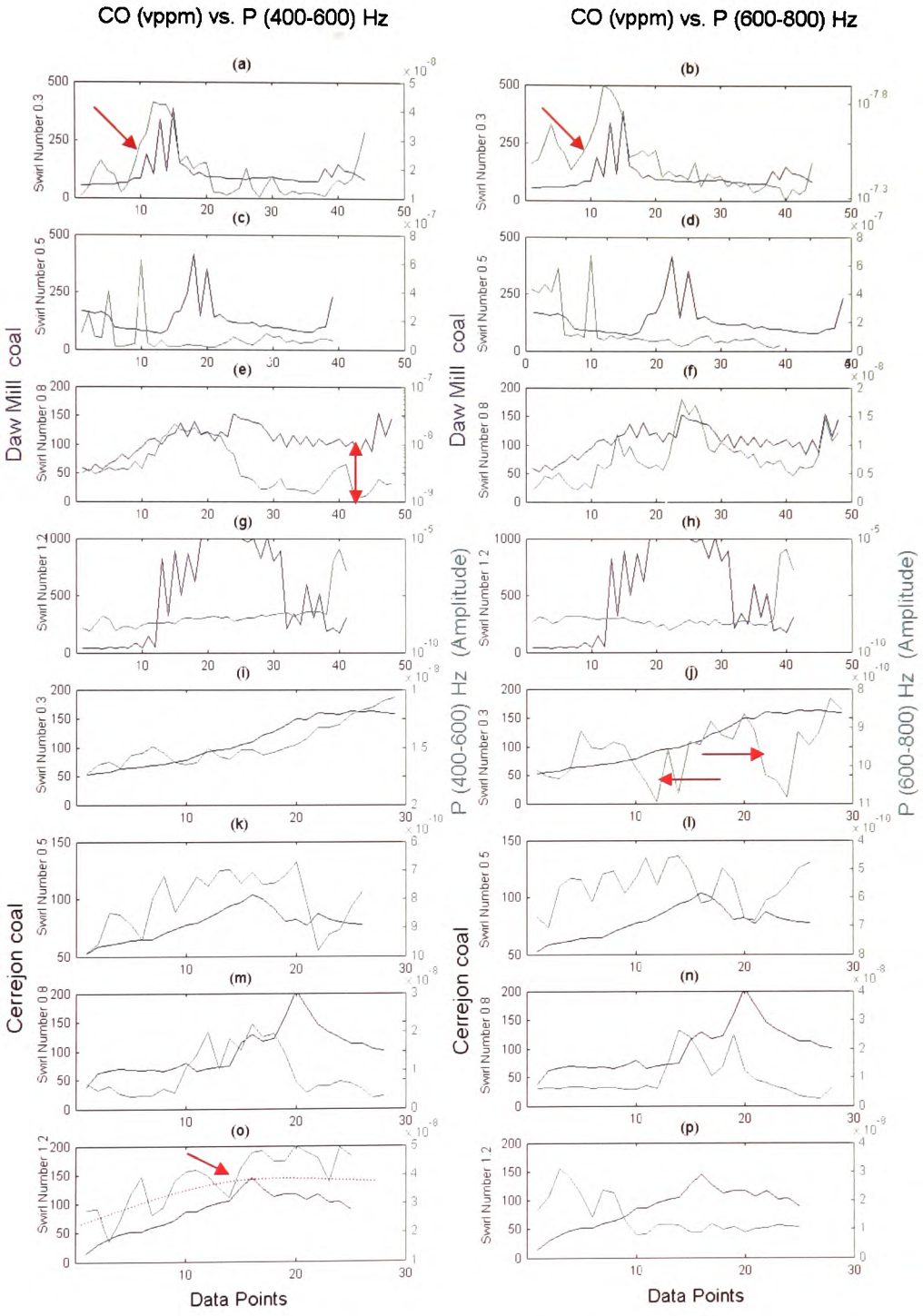

Figure 4.19 CO and the *Average Energy* in the bands of 400-600 and 600-800 for the IR sensor

The *RMS* and *Kurtosis* features for the IR sensor are compared to the O_2 concentrations with the best representations of the trends being found in Figures 4.20 (b), (c), (d), (e), (f), (g), (h), (j), (k) and (l). However, there were also cases where the agreement was less obvious and regions with substantial differences are highlighted.

The *Average Energy*, in the bands of 400-600 and 600-800 Hz for the IR sensor, are compared with the flue gas O_2 in Figures 4.21. As in previous cases, Figures 4.21 (a) and (b) indicate that these features do not detect a step change as shown by the red circles. Figures 4.21 (c), (d) and (f) are good examples of instances when the features are closely correlated to the O_2. Once more, a longer averaging time would be required to reduce the difference as indicated as a red curve (Figures 4.21 (l)).

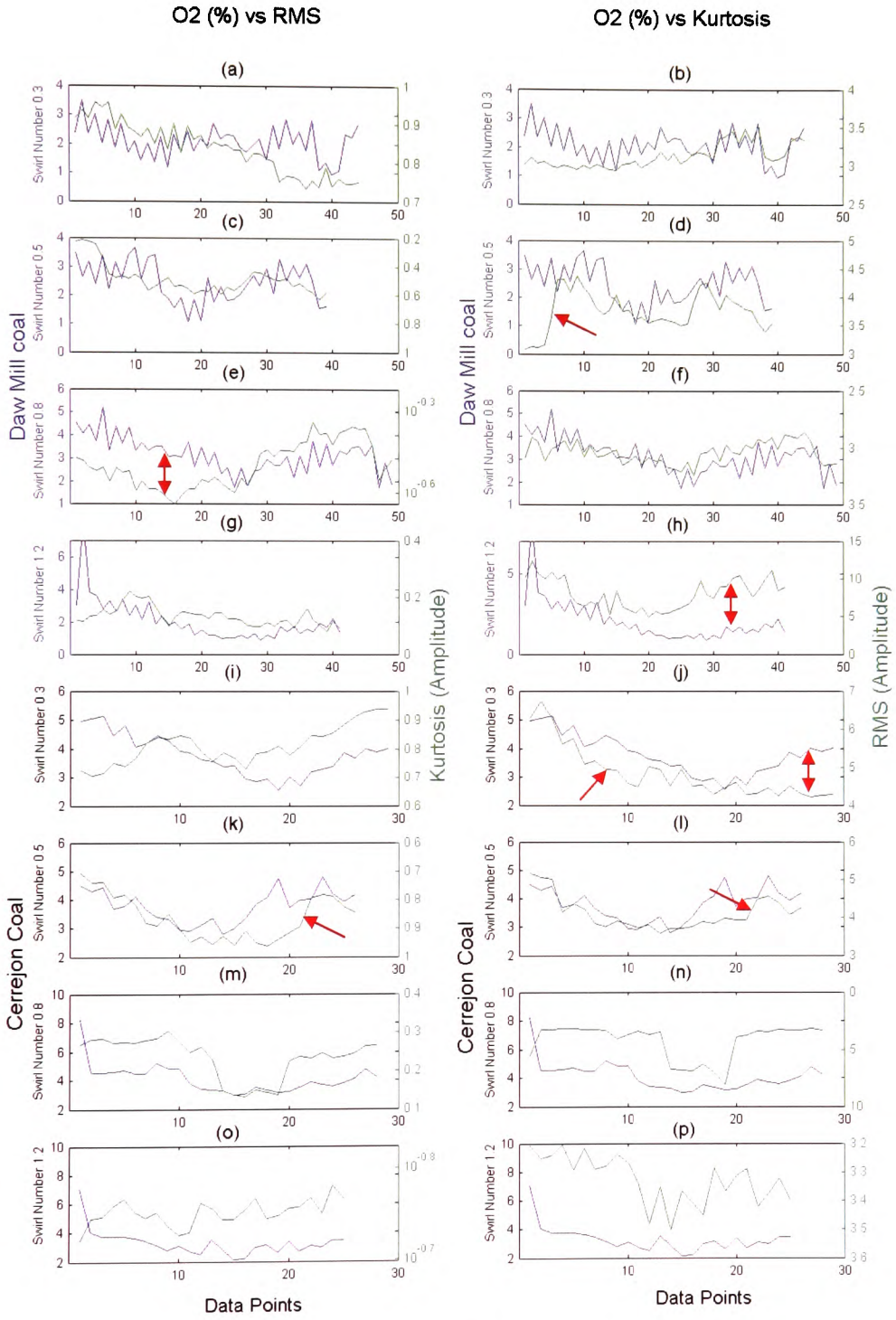

Figure 4.20 O_2 and the *RMS* and *Kurtosis* for the IR sensor

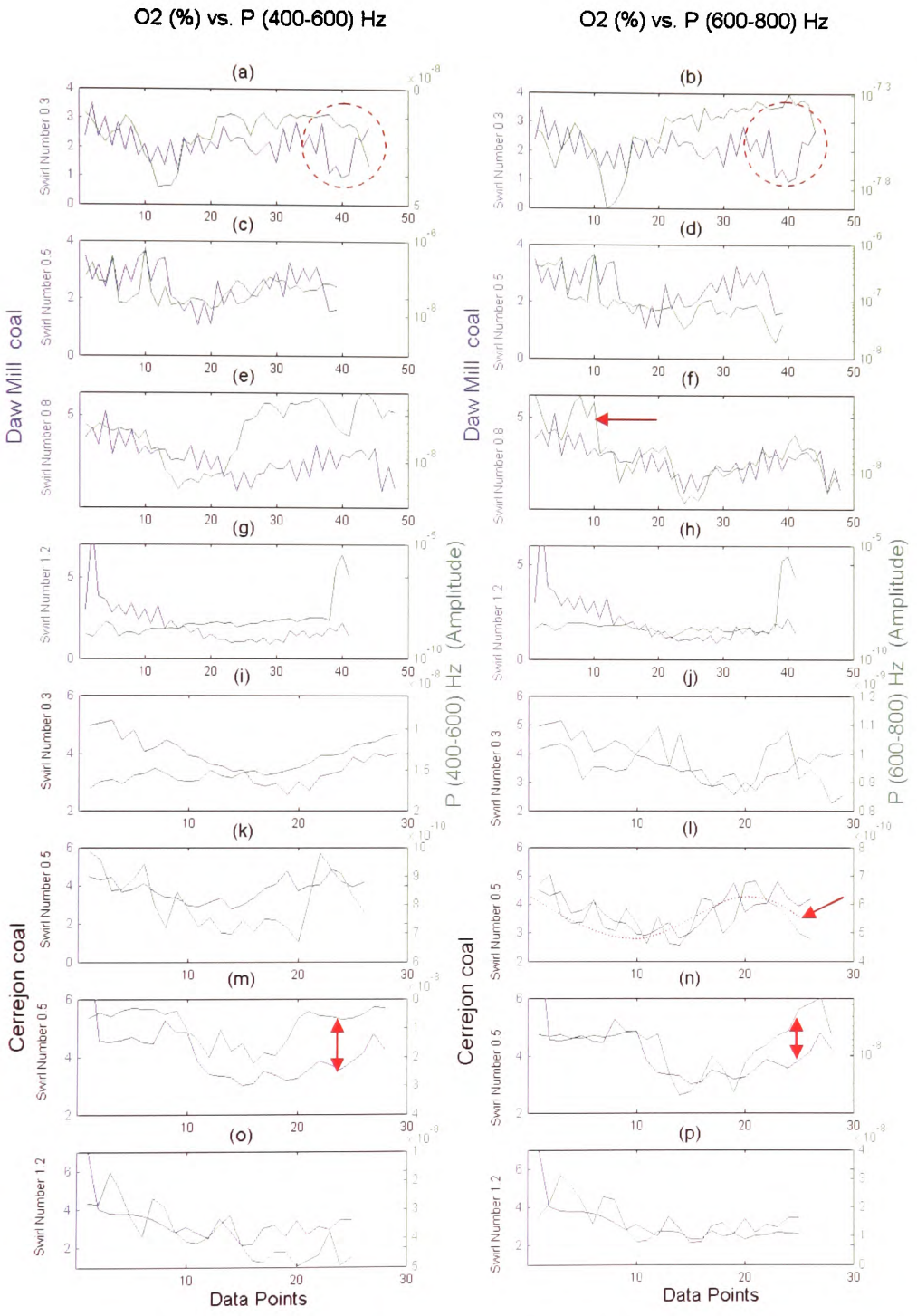

Figure 4.21 O_2 and the *Average Energy* in the bands of 400-600 and 600-800 Hz for the IR sensor

4.4.2 Comparison of Typical Microphone Features with the Flue Gas Concentrations and Secondary Airflow Rate

This section is concerned with the microphone features. Again *RMS*, *Kurtosis,* and the *Average Energy* in the bands of 400-600 and 600-800 Hz were compared with the NOx, secondary airflow rate, CO and O_2 respectively.

Figures 4.22 (a), (c), (e), (f), (g), (m), (n), and (o) below illustrated cases in which the *RMS* and *Kurtosis* of the microphone signals were reasonably related to the NOx. Major differences are highlighted using red arrows and circles as shown in Figures 4.22 (a), (g), and (n). In addition, the trends in the *Average Energy* in the bands of 400-600 and 600-800 Hz which also correlated with the NOx are presented in Figures 4.23 (a), (b), (i), (m) and (n). The microphone features appear to be able to follow step changes in combustion conditions as illustrated in Figure 4.22 (a), and Figures 4.23 (a) and (b). This complemented one of the major limitations of using the IR sensor especially when trying to estimate the combustion gases.

Overall, reasonable correlations existed for every swirl number and coal type, except for the Cerrejon test data at a swirl number of 0.5. It is also worth nothing that some of the other features (not presented in this part of the thesis) can also make reasonable predictions of the NOx emissions although all features exhibit scatter in the individual measurement points.

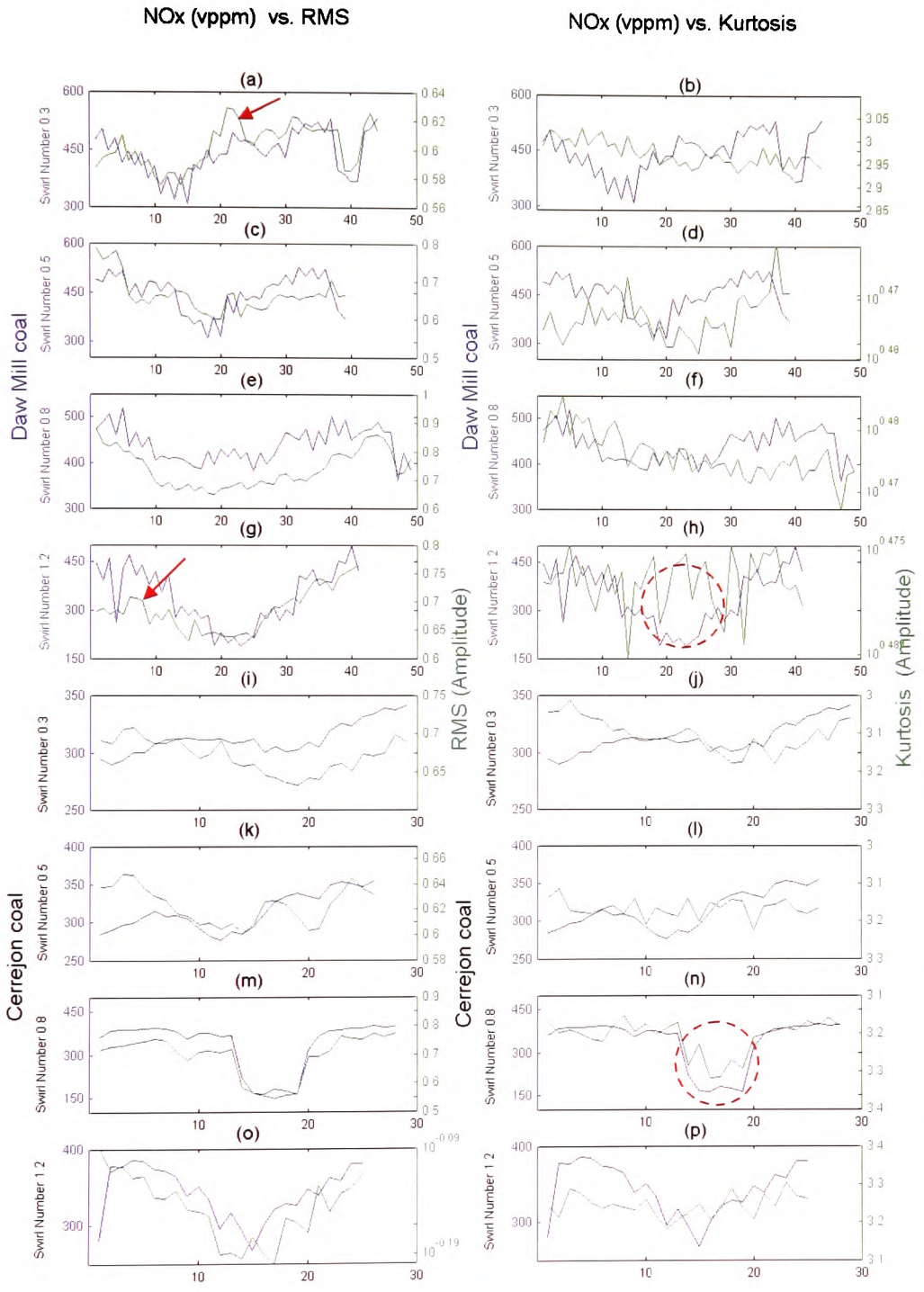

Figure 4.22 NOx and *RMS* and *Kurtosis* for the Microphone

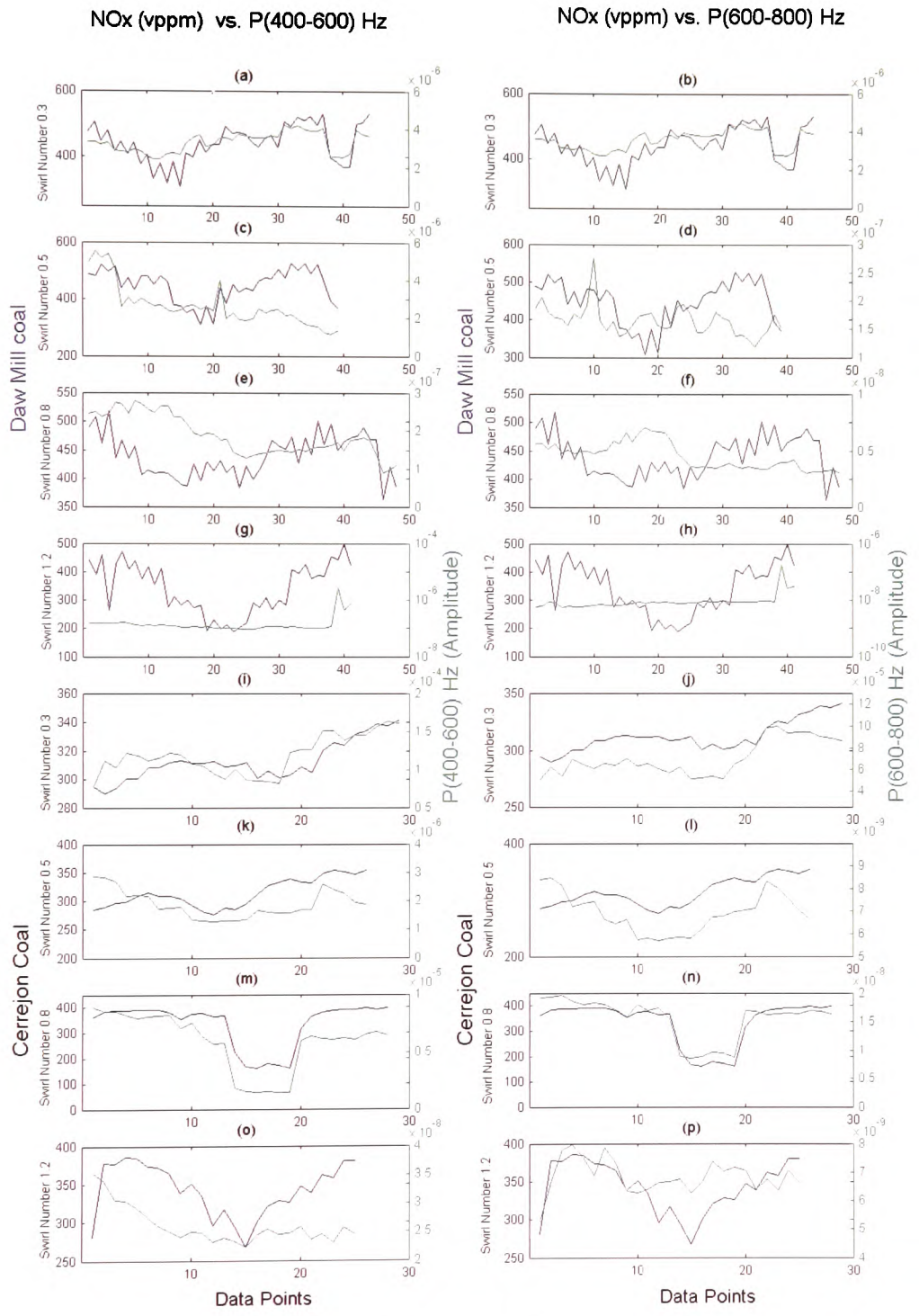

Figure 4.23 NOx and the *Average Energy* in the bands of 400-600 and 600-800 Hz for the Microphone

The similarity of the variation in the secondary airflow rate to the NOx has led a similar set of results. It was established that good correlations existed in Figures 4.24 (a), (e), (g), (i), (k), (l), (m) (n) and (o) in which the *RMS* and *Kurtosis* of the microphone are compared to the secondary airflow rate. Deviations are highlighted by red arrows as shown in Figures 4.24 (a), (e), (g), (k), and (n). Also, the *RMS* and *Average Energy* of the microphone have gracefully followed the large step change (Figures 4.24 (a), and Figures 4.25 (a) and (b)). Figures 4.25 (k), (l), (m), (n), and (o) were among the best features.

Overall, the microphone features have effectively followed the secondary air profile for every swirl number and coal type, except for the Daw Mill data with a swirl number of 0.5. Nevertheless, good correlations were achieved through the computation of other features (Table 4.1).

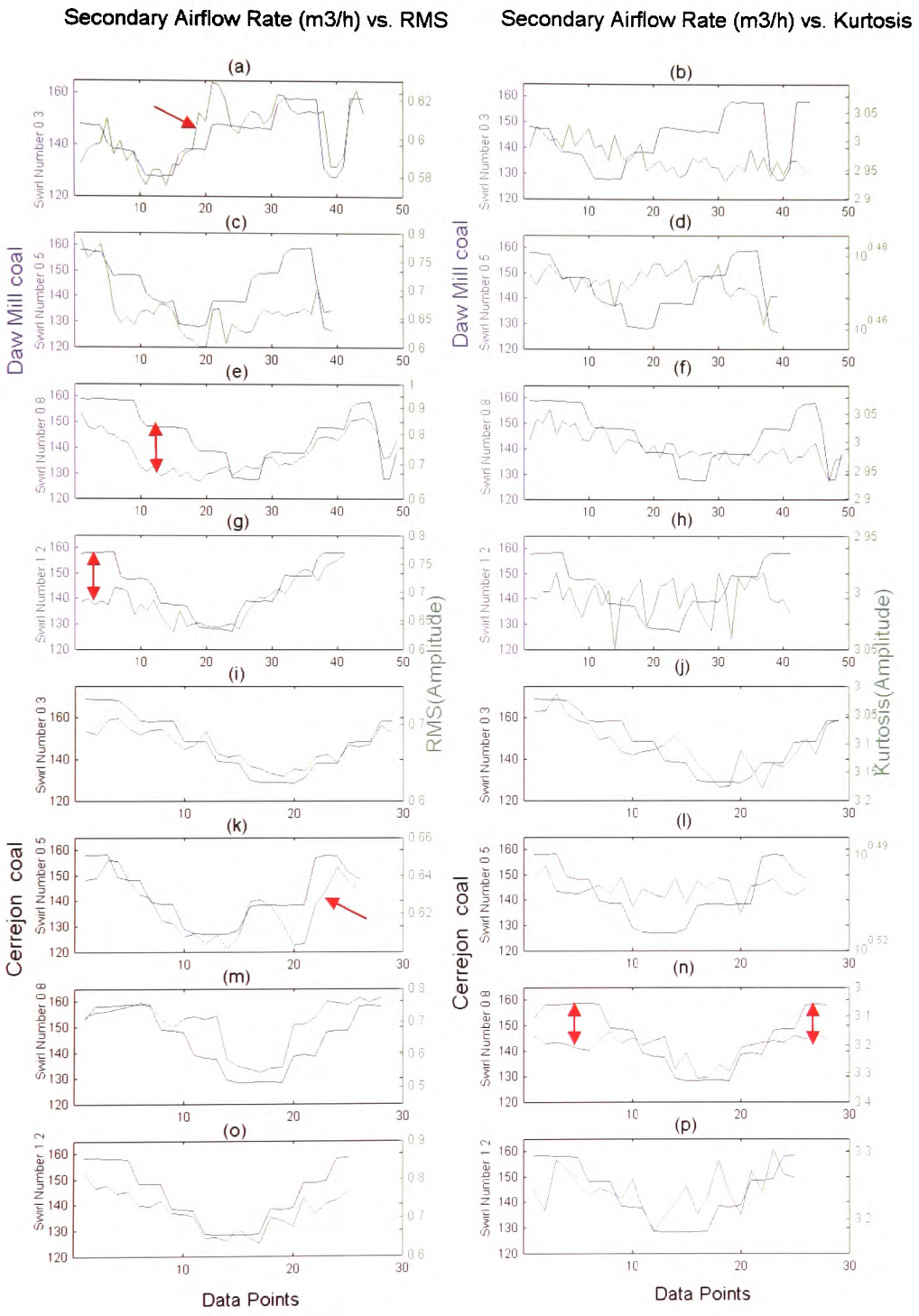

Figure 4.24 Secondary Airflow Rate and *RMS* and *Kurtosis* for the Microphone

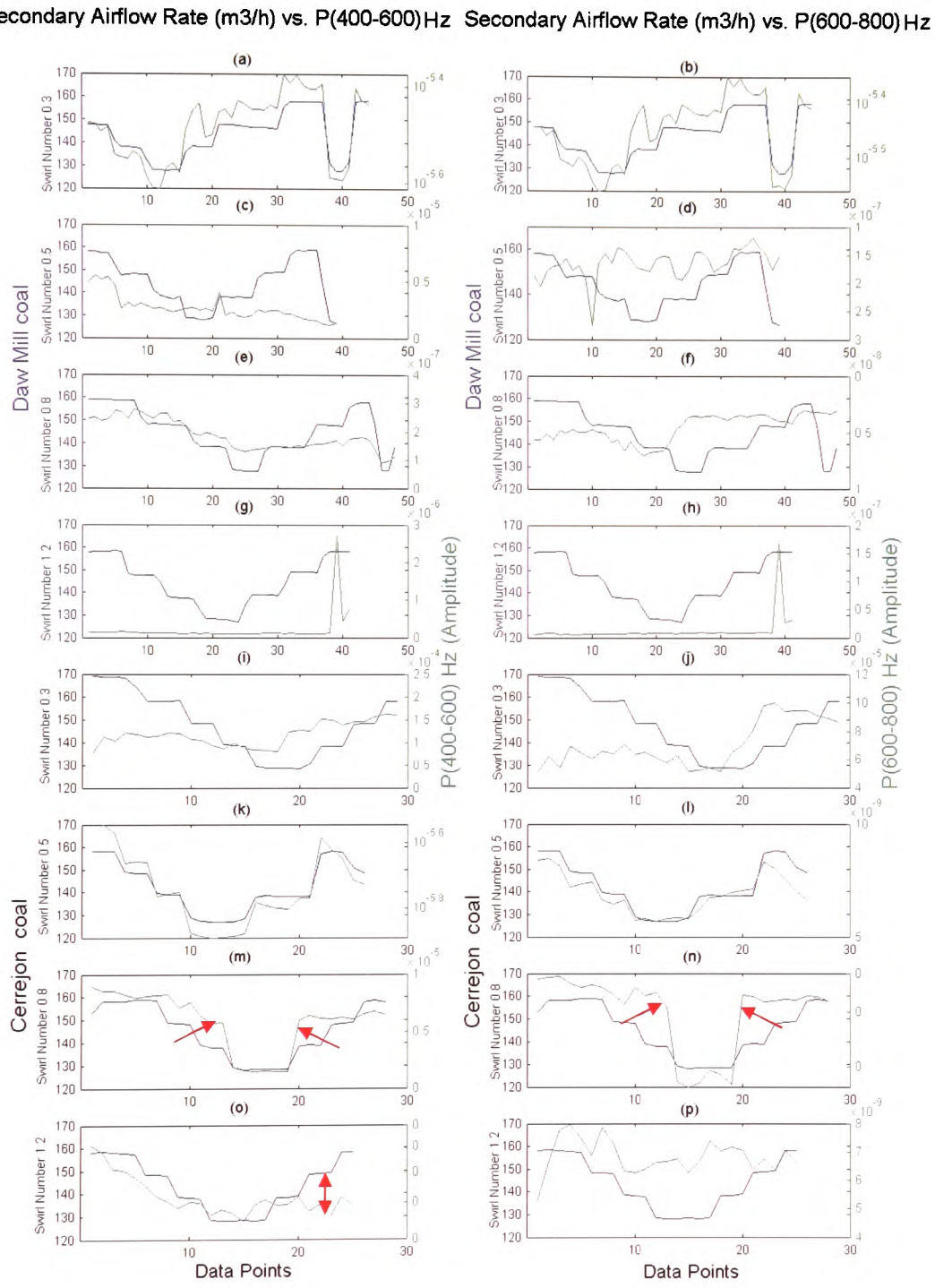

Figure 4.25 Secondary Airflow Rate and the *Average Energy* in the bands of 400-600 and 600-800 Hz for the Microphone

The large peak CO values that were experienced for some of the swirl numbers during the experiments have contributed to the larger differences as the features did not exhibit such a large variation. However, the *RMS* and *Kurtosis* of the microphone signal (Figures 4.26 (a), (b), (e), (f), (g), (i), (j), (k), (m), (n), (o), and (p)) exhibited a similar variation to the CO. As usual, red arrows are used to highlight differences. Also, Figures 4.27 (a), (b), (e), (f), (i), (j), (k), (l), (n) and (o) show examples of the *Average Energy* in the 400-600 and 600-800 Hz frequency range that are related to the microphone and target CO.

Despite large differences in these results, features of the microphone signal can be related with CO for most swirl numbers and coal types, except for the Daw Mill test data at a swirl number of 0.5. Still, there were also other features that were representative of CO for this swirl number that are not presented here.

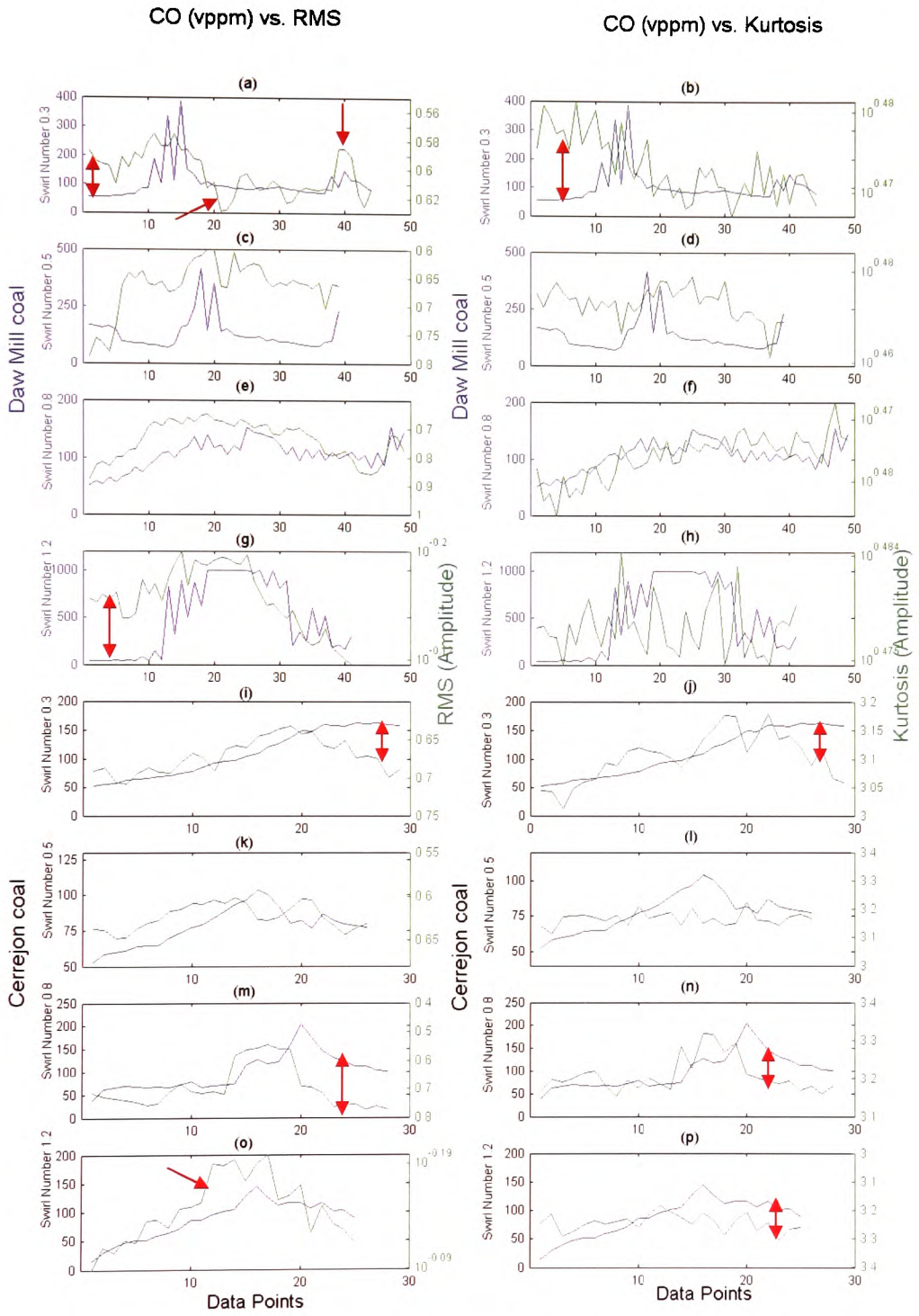

Figure 4.26 CO and the *RMS* and *Kurtosis* for the Microphone

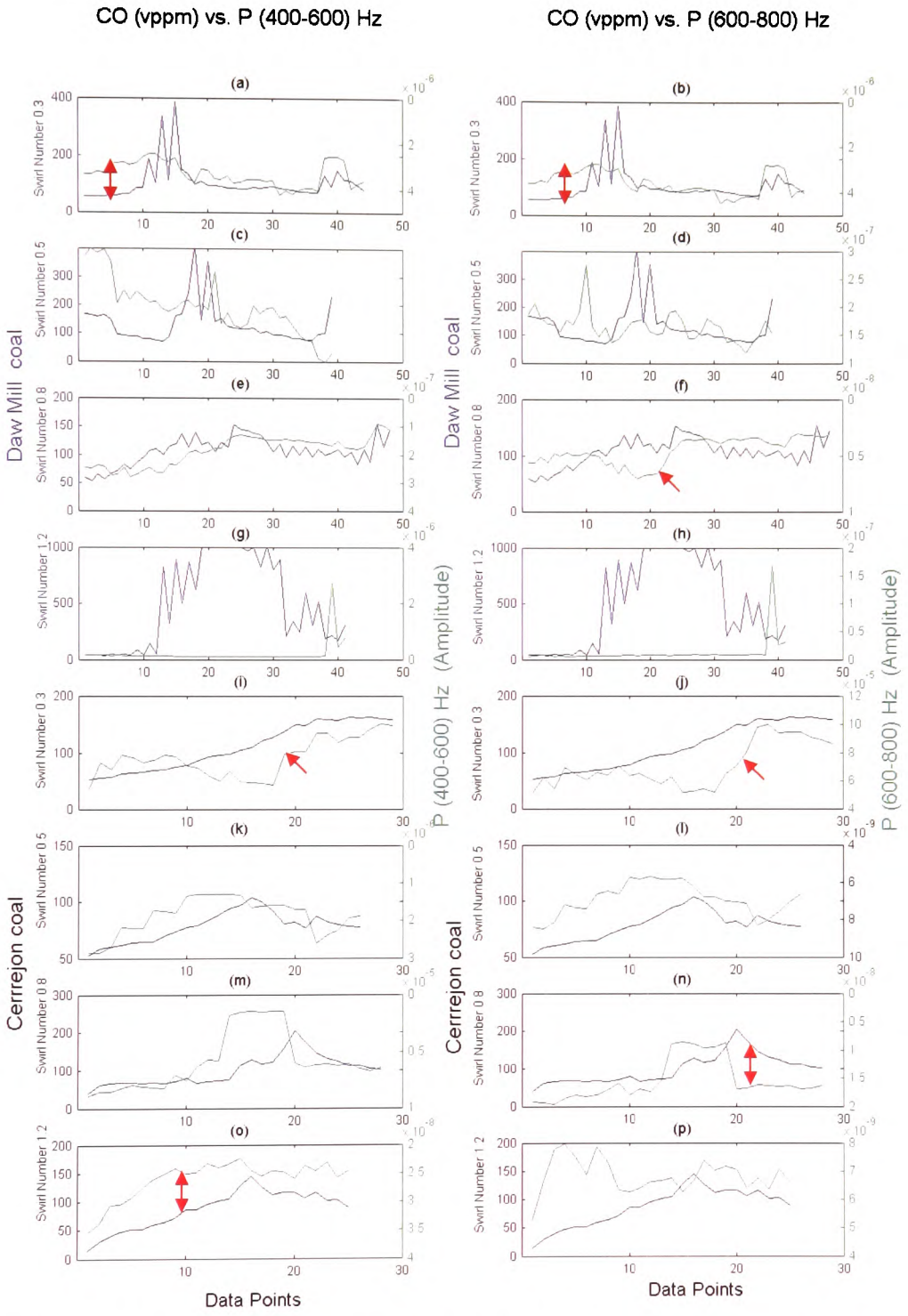

Figure 4.27 CO and *Average Energy* in the band of 400-600 and 600-800 Hz for the Microphone

The *RMS, Kurtosis* and *Average Energy* in the bands of 400-600 and 600-800 Hz features that exhibited good results for the microphone and O_2, were found in 4.28 (a), (b), (c), (d), (e), (f), (i), (j), (k), (l), (m), (n), (o) and (p) and Figures 4.29 (a), (b), (e), (f), (k), (l), (j), (m), (n) and (o). The differences for both Figures 4.28 and 4.29 are highlighted and ideally there appear to be good microphone features for every swirl number and coal type.

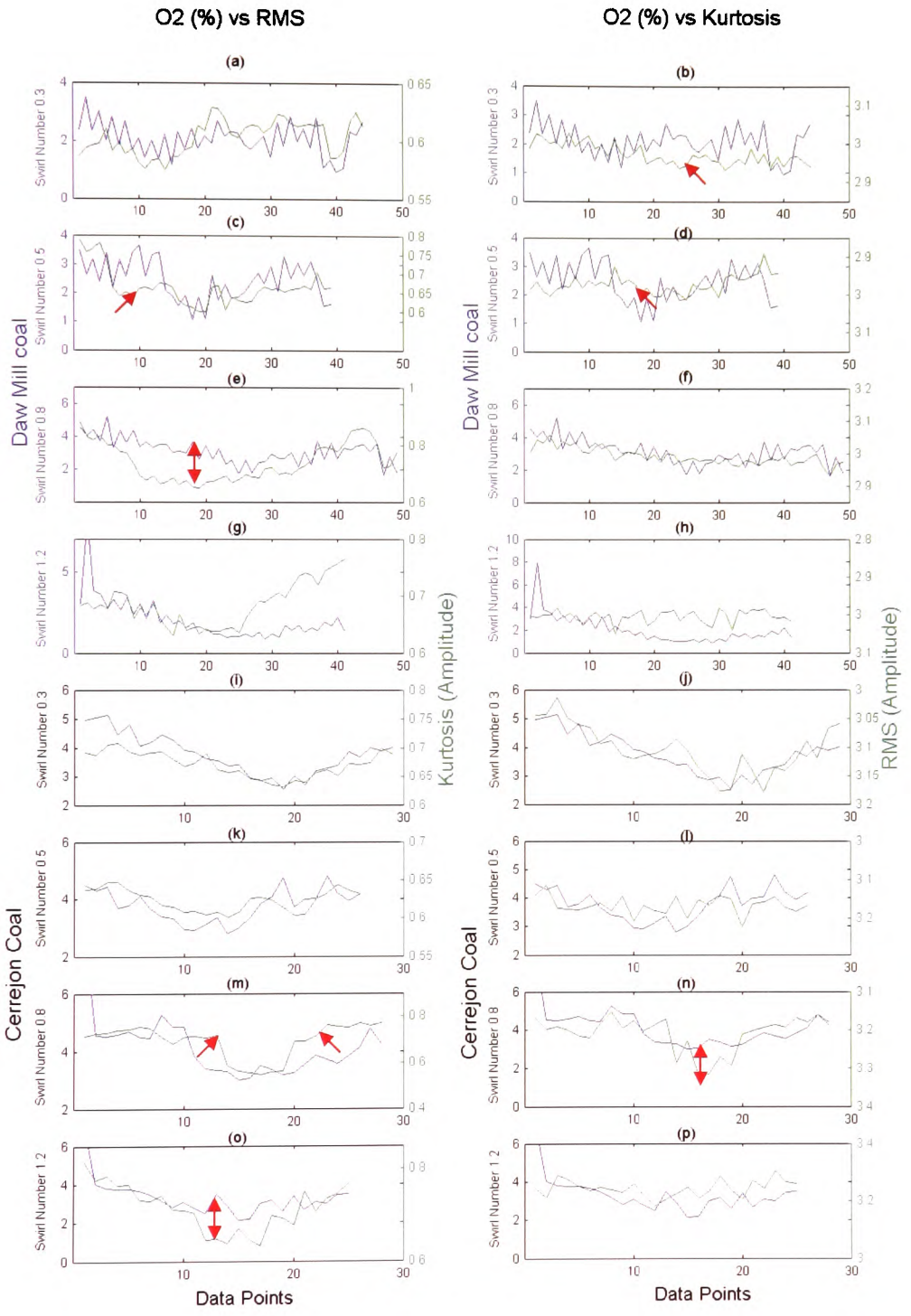

Figure 4.28 O_2 and the *RMS* and *Kurtosis* for the Microphone

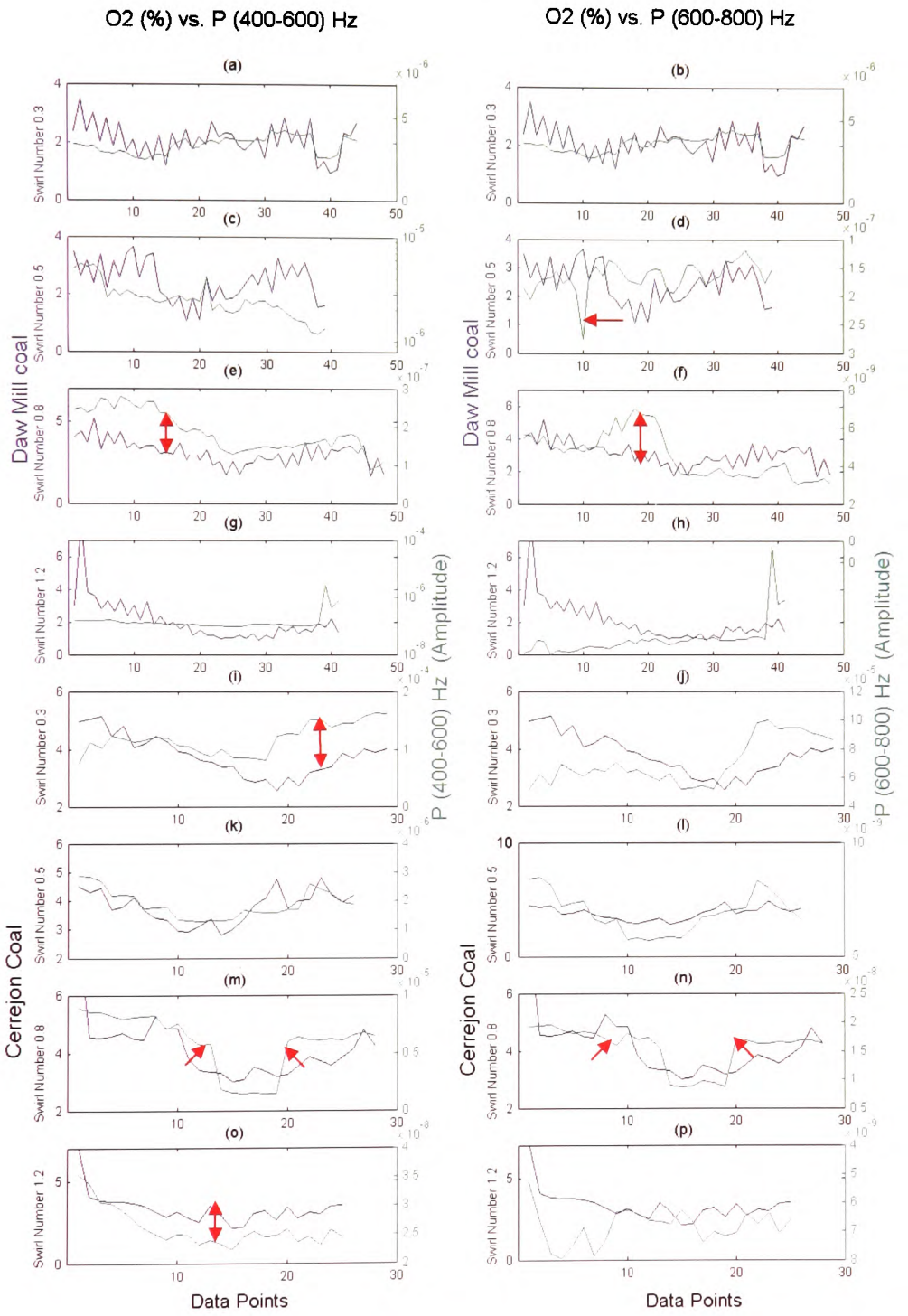

Figure 4.29 O_2 and the *Average Energy* in the bands of 400-600 and 600-800 Hz for the Microphone

4.4.3 Comparison of Typical AE Features with the Flue Gas Concentrations and Secondary Airflow Rate

Fundamentally, AE occurs at high frequencies and so the *Average Energy* in the bands of 300-400 and 700-800 kHz were compared. In a similar manner to the previous results, the AE were plotted against the NOx, secondary airflow rate, CO and O_2 respectively.

The results of the *RMS* and *Kurtosis* of the AE that can be related to the NOx are presented in Figures 4.30 (d), (e), (f), and (j). Unfortunately, only a limited number of statistical features were found related, in comparison to the IR and microphone features. The results of the *Average Energy* in the bands of 300-400 and 700-800 kHz of the AE sensor that can be related to the gaseous NOx are presented in Figures 4.31 (a), (b), (f), (i), (l) and (p). The results suggest that the AE features were not related to the NOx for every swirl number and coal type. This also emphasises the importance of considering more features to increase the chance of relating the AE signals to NOx. In addition, AE was insensitive to the step change of the NOx (Figures 4.30 (a) and (b) and Figure 4.31 (a) and (b)). Other matters of interest include the presence of larger fluctuations (Figures 4.30 and 4.31) which would required a longer averaging time to achieve a better representation as illustrated by the red curve in Figure 4.31 (p).

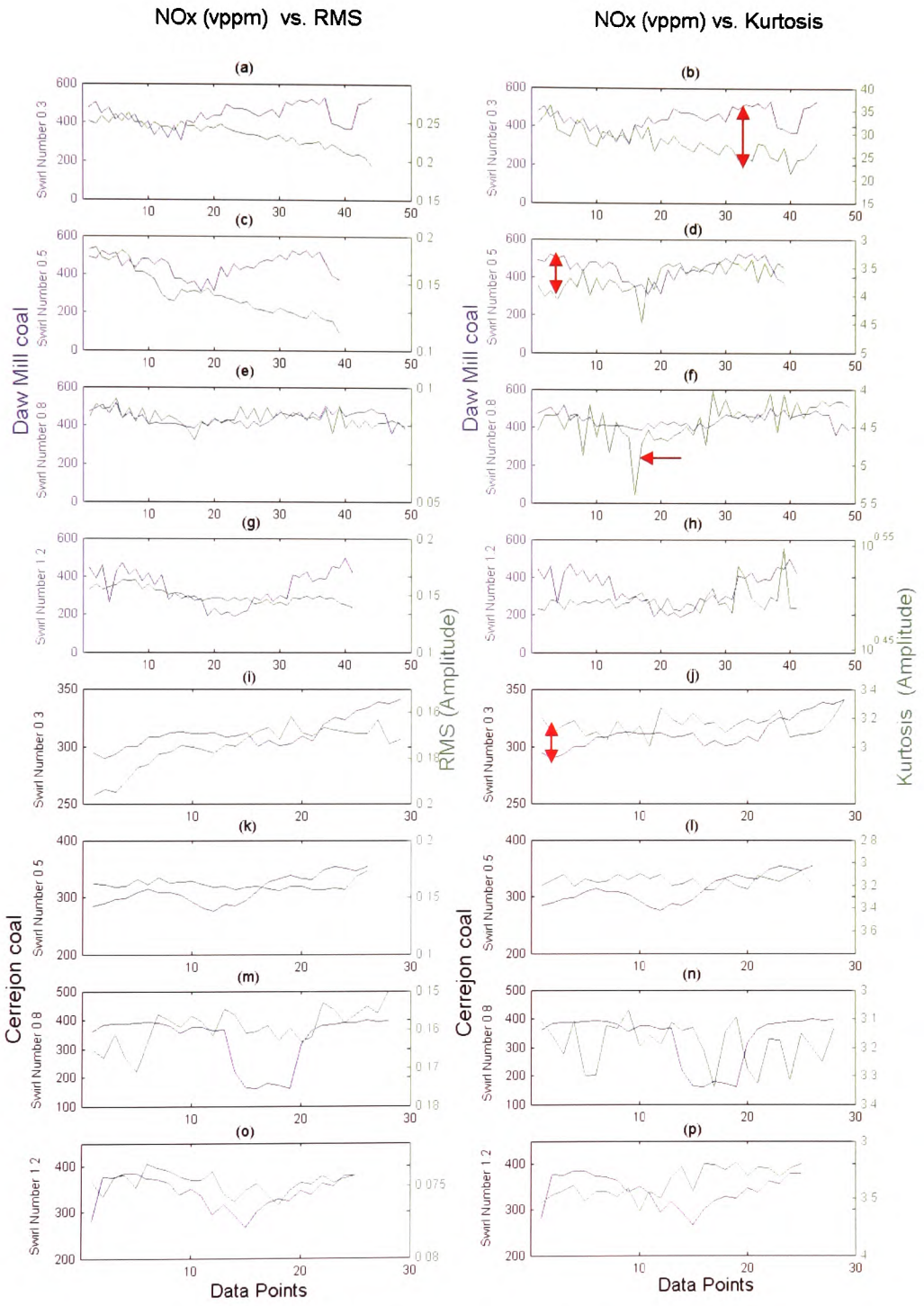

Figure 4.30 NOx and the *RMS* and *Kurtosis* for the AE sensor

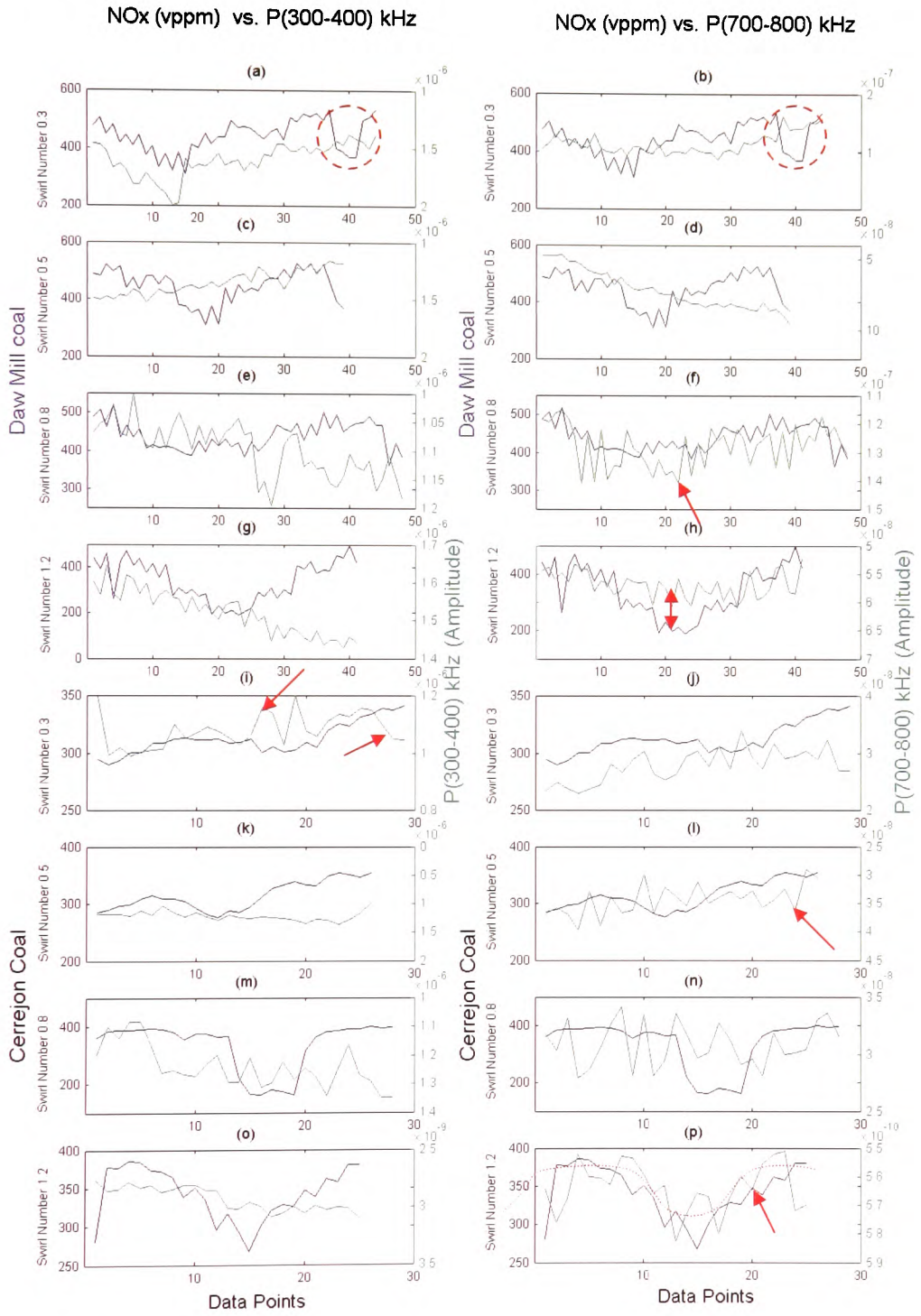

Figure 4.31 NOx and the *Average Energy* in the bands of 300-400 and 700-800 kHz for the AE sensor

For the secondary airflow rate, the *RMS* of the AE signal for the Cerrejon coal data with a swirl number of 0.3 was the only feature that exhibited a corresponding variation (Figure 4.32 (i)). Figures 4.33 (a), (i), (j), and (m) show the *Average Energy* of the AE which appeared to be more related to the secondary airflow rate. Differences are highlighted by red circles although none of the AE features responded to the step change in the secondary airflow rate (Figures 4.32 (a) and (b), and Figures 4.33 (a) and (b)). In general, fewer features were observed to be related, meaning that more features would have to be analysed in the hope of finding related features for every swirl number and coal type.

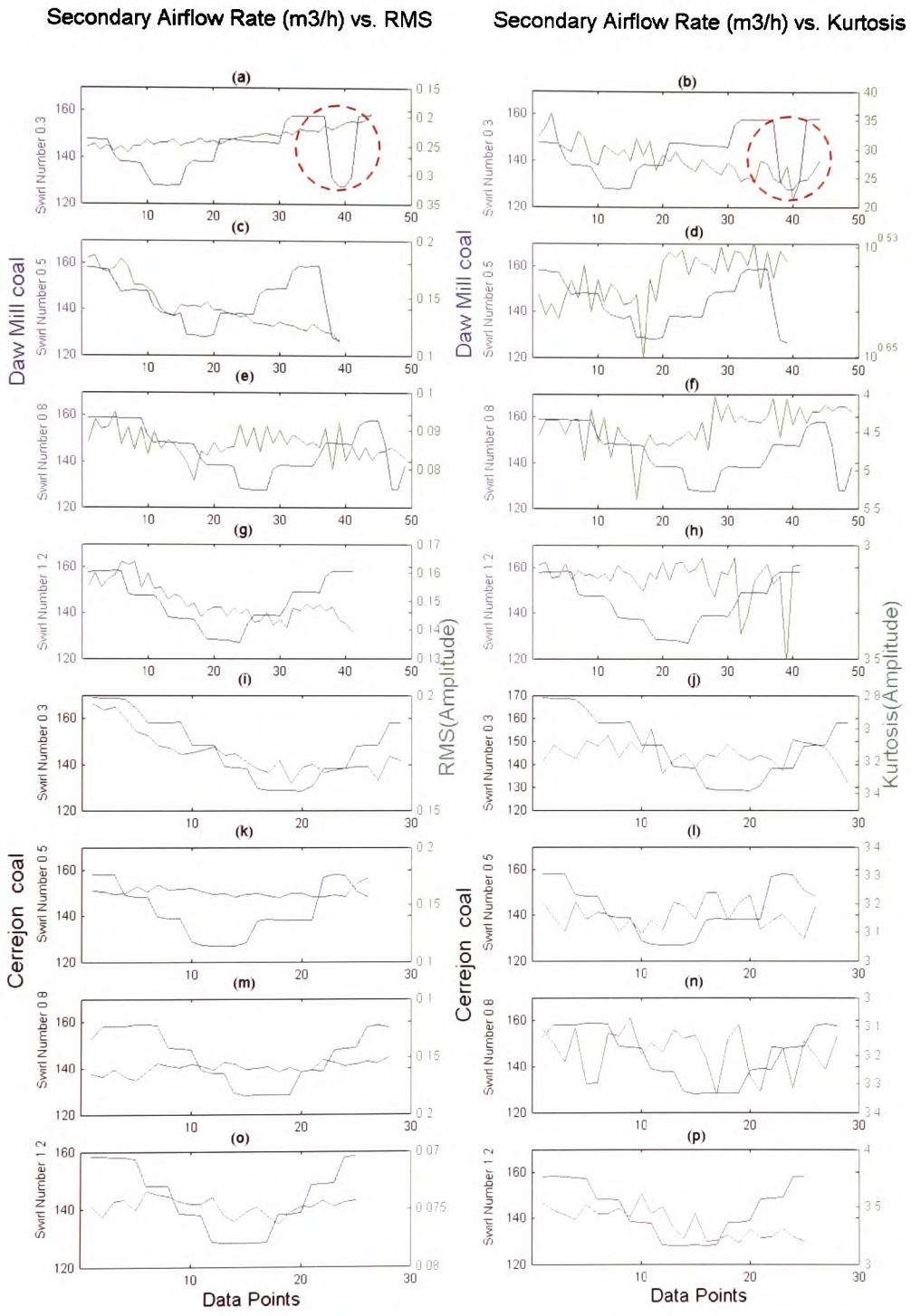

Figure 4.32 Secondary Airflow Rate and the *RMS* and *Kurtosis* for the AE sensor

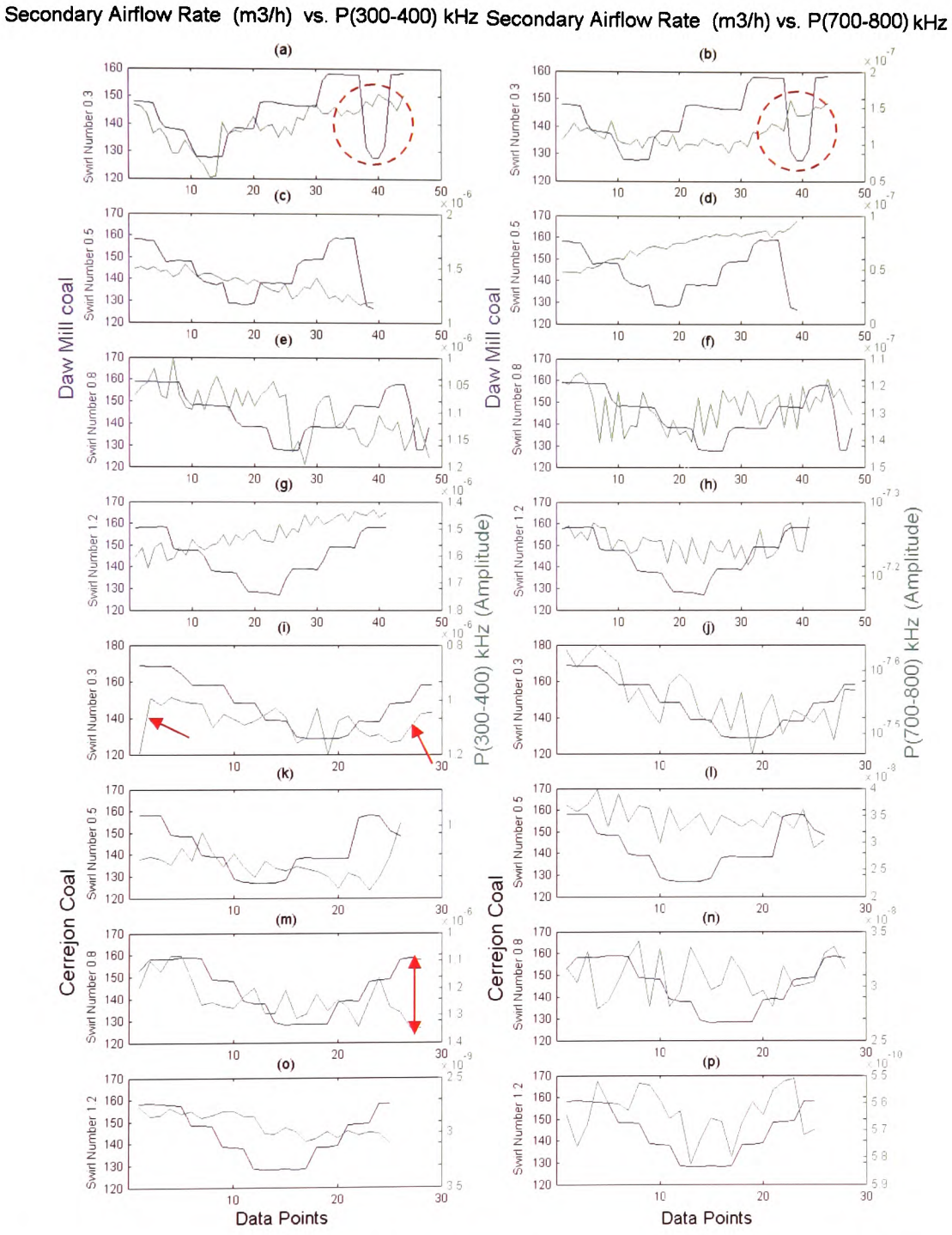

Figure 4.33 Secondary Airflow Rate and the *Average Energy* in the bands of 300-400 and 700-800 kHz for the AE sensor

The results of *RMS* and *Kurtosis* of the AE that were related to the CO are presented in Figures 4.34 (d), (e) (f), (g), (i) and (j) and the *Average Energy* in the bands of 300-400 and 700-800 kHz of the AE signal which correlated with the CO variations are presented in Figures 4.35 (a), (e), (f), (g), (j) and (o). In reality, the acceptable results were limited to the Daw Mill test data for swirl numbers of 0.5, 0.8, and 1.2, and the Cerrejon test data for swirl numbers 0.3 and 1.2. This implies that the AE features were not as good at representing the CO as IR and the microphone. However, this should not lead to abandoning the use of AE for monitoring combustion because good features could still exist when other analysis is undertaken.

In the final presentation, the results of the *RMS* and *Kurtosis* features of the AE that were found to correlate with O_2 are presented in Figures 4.36 (b), (d), (f) and (p) and the *Average Energy* in the bands of 300-400 and 700-800 kHz of the AE were correlated with the O_2 in Figures 4.37 (a), (b), (e), (f), (g), (h), (j) and (l). Correlated features were found exist for almost every swirl number and coal type. This is certainly an improved result compared with the previous two sections where the secondary airflow rate and CO corresponding to AE features were discussed.

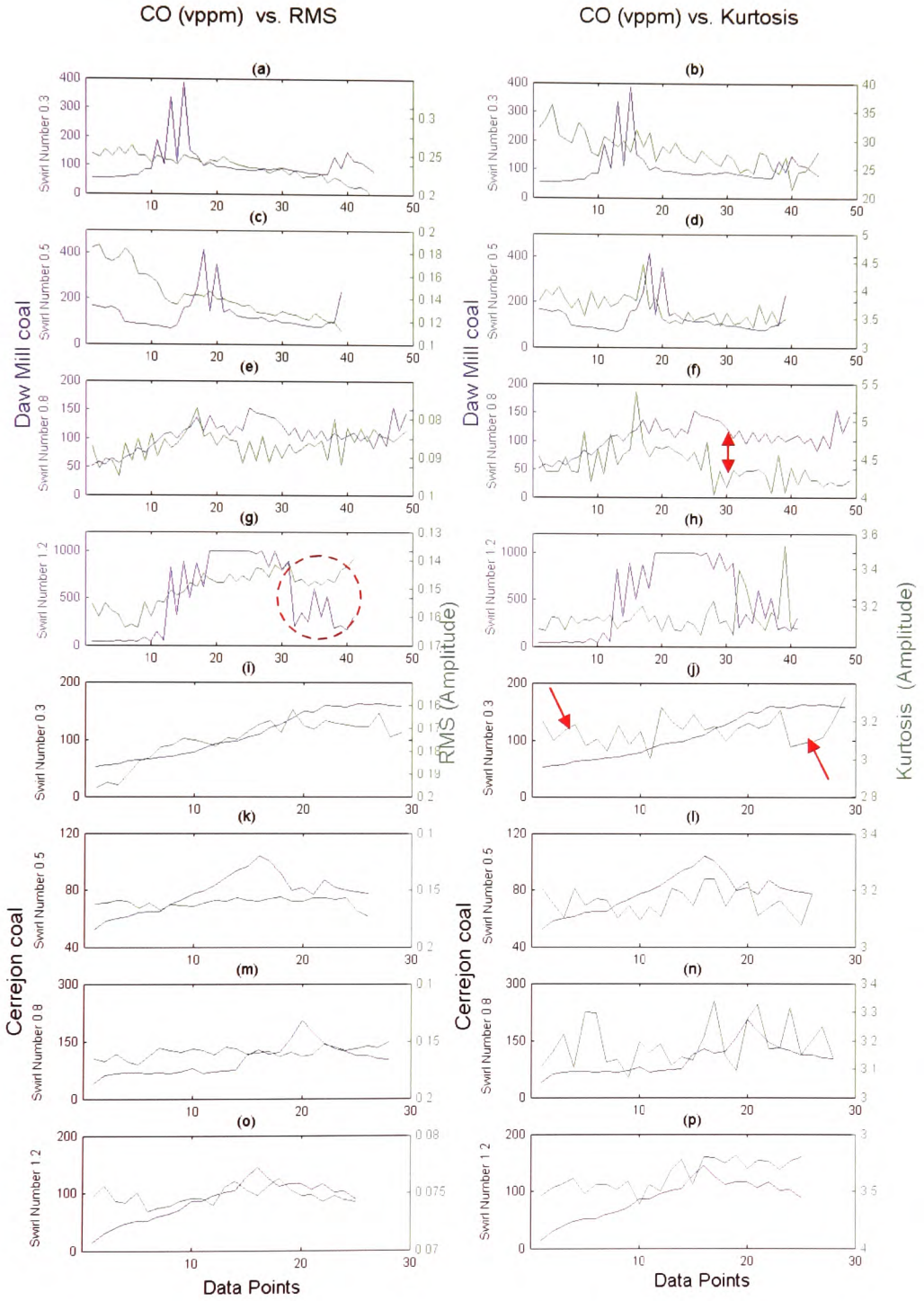

Figure 4.34 CO and the *RMS* and *Kurtosis* for the AE sensor

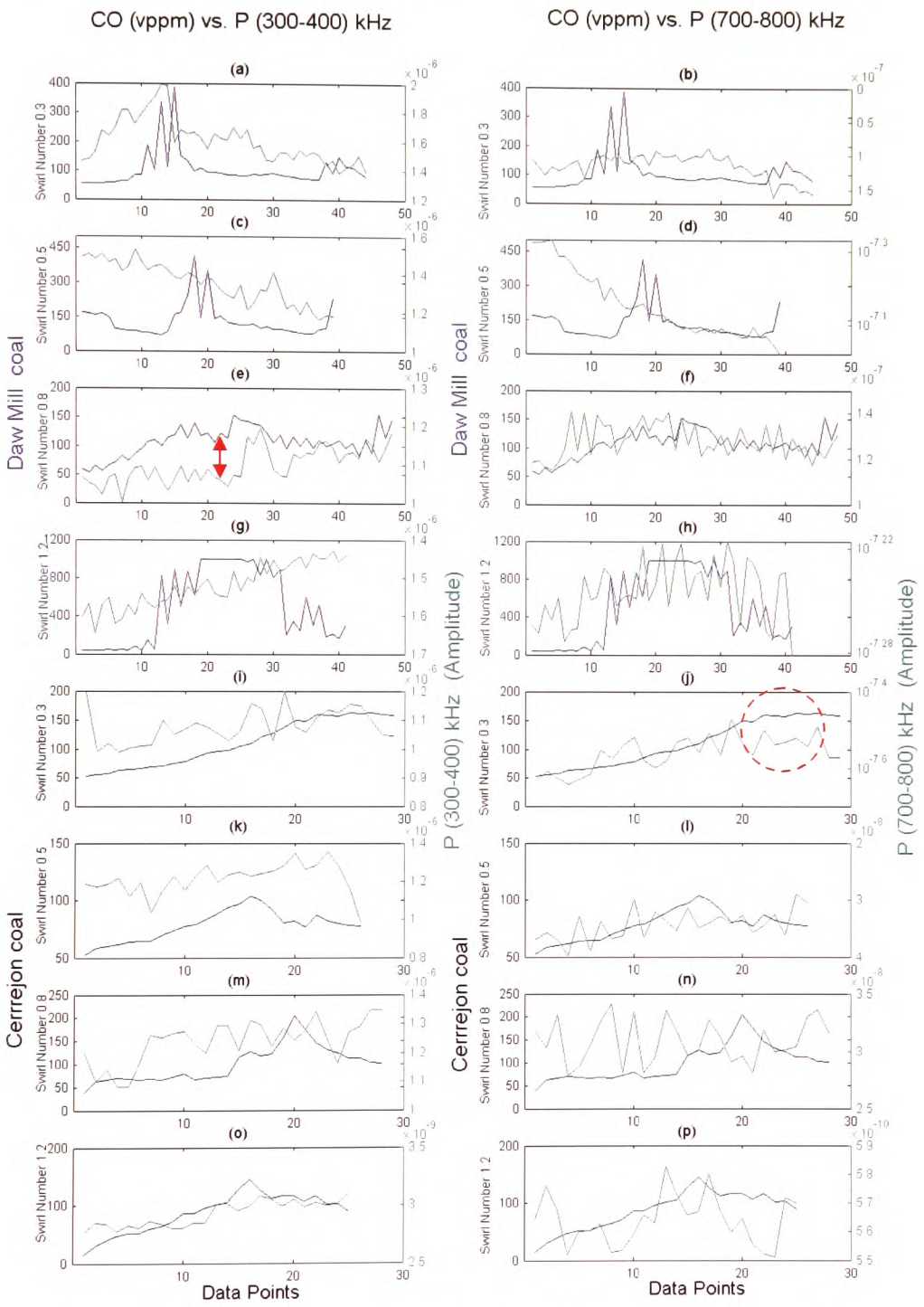

Figure 4.35 CO and the *Average Energy* in the bands of 300-400 and 700-800 kHz for the AE sensor

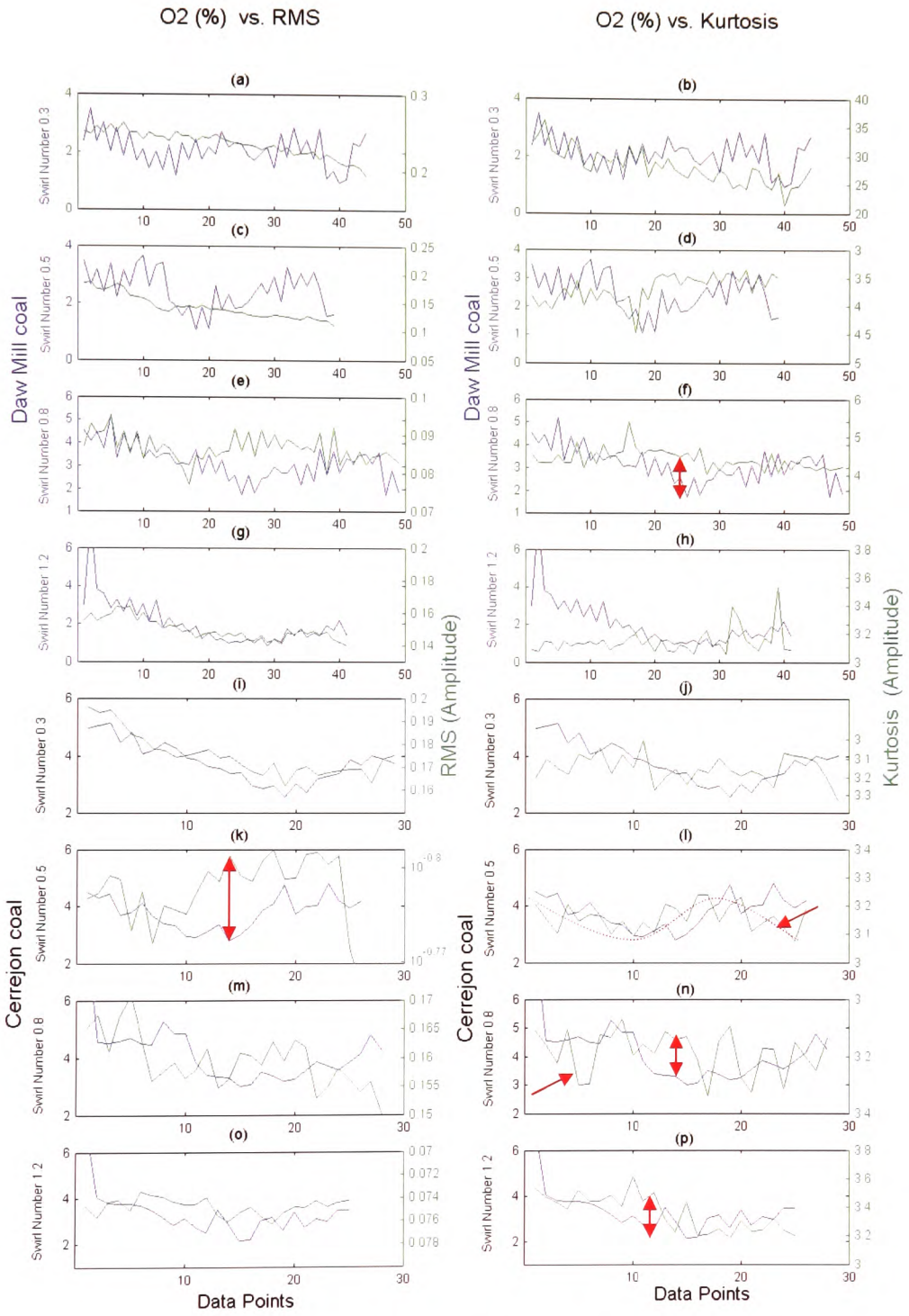

Figure 4.36 O_2 and the *RMS* and *Kurtosis* for the AE sensor

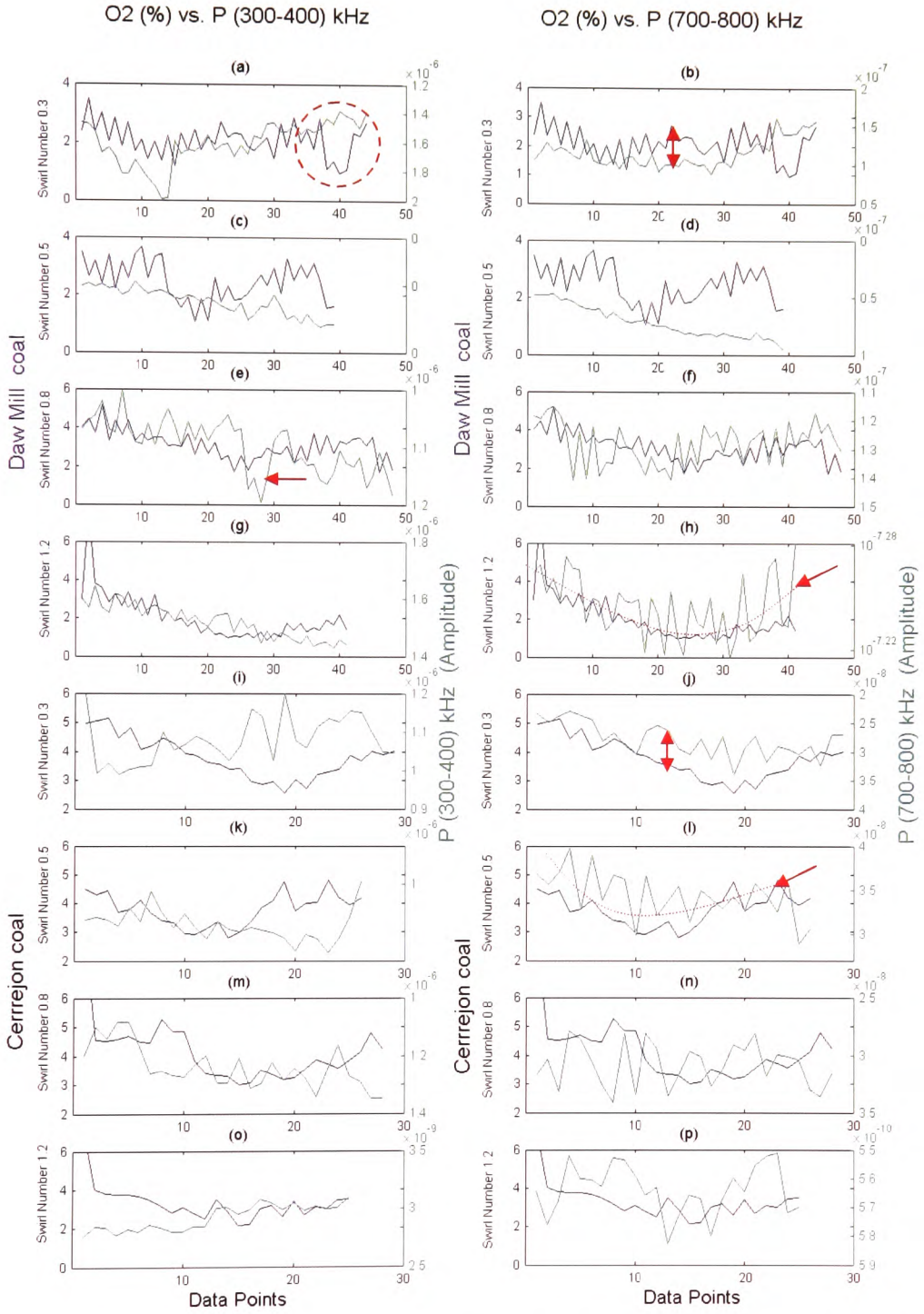

Figure 4.37 O_2 plots against *Average Energy* in the bands of 300-400 and 700-800 kHz for the AE sensor

4.5 Summary of Selected Features Analysis

Even though a large number of features were selected (Table 4.1), it was impossible to present every feature response to every swirl number and coal type. As a result, a selection of features (specifically two time and frequency domain features) for the different swirl numbers, coal types, and sensor type were presented. The arrangement of the results in sections 4.4.1, 4.4.2, and 4.4.3 has enabled the consistency of the chosen features to be compared for each swirl number and coal type.

It was found that every set of results exhibited different degrees of correlation. The features of the IR and microphone sensors had the greatest consistency at representing the gaseous emissions for each swirl number and coal type. This suggests that the AE sensor was the least capable sensor because the correlation of the AE features to some operating condition of the burner was not achieved.

One can conclude that a "universal" feature that consistently estimated the gases for every swirl number and coal type did not appear to exist. Other interesting observations were that the microphone was able to detect step changes in the gases and that there were examples where a long average of the features allowed the feature to estimate the variation in the gases.

4.6 Summary of Chapter 4

Chapter 4 comprised two major discussions: firstly, it discussed a study of the gaseous emission profiles for different burner operating conditions as the experiments were conducted by varying the secondary airflow rate and swirl setting, secondly, it presented the search for a suitable signal processing algorithm, so that the IR, microphone, and AE signals could be transformed into a series of useful features that were comparable to the emission gases.

The purpose of these experiments as conducted in the 150 kW PF combustion test facility was to study the gaseous emission profiles of different coals and burner settings.

In summary, the experiments confirmed that NOx reduced as the secondary airflow rate decreased. However, CO increased rapidly if there was insufficient O_2. Other factors that affected the dynamics of the PF burner included the swirl setting and combustion rate, and a swirl number of 0.8 for both the Daw Mill and Cerrejon was found to be optimal.

The techniques of signal processing both in the time and frequency domains also were discussed. A selection of sensor features were compared to the combustion gases with the conclusion being that the IR and microphone features better represent the gases for almost every swirl number and coal type as compared to the use of AE features. As it was not found to be possible to utilise one feature to estimate emissions for all swirl numbers and for both coals, a technique is required that brings together the "good" features so as to be able to make estimates over as large a range of the swirls tested as accurately as possible.

Chapter 5 The Modelling of Gas Emission in Pulverised Coal system

It was acknowledged in Chapter 4 that there were correlations between the sensor features and the combustion gases. Besides, it was found that no single feature could represent a particular gas reading for every operating condition and so this statement led to the view that a combination of features using Artificial Neural Network (ANN) techniques would provide the best approach for the estimation of the gaseous emissions so that appropriate control actions could take place in real-time.

5.1 Introduction

Generally, there are two ways to perform system (process) modelling. This can either be through, (a) first principles, in which the physical and chemical relationships such as reaction kinetics, material balances, and thermodynamics are modelled, or (b) to generate a mathematical function where empirical relationships are of more concern. In this application, the approach adopted was (b) for the following reasons: -

1. Combustion systems vary significantly due to the high nonlinearity in different operating regions [Russell *et al.*, 1997].

2. Models based on first principles require specific plant data, which can be difficult or expensive to measure.

3. There is no universal kinetic relationship which can adequately describe the combustion system, for example, the gasification of the nitrogen remaining in the char is frequently undetermined [Niska *et al.*, 1996; Stanmore, 1999].

Wojcik (2003) suggested that good predictive results could be difficult to obtain if the model is to be trained with a single variable. Ideally, the ANN is used as a "software sensor[1]" in which they are trained by the historical data and then used to perform online predictions. The trained gases models of Wojcik were integrated to a close-loop control framework in which they predicted gaseous emissions so that the optimisation could be achieved in a routine fashion. The motivation of using ANNs in this project is as follows [Lizarraga, 1998; Sankar *et al.*, 1996]: -

1. ANN is a computational model composed of many "nonlinear" processing elements and so it is suitable for modelling nonlinear processes.

2. ANN has the ability to find an approximate solution to a precisely (or an imprecisely) defined problem in the real world which benefits from its parallel processing capability.

3. ANN learns by adapting its synaptic weights to changes in the surrounding environment and generalises from known tasks or examples to an unknown one.

Among the most popular implementations are the Hopfield, Multilayer Perceptron, (MLP), Elman (Recursive), Self-Organizing Feature Map (SOFM), Learning Vector Quantisation (LVQ), Radial Basis Function (RBF) and Adaptive Resonance Theory (ART) networks. Though with function approximation in mind, the MLP and Elman networks which can approximate any given function with arbitrary precision [Bing, 1997] were evaluated in this project. In addition, a "one-step-ahead" Neural Network of Auto-regressive with Exogenous Inputs (NNARX) structure network developed by Nørgaard (2000) was tested. Nevertheless, only one of these three models will be used in the controller experiments (Chapter 6).

Modelling with an ANN is predominantly dependent to its input signals. Wildman (1994) suggested the use of additional information via data fusion could improve the modelling result. Feature-level data fusion involves the extraction of representative features from

[1] Software monitoring requires instrumenting the application source code, system libraries, or compiler. Software approaches are generally more portable and present information at an abstraction level closer to the users' way of thinking than, say, binary code, or assembly language instructions.

multiple sensor observations, followed by combination into a single concatenated input before modelling. Decision-level fusion, on the other hand, assumes that features in each independent sensor chain are sufficient to perform independent detection. Decision-level fusion theory implies that simulating different networks based on one common data set helps in searching for a good model architecture. In summary, Chapter 5 aims to find a routine that could possibly achieve the best prediction using ANNs.

5.2 Why Artificial Neural Networks?

Frequently in engineering, science, and business, data is collected and plotted graphically in order to assess an association between the variables by connecting the "points" with a line. Once drawn, the line is examined and a "model", then "fitted" and used to replace the existing set of data points as "the appropriate model". This is often followed by finding the coefficients of a polynomial function through the least square[2] algorithm that leads to an overdetermined[3] system as shown: -

$$y = a_0 + a_1 x + a_2 x^2 + a_3 x^3$$

where a_0, a_1, a_2 and a_3 are unknown coefficients

The Simple Regression (SR) model is straightforward and can successfully approximate many processes (at least over a limited range). Since many physical processes are nonlinear, the exploration of other trendline functions such as exponential, power, and logarithmic, have become familiar. However, choosing the wrong model can lead to instability of the model with higher order polynomials [Linko, 1999].

For multivariate systems, Multiple Regression (MR) models have been claimed to provide a more comprehensive solution by assuming that if y is a function of more than

[2] Least squares is a mathematical optimisation technique that attempts to find a "best fit" to a set of data by attempting to minimise the sum of the squares of the differences (called *residuals*) between the fitted function and the data.

[33] Algebraic systems that have more equations than unknowns.

one independent variable, the matrix equations that express the relationships among the variables can be expanded to accommodate additional data which can be expressed as: -

$$y = a_0 + a_1 x_1 + a_2 x_2$$

MR solves the unknown coefficients of a_0, a_1 and a_2 much in the same way to SR model. The approximation of MR is improved by increasing the number of positive independent variables [Advanced Statistics (Multiple Regressions) – *http://www.maths.ex.ac.uk/~wjk/psy6010/multreg1.html*; Last Accessed 10 April 2005]. Nevertheless, MR is fundamentally a linear model and using a linear criterion in a nonlinear context is far from optimal [Lendesse *et al.*, 2002].

Artificial Neural Networks (ANNs), on the other hand, have a proven ability for handling nonlinear and ill-defined problems. ANN determines the input-output relationships from a set of good examples, much in the same way that people learn through experimentation and interaction with their environment [Salehfar *et al.*, 1997]. Although the statistical methods such as SR and MR are still commonly used in the development of empirical relationships between them, this procedure is often complex and circuitous. In contrast, to formulate the statistical model process in an ANN is much easier and direct, for there is no necessity to specify a mathematical relationship between the input and output variables [Yin *et al.*, 1998]. With improved computer processing power, the ANN has become a practical tool for regular applications [William *et al.*, 1992] especially in the situation where online adaptation is required. Since there are various network types and architectures, the assessment of different network performances were undertaken and reported in the following sections.

5.3 Modelling of Pulverised Coal-fired Systems

Combustion is regarded as a highly complex and nonlinear system and because many boiler characteristics are not well understood, the empirical rather than first principle model is preferred [Kenneth *et al.*, 1994]. The earliest models were mainly based on global kinetics and these models have limitations in practical applications as they involve complex calculations using parameters that are not readily available and are accurate only to certain coals [Zhu *et al.*, 1999]. Yin (1998) stated that although there are several conventional techniques for estimating, for example, ash fusion temperatures from chemical composition, it is a complex question characterised by a number of interacting factors in which the relationship between these factors is not precisely known. In addition, the data associated with these parameters are usually erroneous and so developing empirical relationships using an ANN to predict the ash fusion temperature is favoured [Yin *et al.*, 1998]. From the above discussions, it is clear that the ANN is more appropriate for the use in combustion processes than many other mathematical based models.

5.4 Data Fusion

An appropriate combination of features greatly improves the chance of a good result in modelling whereas a poorly chosen set of features tends to lead to a poor estimation [Tan, 2003]; for example, Sharkey (1996) claimed that the use of combined features of temperature and pressure data achieved better prediction of faults in a marine diesel engine. However, to combine features requires an assessment of the "features" fitness for purpose and this can be achieved through techniques such as an examination of the correlation coefficient of each feature, or to identify good features through visual inspection.

5.4.1 The Importance of Data Fusion

Methods to combine or fuse data are drawn from a diverse set of more traditional disciplines, including digital signal processing, statistical estimation, control theory, artificial intelligence, and classical numerical methods. Data fusion techniques combine data from multiple sensors and relate information to achieve more specific inferences

than could be achieved using a single, independent sensor. For example, multi-sensor data (e.g., smell, touch, and vision) fusion is naturally performed by animals and humans to assess more accurately the surrounding environment and to identify threats, thereby improving their chances of survival.

The advantage of deploying multiple sensor fusion is to corroborate useful information from diverse feature vectors from different sensors. Three basic alternatives can be used for multi-sensor data: -

1. Direct fusion of sensor data.

2. Representation of sensor data via feature vectors, with subsequent fusion of the feature vectors.

3. Processing of each sensor to achieve high-level inferences or decisions, which are subsequently combined.

Hall *et al* (2000) stated that if the multi-sensor data can be derived from sensors measuring the same physical phenomena, such as two visual image sensors or two acoustic sensors, then the raw sensor data could be directly combined. Conversely, if the sensor data are non-commensurate, then the data must be fused at the feature/state vector level or decision level. Consequently, only (a) feature-level and (b) decision-level fusions are to be discussed here.

5.4.2 Feature-Level and Decision-Level Fusion

Feature-level fusion involves the extraction of representative features from multiple sensor observations followed by their combination into a single concatenated feature vector before input to the ANN. A schematic of a feature-level fusion based model is illustrated in Figure 5.1.

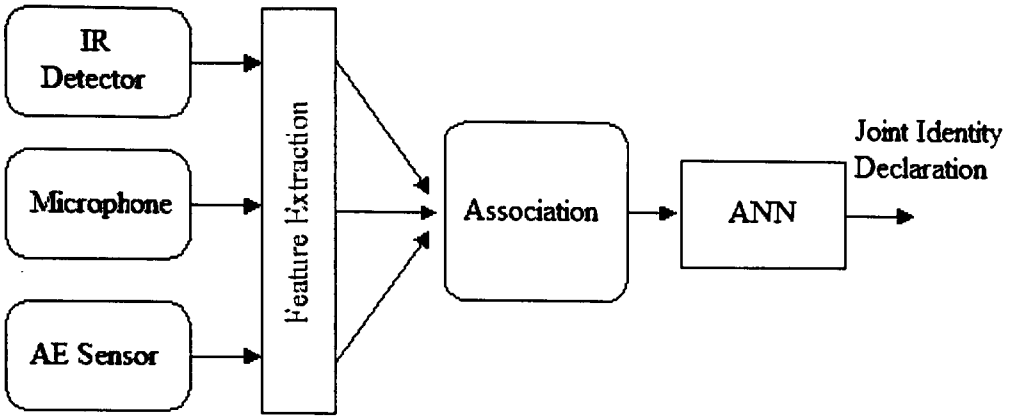

Figure 5.1 Feature-Level Fusion Model

In contrast, decision-level fusion combines sensor information after each sensor has made a preliminary determination of the identity of the class. This approach inherently assumes that the signals and features in each independent sensor chain are sufficient to perform independent detection before the sensor decisions are combined. Hall *et al* (2001) suggested that the final outcome of the decision-level fusion could be achieved through a voting technique. The output decision can be determined by selecting the least error model of ANN, which can be mathematically described as in Equation 5.3.

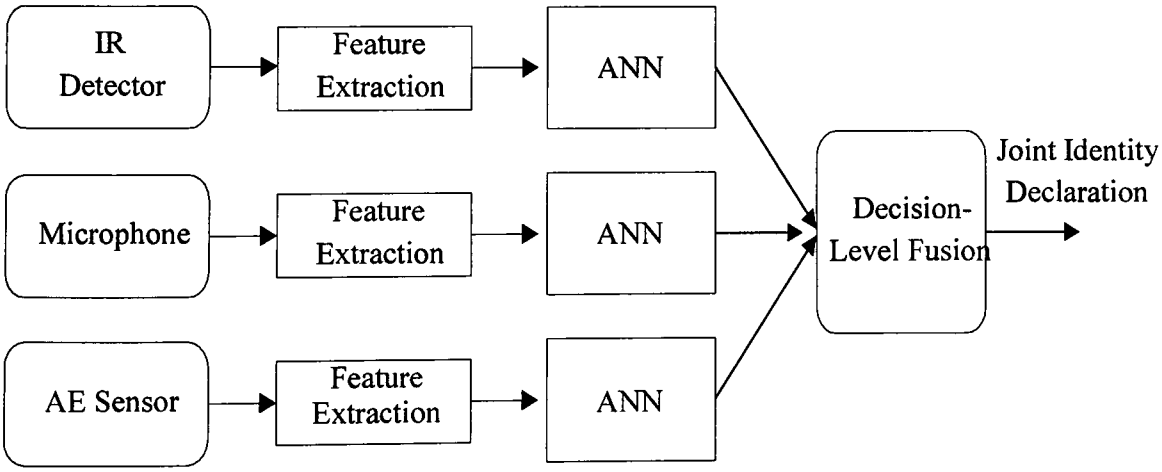

Figure 5.2 Decision-Level Fusion Model

$$\text{Final Decision} = \text{Min}\left[ME\left(\begin{pmatrix} P1 \\ P2 \\ P3 \end{pmatrix}_{IEDetector} + \begin{pmatrix} P1 \\ P2 \\ P3 \end{pmatrix}_{Microphone} + \begin{pmatrix} P1 \\ P2 \\ P3 \end{pmatrix}_{AESensor} \right) \right] \quad [5.3]$$

where P_1, P_2, and P_3 represent the sensor features used for training an individual ANN model.

It is obvious that the search for the "best" model for predicting the gaseous emissions resulting from combustion could involve both (a) feature-level fusion (b) decision-level fusion.

5.5 Gas Predictions by Artificial Neural Networks

The results in Chapter 4 show one feature can be more related to combustion gases than another. In addition, the correlated features varied from one swirl number to another and so a "universal" feature set, which can be used in every burner condition, does not appear to exist. Consequently, different ANN models designed for particular swirl numbers were used. Each swirl number was used to generate data for 6 ANN simulations corresponding to (a) IR, (b) microphone, (c) AE, (d) combined features from all sensors, (e) the 3 most highly correlated features, and (f) use of a visually inspected set of features. The descriptions and test results of the simulations are tabulated in Tables 5.1 and 5.2 for the Daw Mill and Cerrejon test data. Columns 1 and 2 indicate the swirl number and target gases that the ANN was being used to model. Column 3 is the simulation test number in systematic order, and Column 4 illustrates how the features were used in the predictions.

A MLP network with a hidden layer of hyperbolic tangent activation function neurons and an output layer of linear activation transfer function neurons was programmed in Matlab™. The choice for the hidden neurons was determined through counting the number of effective parameters during the training. Some 10 hidden neurons were found to be sufficient to the model combustion gases based entirely on the sensor features (Table 4.1). Levenberg-Marquardt, a gradient descent back propagation method was used to adjust the network during training. In addition, network regularisation by the early stopping routine implemented in Matlab™ (Figure 5.4) was used to optimise the training time (size) of the trained network [Zhu *et al.*, 1999].

The first half of the data set was used for training with the rest for validation (unless otherwise specified). The same network model was trained a number of times in order to avoid the effect of local minima and to obtain best network performance [Tan *et al.*, 1999]. Since a neural network model is directly influenced by its input it is possible to examine the model predictions by knowing the input signals.

Knowing that the predictions directly depended on the sensor features, high frequency components (noise) were modelled in addition to the underlying signal. For this reason, it was decided to average the predictions as a means to reduce prediction errors, rather than filter the features, as it was felt that there might be useful information in the high frequency content. The averaging of the predictions that will be discussed in Chapter 6 shows that averaging the predictions over a sufficiently long period of time yielded a reliable estimate of CO and NOx. In addition, evidence of the neural network being only sensitive to the underlying gas signal (exclusive of its periodic oscillation) was found in Chapter 5.

Table 5.1 Simulation of ANN based of Daw Mill test data

Swirl Number	Target	Simulation No.	Simulation Details	Swirl Number	Target	Simulation No.	Simulation Details
0.3	NOx	Simulation 1.1	IR Features	0.5	NOx	Simulation 2.1	IR Features
		Simulation 1.2	Microphone Features			Simulation 2.2	Microphone Features
		Simulation 1.3	AE Features			Simulation 2.3	AE Features
		Simulation 1.4	All Sensor Features			Simulation 2.4	All Sensor Features
		Simulation 1.5	3 Most Highly Correlated Features			Simulation 2.5	3 Most Highly Correlated Features
		Simulation 1.6	Visually Inspected Features			Simulation 2.6	Visually Inspected Features
	CO	Simulation 1.7	IR Features		CO	Simulation 2.7	IR Features
		Simulation 1.8	Microphone Features			Simulation 2.8	Microphone Features
		Simulation 1.9	AE Features			Simulation 2.9	AE Features
		Simulation 1.10	All Sensor Features			Simulation 2.10	All Sensor Features
		Simulation 1.11	3 Most Highly Correlated Features			Simulation 2.11	3 Most Highly Correlated Features
		Simulation 1.12	Visually Inspected Features			Simulation 2.12	Visually Inspected Features
	O_2	Simulation 1.13	IR Features		O_2	Simulation 2.13	IR Features
		Simulation 1.14	Microphone Features			Simulation 2.14	Microphone Features
		Simulation 1.15	AE Features			Simulation 2.15	AE Features
		Simulation 1.16	All Sensor Features			Simulation 2.16	All Sensor Features
		Simulation 1.17	3 Most Highly Correlated Features			Simulation 2.17	3 Most Highly Correlated Features
		Simulation 1.18	Visually Inspected Features			Simulation 2.18	Visually Inspected Features

Cont'

0.8	NOx	Simulation 3.1	IR Features	1.2	NOx	Simulation 4.1	IR Features
		Simulation 3.2	Microphone Features			Simulation 4.2	Microphone Features
		Simulation 3.3	AE Features			Simulation 4.3	AE Features
		Simulation 3.4	All Sensor Features			Simulation 4.4	All Sensor Features
		Simulation 3.5	3 Most Highly Correlated Features			Simulation 4.5	3 Most Highly Correlated Features
		Simulation 3.6	Visually Inspected Features			Simulation 4.6	Visually Inspected Features
	CO	Simulation 3.7	IR Features		CO	Simulation 4.7	IR Features
		Simulation 3.8	Microphone Features			Simulation 4.8	Microphone Features
		Simulation 3.9	AE Features			Simulation 4.9	AE Features
		Simulation 3.10	All Sensor Features			Simulation 4.10	All Sensor Features
		Simulation 3.11	3 Most Highly Correlated Features			Simulation 4.11	3 Most Highly Correlated Features
		Simulation 3.12	Visually Inspected Features			Simulation 4.12	Visually Inspected Features
	O_2	Simulation 3.13	IR Features		O_2	Simulation 4.13	IR Features
		Simulation 3.14	Microphone Features			Simulation 4.14	Microphone Features
		Simulation 3.15	AE Features			Simulation 4.15	AE Features
		Simulation 3.16	All Sensor Features			Simulation 4.16	All Sensor Features
		Simulation 3.17	3 Most Highly Correlated Features			Simulation 4.17	3 Most Highly Correlated Features
		Simulation 3.18	Visually Inspected Features			Simulation 4.18	Visually Inspected Features

Table 5.2 Simulation of ANN based of Cerrejon test data

Swirl Number	Target	Simulation No.	Simulation Detail	Swirl Number	Target	Simulation No.	Simulation Detail
0.3	NOx	Simulation 5.1	IR Features	0.5	NOx	Simulation 6.1	IR Features
		Simulation 5.2	Microphone Features			Simulation 6.2	Microphone Features
		Simulation 5.3	AE Features			Simulation 6.3	AE Features
		Simulation 5.4	All Sensor Features			Simulation 6.4	All Sensor Features
		Simulation 5.5	3 Most Highly Correlated Features			Simulation 6.5	3 Most Highly Correlated Features
		Simulation 5.6	Visually Inspected Features			Simulation 6.6	Visually Inspected Features
	CO	Simulation 5.7	IR Features		CO	Simulation 6.7	IR Features
		Simulation 5.8	Microphone Features			Simulation 6.8	Microphone Features
		Simulation 5.9	AE Features			Simulation 6.9	AE Features
		Simulation 5.10	All Sensor Features			Simulation 6.10	All Sensor Features
		Simulation 5.11	3 Most Highly Correlated Features			Simulation 6.11	3 Most Highly Correlated Features
		Simulation 5.12	Visually Inspected Features			Simulation 6.12	Visually Inspected Features
	O_2	Simulation 5.13	IR Features		O_2	Simulation 6.13	IR Features
		Simulation 5.14	Microphone Features			Simulation 6.14	Microphone Features
		Simulation 5.15	AE Features			Simulation 6.15	AE Features
		Simulation 5.16	All Sensor Features			Simulation 6.16	All Sensor Features
		Simulation 5.17	3 Most Highly Correlated Features			Simulation 6.17	3 Most Highly Correlated Features
		Simulation 5.18	Visually Inspected Features			Simulation 6.18	Visually Inspected Features

Cont'

0.8	NOx	Simulation 7.1	IR Features	1.2	NOx	Simulation 8.1	IR Features
		Simulation 7.2	Microphone Features			Simulation 8.2	Microphone Features
		Simulation 7.3	AE Features			Simulation 8.3	AE Features
		Simulation 7.4	All Sensor Features			Simulation 8.4	All Sensor Features
		Simulation 7.5	3 Most Highly Correlated Features			Simulation 8.5	3 Most Highly Correlated Features
		Simulation 7.6	Visually Inspected Features			Simulation 8.6	Visually Inspected Features
	CO	Simulation 7.7	IR Features		CO	Simulation 8.7	IR Features
		Simulation 7.8	Microphone Features			Simulation 8.8	Microphone Features
		Simulation 7.9	AE Features			Simulation 8.9	AE Features
		Simulation 7.10	All Sensor Features			Simulation 8.10	All Sensor Features
		Simulation 7.11	3 Most Highly Correlated Features			Simulation 8.11	3 Most Highly Correlated Features
		Simulation 7.12	Visually Inspected Features			Simulation 8.12	Visually Inspected Features
	O_2	Simulation 7.13	IR Features		O_2	Simulation 8.13	IR Features
		Simulation 7.14	Microphone Features			Simulation 8.14	Microphone Features
		Simulation 7.15	AE Features			Simulation 8.15	AE Features
		Simulation 7.16	All Sensor Features			Simulation 8.16	All Sensor Features
		Simulation 7.17	3 Most Highly Correlated Features			Simulation 8.17	3 Most Highly Correlated Features
		Simulation 7.18	Visually Inspected Features			Simulation 8.18	Visually Inspected Features

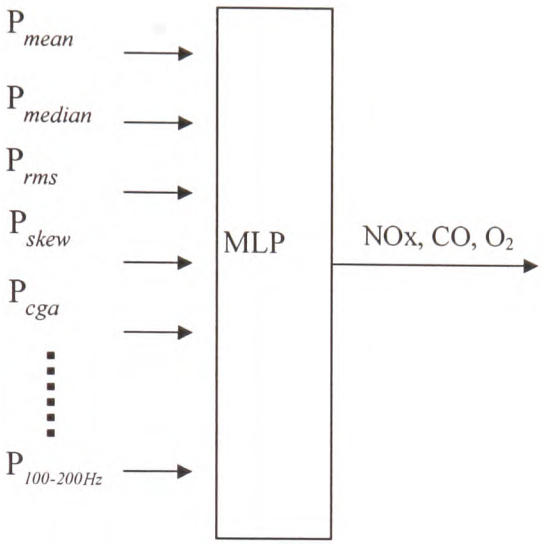

Figure 5.3 Modelling of the Combustion Gases

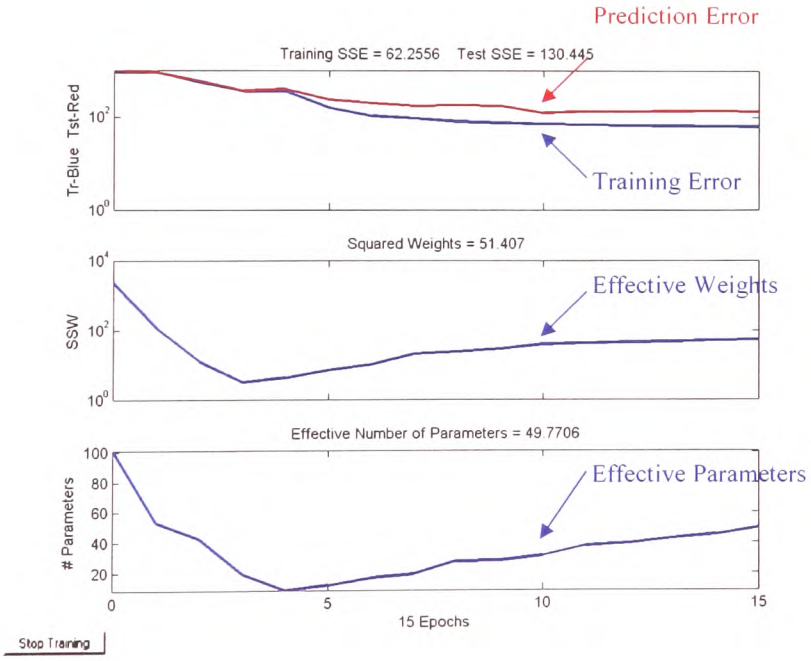

Figure 5.4 Early Stopping in Matlab™

5.5.1 Predictions of NOx, CO and O_2 for Daw Mill test data at Swirl Number 0.3

A feedforward MLP network was used for modelling the NOx, CO and O_2. *The Mean Error (ME) (i.e., square root of Mean Square Error) for each simulation test was calculated and used as a benchmark as to how the system performed.* Six separate figures corresponding to the 6 different ways in which the features were combined was plotted in Figure 5.5 (a). Also, the MEs were presented as bar charts in Figure 5.5.

For simulations 1.1 to 1.6, the first half of the data set was for training and the other half (the unseen data) for validation. Reasonable predictions, except in simulation 1.3 for the AE features which has an increased, ME of 73 ppm. The reduced predictive capabilities with the insufficient AE signal in predicting NOx was probably affected by reduced turbulent combustion conditions with the lower swirl number of 0.3.

Figure 5.5 (a) indicates every simulation generated slightly different results. The trained model of the IR features in simulation 1.1 predicts both the periodic oscillation and underlying signal trend, as this led to an increased ME when compared with simulation 1.2 of the microphone features. In addition, simulations 1.4, 1.5, and 1.6 corresponding to all sensor features, the 3 most highly correlated and the visually inspected features have MEs of less than 54 ppm. This suggests that the use of combined features that depended on more than one sensor data stream could deliver better prediction accuracy.

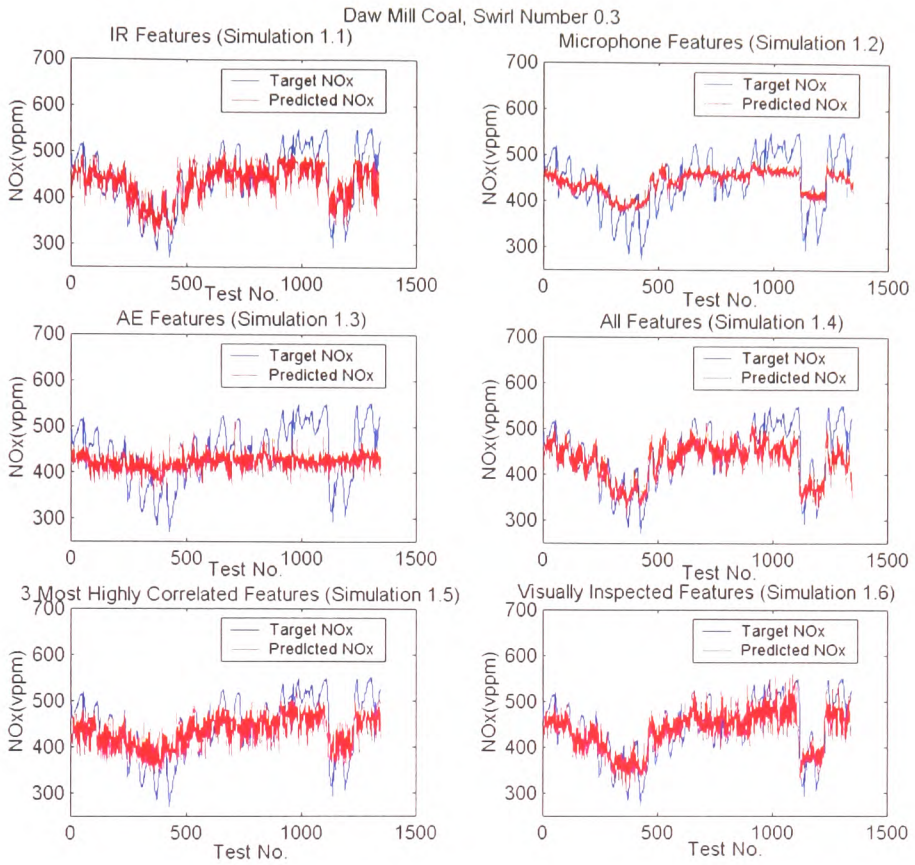

Figure 5.5 (a) Simulations 1.1 to 1.6

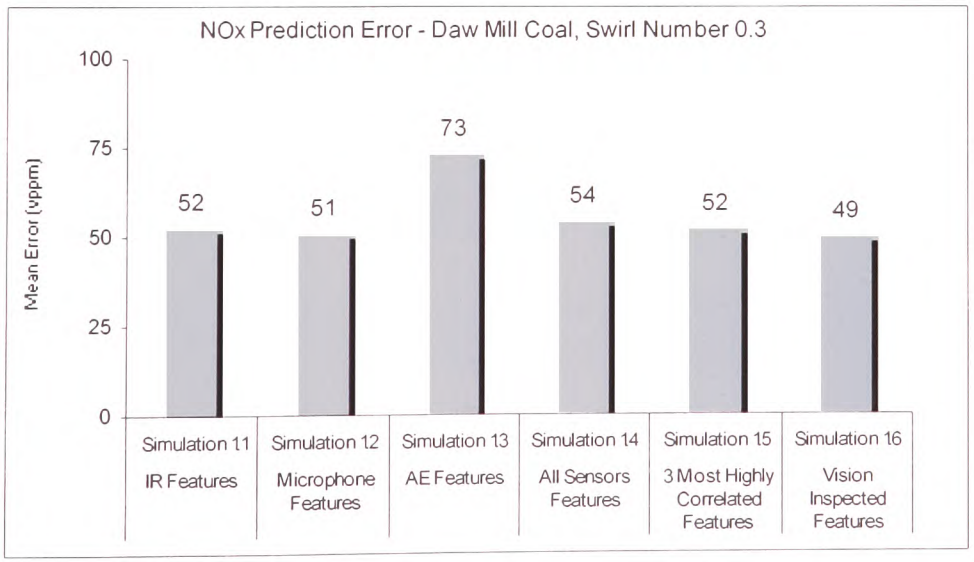

Figure 5.5 (b) Mean Errors for Simulations 1.1 to 1.6

For the prediction of CO, the first 400 data points were used for training with the rest being used for validation. The idea was to make sure the data used for training and validation covered the entire gas range being modelled. All simulations achieved acceptable predictions of MEs less than 67 ppm, except simulations 1.9 and 1.11 corresponding to AE and the 3 most highly correlated features which have increased MEs of 75 ppm.

In Figure 5.6 (a), there are large excursions in the CO readings between the data points 300 and 500. The transient in the CO resulted in localised signal deviations that led to significant errors. This applied to all 6 cases of Figure 5.6 (a). One possible explanation would be that the trained model of IR features (simulation 1.7) is that the trained IR model was capable of representing CO much better than any other simulations in Figure 5.6 (a). This finding is probably due to a constant flame radiation particularly with a lower swirl setting which yielded a more reliable signal. To operate a burner with a lower swirl condition, however, resulted in a less turbulent combustion condition and consequently reduced pressure fluctuations. Therefore, the insufficient AE signal prevented the trained model to predict gas CO as in simulation 1.9.

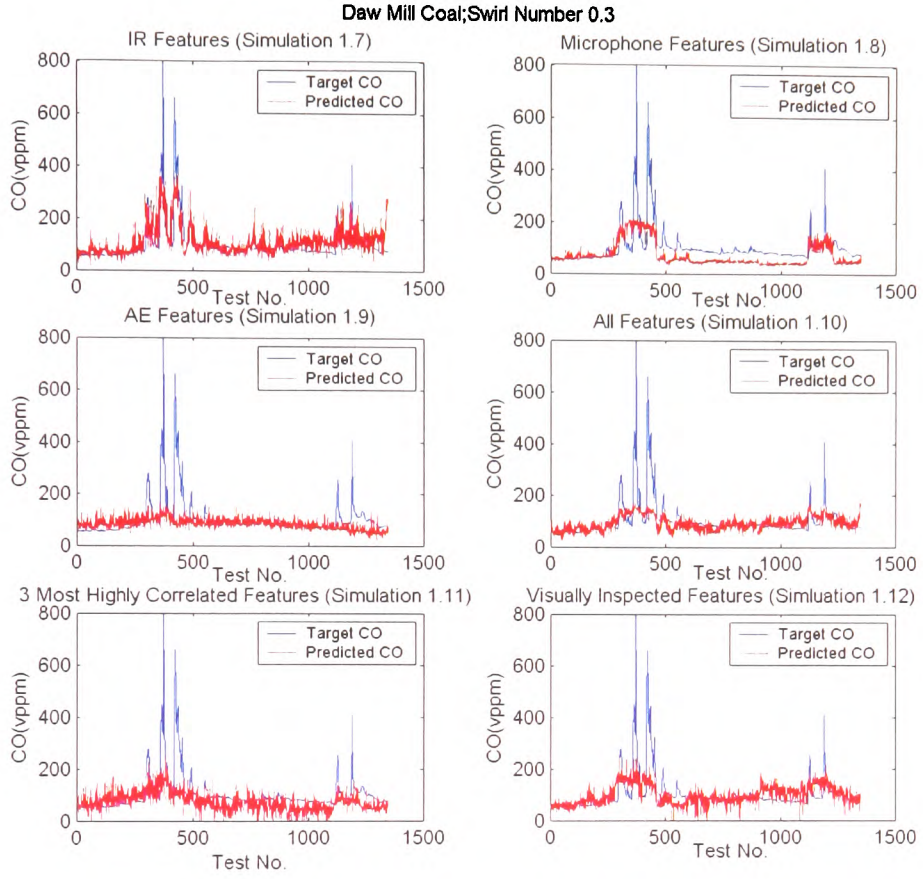

Figure 5.6 (a) Simulations 1.7 and 1.12

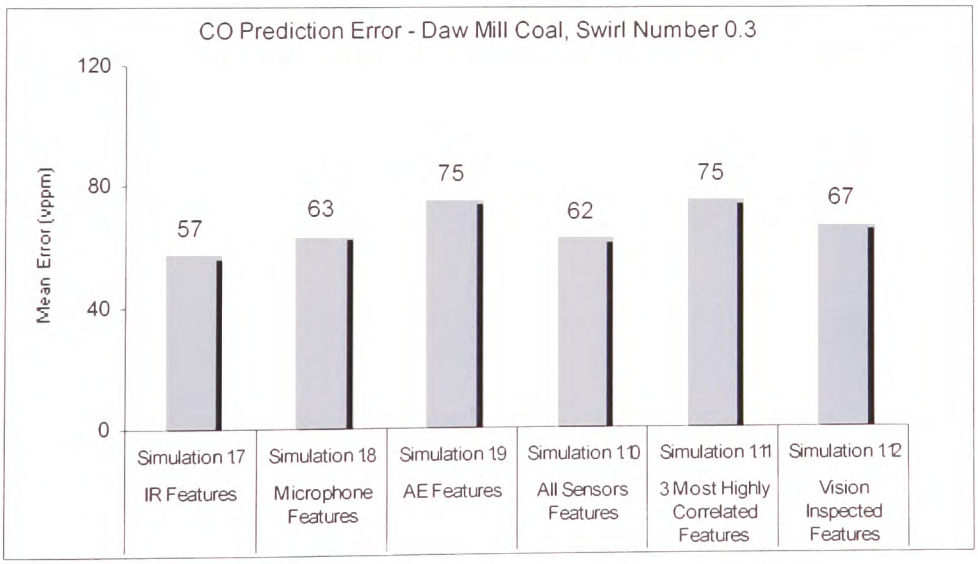

Figure 5.6 (b) Mean Errors for Simulations 1.7 to 1.12

For the O_2 simulation, half of the data were used to train a network model with another half for validation. The fluctuation in the O_2 results from the slightly uneven fuel supply that potentially led to an increased ME. *One should take note that because O_2 appears as a percentage (%) so the corresponding ME of O_2 must also be presented as the percentage error.*

Simulation 1.13 demonstrates the IR features offered sufficient indication to predict both the periodic oscillations and the underlying O_2 signal. This assumption has been made with a belief that the IR was better than the microphone, or AE sensor in predicting O_2. This assertion is in agreement with the previous test results that involved both NOx and CO. The poor AE response, on the other hand, probably resulted from a more stable combustion condition led to no signal. The use of combined features from different sensor data streams, on the contrary, has improved the prediction efficiency.

It was learned that a relatively large signal oscillation in the O_2 resulted in increased MEs for all 6 cases (Figure 5.7 (a)). The fluctuations in the signal were purely a disturbance that is of no use in the process monitoring.

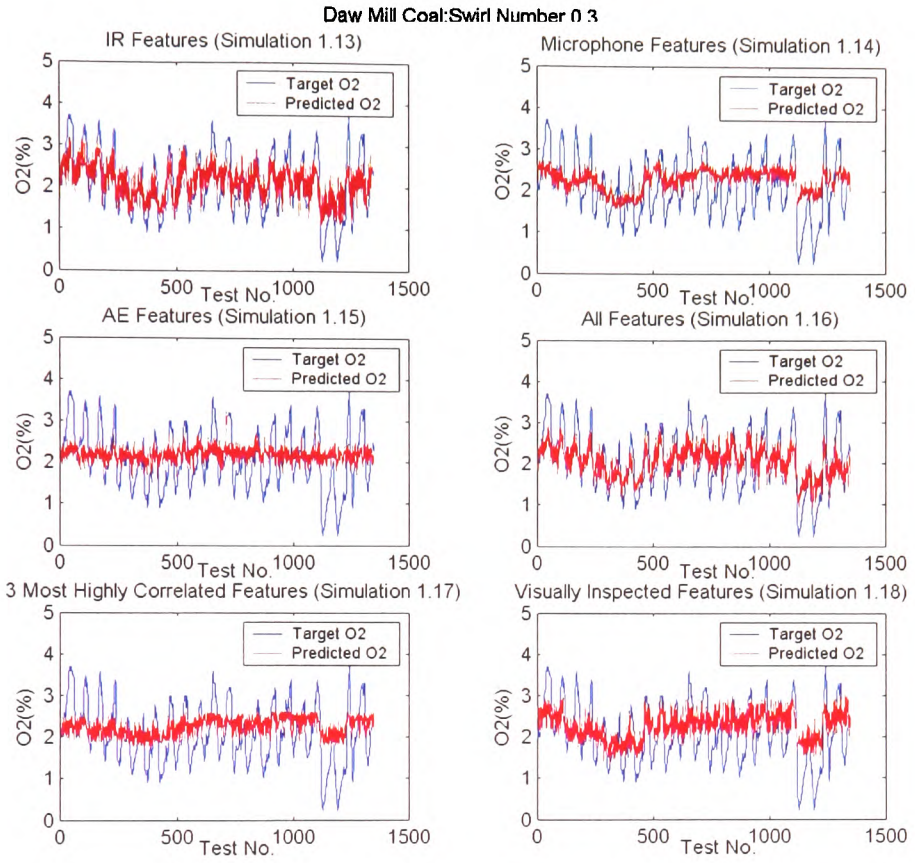

Figure 5.7 (a) Simulations 1.13 to 1.18

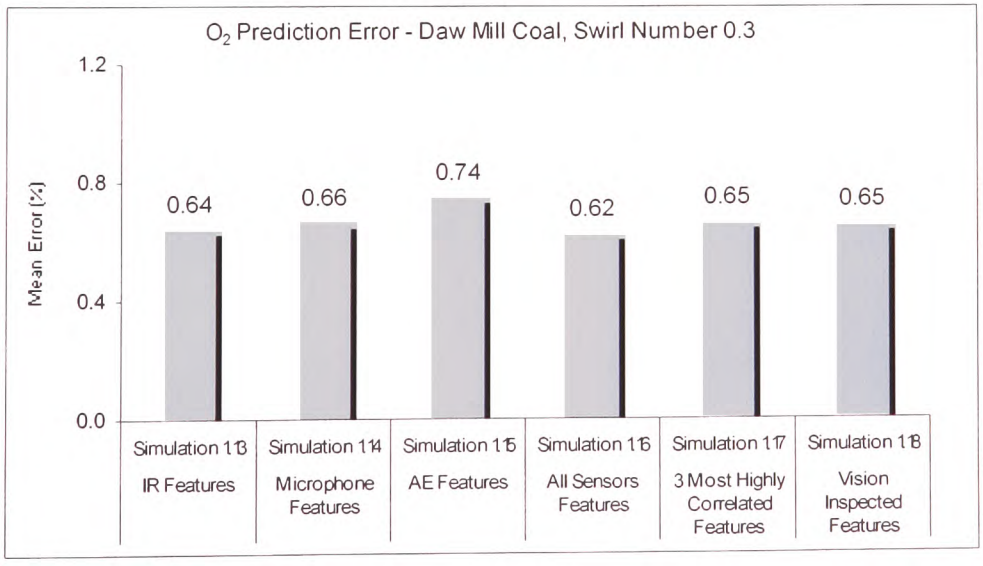

Figure 5.7 (b) Mean Errors for Simulations 1.13 to 1.18

5.5.2 Simulations of NOx, CO and O_2 of Daw Mill Coal at Swirl Number 0.5

For the Daw Mill test with a swirl number of 0.5, the first half of the data set was used to train the ANN followed by validating the model with the remaining data. The trained NOx models corresponding to simulation 2.1, 2.5, and 2.6 of the IR and 3 most highly correlated and the visually inspected features yielded MEs of less than 74 ppm. This suggests the trained IR could be better than the microphone or AE models with a lower swirl number of 0.5, and, the combined features offered better model prediction.

One major finding in Figure 5.8 (a) is that the NOx did not appear to be consistent when subject to the same secondary airflow rate at the beginning and somewhere towards the end in all 6 cases. Such signal deviations could have resulted from variations in the flame signature that was affected by factors such as the coal size distribution and moisture content. Also the predictions made by the trained model of the microphone features in simulation 2.2 have MEs as high as 104 ppm. These signal deviations, however, were affected by factors such as slight changes in the coal properties, or the noise generated by the suction pump when refilling the coal feeder.

Some green circles were added to indicate the location of errors that made significant contribution to the overall MEs of Figure 5.8 (a). In addition, to operate the burner with a low swirl number of 0.5 appears to result in a stable combustion condition and consequently diminished the AE signal that then yielded no prediction (simulation 2.3).

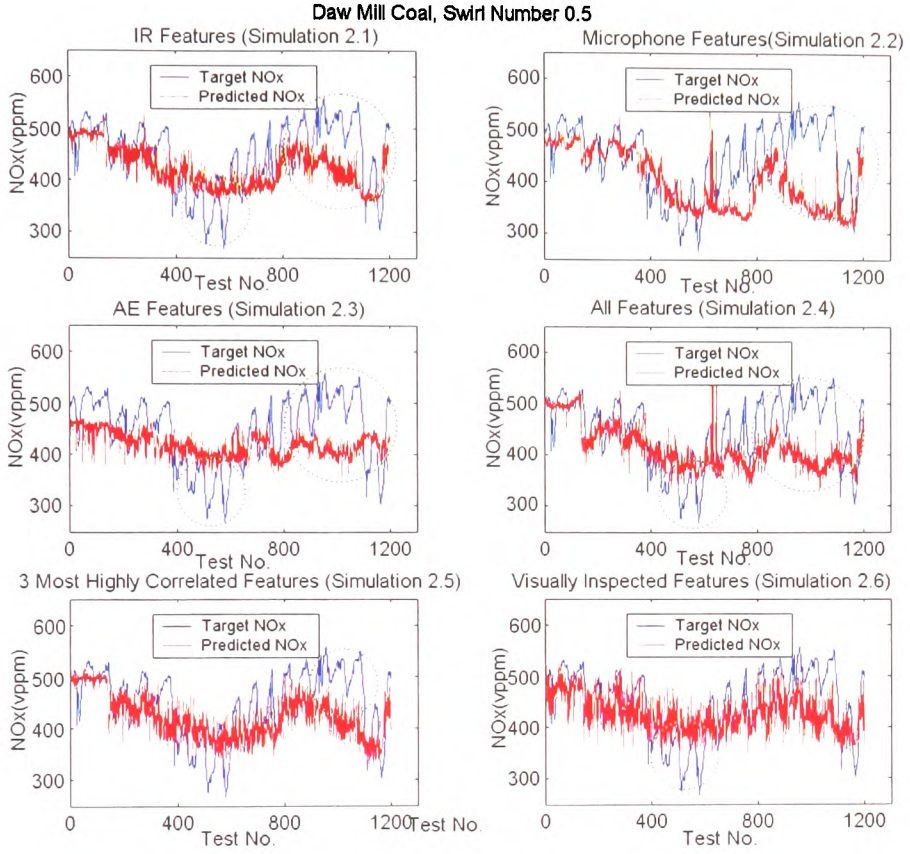

Figure 5.8 (a) Simulations 2.1 to 2.6

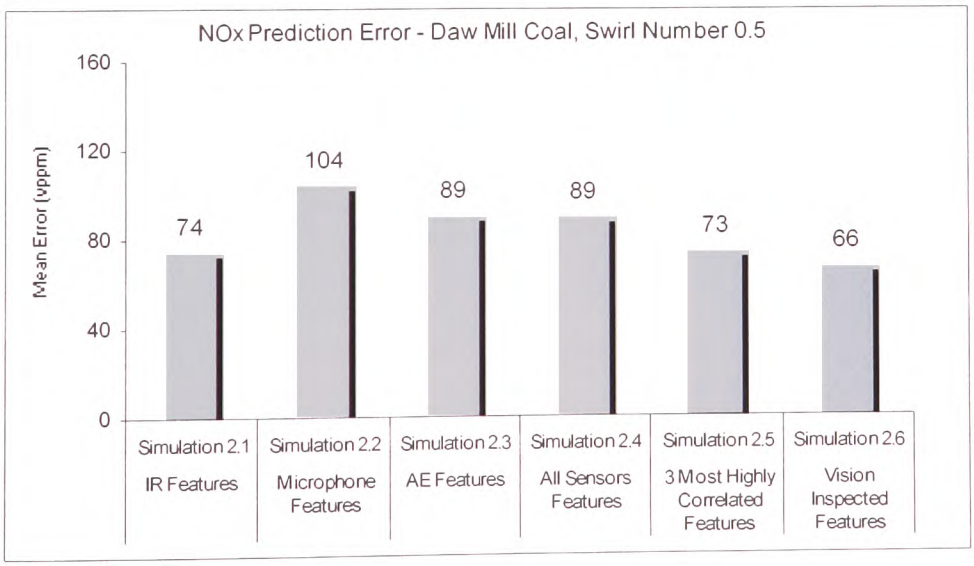

Figure 5.8 (b) Mean Errors for Simulations 2.1 to 2.6

The CO model with a swirl number of 0.5 was trained and validated in a similar way to the NOx model. All 6 simulations showed somewhat consistent in terms of ME calculated. The extremely poor predictions resulted from the set of features that failed to match the change in the gaseous CO (noticeable between the data points 400 and 700) were found in Figure 5.9 (a).

The unsuccessful prediction in simulation 2.9 was due to missing AE signal. Perhaps homogeneity in the combustion condition did not generate significant AE for the neural network. Besides, the wrongly chosen features, in simulation 2.12, have resulted in no prediction at all. One should pay attention to the unsuccessful predictions in simulations 2.9 and 2.12 of the AE and visually inspected features, which have MEs as low as 82 and 80 ppm when compared to other simulations. Such a misleading error for simulations 2.9 and 2.12 demonstrates the need to check visually the target and prediction signals in addition to calculating the prediction errors.

Unfortunately, Figure 5.9 (a) demonstrates a very weak correlation. However, one may consider using CO models as an indicator to which "relative" rather than "absolute" information is of more importance.

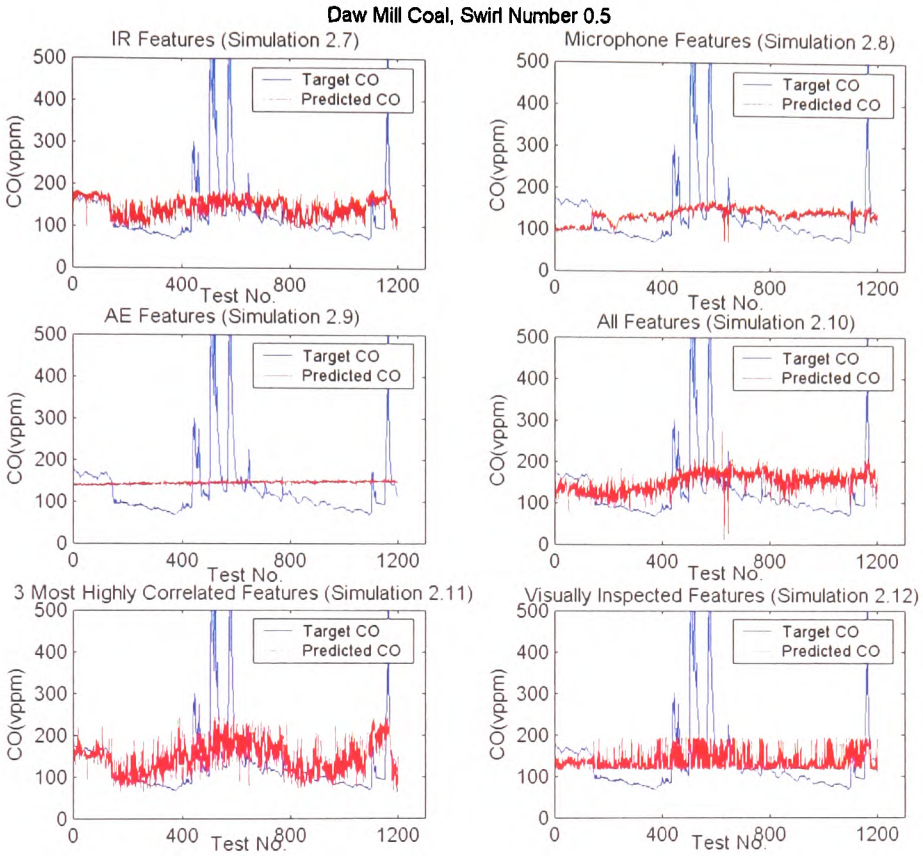

Figure 5.9 (a) Simulations 2.7 to 2.12

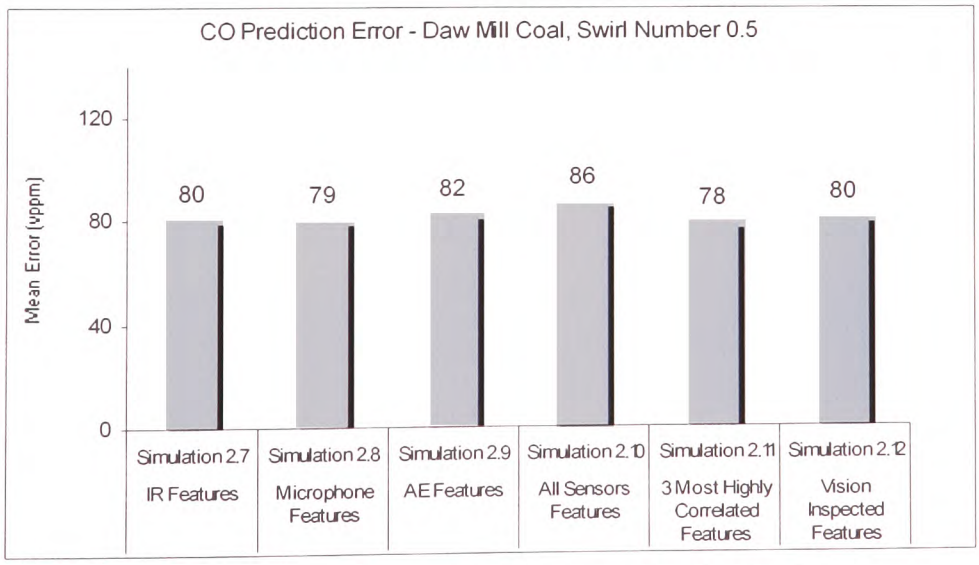

Figure 5.9 (b) Mean Errors for Simulations 2.7 to 2.12

In the prediction of O_2, the data that was used to train NOx and CO were adopted for training the O_2 model. It can be observed that simulations 2.13, 2.17, and 2.18 (the IR, 3 most highly correlated and visually inspected features) have lower MEs of 0.72, 0.74, and 0.74 % respectively. This indicates the trained model of the IR outperformed the microphone or AE features, even though the predictions loosely followed the gas O_2.

As O_2 was consistent with the same secondary airflow rate in simulation 2.14, the error for the trained model of the microphone features probably resulted from additional noise sources, for example, an audible sound generated by the suction pump when refilling the coal feeder. The deviations in the target and prediction signals corresponding to simulation 2.14 were highlighted.

Unlike the trained AE model with a swirl number of 0.5 in predicting both NOx and CO in simulations 2.3 and 2.9 a smaller O_2 response has allowed the trained model of the AE features to predict the gas O_2 (simulation 2.15). This implies that the predictable condition using a trained AE model resulted from either the increased swirl setting hence a greater signal, or due to a smaller O_2 response, or both.

Simulations 2.17 and 2.18 of 3 most highly correlated and the visually inspected features have reasonable predictions. The improve predictions almost certainly resulted from a larger data dimension and effectively better network inference. In addition, the oscillation in the signal O_2 in Figure 5.20 suggests these models were trained only to recognise the underlying O_2 signal trend.

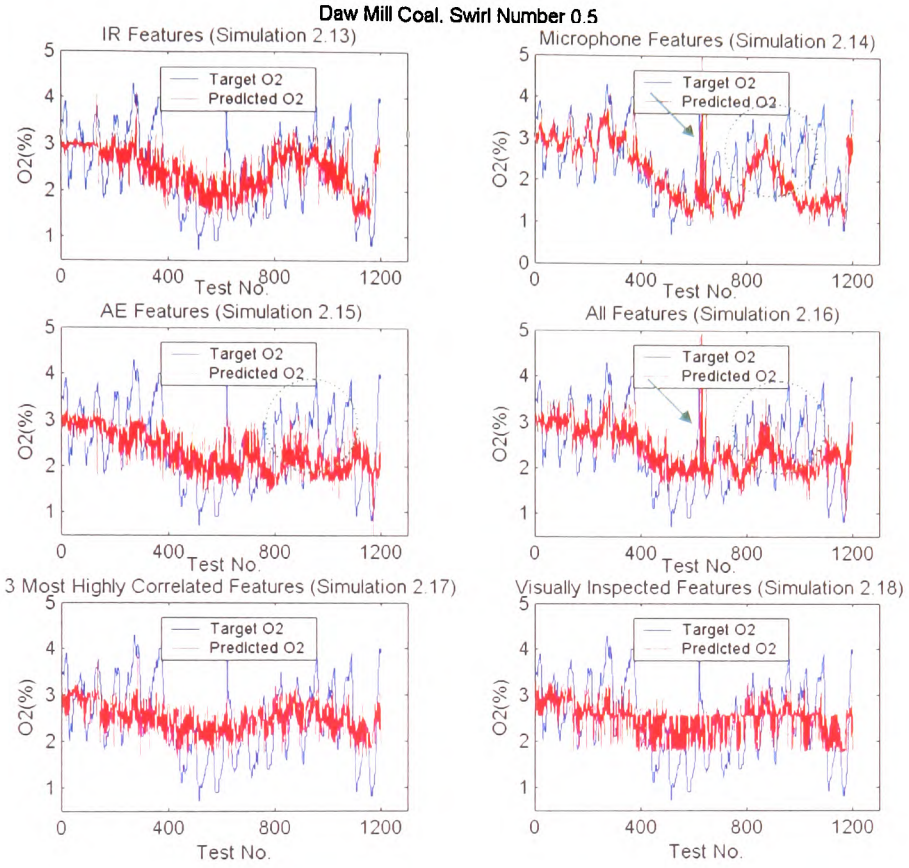

Figure 5.10 (a) Simulations 2.13 to 2.18

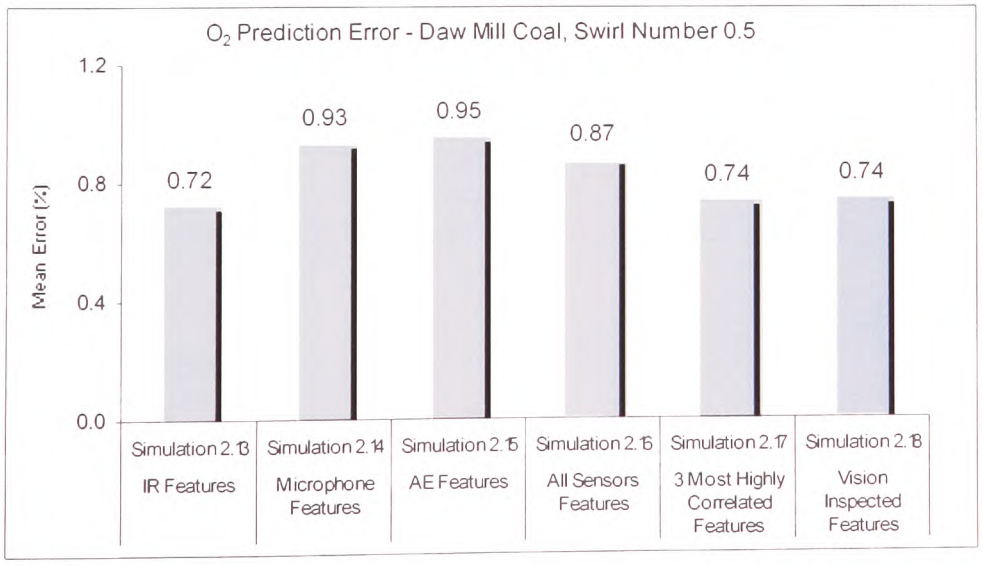

Figure 5.10 (b) Mean Errors of Simulations 2.13 to 2.18

5.5.3 Simulations of NOx, CO and O_2 for Daw Mill Coal at Swirl Number 0.8

In the simulations where Daw Mill test data for a swirl number of 0.8 was used, the first 800 data points were for training with the rest for validation. This arrangement applied to all 3 models in response to NOx, CO and O_2. Simulations 3.1, 3.4, 3.5 and 3.6 (the IR, all sensor features, 3 most highly correlated and the visually inspected features) (Figure 5.11 (a)) achieved reasonable prediction with MEs of less than 30 ppm.

The signal deviations in simulation 3.2 of the microphone features (as highlighted) were thought to be affected by additional noise sources. This is unlikely to happen in any practical boiler as the auxiliary plants, for example, the forced draft fan and suction pump usually placed many meters away from the main boiler. For a swirl number of 0.8 the model trained with the AE features matched he actual NOx for the first 900 data points. However, the remaining data is not predicted as well which perhaps resulted from small changes in the airflow setting.

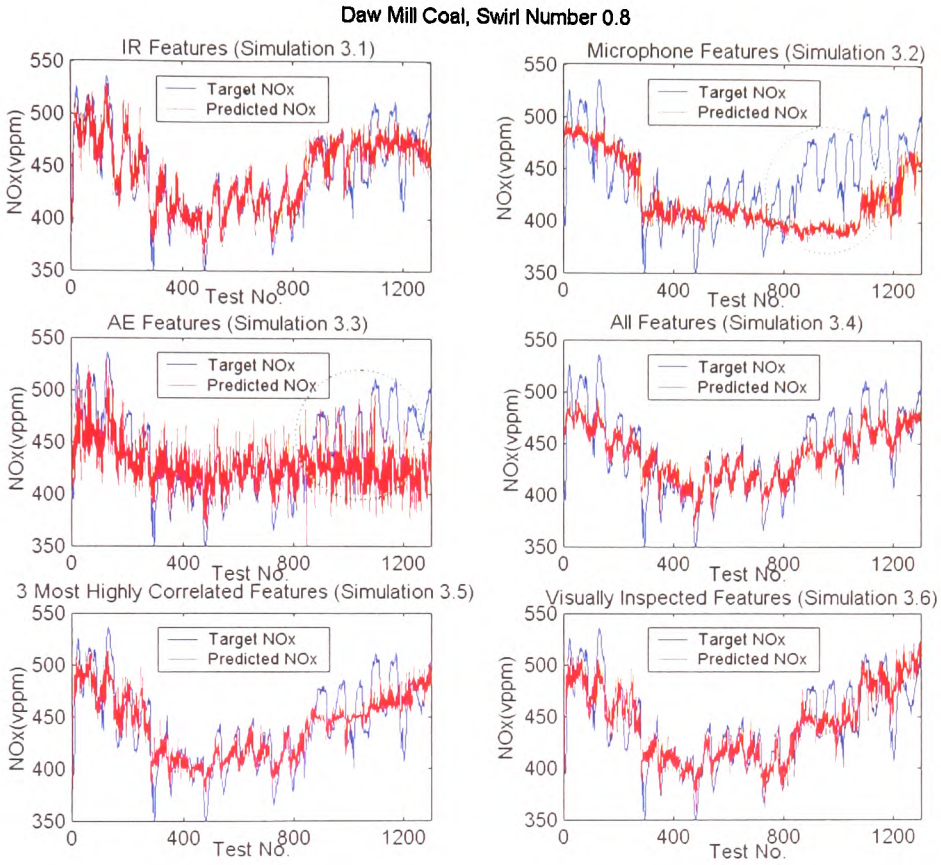

Figure 5.11 (a) Simulations 3.1 to 3.6

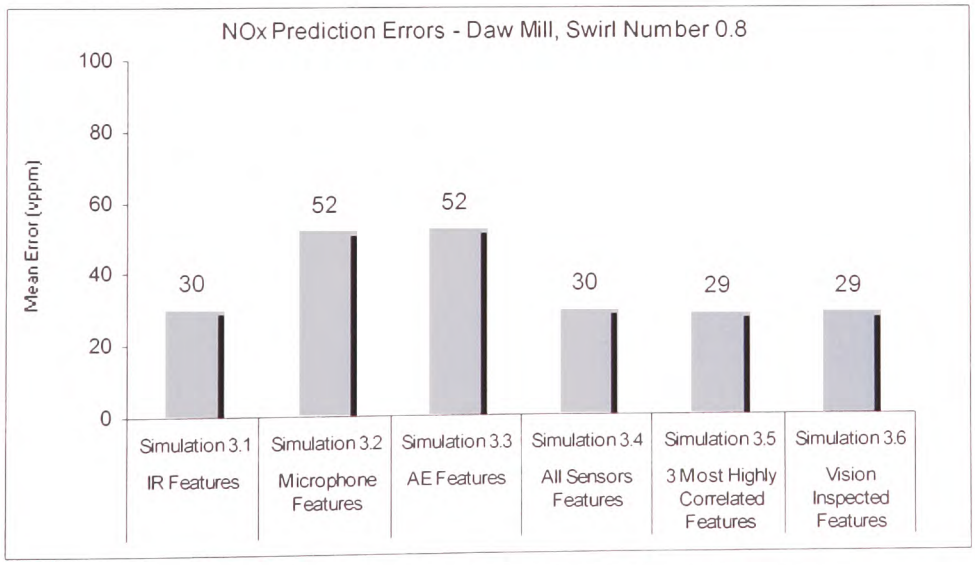

Figure 5.11 (b) Mean Errors for Simulations 3.1 to 3.6

For the predictions of CO, the overall MEs were reasonably low (< 30 ppm) (Figure 5.12 (b)). Such a promising simulation result benefited from CO with no large excursions. The increased error in simulation 3.8 of the microphone features, on the other hand, resulted from unexpected noise sources. This judgment was made with a reason that no such signal interference was found in both simulations 3.7 and 3.9 of the IR and AE features. In addition, simulations 3.10, 3.11, and 3.12 suggest better predictions could be obtained when using combined sensor features.

One remarkable finding in monitoring gas CO is concerned with the problem where the CO levels were different when subject to the same secondary airflow rate. The drifting in the CO gas analysis was probably due to some considerable unburned carbon in the fly ash settled around the gas sampling point after a prolonged period of operation. One way to alleviate this problem is to purge the CO sampling point with compressed air on a regular basis. However, this existing feature in the burner was disabled as the introduction of an air purge scheme led to an incursion of O_2 and subsequently incorrect gas readings owing to dilution. Such inconsistency in the CO readings, therefore, refers to inaccuracies in the gas analyser.

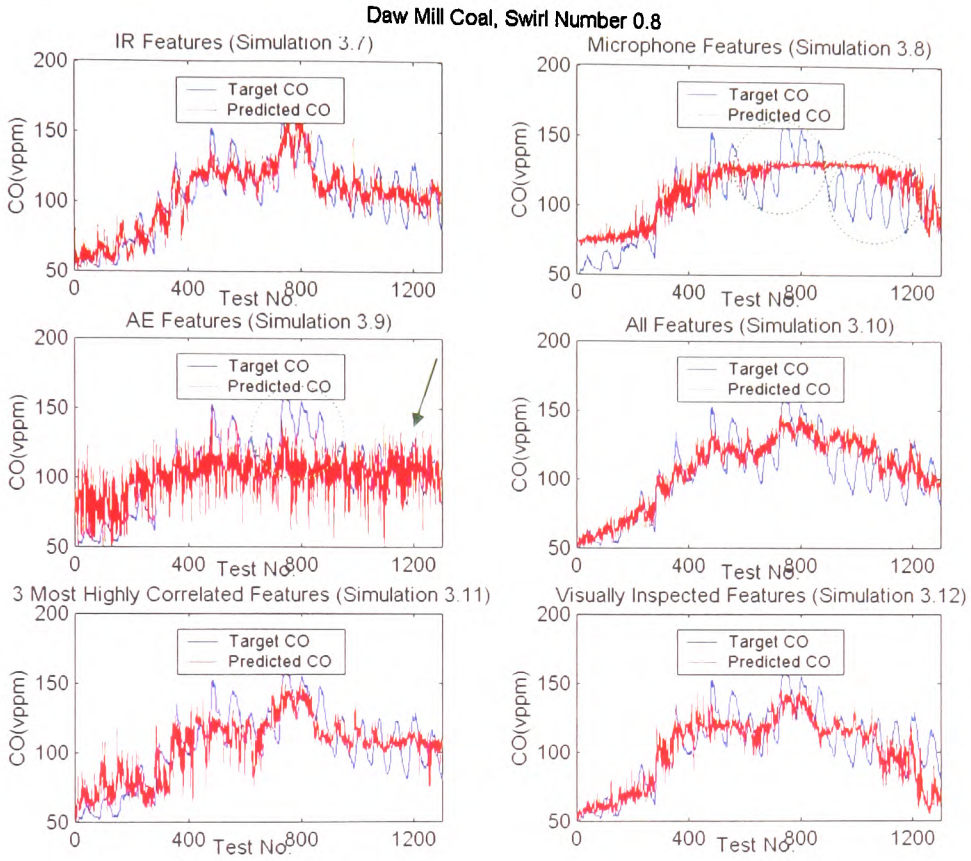

Figure 5.12 (a) Simulations 3.7 to 3.12

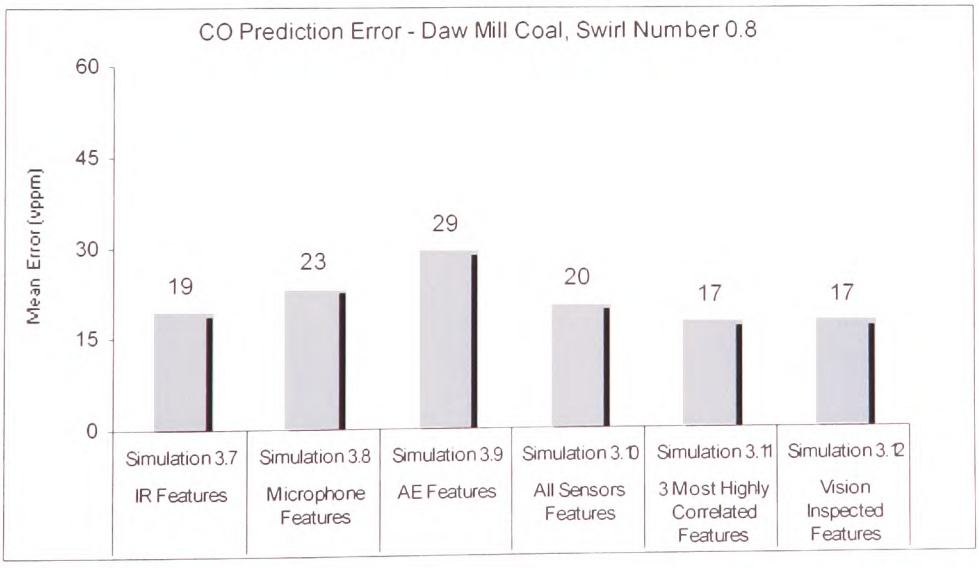

Figure 5.12 (b) Mean Errors for Simulations 3.7 to 3.12

It is felt that in Figure 5.13 (a), reasonable predictions were achieved, except simulation 3.13 and 3.15 of the IR and AE features. The high ME with the trained model of the IR features in simulation 3.13 resulted from an "offset" between the predicted and target O_2 as highlighted with a green circle. This offset in the readings could be due to an inaccuracy in the gas analyser readings due to the fact the secondary airflow rate was the same at the beginning and the end of the simulation. For this condition, however, the microphone features results in an excellent prediction therefore, there must be an aspect of the microphone features that has matched the O_2 signal.

The increase error in simulation 3.15, on the other hand, shows AE features were unable to predict gas O_2. This refers to insufficient AE signal that resulted from a steady combustion condition. One should also pay attention to low MEs in simulations 3.16, 3.17, and 3.18 in which the combined features have persistently improved model prediction accuracy.

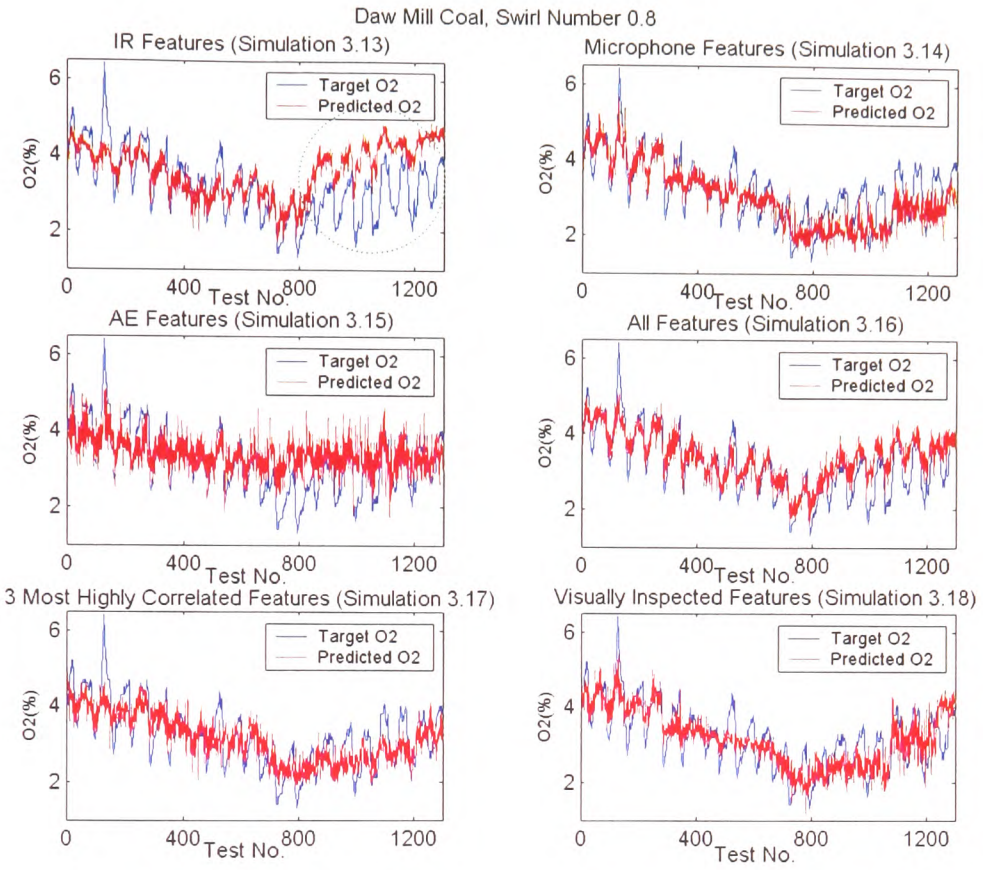

Figure 5.13 (a) Simulations 3.13 to 3.18

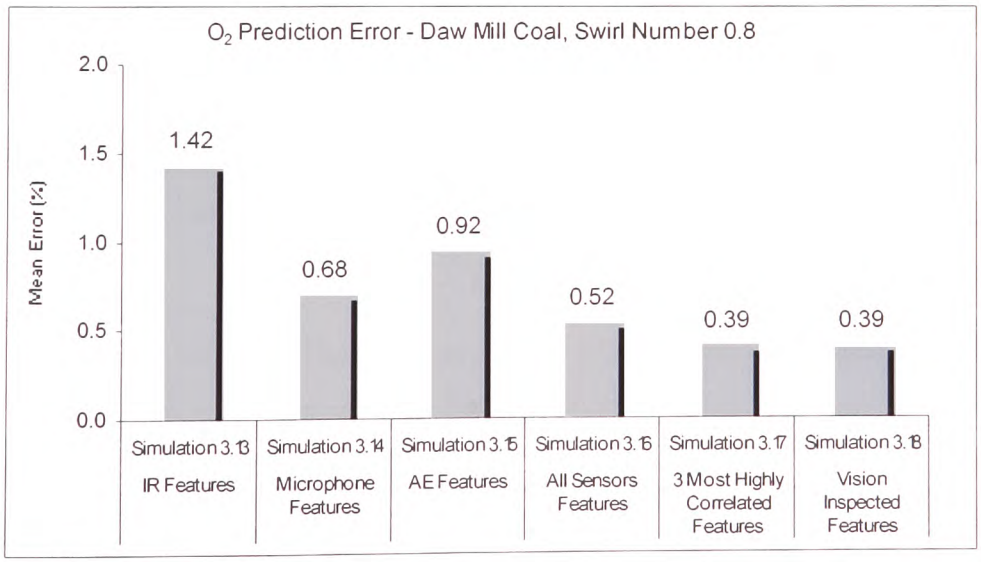

Figure 5.13 (b) Mean Errors for Simulations 3.13 to 3.18

5.5.4 Simulations of NOx, CO and O_2 for Daw Mill Coal at Swirl Number 1.2

Figure 5.14 illustrates a problem of monitoring CO which when subject to the same secondary airflow rate (i.e., 150 m^3/h) different CO values were recorded at the beginning and end of the test. The implication being that a model trained with the first half of the CO data and validated with second half would have predicted values corresponding to the first half. This result in signal deviations when the prediction, corresponding to the beginning, was presented against the target CO of the second half of Figure 5.14. To avoid this, the CO model was trained and validated using even and odd number data from the same data set and the same procedure applied to all three models in response to NOx, CO and O_2. One may realise a high CO concentration has saturated the gas analyser so that the prediction made by using this data set has maximum predictions of a 1000 ppm, which can be considered to be a high reading.

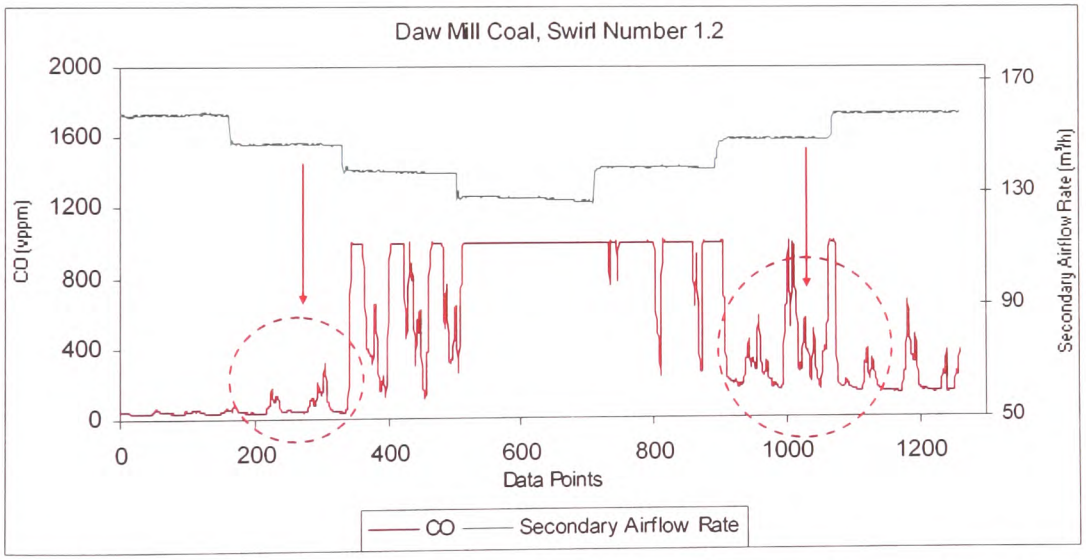

Figure 5.14 The "off-set" effect happened to CO when subject to the same Secondary Airflow Rate of 150 m^3/h

In simulations 4.2 and 4.4, the predictions made by the microphone and all sensor features have lower MEs of 53 ppm and 55 ppm. It is felt that with a high swirl number of 1.2, the microphone features in simulation 4.2 have become dominant consequently allowing better predictions, when the trained model of microphone features and compared with the IR features. This probably resulted from increased turbulence in the combustion condition and hence greater sound intensity. In addition, the increased swirl number also led to increase structural vibrations as the AE signal was found to be driven by pressure fluctuations that were generated inside a burner.

Simulations 4.4 and 4.5 of Figure 5.15 demonstrated the advantage of using the combined features as a larger data dimension helps the neural network match the variable signal. Also, the predictions in simulation 4.6 suggest the wrongly chosen feature led to a total failure.

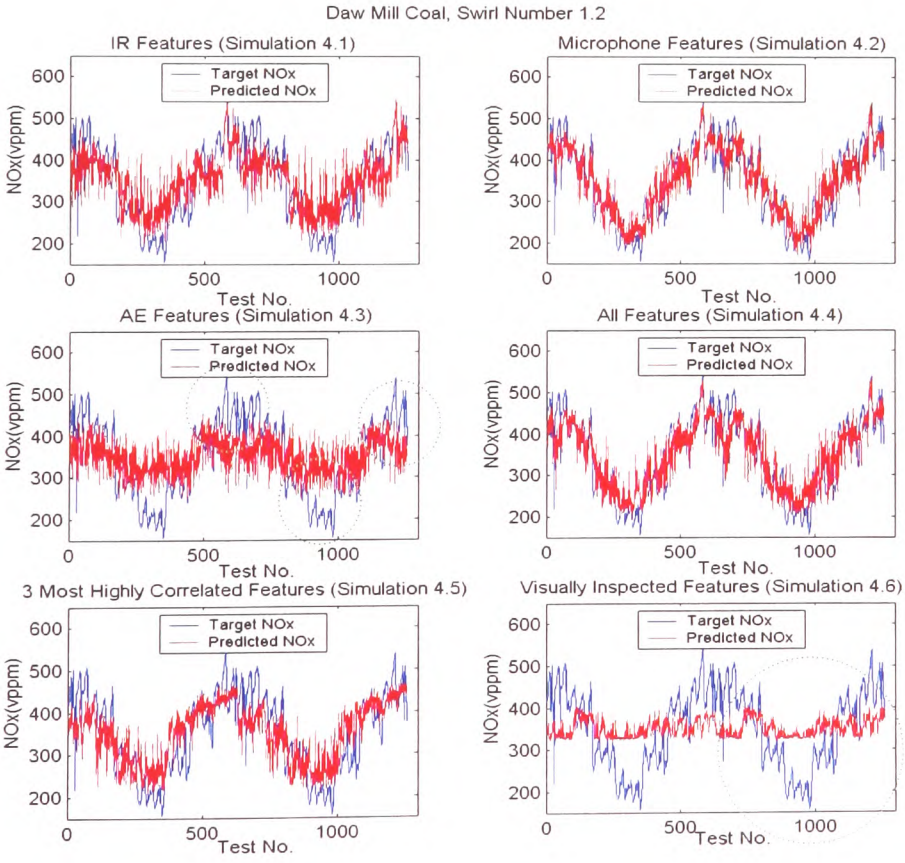

Figure 5.15 (a) Simulations 4.1 to 4.6

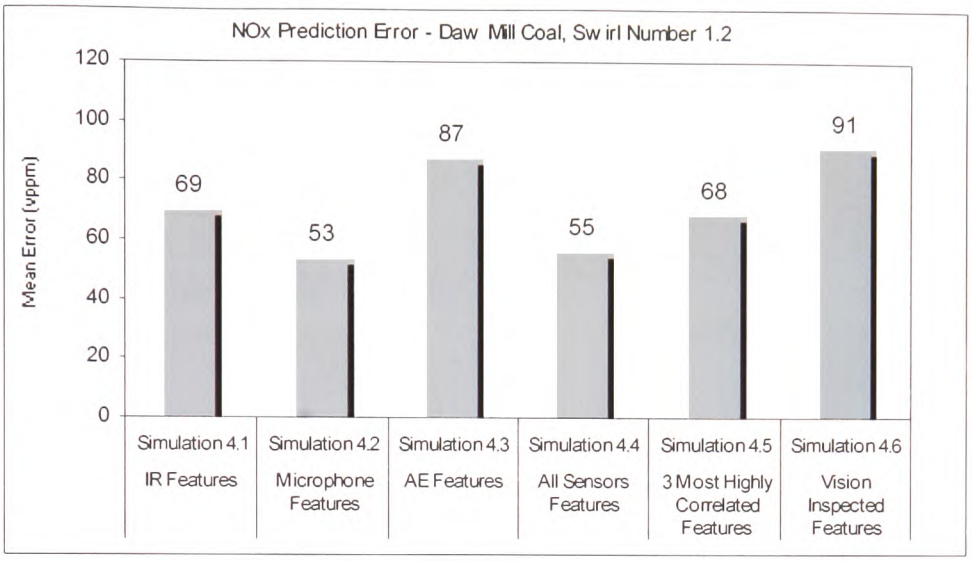

Figure 5.15 (b) Mean Error for Simulations 4.1 to 4.6

Given that the CO was found to be the most unpredicted combustion parameter, it is of very little surprise that the MEs of as high as 377 ppm (simulations 4.7 to 4.12) were found. The high MEs happened for all 6 simulations in Figure 5.16 (a) and they were in some way affected by large signal deviations that coincided with the transients in the CO.

The increased swirl number to 1.2 resulted in a higher turbulent flame consequently better sound intensity (simulation 4.8). In addition, it is felt that the increased swirl number also accompanied by the increase in the AE signal. This in turn can be observed from an improved prediction in simulation 4.9 using the trained AE model.

Finally, simulations 4.10 and 4.11 of all sensor and the 3 most highly correlated features demonstrated reasonable predictions. One may discover the network estimates are sometimes higher than the maximum training value of 1000 ppm as the network predicts "noise" in addition to the underlying signal.

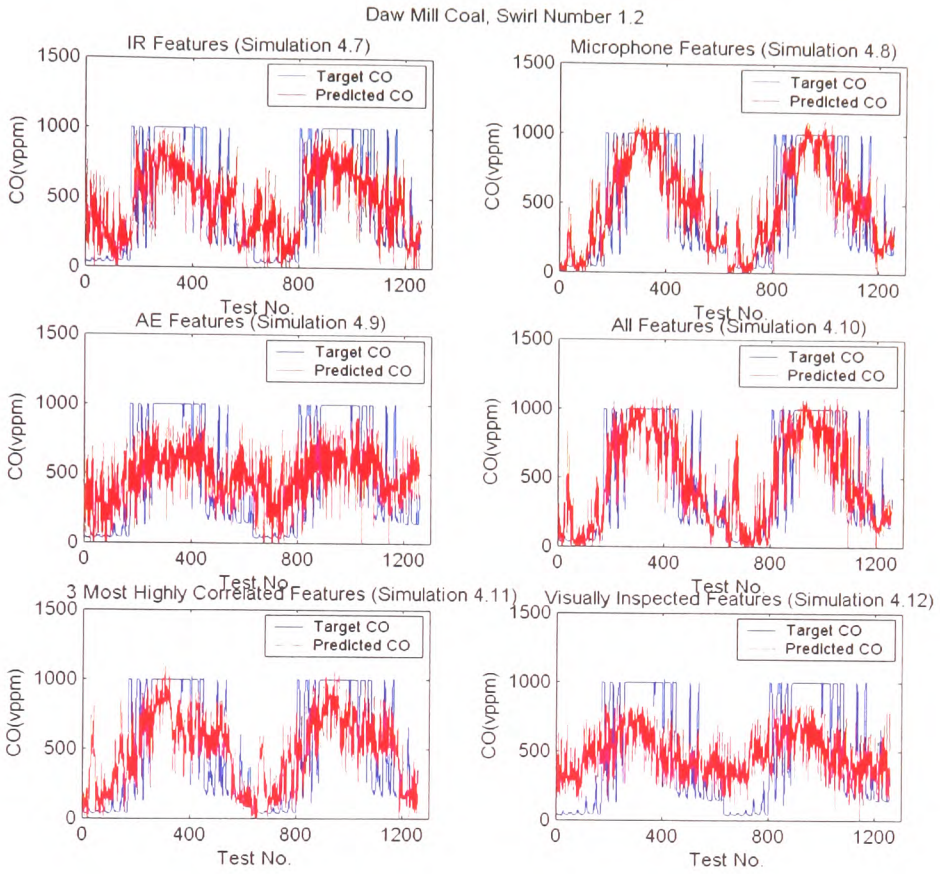

Figure 5.16 (a) Simulations 4.7 to 4.12

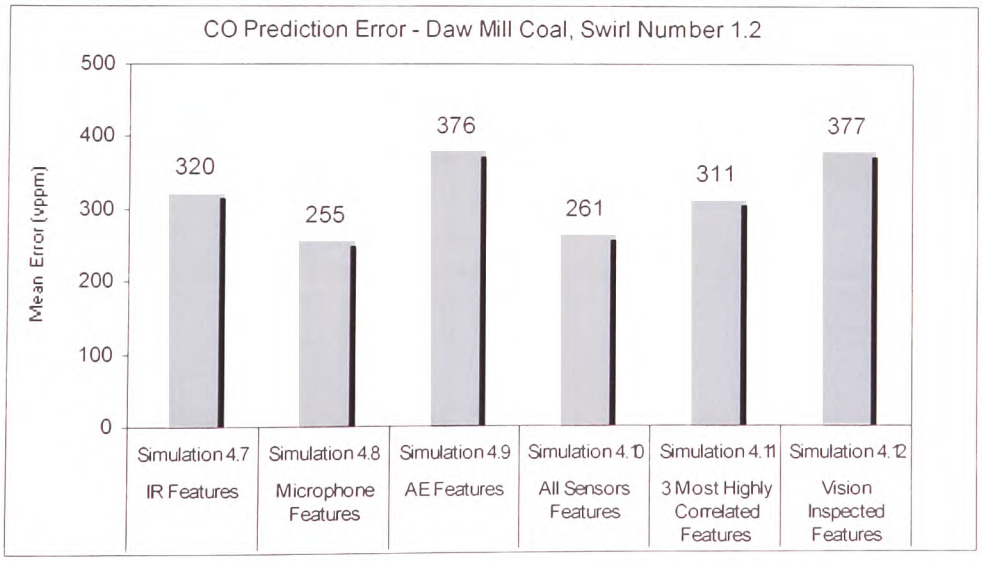

Figure 5.16 (b) Mean Errors for Simulations 4.7 to 4.12

In the predictions of O_2, simulations 4.14, 4.15 and 4.16 (the microphone, AE and all sensors features) (Figure 5.17 (a)) have reasonable MEs not more than 0.55 %. The trained model of microphone features, again, offered good prediction performance as a result of more discriminate features. In addition, simulation 4.15 shows reasonable predictions of the gas O_2 when using trained model of AE features, as this situation did not happen to other swirl numbers (i.e., 0.3, 0.5, and 0.8) where the AE features were involved.

Large signal deviations in simulations 4.17 and 4.18, as highlighted, were probably affected by the insufficient number of features being used in the modelling. Both simulations 4.17 and 4.18 used the same features for predicting O_2 and consequently this led to the same ME of 0.76 %.

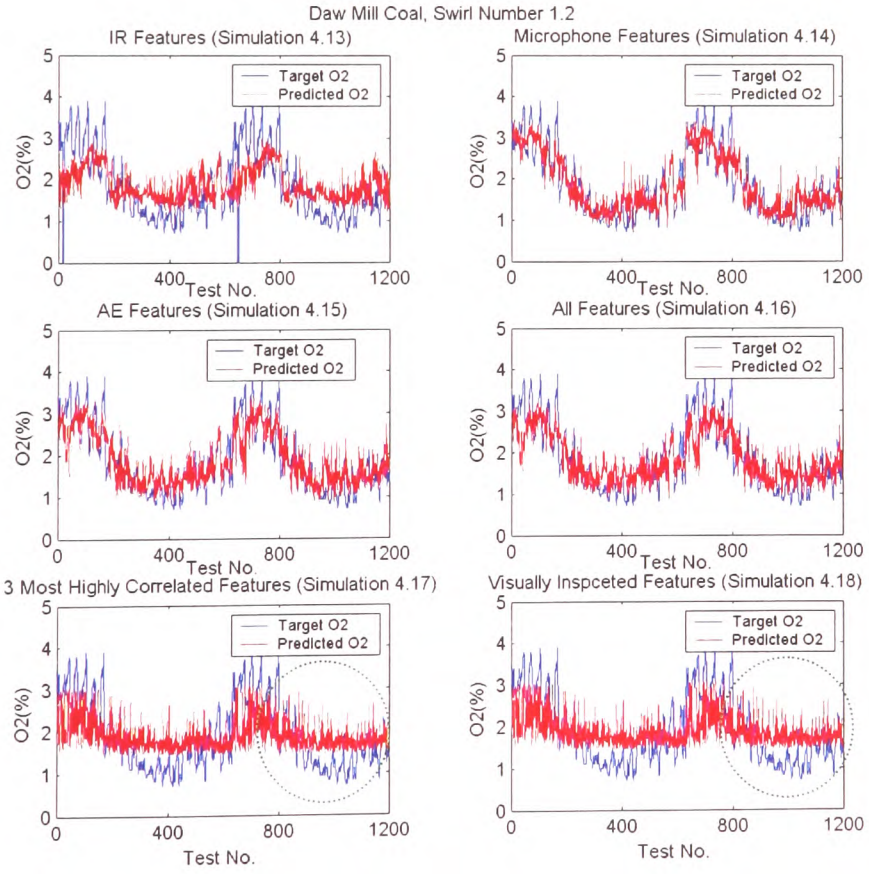

Figure 5.17 (a) Simulations 4.13 to 4.18

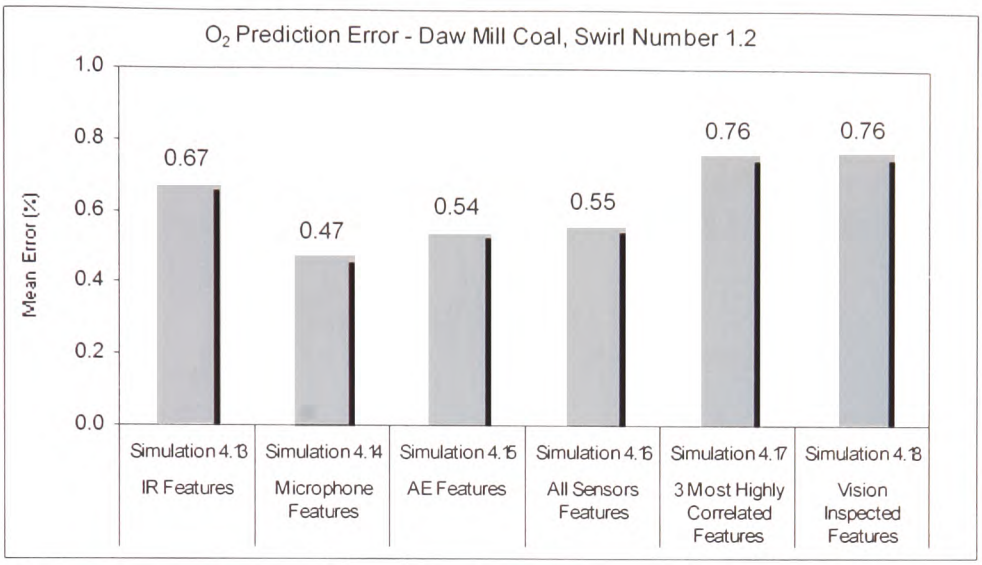

Figure 5.17 (b) Mean Error for Simulations 4.13 to 4.18

5.5.5 Simulations of NOx, CO and O_2 for Cerrejon Coal at Swirl Number 0.3

In a similar way to the result for Daw Mill coal, the Cerrejon test data were used for the prediction of the combustion gases corresponding to swirl numbers 0.3, 0.5, 0.8, and 1.2. Figure 5.18 shows that the first half of the data set does not cover the entire range of the second half of the NOx, therefore the NOx was trained using even and odd numbers of the data from the same data set. This was probably due to air leaking or changes in temperature, as the burner started cold. In addition, in order to achieve homogeneity, this arrangement was applied to CO and O_2 in the subsequent modelling events.

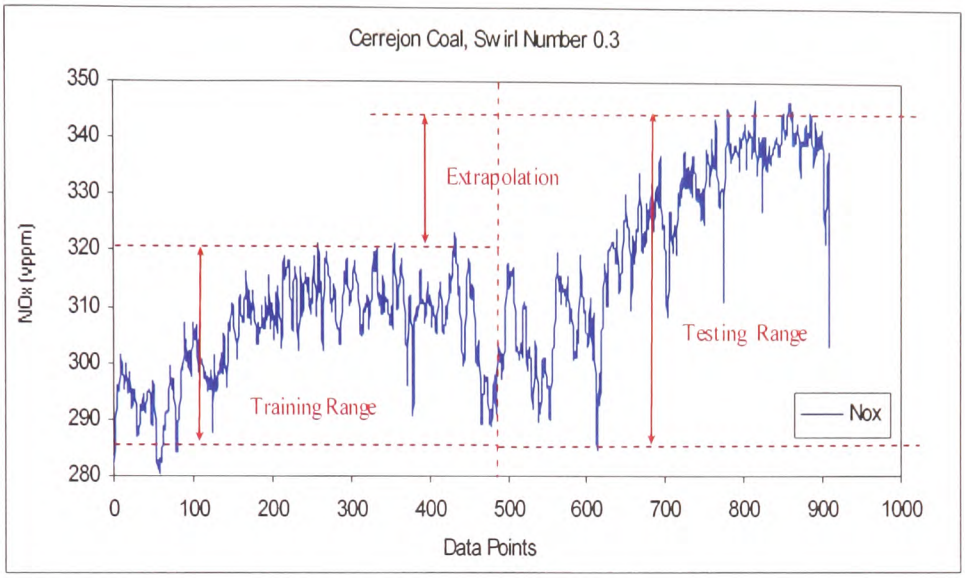

Figure 5.18 The Gaseous NOx corresponding to Cerrejon Coal., Swirl Number 0.3

Simulations 5.1 to 5.6 that involved the predictions of NOx have MEs of less then 13 ppm (Figure 5.19 (b)). It is felt that the simulations based on even and odd numbers of the data set for training and validating, have lower errors when compared to Daw Mill results simply because the odd data series is analogous to the even numbers of the same data set. One may argue that by doing this, the generalised property of the network has not been tested simply because of the similarity between the training and validation data sets. Still, they were differences between the training and validation results thus allowing the different networks to be compared. Simulations 5.2, 5.3 and 5.6 show the differences (highlighted by green arrows and circles) which appeared to both training and validation hence increasing the MEs.

It is evident that the improved microphone and AE signals occurred at higher swirl numbers. As a result, the trained model of the AE features in simulation 5.3 and with a lower swirl setting of 0.3, turned out to be the poorest out of the 6 simulation tests in Figure 5.19. Also the trained model of the IR (simulation 5.1), at a lower swirl number of 0.3, was slightly better than the microphone features in simulation 5.2. This is comparable to the simulations 1.1 and 1.2 of Daw Mill experiments. The predictions using combined features corresponding to all sensors and the 3 most highly correlated

features have low MEs. In addition, the visually inspected features technique that persistently led to poor prediction based upon human judgement must be avoided whenever is possible.

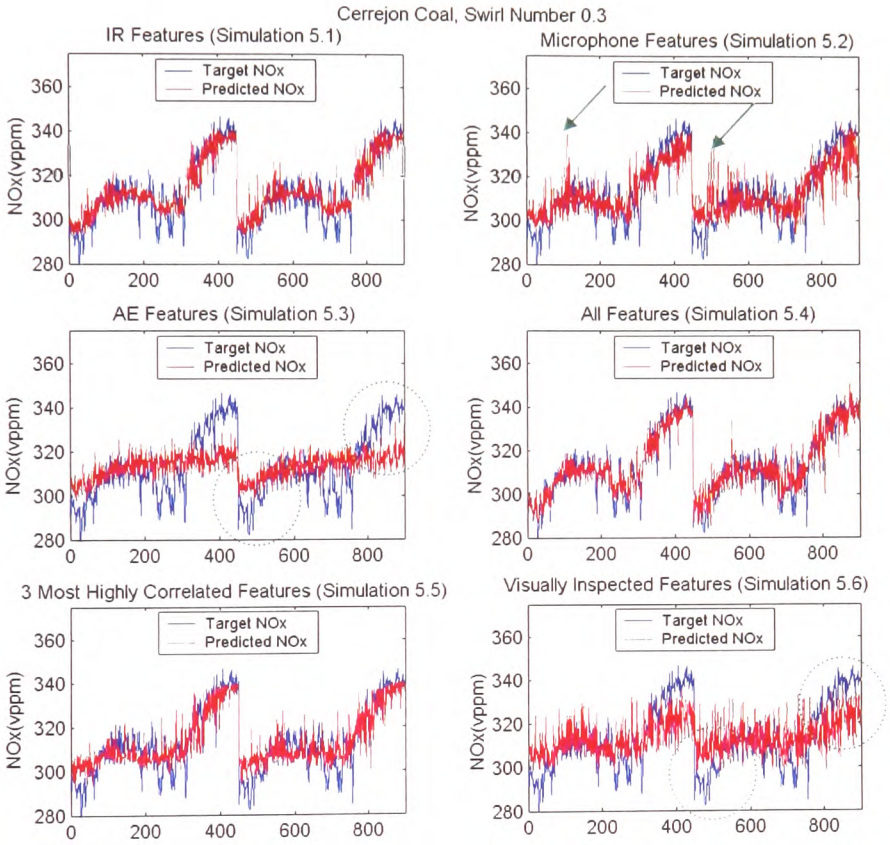

Figure 5.19 (a) Simulations 5.1 to 5.6

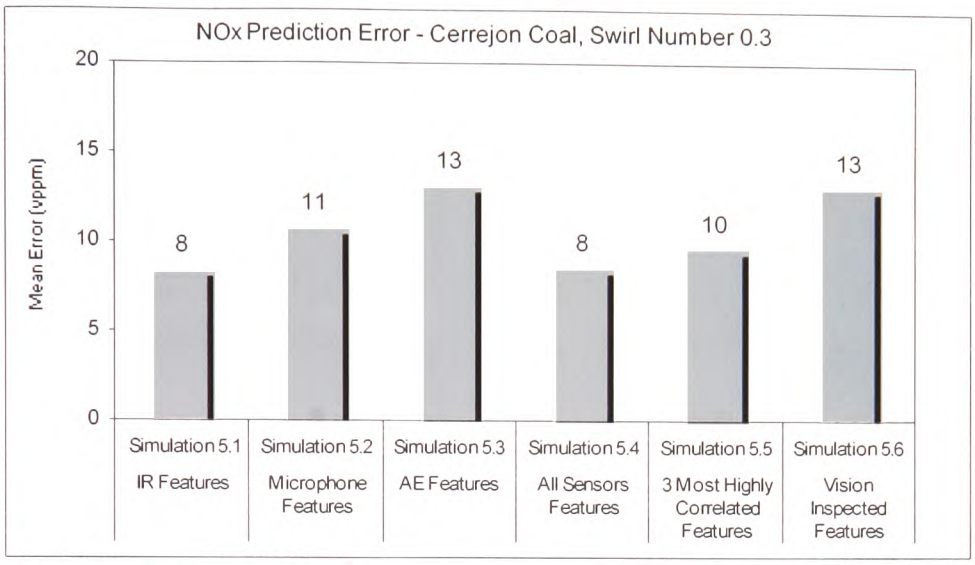

Figure 5.19 (b) Mean Errors for Simulations 5.1 to 5.6

In the prediction of CO, simulations 5.10 and 5.11 (all sensor and the 3 most highly correlated features) have MEs of less than 12 ppm. This further consolidates the idea to combine features for better predictions. Simulations 5.7 and 5.8 of both the IR and microphone features achieved relatively low MEs of no more than 23 ppm and with a view that the trained IR model was marginally better under a lower swirl condition of 0.3. From this, one may confirm a well-trained model of IR features with a low swirl setting could result from to a homogeneous flame radiation condition. In contrast, the trained model of AE features has limited representation to the gas CO particularly at the lower gas CO region. Finally, the trained model of the visual inspection technique was once again found to be the weakest.

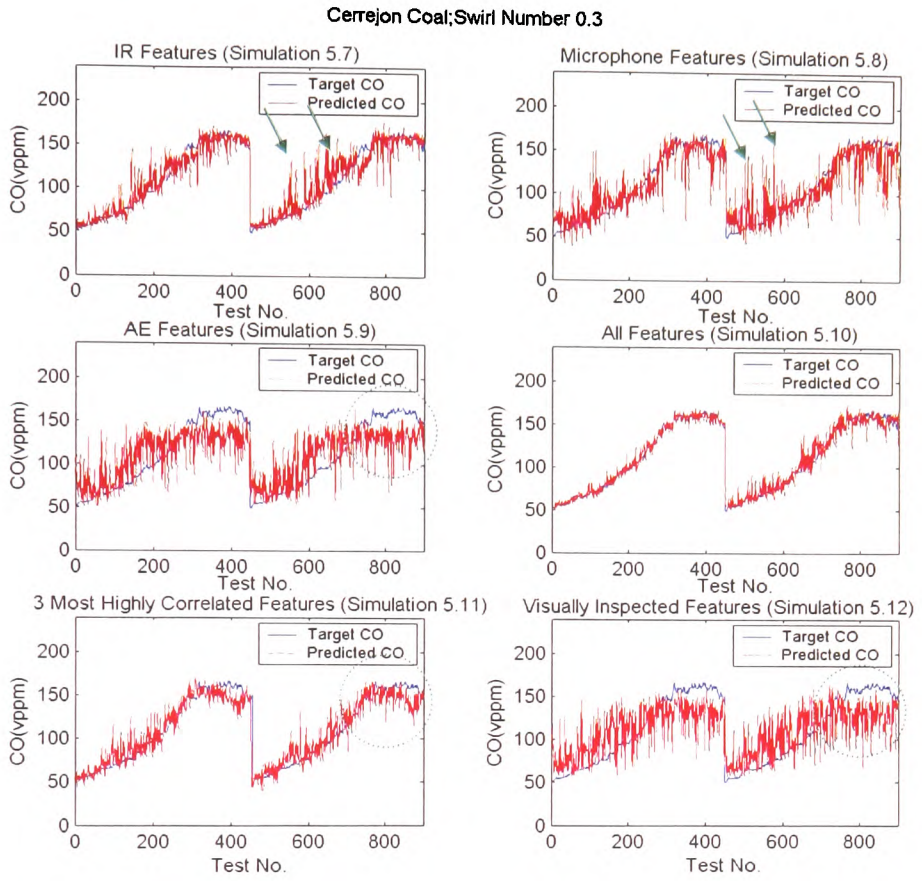

Figure 5.20 (a) Simulations 5.7 to 5.12

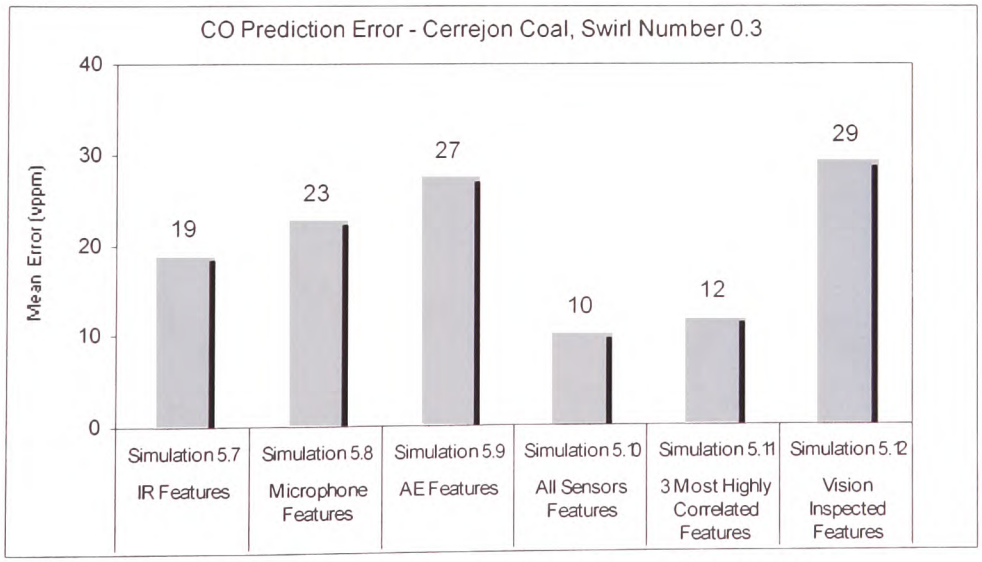

Figure 5.20 (b) Mean Error for Simulations 5.7 to 5.12

In the prediction of O_2, the simulation 5.13 of the trained model of the IR appeared to be better than the microphone features. This finding is effectively in agreement with simulations 5.1 and 5.7 involving both NOx and CO resulted from a more stable flame signal. Reasonable predictions from all sensors, 3 most highly correlated and the visually inspected features of simulations 5.16, 5.17 and 5.18, highlighted the best use of the combined features to ensure better prediction accuracy. Another remarkable discovery, which contradicted the idea where AE signal could hardly be found, when the burner operated at a lower swirl number, refers to a smaller O_2 response. This situation has allowed the trained model of the AE features to predict gas O_2. As a result, this led to the conclusion that AE could be affected by both the swirl setting and target signal.

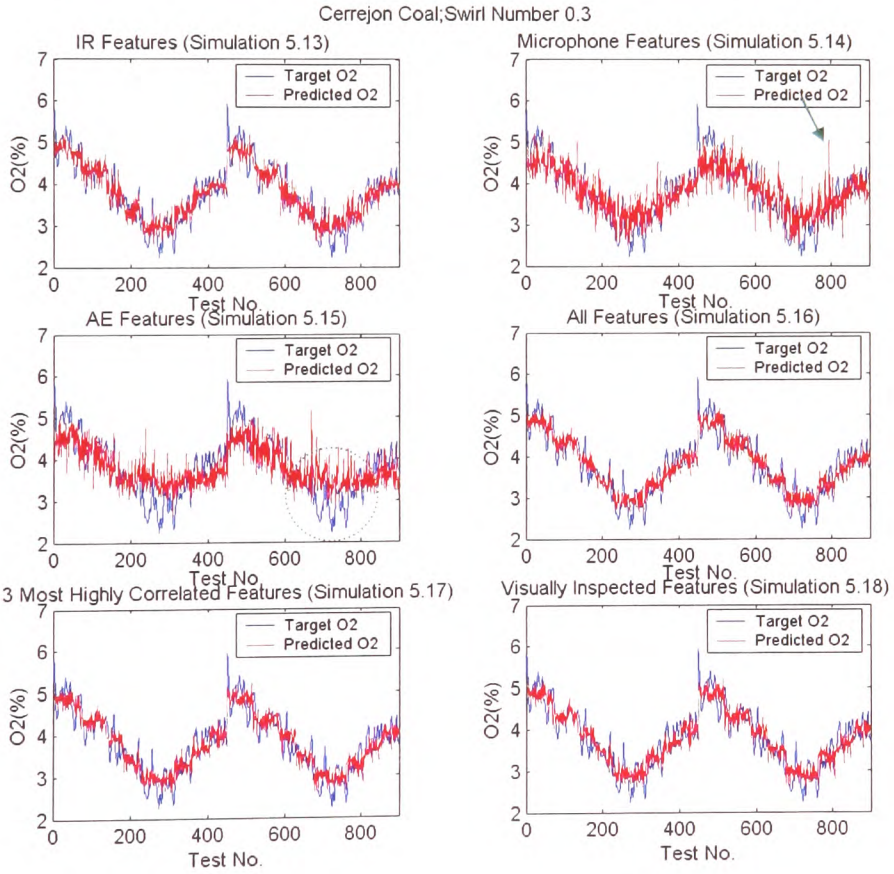

Figure 5.21 (a) Simulations 5.13 to 5.18

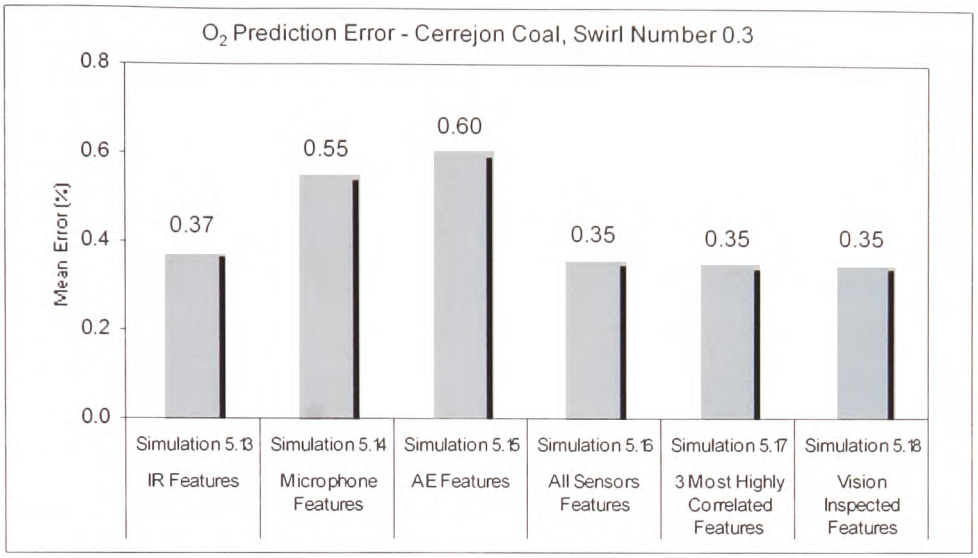

Figure 5.21 (b) Mean Errors for Simulations 5.13 to 5.18

5.5.6 Simulations of NOx, CO and O_2 for Cerrejon Coal at Swirl Number 0.5

The simulations in this section were trained and validated using even and odd numbers of the same data set. The sound increases as the swirl in the secondary air rises and overall this led to an improved microphone signal. Judging from the fact that the NOx should lie in the same level at the beginning and the end when subject to the same secondary airflow rate, thus resulted in localised signal deviations (as highlighted) in Figure 5.22 (a). Simulations 6.1 and 6.2, on the other hand, indicate signal deviations using both the IR and microphone features most likely resulting from either inaccuracies in the gas analyser, or variations in the combustion flame.

Recognising that the position of each sensor has a slightly different signal response over the entire burner operation conditions, the use of the combined features could lead to a more complete solution in terms of prediction performance. This justification can be applied to simulation 6.4, where the trained model corresponding to all sensor features, capable of predicting upper NOx region. The unpredicted NOx in simulations 6.5 and 6.6 of 3 most correlated and the visually inspected features, however, were most likely due to inaccuracies in the gas analyser.

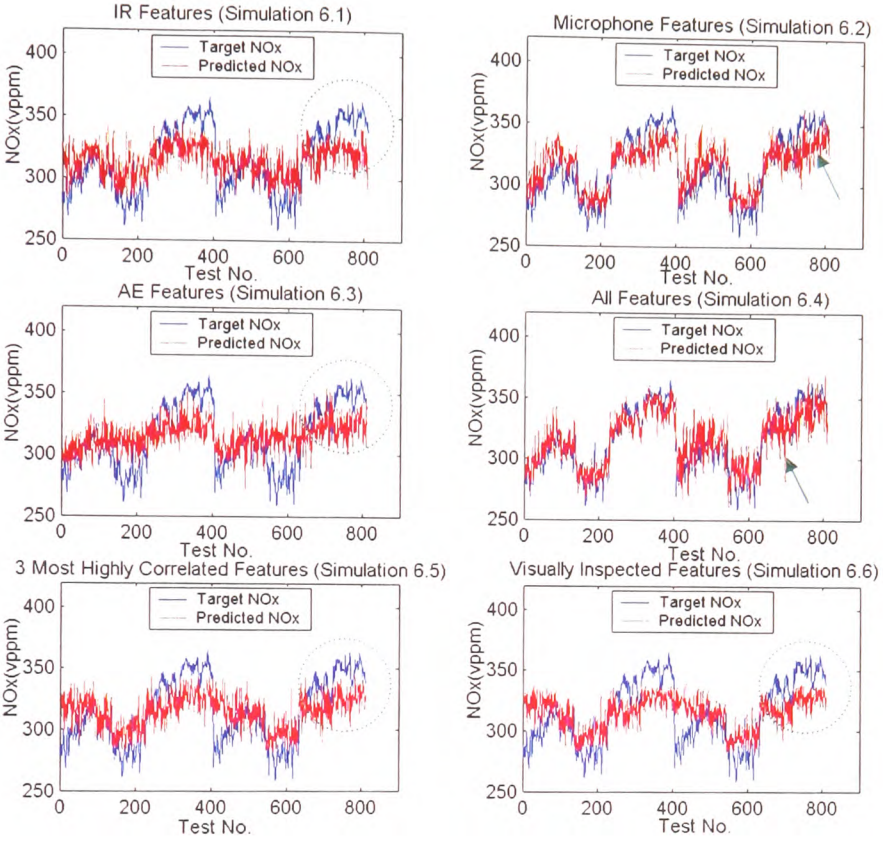

Figure 5.22 (a) Simulations 6.1 to 6.8

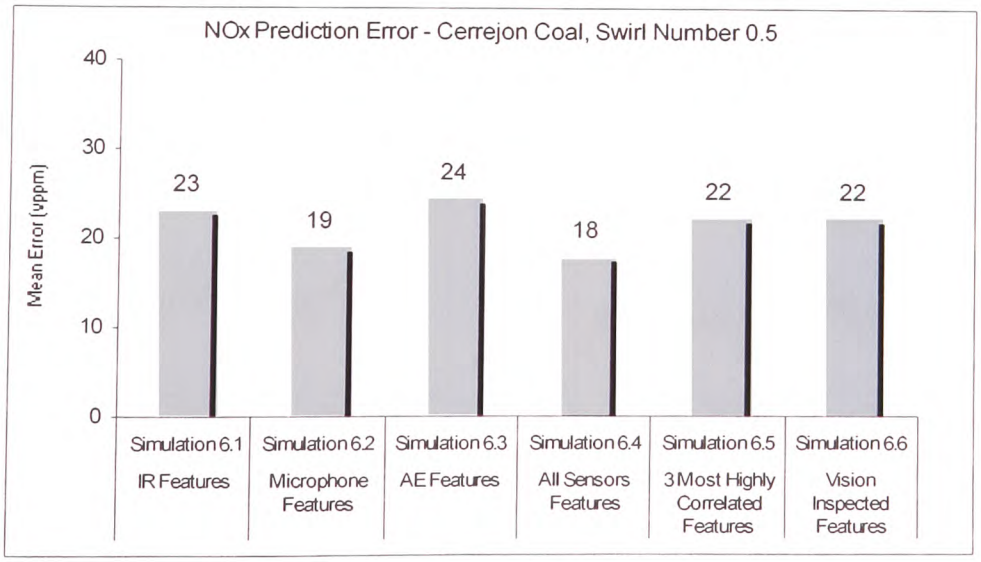

Figure 5.22 (b) Mean Errors for Simulations 6.1 to 6.6

One significant deviations in simulations 6.7 to 6.12 of Figure 5.23 (a) is that these trained models failed to predict the highest CO (error of 120 ppm). It is felt that as the flame physical changes at a different rate when compared with the gas CO so, only partial changes in the flame were recorded. Nevertheless, the increased microphone signal in simulation 6.8 led be a much better prediction with a swirl number of 0.5.

However, even with an increased swirl number the predictions using AE features in simulation 6.9 were not found to be much better due to insufficient AE signal features. Simulation 6.10 with the all sensor features, on the other hand, outperformed both simulations 6.11 and 6.12 of the 3 most correlated and visually inspected features and overall, the improved prediction using the combined features benefited from a larger data dimension.

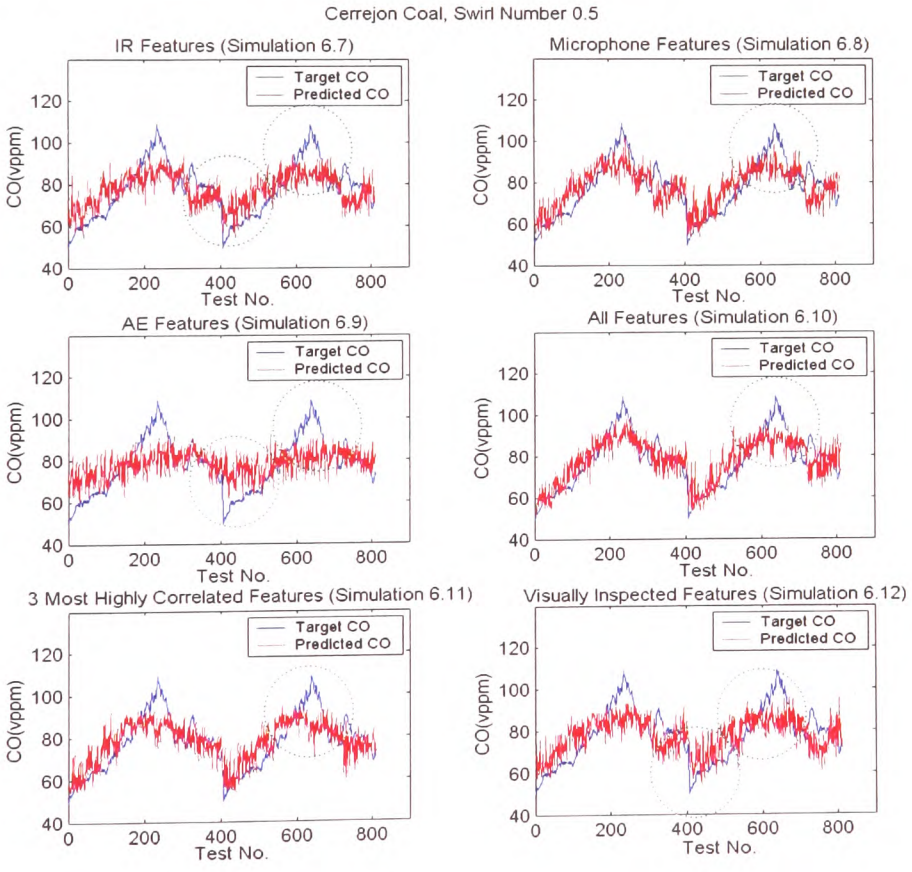

Figure 5.23 (a) Simulations 6.7 to 6.12

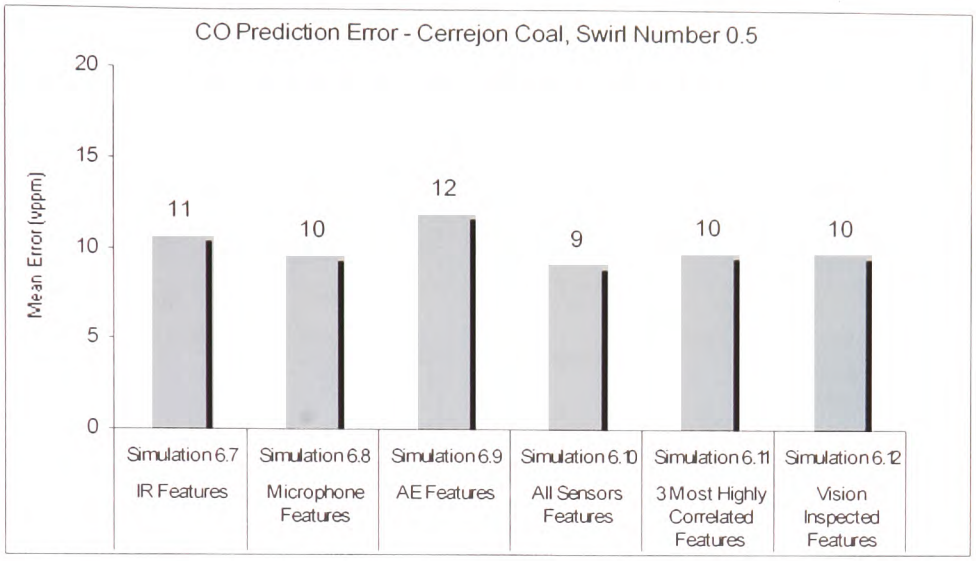

Figure 5.23 (b) Mean Errors for Simulations 6.7 to 6.12

A slight increase in swirl number of 0.5 has led to improve microphone response. This assertion is can be evident in simulation 6.14 where the trained model of microphone features successfully covered the entire range in O_2 gas. In addition, it was found that the trained model of AE features failed to predict the O_2 and so this implies a further increase in the swirl number may be required before a satisfactory level of AE signal can be found. Simulations 6.16, 6.17 and 6.18 of all sensor, 3 most correlated and the visually inspected features, on the other hand, demonstrated some better predictions because of the use of multiple sensor information.

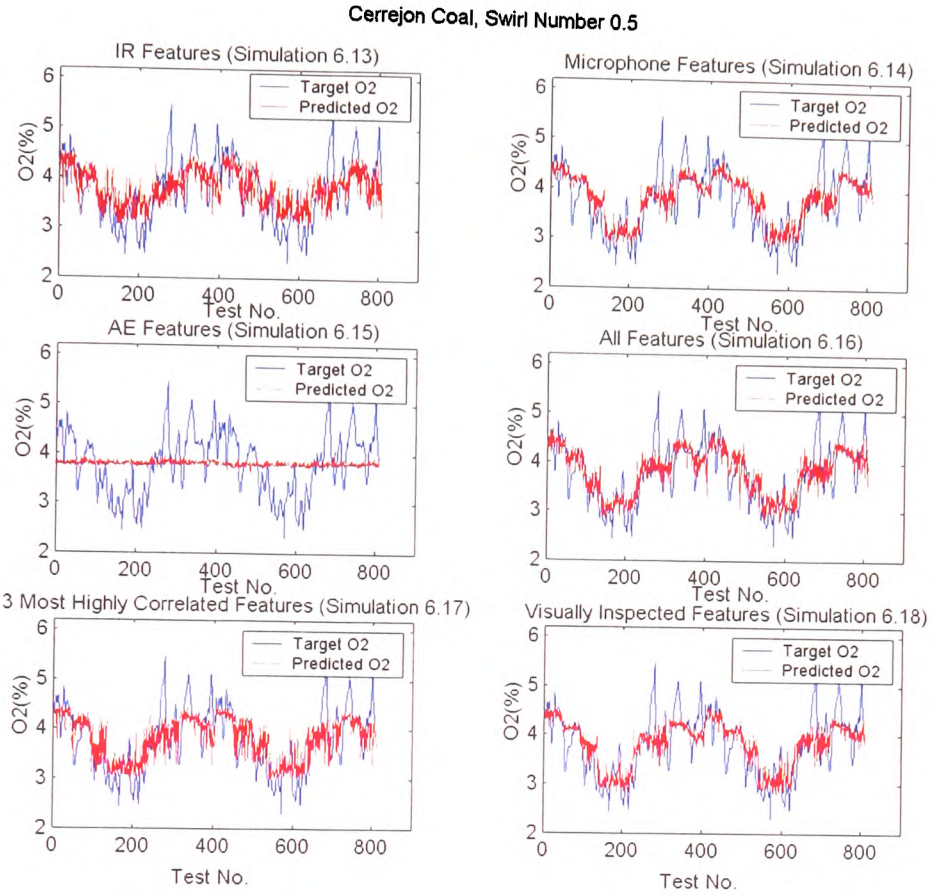

Figure 5.24 (a) Simulations 6.13 to 6.18

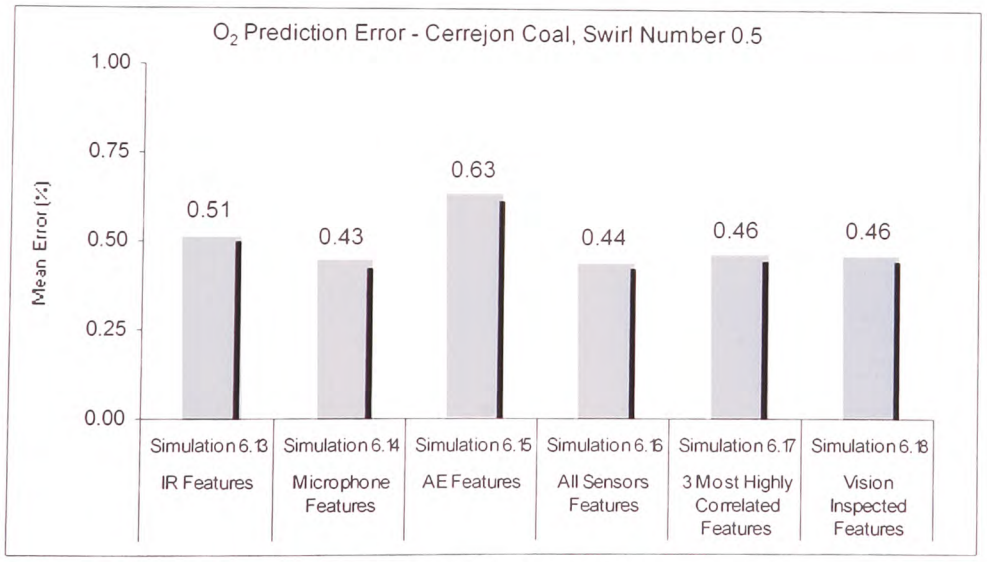

Figure 5.24 (b) Mean Errors for Simulations 6.13 to 6.18

5.5.7 Simulations of NOx, CO and O_2 for Cerrejon Coal at Swirl Number 0.8

In the following simulations where Cerrejon test data for a swirl number of 0.8 were used, the first 500 data samples were used for training with the remaining being used for validation. It is felt that the MEs of Figure 5.25 (a) were reasonably low except simulation 7.3 of the AE features where no prediction was found. The missing AE even at an increased swirl number of 0.8 did not produce significant pressure fluctuation in the combustion condition of Cerrejon coal. Both trained models of the IR and microphone features achieved acceptable predictions. However, the localised deviations in simulation 7.1 (as highlighted) probably resulted from unknown disturbances, for example, temporarily settlement of fly ash that obstructs the optical lens of the IR sensor could have led to some irregularity in the measurement. Other discovery includes the combined features that offered reliable predictions as in simulations 7.4, 7.5 and 7.6.

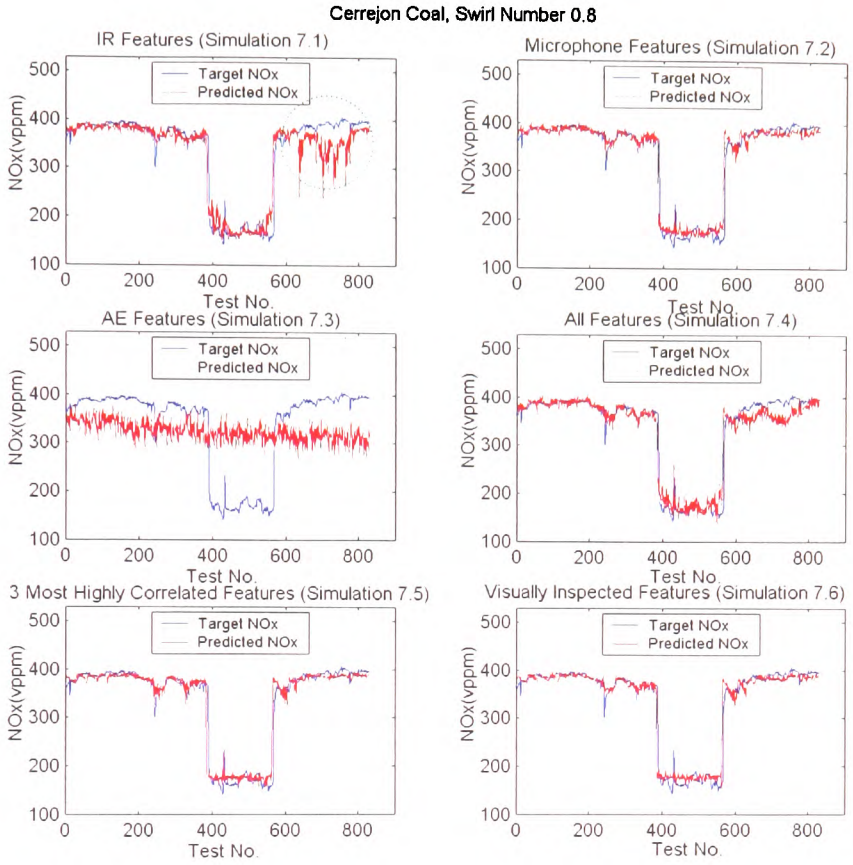

Figure 5.25 (a) Simulations 7.1 to 7.6

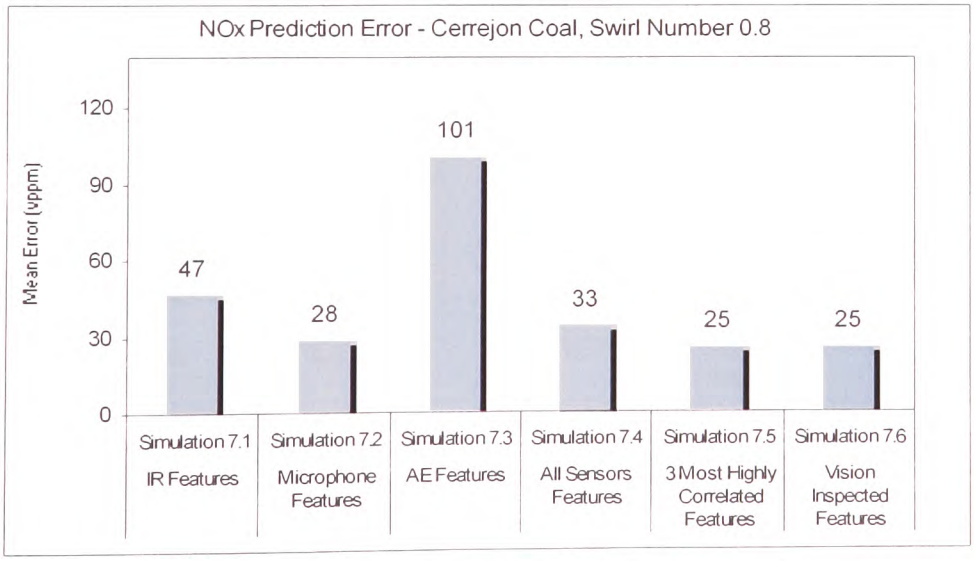

Figure 5.25 (b) Mean Errors for Simulations 7.1 to 7.6

The homogeneity in the combustion condition with a swirl number of 0.8 led to no prediction in simulation 7.7 of AE sensor. It is felt that the trained data corresponding to the first 500 data points did not cover the second half of the validation data set and overall this resulted in large signal deviations that happened to all 6 simulations in Figure 5.26.

The use of combined features in simulations 7.10, 7.11, and 7.12 offered a less fluctuating prediction signal. In addition, the transients in the CO and predictions took place at two separate instances. The time-delay pattern has led to localised errors and so greater MEs.

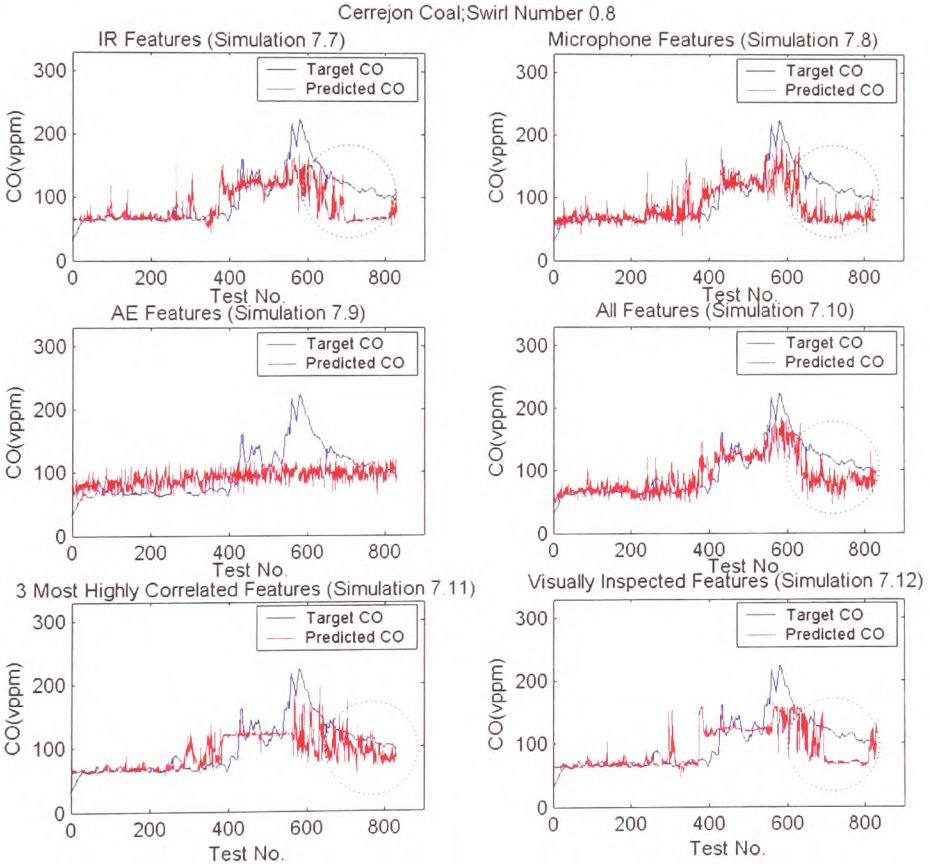

Figure 5.26 (a) Simulations 7.7 to 7.12

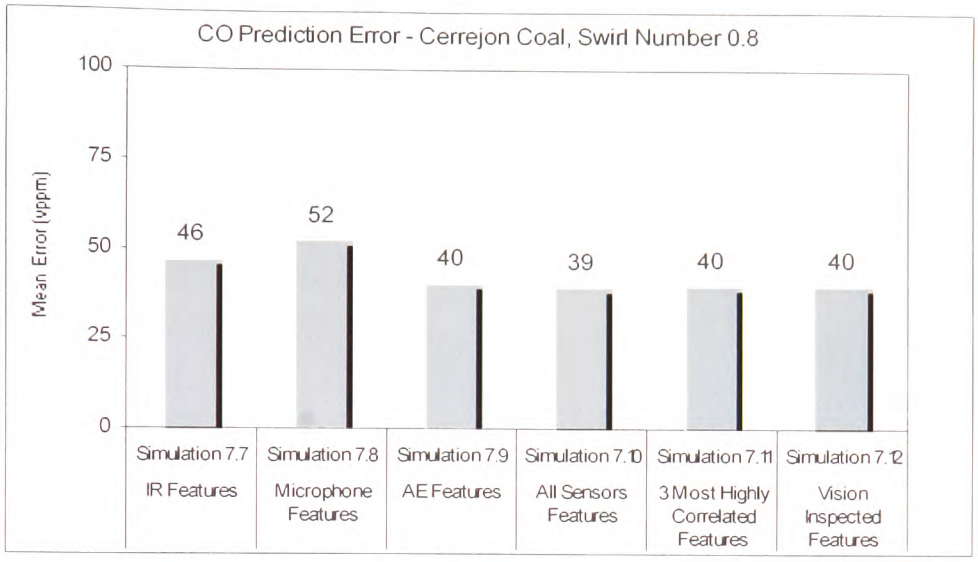

Figure 5.26 (b) Mean Errors of Simulations 7.7 to 7.12

In the prediction of O_2, the models were trained in the same way to the NOx and CO. The missing AE signal (simulation 7.15) with a swirl number of 0.8 resulted in no prediction. As the O_2 is different in the first and second half when subject to a secondary airflow rate describes the inaccuracies in the gas analyser as in simulation 7.13. Simulations 7.16, 7.17 and 7.18 of all sensors, the 3 most highly correlated and visually inspected features, on the other hand, give emphasis to the combined features and hence better prediction accuracy.

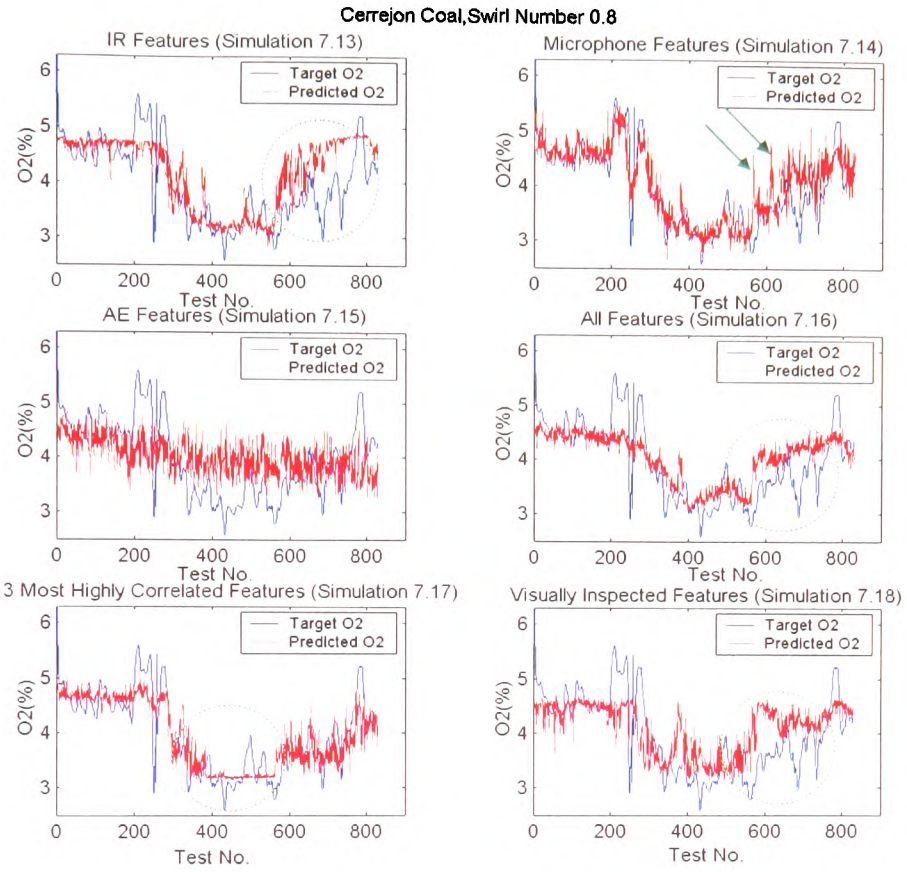

Figure 5.27 (a) Simulations 7.13 to 7.17

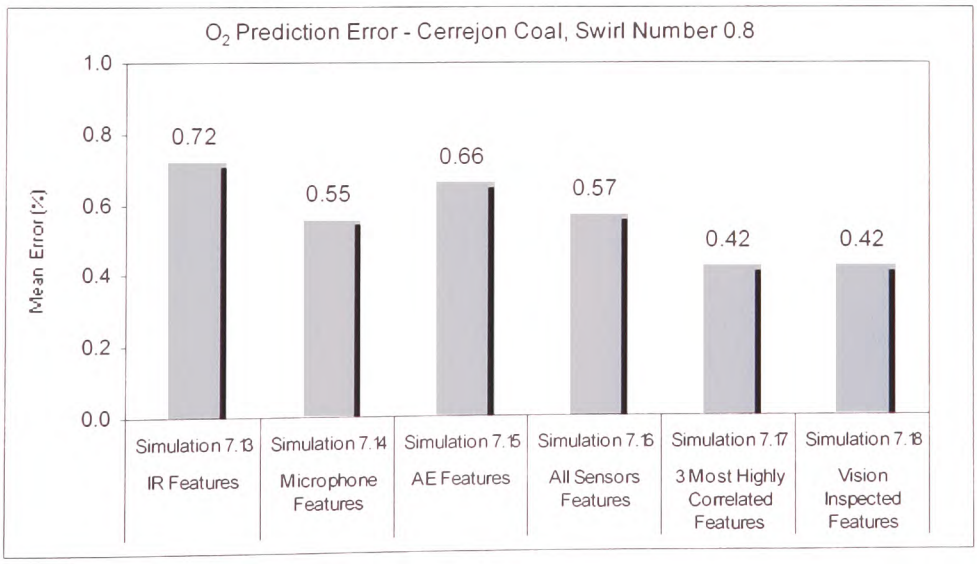

Figure 5.27 (b) Mean Errors for Simulations 7.13 to 7.17

5.5.8 Simulations of NOx, CO and O_2 for Cerrejon Coal., Swirl Number 1.2

The final of simulations concerns the Cerrejon test data for a swirl number of 1.2. One obvious statement applies to all simulation tests involving both Daw Mill and Cerrejon coal data is that the microphone signal increases as the swirl number increases. For this reason, the trained model of the microphone features in simulation 8.2 has a better prediction. On the other hand, simulation 8.1 of the trained model of IR features offered reasonable predictions. Nevertheless, evidence of insufficient AE signal even with a higher swirl number of 1.2 was found. This situation can be witnessed in simulation 8.3 in which, only limited predictions were obtained and it is also felt that a swirl number greater than 1.2 may be required if Cerrejon coal is to be fired. Therefore, one may argue that the AE sensor could be more suitable to monitor other burner activities, for example, soot blowing entailed valve movements hence greater AE signal when compared with current application to monitor gases. Finally, it was learned from simulations 8.4, 8.5, and 8.6 that the use of the combined features has again offered much better predictions and was irrespective of the swirl setting.

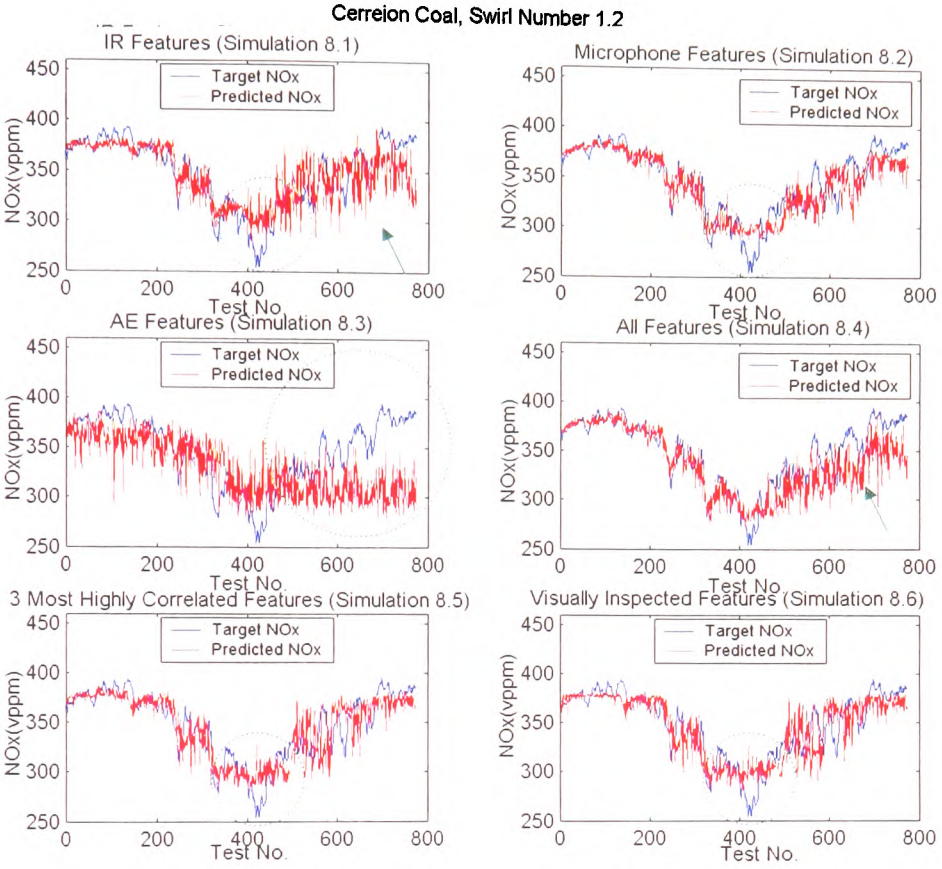

Figure 5.28 (a) Simulations 8.1 to 8.6

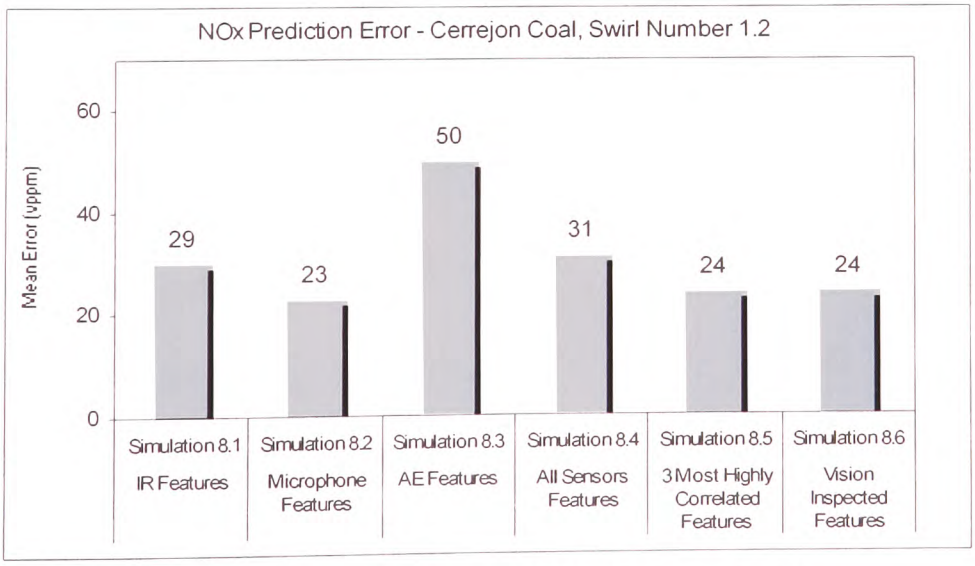

Figure 5.28 (b) Mean Errors of Simulations 8.1 to 8.6

The CO models were trained with the first 400 data points and validated with the remaining data. There were cases where the trained CO models were unable to predict the peak CO at around data point 420. This happened due to the peak CO which was not included in the training and so no prediction corresponding to that upper CO region was found. Other discoveries included different CO readings when subject to a same secondary airflow rate at the beginning and the end of the experiment led to signal deviations, and, the use of the combined features corresponding to all sensors and the 3 most correlated features produced some better predictions. It was also learned that the wrongly chosen features in simulation 8.12 corresponding to the visually inspection features could be the reason which led to a restricted accuracy when modelling gas CO.

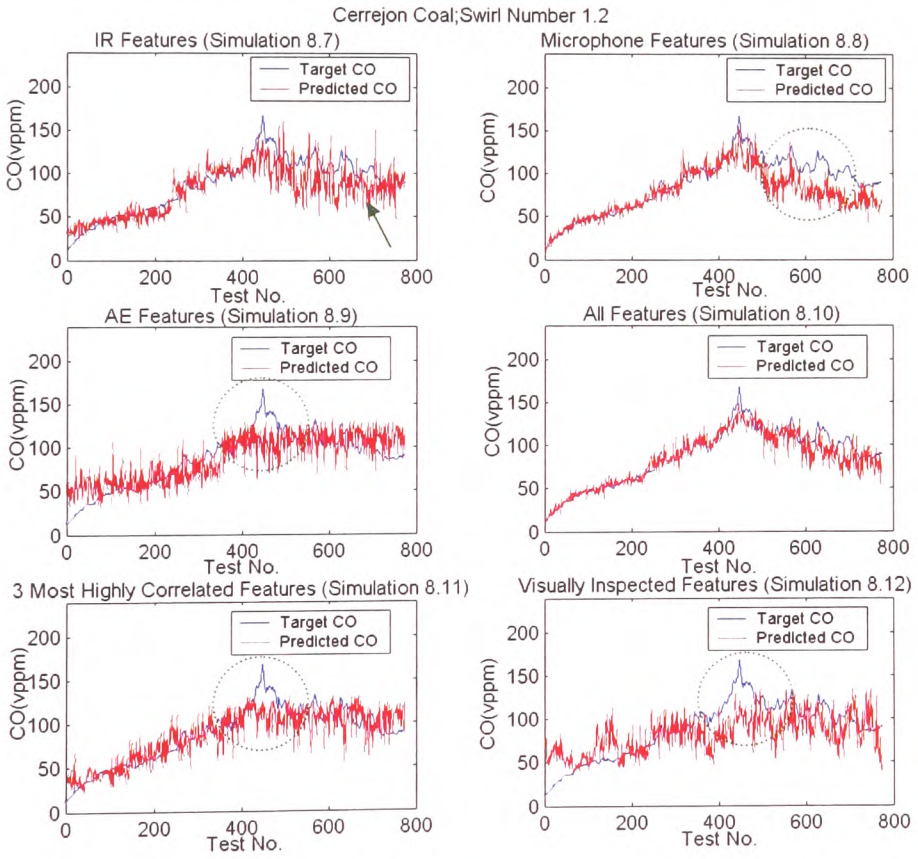

Figure 5.29 (a) Simulations 8.7 to 8.12

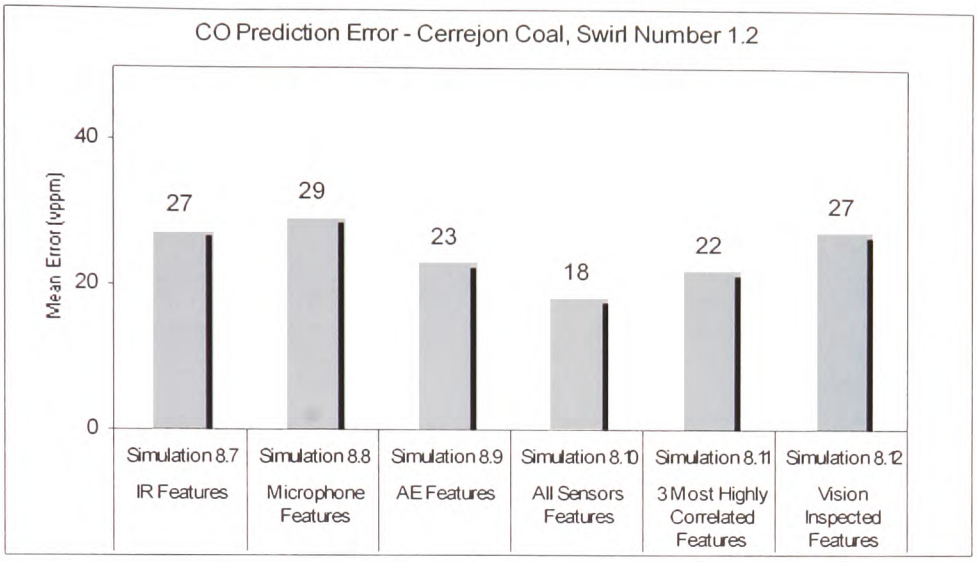

Figure 5.29 (b) Mean Errors for Simulations 8.7 to 8.12

In agreement to the previous simulation tests that involved both NOx and CO with a swirl number of 1.2, the high swirl setting led to increased turbulence in the combustion condition hence greater sound intensity, and as a result, the trained model of microphone features in simulation 8.14 were found to achieve better model prediction. In addition, it was learned that unlike in simulation 8.13, the trained model of the IR microphone features was insensitive to the oscillation in the gas O_2. This demonstrates a neural network could circumvent the unwanted signal noises of the predictions and concentrate on the underlying O_2.

It is felt that there is very little indication of increased AE signal with a swirl number of 1.2 and consequently only limited prediction was found in simulation 8.14. In addition, one may need to further increase the swirl number until sufficient AE allows reasonable predictions to obtain.

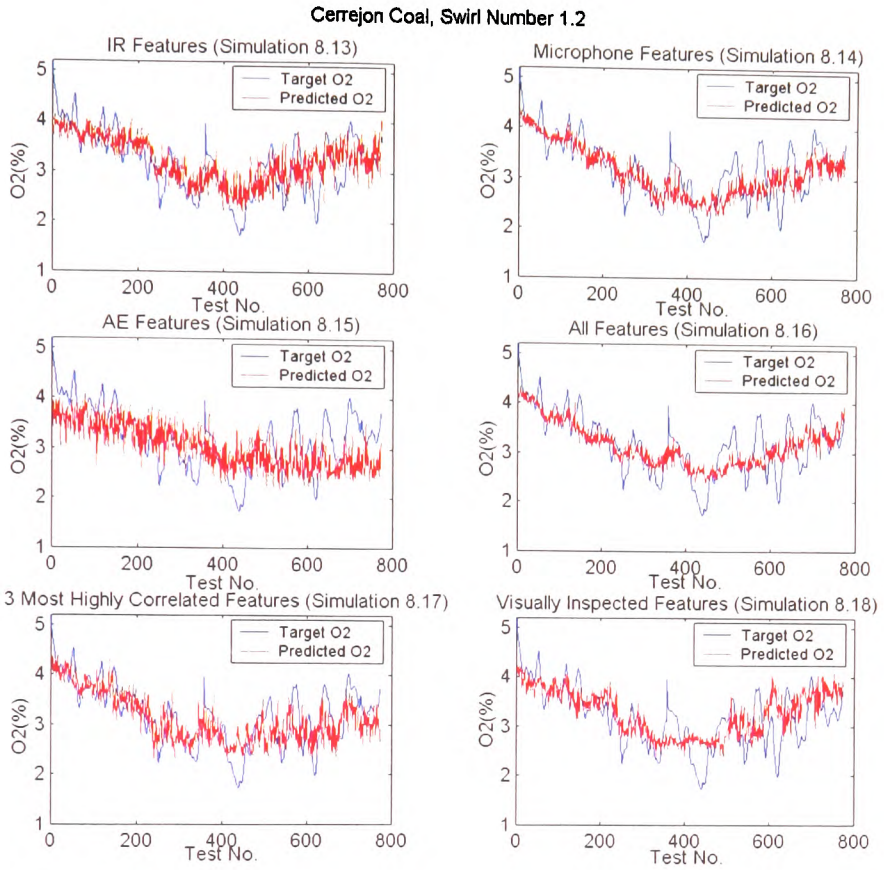

Figure 5.30 (a) Simulations 8.13 to 8.17

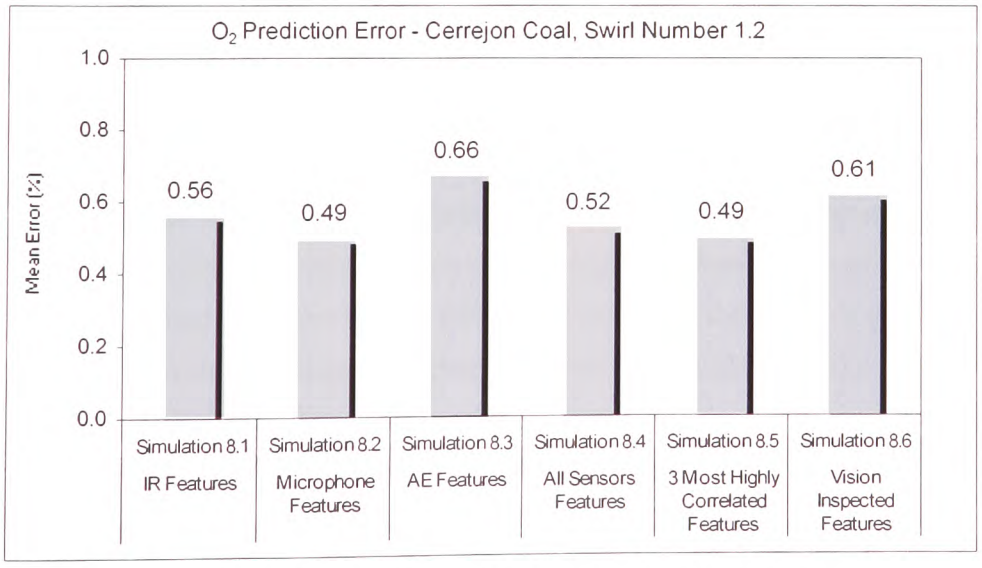

Figure 5.30 (b) Mean Errors for Simulations 8.13 to 8.17

5.6 Summary of Section 5.5

At lower swirl numbers, the homogeneity in the combustion condition generated a more steady flame and so this led to a uniform IR signal hence better predictions. In addition, the increase in the swirl improved the turbulence in the secondary air and this overall resulted in a greater sound intensity. This indicates that a trained model of microphone features becomes dominant as the swirl increases. This happening, however, depended on factors such as the coal property and swirl intensity as such transition took place in different swirl numbers with different coal types.

It is felt that the increased swirl number also introduced greater pressure fluctuation under a highly turbulent combustion condition. Consequently, this explains the increased AE signal particularly at a higher swirl number. However, unlike in simulations that involved Daw Mill coal, a distinctive AE source has not been found. This subsequently suggested a further increase in the swirl number may be required. Even so, one must bear in mind that this may not be feasible as every burner has its own operating boundary and to operate the burner outside this limit could lead to an adverse impact and as a result undesirable operation.

One may determine the best feature set by calculating the percentage errors corresponding to all simulations in section 5.5. Essentially, the idea is to normalise the MSE to a unit area so that simulations involved all 3 gases of NOx, CO and O_2 in section 5.5 could be compared. The (a) average, and (b) standard deviations, of the percentage errors corresponding to different swirl numbers and for both the Daw Mill and Cerrejon test data have been calculated. The standard deviation of the percentage errors was used to indicate how "reliable" a feature set was. Three separated figures consisting of both the average and standard deviation of the percentage errors of the network predictions for NOx, CO and O_2 were plotted and compared (Figures 5.31, 5.32 and 5.33).

In Figure 5.31, the models trained with AE features have the highest average percentage errors. The use of the IR and microphone features have lower average percentage errors and so they were better sensors than the AE. In addition, the models of the combined sensors, 3 most highly correlated and visually inspected features outperformed the use of

individual sensor features of the IR, microphone and AE for trainings. However, the simulation of the visually inspected features has a greater standard deviation. As a result, the combination of all sensor features and the 3 most highly correlated features were the best. Given that the Daw Mill coal (as opposite to Cerrejon coal) was more sensitive to the secondary airflow change, it exhibited a greater variation in the gaseous emissions and so a greater percentage error.

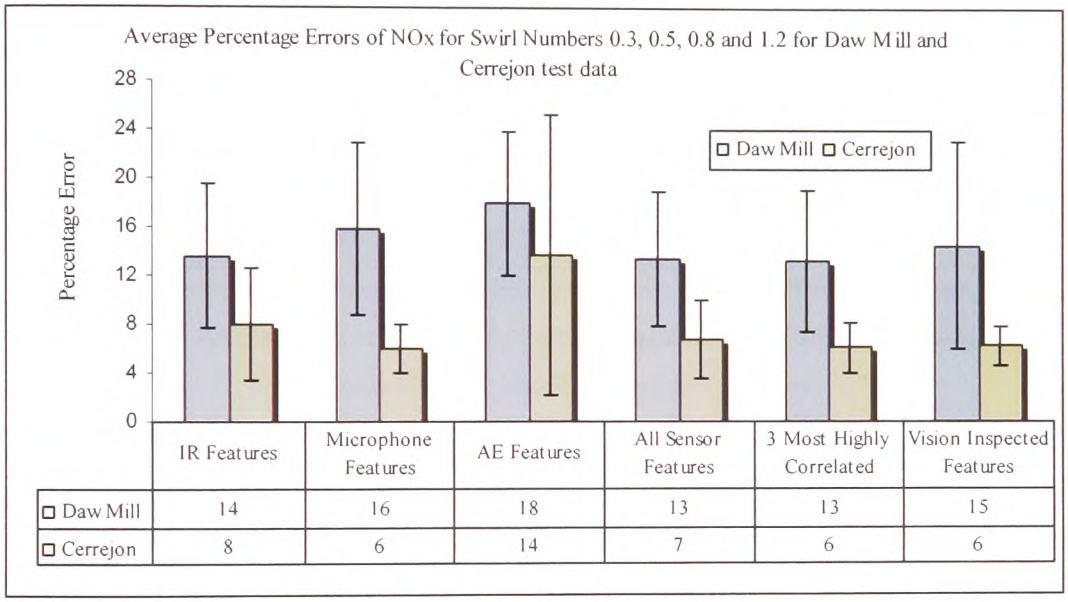

Figure 5.31 Average Percentage Errors and Standard Deviations for Modelling NOx corresponding to Swirl Numbers 0.3, 0.5, 0.8 and 1.2

Figure 5.32 shows the average percentage errors and standard deviations for modelling CO. There were mixed results but one can confirm that simulations made by all sensor features and the 3 most highly correlated features again have the lower average percentage errors. The overall standard deviation was consistent. The predictions made by the IR and microphone have outperformed the AE features. Visually inspected features, on the other hand, have a mixed performance and the average percentage error was very good for the Cerrejon but not for the Daw Mill test data as shown in Figure 5.32. The percentage errors of the CO simulation, however, are commonly greater because of large excursions in the CO, which make them the most unpredictable combustion parameter.

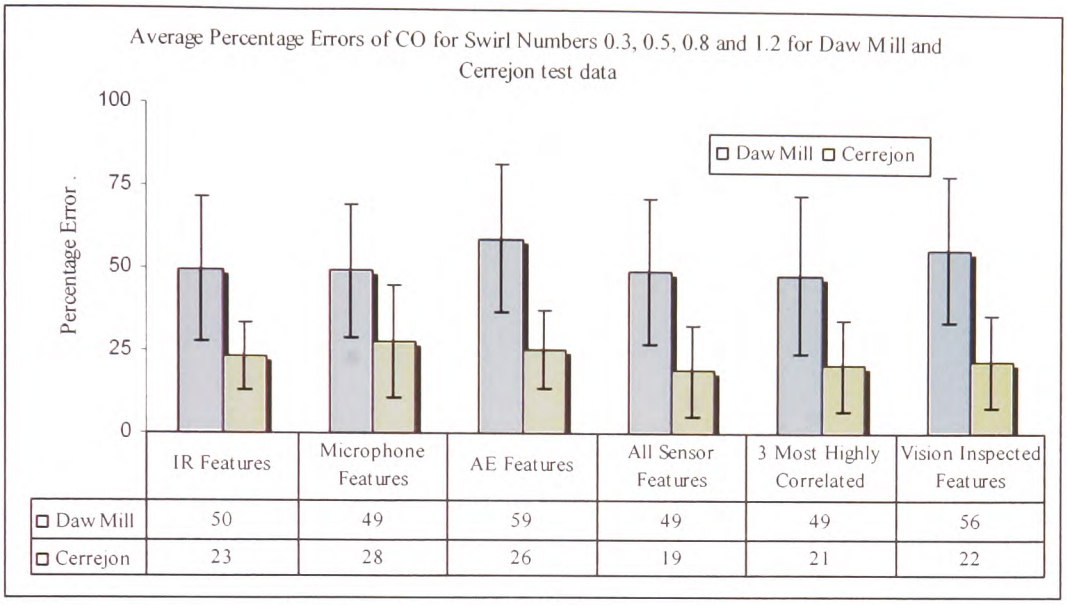

Figure 5.32 Average Percentage Errors and Standard Deviations for Modelling CO correspond to Swirl Numbers 0.3, 0.5, 0.8 and 1.2

Figure 5.33 indicates the average and the standard deviations of the percentage errors when modelling O_2. It was observed that the models of the IR, microphone and AE features have very similar results. However, the model of the microphone features has turned out to be the best. In addition, the models belonging to all sensors, the 3 most highly correlated and the visually inspected features have again achieved lower average percentage errors as well as no increased standard deviations being observed. Despite the fact that O_2 behaves in a similar way to the NOx, the percentage errors of O_2 were found to be greater. This is because a larger response in the gas O_2 to the periodic fluctuations of coal feed mechanism has relatively more percentage errors when compared to the simulations of NOx.

From this point, one may draw a conclusion signifying that the calculated percentage errors were effectively influenced by the transients in the target gases to be modelled. The signal variations as a result of the transient in the gases could happen through sudden incursions in the gas readings (as was happened to most CO cases), or resulted from significant periodic oscillations (as normally happened to O_2).

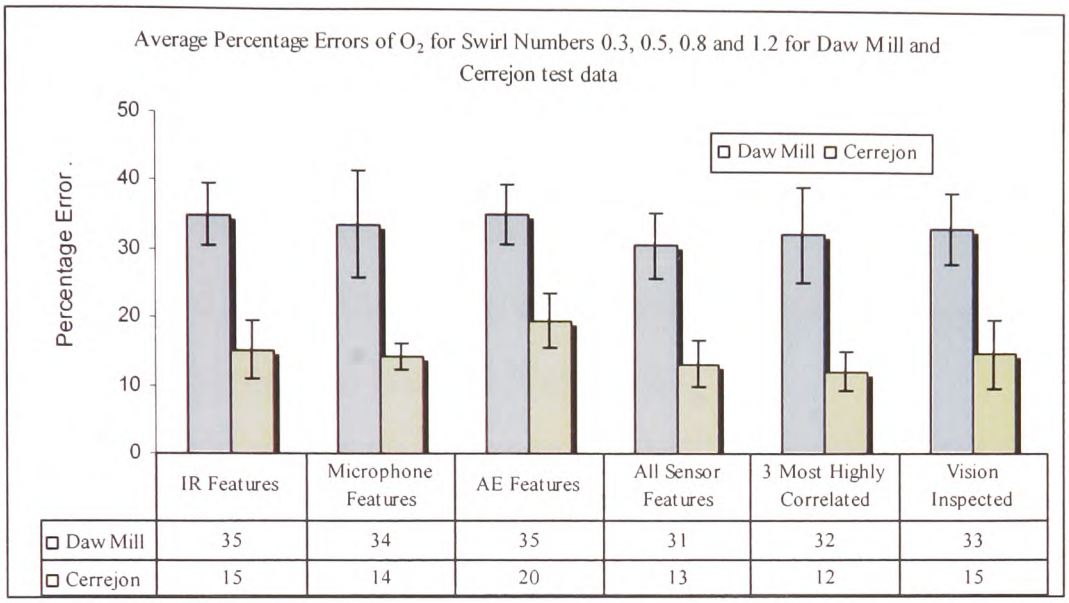

Figure 5.33 Summary of Percentage Errors for CO predictions of Swirl Number 0.3, 0.5, 0.8 and 1.2, both Daw Mill and Cerrejon coal test data

Another major discovery is the lack of repeatability in the gas readings either due to a "drift" in the gas analysis as a result of high unburned carbon settled around the sampling point (e.g., Figure 5.14), or slight changes in the coal property (e.g., simulation 3.13). Other possibilities include air leaking, which resulted from incursions of air when the viewing port window opened for routine inspections, changes in temperature as the burner started up cold (e.g., Figure 5.18), and unforeseen events such as temporary signal disturbances, for examples, additional noise source from other plant operation (e.g., simulation 3.2) and settlement of fly ash obstructed the optical lens (i.e., simulation 7.1). Further to this, large signal deviations could also be affected by a delay in the analyser readings when compared with the predictions (e.g. simulations 7.7 to 7.12). Therefore, all the reasons described in the above led to increased percentage errors.

Knowing that these sensors have variations in terms of signal sensitivity under varies operating conditions. As such, this consolidated the idea to combine features in order to obtain signal inference. In summary, the model trained with all sensors and the 3 most highly correlated features consistently maintained the lowest prediction errors. For

smaller network parameters and faster training in mind, the use of the 3 most highly correlated features for modelling the combustion gaseous was the best. Also, the results indicate the models corresponding to the IR and microphone were better than the AE for an instance where only one of the three sensors is installed.

5.7 Improved Model Predictions by the Recursive and Feedforward of Auto Regressor with Exogeneous Input (NNARX) Structure Neural Networks.

It should be clear by now that the feedforward (i.e., MLP) neural networks have no way of predicting feature outputs, as these networks are ideal for solving problems that require the computation of a static function (i.e., a function whose output depends only upon the current input and not on any previous inputs). However, in the real world, one encounters many problems, which cannot be solved by learning a static function because the function being computed changes with each input received. This situation can be catered for by the introduction of feedback connections within the network and so the network activation produced by past inputs can cycle back and affect the processing of future inputs. As a result, the prediction of the combustion system based on the recursive neural network and the "one-step-ahead" NNARX model was evaluated in the hope that one of these suggested models had improved results.

A series of tests were conducted (Table 5.3) where a recursive model with a hidden layer of hyperbolic tangent activation function neurons and an output layer with a linear activation transfer function was used. The numbers of hidden and output neurons were 10 and 1 with gradient descent back-propagation and early stopping functions being standard. The simulation of the NNARX network had past output and input values and delays were set at 2, 2 and 1 respectively.

Daw Mill and Cerrejon data at a swirl number of 0.8 were used for the experiment. The experimental descriptions as well as the calculated percentage errors are presented in Table 5.3. Columns 1 and 2 show the coal test data and target gases to be modelled. Column 3 indicates the types of networks used in the simulation tests and columns 4 to 9

are the calculated percentage errors for the different feature sets. The statistics indicate that in general, the NNARX has the lowest percentage error of less than 9 %. However, one should bear in mind that the NNARX requires actual gas readings from a gas analyser that inhibits the application of the NNARX in practice because the gas information per burner is generally not available. Finally, it was concluded that the predictions made by the recursive network outperformed the ordinary MLP.

Some example results (from Table 5.3) were plotted and presented accordingly in Figures 5.34 to 5.39. Figures 5.34 (a) and (b) illustrate the result for the prediction of NOx of Daw Mill test data, swirl number of 0.8. The recursive network has a marginal improvement over the MLP with 3 % and 1 % reduction in error respectively. A green circle was used to highlight the improvement of the recursive network in prediction. Also, the NNARX networks have as little as 2 % errors.

Table 5.3 Comparison of Network Performances based on Daw Mill and Cerrejon coals of Swirl Number of 0.8

Coal Type	Combustion Gases	Type of Network	Percentage Error (%) in Prediction					
			IR Features	Microphone Features	AE Features	All Sensor Features	3 Most Highly Correlated Features	Visually Inspected Features
Daw Mill	NOx	MLP network	7	11	12	7	6	7
		Recursive Network	7	8	13	6	8	7
		MLP of ARX Structure	3	2	2	2	2	2
	CO	MLP network	18	21	26	18	17	23
		Recursive Network	18	20	22	17	17	18
		MLP of ARX Structure	4	3	3	4	4	3
	O_2	MLP network	41	28	33	25	21	26
		Recursive Network	22	25	25	20	21	23
		MLP of ARX Structure	7	6	6	8	6	6
Cerrejon	NOx	MLP network	14	8	30	10	8	8
		Recursive Network	10	8	30	9	8	8
		MLP of ARX Structure	4	4	3	2	4	3
	CO	MLP network	36	50	40	39	40	40
		Recursive Network	31	36	31	26	30	30
		MLP of ARX Structure	3	3	3	3	3	3
	O_2	MLP network	19	15	24	15	11	18
		Recursive Network	13	14	16	15	11	11
		MLP of ARX Structure	3	3	2	2	2	3

(a)

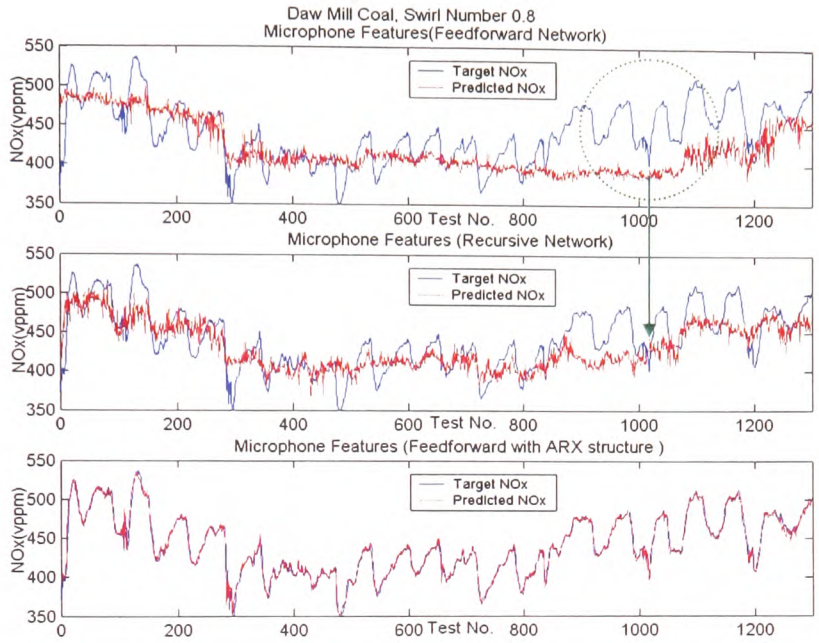

(b)

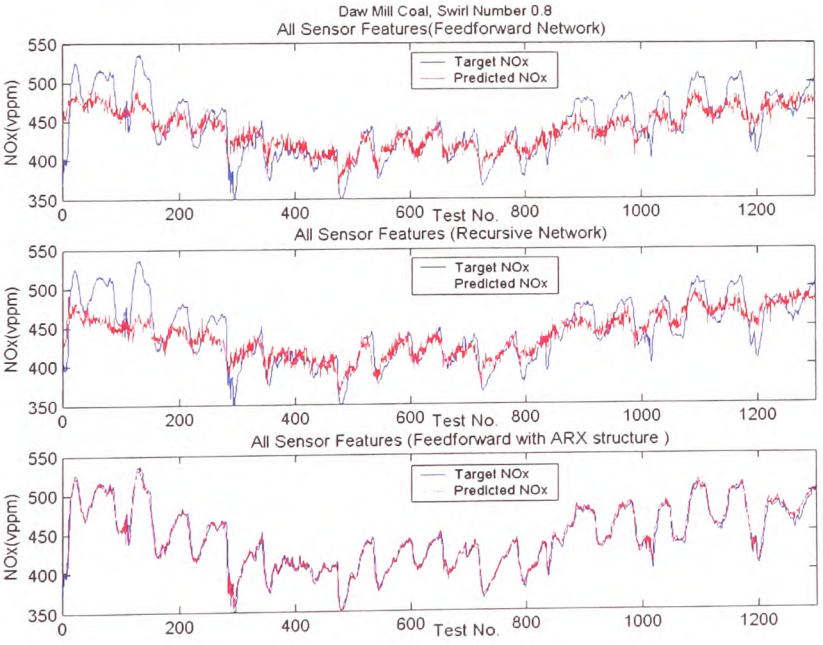

Figure 5.34 The Prediction of NOx by the MLP, Recursive and NNARX networks based on the (a) Microphone, and (b) All sensor features, of Daw Mill test data, Swirl Number of 0.8

Figure 5.35 demonstrates the prediction of CO based on the Daw Mill test data, where a 1% of reduction in error was found using the recursive model, which indicated by a green arrow. The prediction made by NNARX has an outstanding result of 3 % error.

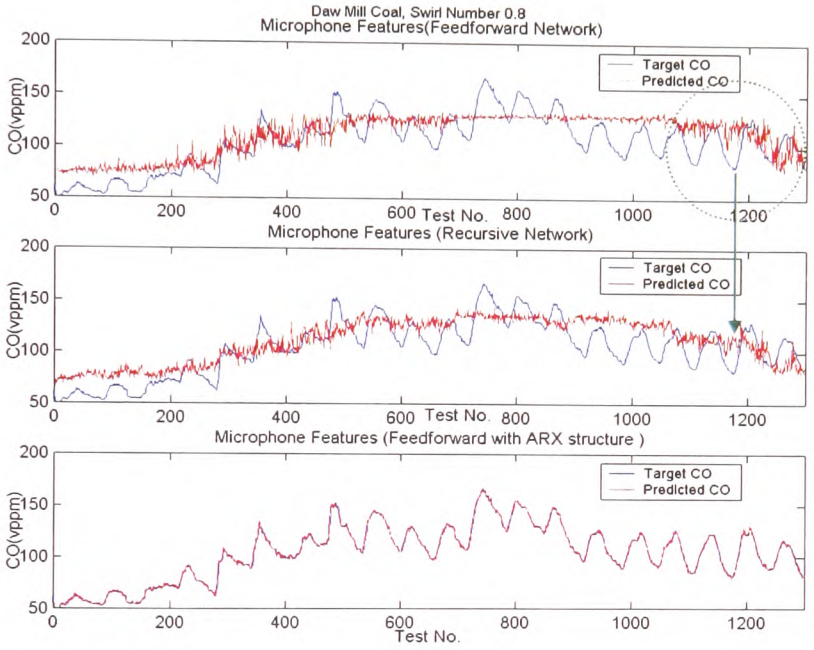

Figure 5.35 Prediction of CO by MLP, Recursive and NNARX Network based on the Microphone features, of Daw Mill test data, Swirl Number of 0.8

Figures 5.36 (a) and (b) show the prediction of O_2 based on the Daw Mill test data. Figure 5.36 (a) shows that the predicted signal has regions where the network has problems predicting the O_2 (as highlighted). A significant error reduction from 41 % to 22 % for the MLP and recursive networks was recorded respectively. Although there were hardly any observable changes found in Figure 5.36 (b). An error of 5 % was found and for the NNARX (Figure 5.36 (c)) the error was less than 8 %.

(a)

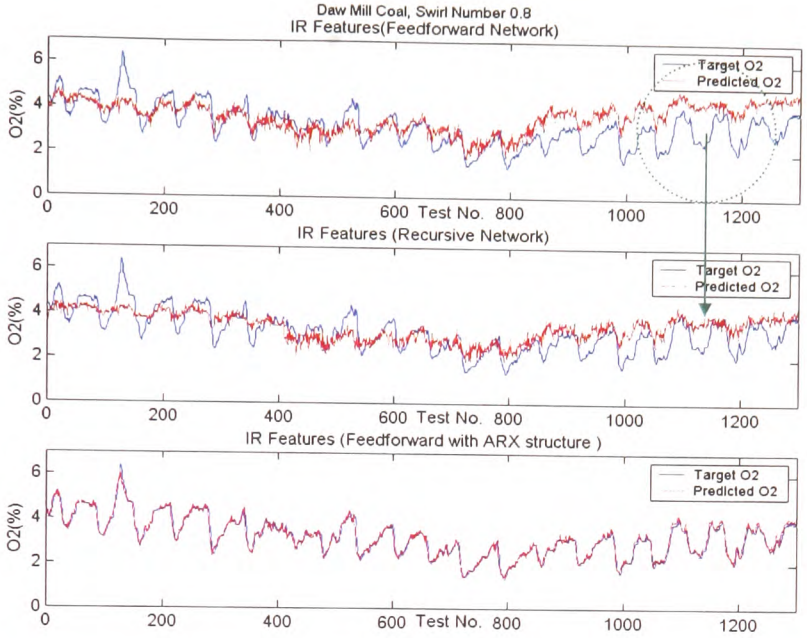

(b)

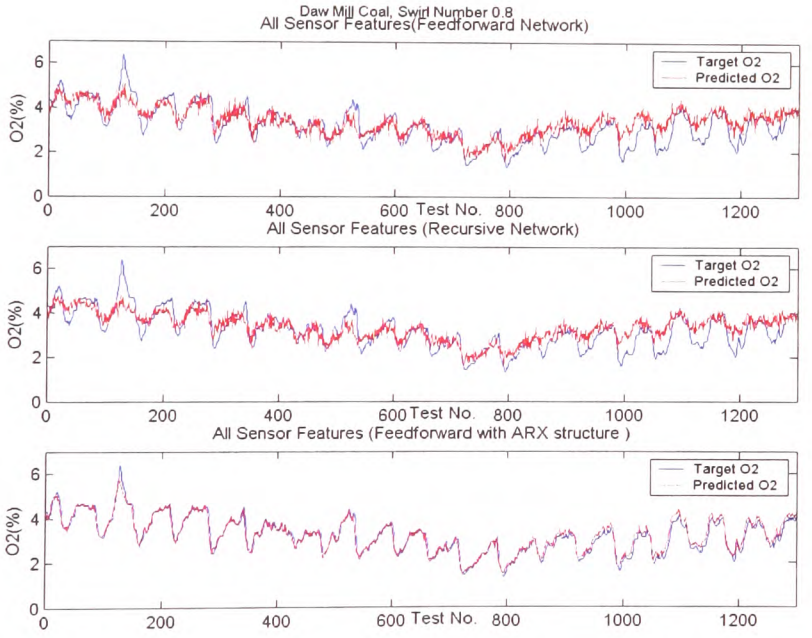

Figure 5.36 Prediction of O_2 by MLP, Recursive, and NNARX networks based on (a) IR, and (b) All sensor features, of Daw Mill test data, Swirl Number of 0.8

Figure 5.37 shows the prediction of NOx based on the Cerrejon test data for a swirl number of 0.8. A 4 % reduction in error was found with the recursive network as compared to the MLP. The region as highlighted yielded the greatest percentage reduction in error. Also, the NNARX had only 4 % error.

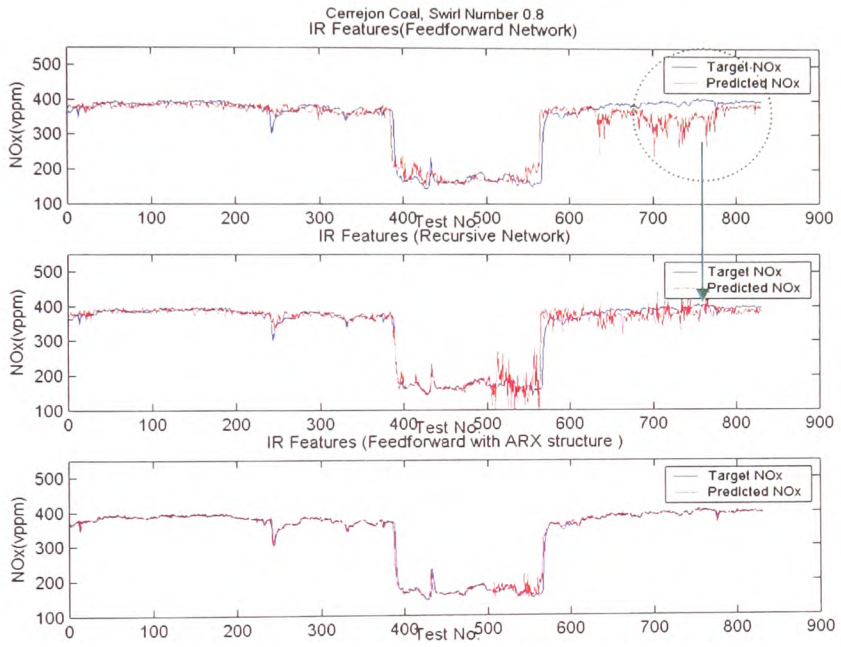

Figure 5.37 Prediction of NOx by MLP, Recursive and NNARX networks based on IR features of Cerrejon, Swirl Number of 0.8

Figure 5.38 (a) shows the predictions of CO based on the Cerrejon test data. A 14% reduction in error was recoded using the recursive network as compared to the MLP, even though the improvement can hardly be observed. The same observation can be applied to Figure 5.38 (b) for which the prediction error fell from 39 % to 26 %. The prediction of NNARX has only 3 % error for both Figures 5.38 (a) and (b).

(a)

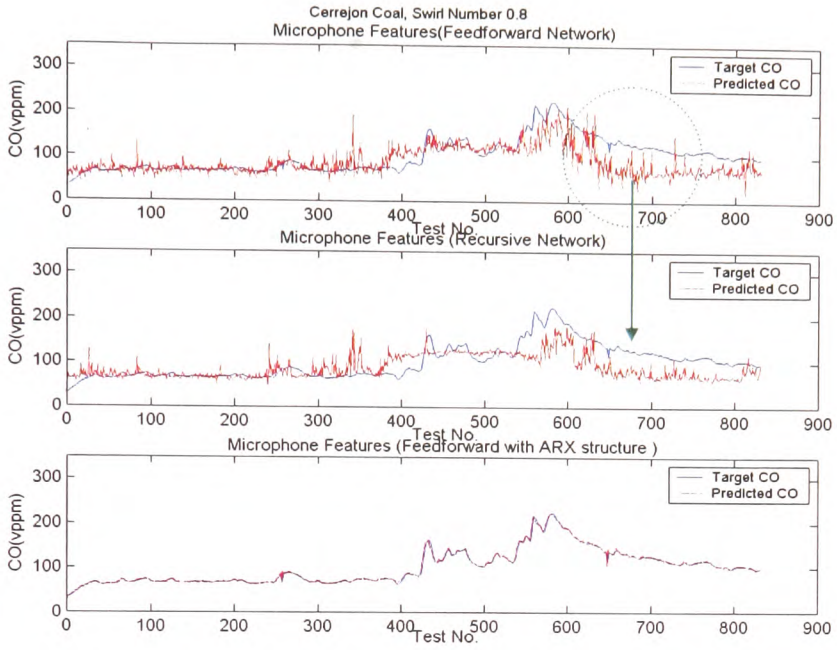

(b)

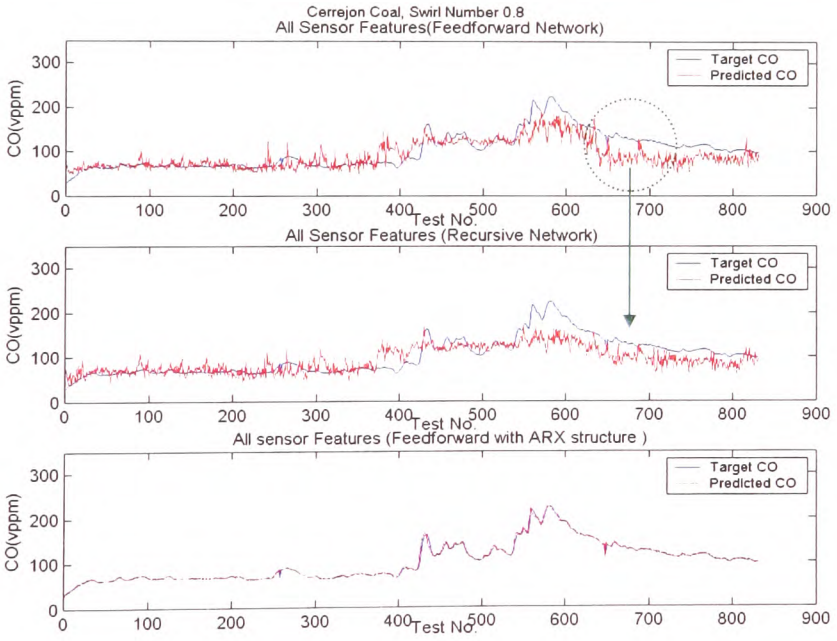

Figure 5.38 Prediction of CO by MLP, Recursive, and NNARX networks based on (a) Microphone, and (b) All sensor features, of Cerrejon test data, Swirl Number of 0.8

Figures 5.39 (a) and (b) show the predictions of O_2 for the Cerrejon test data. Figure 5.39 (a) shows the prediction made by the recursive network which has an error that is 6 % lower than the error achieved by the MLP of 19 % error. One significant improvement is that the recursive network has matched the underlying dynamics of the O_2 signal that the MLP network failed to achieve (Figure 5.39 (b)), as a result, an 8 % reduction in error was obtained. Again, the NNARX has no more than 3 % of error for both Figures 5.39 (a) and (b).

(a)

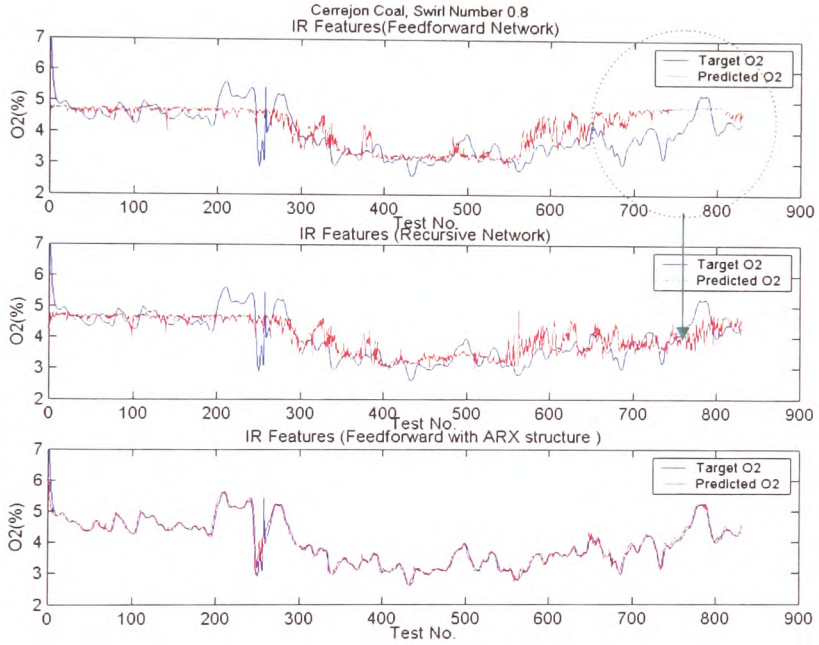

(b)

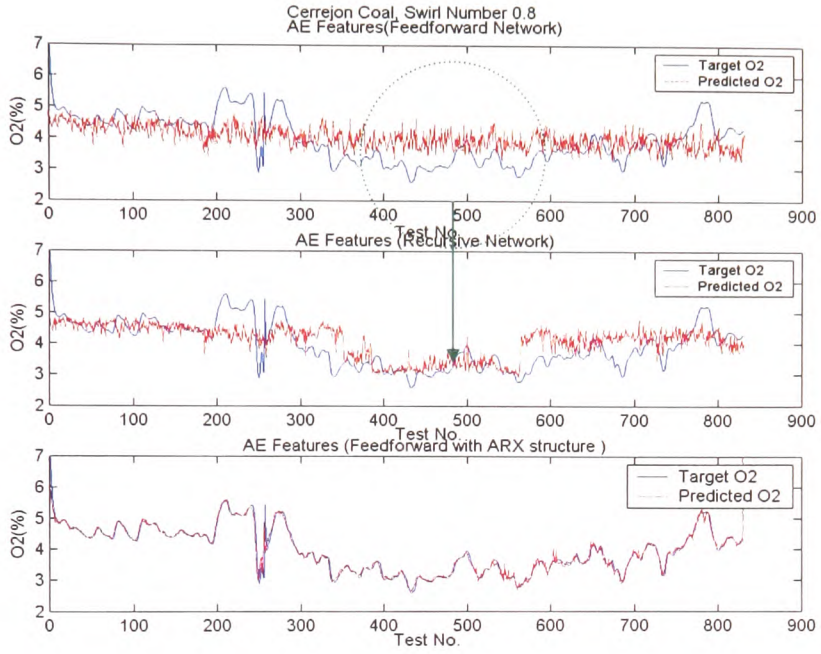

Figure 5.39 Prediction of O_2 by MLP, Recursive and NNARX networks based on (a) IR, and (b) AE features, of Cerrejon test data, Swirl Number of 0.8

5.7.1 The use of Predictions as Inputs to the Neural Network

As the NNARX network was the best performing it was decided to explore this network further. In practice, two approaches can be used to generate the inputs to the NNARX network model predictions: (a) using past plant outputs and (b) feeding back past model predictions [Nørgaard, 1995]. Obviously, the first method cannot be used in the application as there was no plant output (gas analysis) available and for this reason, a prediction can only be made using former predictions to generate the input vector (Figure 5.40). This arrangement was successfully used to model three parameters of an anaerobic digester [Esteves, 2002]. And similar approaches were reported by Van (1995) and Russell (1997). Only the initial measured system output Y*a* is used as an input for the model. All intermediate system outputs are calculated and then network is run to generate the input vector [Tan *et al.*, 1999].

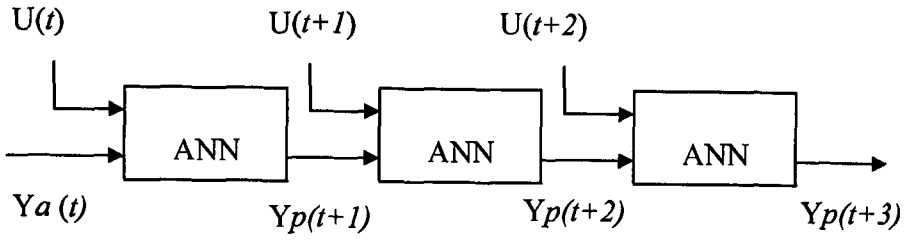

Ya – The initial reading of the actual gaseous
Yp – Former prediction used as the current model input
U – Output from the sensor features

Figure 5.40 Former Predictions as Model Input for subsequent Simulations

Figure 5.41 shows such a simulation generated by the NNARX. The setting of the past outputs, past inputs and number of delays can be found in Table 5.4. Even though it can be seen in Figures 5.41 (a), (b) and (c) that the predictions resemble the dynamics of the target NOx, there were considerable deviations of the two signals. With this approach, the subsequent simulation is affected directly by the former predictions, so small errors can accumulate quickly, and because of restricted accuracy, the NNARX with former predictions used to generate the input vector is not recommended in this application.

Table 5.4 The NNARX network configurations

Simulation No.	Number of Neuron	Number of Past Output	Number of Past Input	Number of Delay
9.1	20	1	3	1
9.2	20	2	4	1
9.3	20	4	5	1
9.4	20	3	1	1

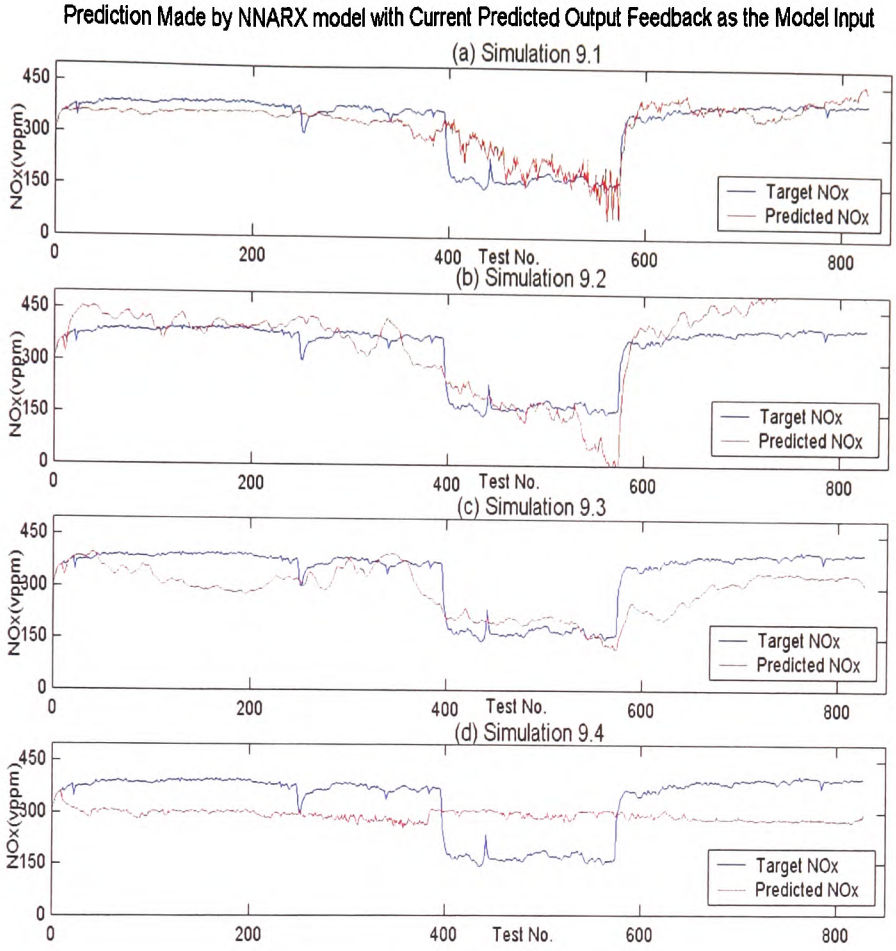

Figure 5.41 The Former Predictions as by the NNARX in which the predicted values were used as past inputs to the model for subsequent predictions.

5.8 Methods to Improve Neural Network Predictions.

Despite the discussion of ANN improvements by a correct set of combined features and network architectures, other methods that could certainly help to enhance network efficiency were the use of a software filter and the Principle Component Analysis (PCA) function. However, PCA is probably not judicious here because it is a linear projection [Lendasse *et al.*, 2002]. Premier (1999) suggested that the use of Butterworth 5th order filters in both chronological directions can help to remove large amounts of signal noise thus improvement the modelling results. Alternatively, the PCA serves two purposes (a) de-correlate training vectors, (b) reduce their dimension

by taking only the first $k < n$ principle components, thus generating new variables of a smaller dimension [MacIntyre *et al.*, 1996; Faller *et al.*, 2000] were also recommended. Nevertheless, the use of both a software filter and PCA required modest considerations and good experience in order not to remove any necessary information for good network prediction [Lendasse *et al.*, 2002].

5.9 Summary of Chapter 5

Using the features derived from the 3 sensors, an investigation of the best possible (a) model based on feature-level fusion, and (b) network architecture via decision-level fusion was undertaken.

The difficulty of modelling the combustion process from first principles has been evident in a large amount of literature. In addition, simple and multiple regressions have tendency of become ill when they performed calculations on numbers that have large variance consequently poor estimation. In addition, Wildman *et al* (1994) suggested that empirical models cannot identify the relationship between the independent variables and various cross products of the dependent variables and so this explains the need for an ANN in combustion.

To generate a good model requires a large amount of representative data [Simula *et al.*, 1996]. In the simulation tests, the standard MLP was tested with the (a) IR, (b) microphone, (c) AE, (d) all sensor, (e) 3 most highly correlated, and finally, (f) visually inspected, features at each swirl number and coal type. The average percentage error corresponding to the results of different swirl numbers was computed both for the Daw Mill and Cerrejon test data, where it was determined that the predictions made by the (a) combined features and (b) 3 most highly correlated features, achieved the lowest average percentage errors. The 3 most highly correlated features technique was chosen because it has the smallest dimension while still preserving the most important metric relationships thus ensuring fast training and good network generalising properties.

Finding a good network architecture is very important and often problem dependent. It was concluded that the predictions made by the recursive network, which can achieve temporal processing, were generally better than that achieved by the static MLP in the modelling of the gaseous emissions. Even though, the NNARX model has a remarkable performance, it has not been used because there were no online gas readings for the model to continue with the prediction. In addition, in the iterative procedure, any errors in the neural network output are fed back into the network, causing an accumulation of errors that can significantly degrade the network's prediction accuracy especially, when the prediction horizon is larger.

Chapter 6 Neural Network based Flame Monitoring and Control System

This chapter will discuss the development and testing of an Artificial Neural Network (ANN) based flame monitoring and control system. Chapters 4 and 5 reviewed details including data collection, signal processing, the choice of the best features and ANN training. In this chapter, all these topics will be brought together in the final controller design.

All experiments were conducted on the 150 kW PF burner rig based at Casella CRE Ltd., UK. The prototype controller was commissioned, debugged, and tuned to yield a satisfactory performance. Although there are large combinations of settings that could be used to achieve good operation of the burner, probably the most effective way is to regulate the excess air so that the burner can always operate at near stoichiometric condition [Chong, 2000; Wojcik *et al.,* 2003]. The design of the Flame Monitoring and Control system (FMCS) is particularly attractive to a multiple burner installation because it would allow individual burner performance within a boiler to be assessed.

6.1 Controller Design

Figure 6.1 shows a schematic of the Flame Monitoring and Control System (FMCS) devised to optimise an individual burner within a boiler. The three sensors, namely, IR, Microphone, and AE monitored the flame. The signals were acquired as per the system hardware design, which can be found in Chapters 3 and 4. The signals were passed through LabVIEW™ and Matlab™ in sequence with data being acquired with an interval of 10 seconds. The sensor signals were transformed to yield the three most highly correlated features that were used to train the ANNs to estimate the CO and NOx. These trained ANNs were then used by the rules embedded in the controller to optimise the combustion.

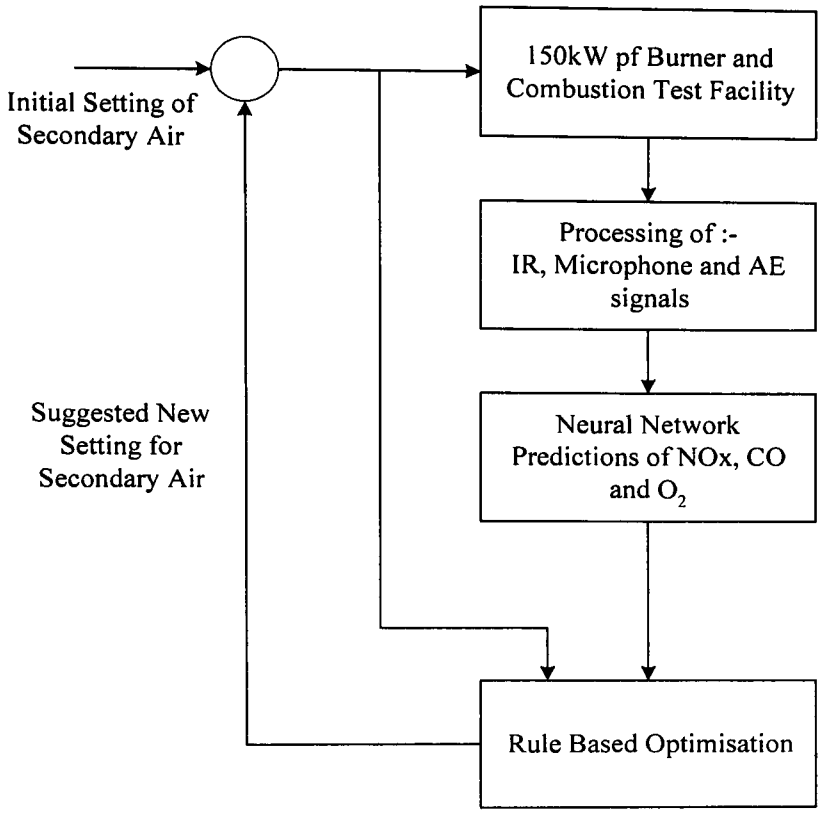

Figure 6.1 Neural Network Monitoring and Control System

The rules for PF burner optimisation were obtained by classifying both NOx and CO within one of three bands, namely, (a) low, (b) average, and (c) high. A total of nine states were identified with their corresponding control actions being shown in Table 6.1. Other design parameters that determined the overall controller performance were: -

1. Selection of higher and lower target bands for NOx and CO.

2. Increasing or reducing the amount of air.

3. Determining the change in the flow rate of air.

Table 6.1 Nine Possible States and their correspond Suggestions for Improvement

	Low CO	**Average CO**	**High CO**
High NOx	7 Reduce Air by 10 m^3h^{-1}	8 Reduce Air by 5 m^3h^{-1}	9 Keep Air Constant
Average NOx	4 Reduce Air by 5 m^3h^{-1}	5 Reduce Air by 2.5 m^3h^{-1}	6 Increase Air by 2.5 m^3h^{-1}
Low NOx	1 Keep Air Constant	2 Reduce Air by 2.5 m^3h^{-1}	3 Increase Air by 5 m^3h^{-1}

Note: Numbers in Each Box Indicate the States

State 1 indicates both NOx and CO fall within "optimum" regions. State 2 shows that NOx is low and CO is slightly over the target. The priority within the controller is with NOx and so a small reduction of excess air can be introduced. State 3 implies serious incomplete combustion therefore a considerable increase in the secondary airflow rate was required. State 4 shows the NOx increasing so a reduction in the secondary airflow rate was required. State 5 implies both NOx and CO fall beyond their targets, and as the NOx has been given priority to a reduction of airflow is suggested. State 6 shows the CO was extremely high and therefore requires immediate attention by increasing the secondary airflow rate. State 7 suggests the NOx was high and so a considerable reduction of the secondary airflow rate for a better time response should be introduced. State 8 shows NOx was too high and will require a reduction in the secondary airflow rate, but on a smaller scale as compared with State 7 as the CO has increased. Finally, State 9 shows both NOx and CO simultaneously are very high. This, however, is unlikely to happen as long as the target bands have been set correctly and as a result nothing can be done.

6.1.1 To Determine Good Controller Settings

In order for the settings of low and high target bands for NOx and CO to be correctly identified, a systematic procedure was adopted. First, the author decided on the concentration at which to maintain the CO. For example, if the objective were not to exceed 300 ppm of CO, the lowest intensity for NOx would be 450 ppm as shown in Figure 6.2 (a). The target bands for both NOx and CO were identified from the data collected for model training; alternatively, historical data corresponding to the boiler of interest could be used. The upper band setting could directly impinge on system behaviour, for example, if the upper NOx band is set too high, it is likely that the predicted NOx will occur between the upper and lower bands and hence a small change in air will be given so that the system will take a longer time to reach the target (i.e. the controller will have a sluggish response). This can be explained by the fact that if the prediction falls in the intermediate region, the signal is considered to be close to the lowest NOx and therefore only a small change of air will be recommended to prevent overshooting. On the contrary, if the distance between the upper and lower bands is small, most probably, the NOx will fall beyond the upper band and subsequently a large change in air would be introduced. As a result, the system will overshoot leading to long transients and combustion instability.

(a)

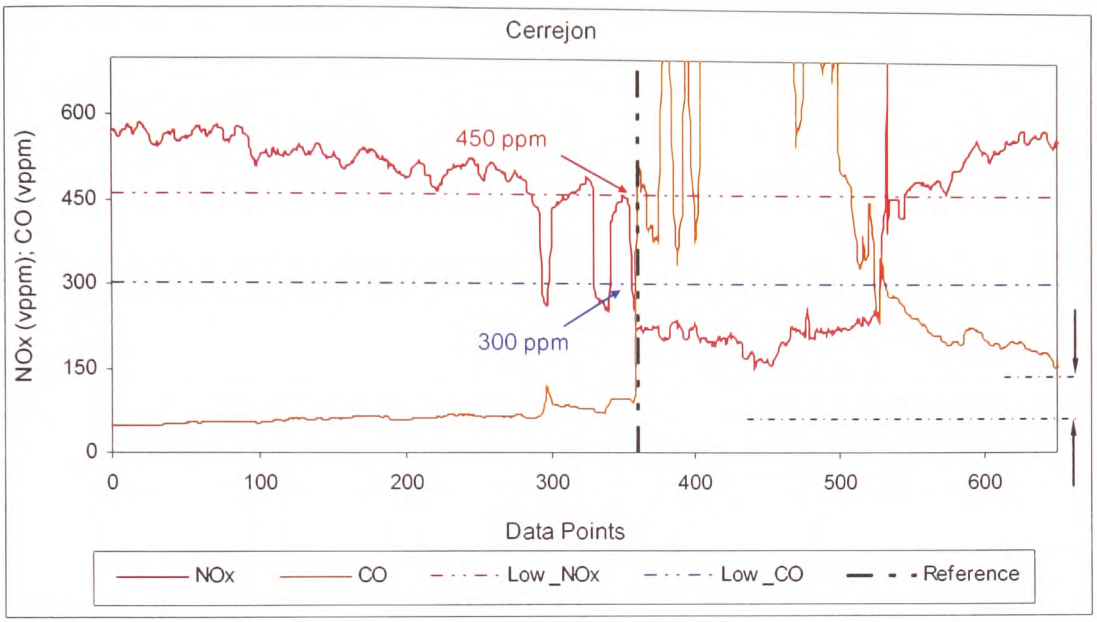

(b)

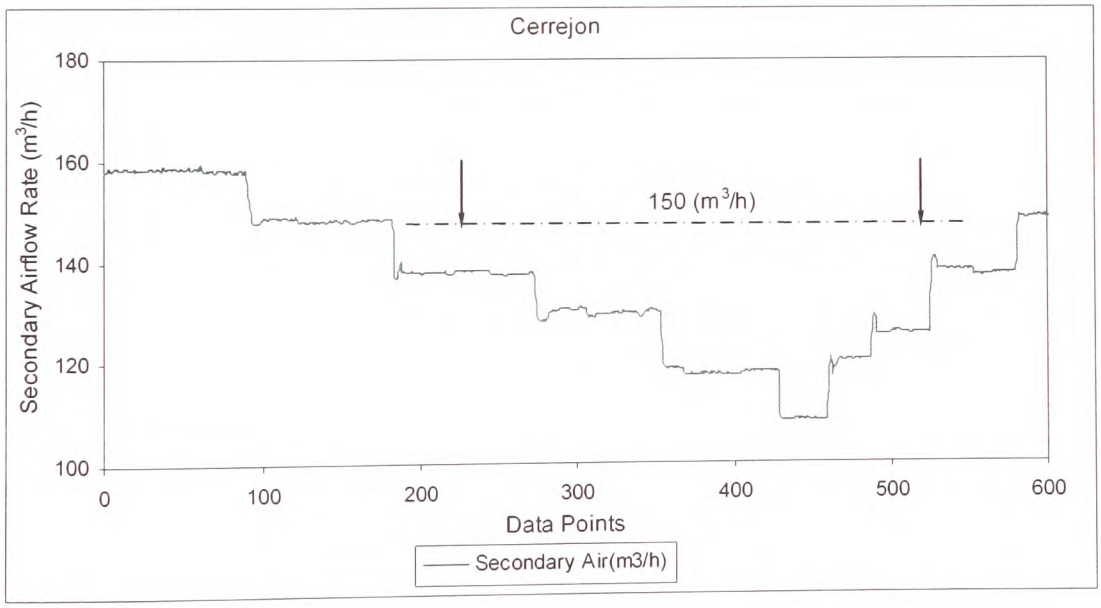

Figure 6.2 Data for: (a) Determining System Target Band Settings and (b) Gaseous Models Training 1 – Cerrejon Coal

6.1.2 Neural Network Training

The gas models of NOx, CO and O_2 were trained using standard recursive network with the input features being arranged as illustrated in Figure 6.3.

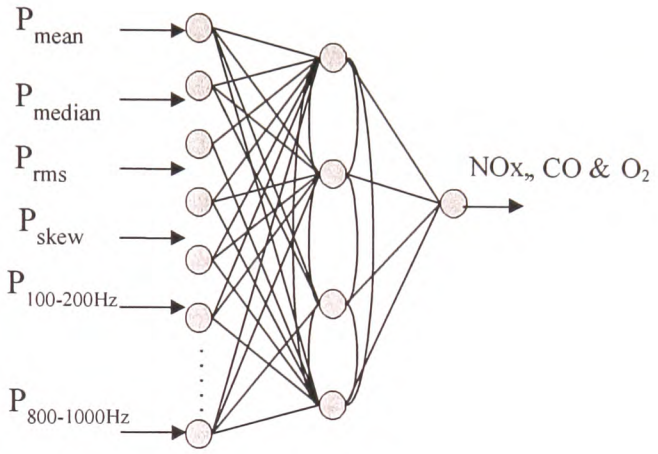

Figure 6.3 Recursive Network as the final ANN for Control Experiments

Figures 6.2 (a) and (b) highlight (arrows) inconsistent trends of CO when the burner was operated with the same secondary airflow (150 m^3/h) at two different times. This implies that a model trained with input vectors from both sections (approximately between data points 0 to 300, and 500 to 650, of Figure 6.2 (a)), the predictions made will be inaccurate because of conflicting training examples. This occurred because unburned carbon in the fly ash settled around the gas sampling point after a prolonged period of operation. Continued operation even at a lower combustion rate will appear to result in high CO concentration. This is not likely to happen in a full-scale boiler in which air is purged through the sampling probes to alleviate clogging resulting from fly ash and the effect of particulate stratification. For this reason, the latter data were excluded from the training of the CO model and a regular cleaning regime for the CO sampling probe was recommended.

6.1.3 Signal Averaging

It is acknowledged that pulverised fuel and other coal combustion systems exhibit a relatively slow response. Conventional combustion monitoring systems provide information that has been averaged over several minutes or hours [Daw *et al.*, 2002]. However, Wilson *et al* (2002) demonstrated that a 5-minute sampling period could adequately control a coal utility boiler without causing system instability. In practice, there is no definitive control interval as numerous factors such as the furnace physical attributes as well as the chemistry of combustion will require different settings.

The IR, Microphone and AE signals inherited variations resulting from factors such as flame flicker, pressure fluctuations and flue gas turbulence that took place during combustion and for this reason there is a need to average the predictions. Furthermore, some gas signals oscillated in a sinusoidal fashion, which were found to be driven by small fluctuations in the coal feed mechanism. This further consolidated the need for signal averaging and therefore a 30-point average was used. This allowed a sample acquired over a control action take placed. Figures 6.4 (a) and (b) present the actual and averaged predictions of NOx and CO respectively, and as can be seen, the average signal captures the trend of the "raw" signals.

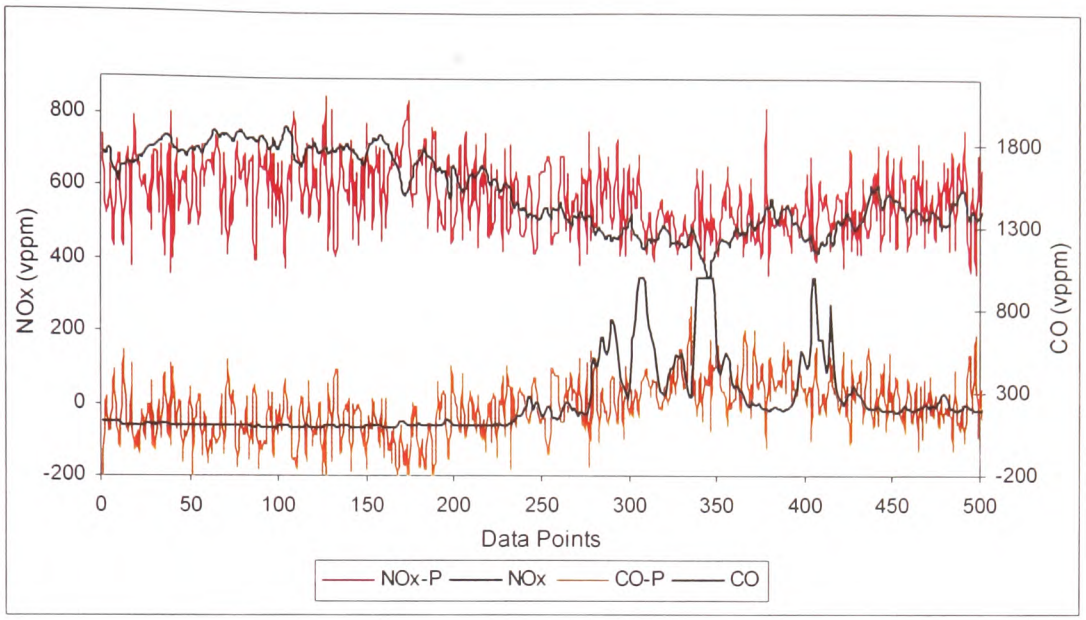

Figure 6.4 (a) The Actual and Predicted NOx and CO

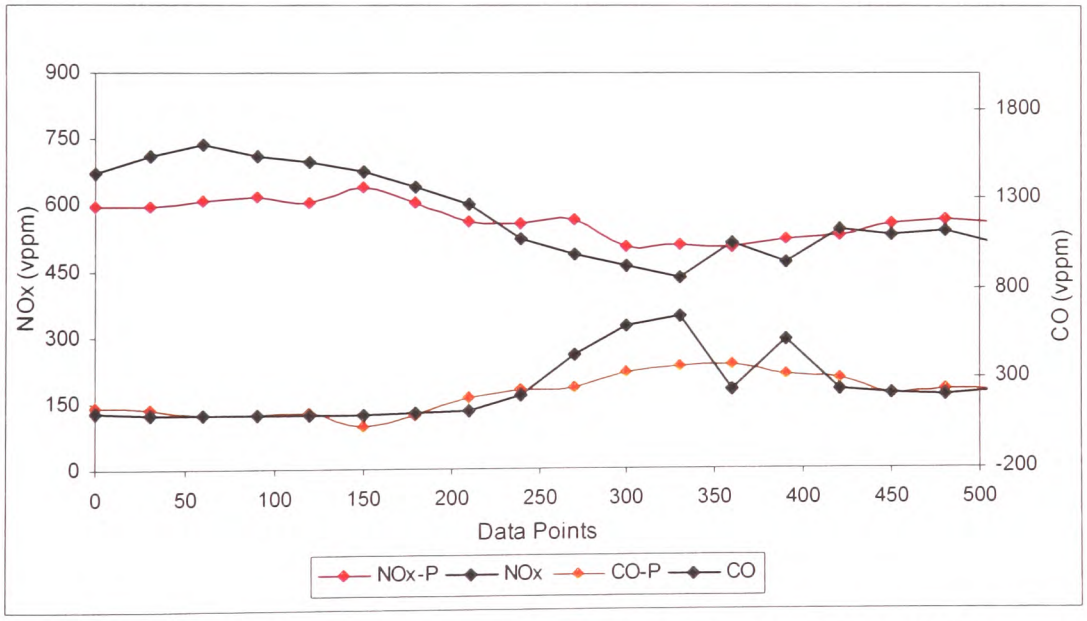

Figure 6.4 (b) The 30-point Average Actual and Predicted NOx and CO

6.2 Flame Monitoring and Control System Testing

In order to test the controller scheme, the work was undertaken in two phases: -

1. Phase 1: collection of data for ANN model training and determination of controller settings (target bands, decisions to increase or to decrease air, amount of change).

2. Phase 2: initialise the control experiment with a high excess air with the controller objective being to tune the burner to a good combustion condition.

6.2.1 Control Experiment 1 – Cerrejon Coal

The burner was initially set to a high secondary airflow rate of 155 m^3/h. The upper and lower limits were 600 and 450 ppm for the NOx, and 450 and 300 ppm for the CO. The solutions for conditions for the controller are given in Table 6.1.

Figures 6.5 (a), (b) and (c) show the results for NOx, CO and O_2 obtained as the experiment proceeded. As can be observed, the gases and the predictions were in good agreement. The NOx reduced as the secondary air decreased (pale green). Because the control experiment was conducted some 12 months after the data collection phase for training and testing of different ANN architectures (Chapter 5) a change in the burner characteristics has resulted in changes to the flame signals leading to different prediction errors. The percentage error for the NOx and CO were 19 % (ME of 84 ppm) and 127 % (ME of 165 ppm) respectively. The increased percentage error for the CO was perhaps due to the offset between the predicted and gas analyser readouts. This arises because the gas sampling probes were cleaned just before the control experiment and so reduced emissions should be expected. Another factor included an estimation of a 5-minute time-delay, which occurred somewhere in between the 3rd and 5th control intervals of Figure 6.2 (b) (highlighted with black arrows). This introduced a significant number of local deviations that were associated with the ME. Both the sensors and gas analysers were

sampled at a 10-second interval. The total duration for Control Experiment 1 was about 1 hour and 20 minutes.

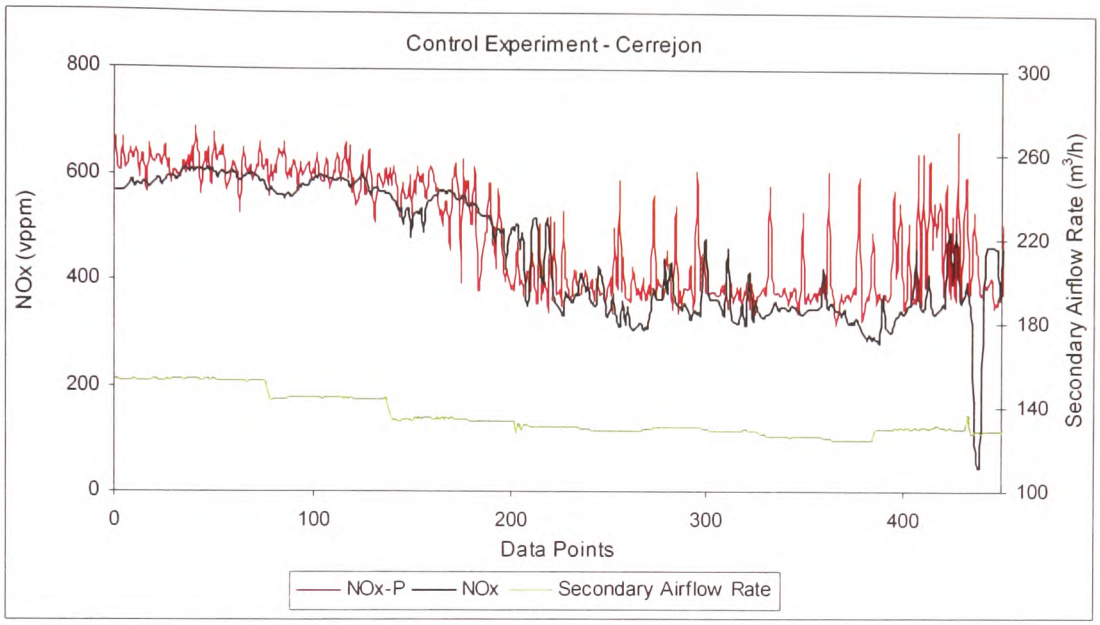

Figure 6.5 (a) Control Experiment 1 – Predicted NOx

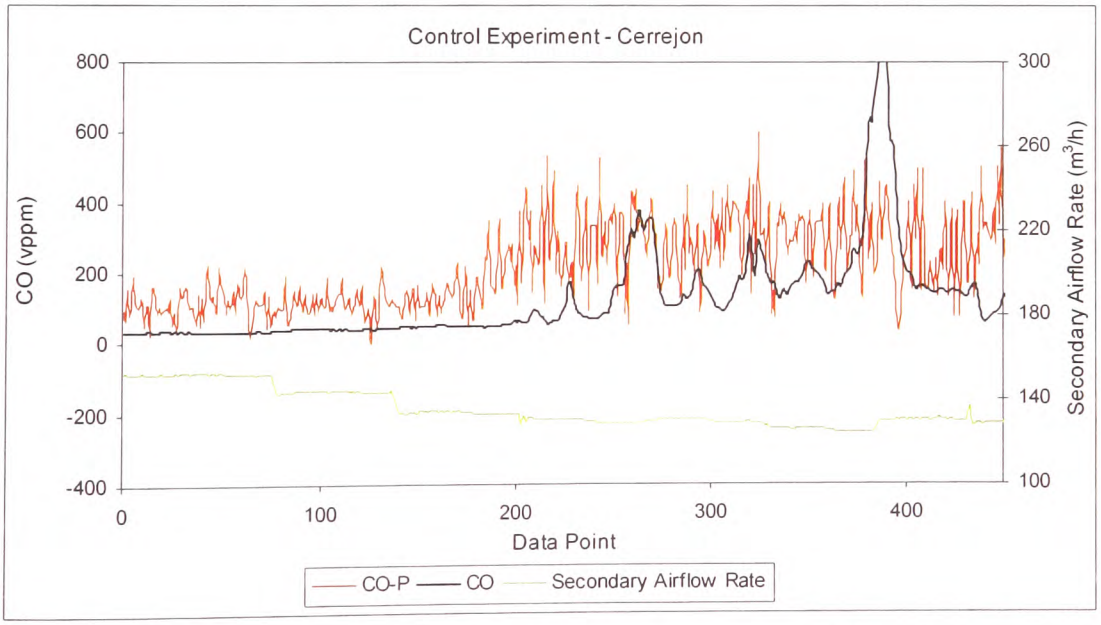

Figure 6.5 (b) Control Experiment 1 – Predicted CO

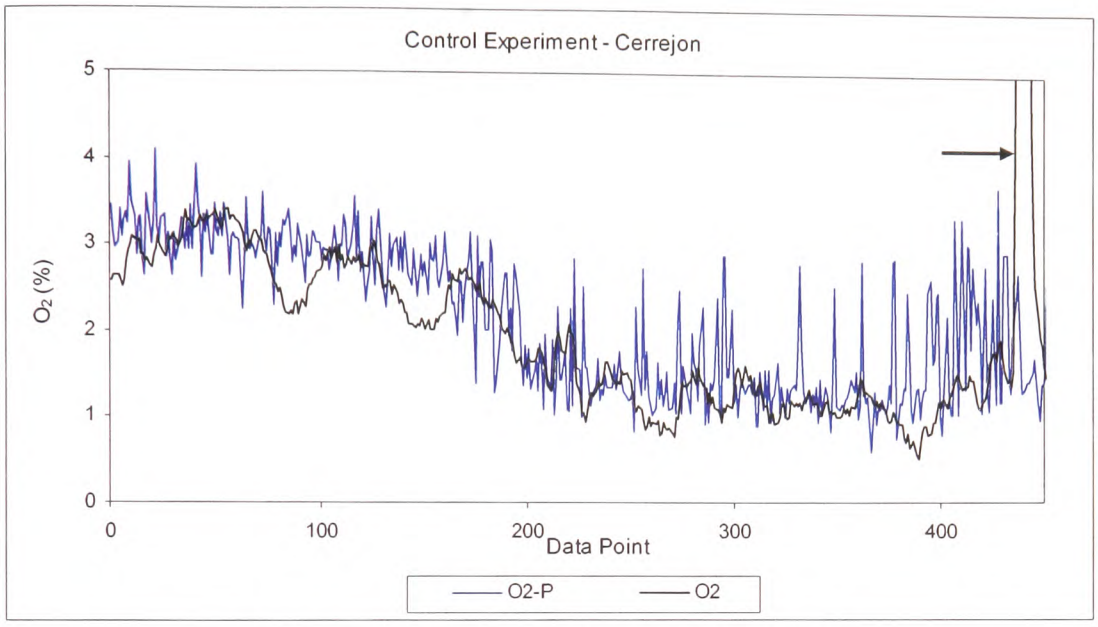

Figure 6.5 (c) Control Experiment 1 – Predicted O_2

Figures 6.6 (a), (b) and (c) show the ensemble averages of the predictions for the NOx and CO with the green and red arrows being used to indicate combustion conditions. The green arrows show good burner performance while the red indicates the system was out of tune. *The desirable combustion condition refers to the time when both NOx and CO arrows were in the green* (i.e. State 1). The results of Figures 6.6 (a) and (b) indicate the system achieved a good combustion condition after the 3rd control action. The controller achieved "good combustion" by allowing the CO to rise to just below the upper limit. This led to the possibility that the CO might rise above the upper threshold, possibly leading to hunting in the controller. However another advantage of the averaging and the rule-based approach to airflow adjustments is that only a sustained increase in CO will lead to an adjustment of the secondary airflow and then only by the pre-defined amount.

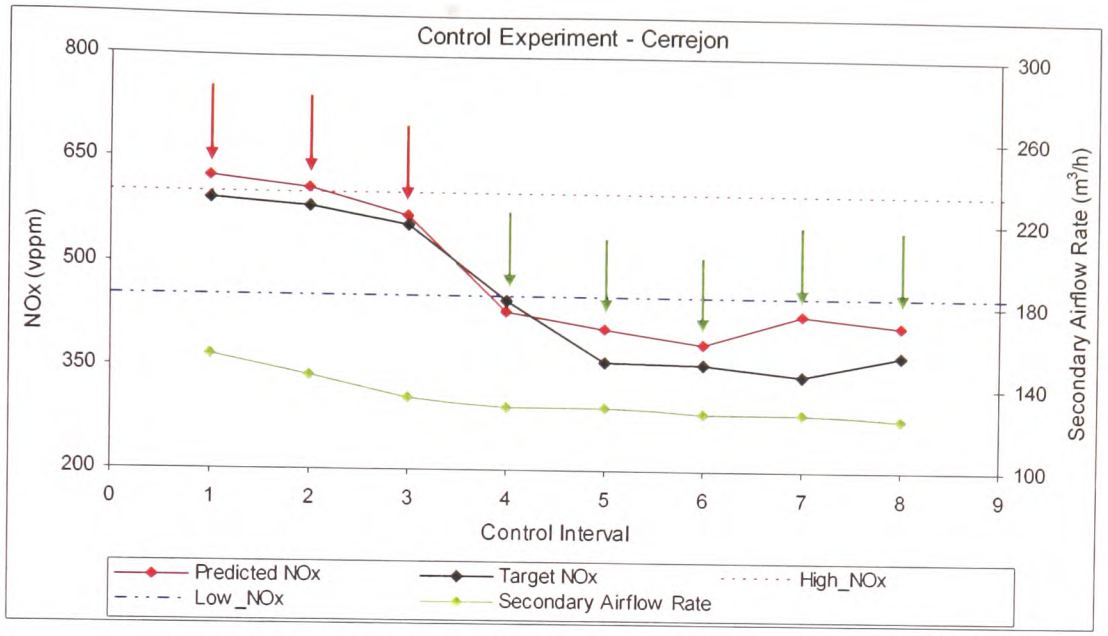

Figure 6.6 (a) Control Experiment 1 – Averaged Predicted NOx

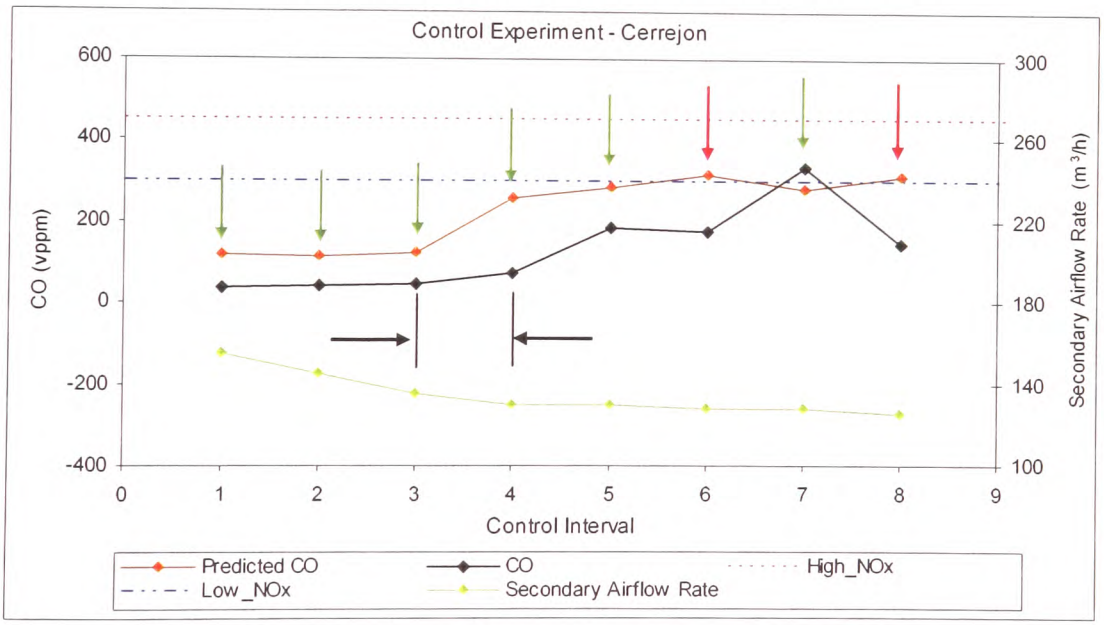

Figure 6.6 (b) Control Experiment 1 – Averaged Predicted CO

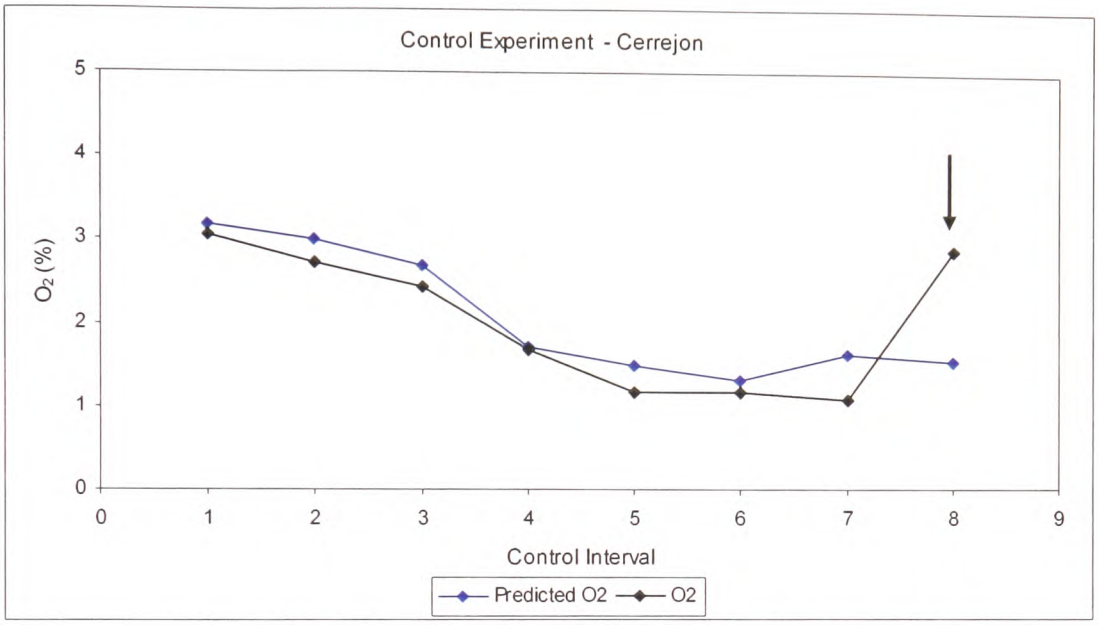

Figure 6.6 (c) Control Experiment 1 – Averaged Predicted O_2

The black arrows in Figures 6.5 (c) and 6.6 (c) indicate a rise in the O_2 reading, which was identified to result from a sudden incursion of air due to an inspection port being opened for a routine inspection. The flame monitor made predictions based solely on the flame measurement, which does not detect the disturbance due to the dilution of oxygen in the flue gases.

A summary for Control Experiment 1 is presented in Table 6.2. The prediction columns of Table 6.2 for NOx and CO are coloured according to low (green), average (yellow) and high emissions (Magenta). The system achieved the target NOx without seriously increasing CO after the 3rd adjustment of the secondary airflow rate. However, as already mentioned, slight increases in the CO will push the reading above the upper threshold (points 6 and 8).

Table 6.2 The Summary of Control Experiment 1 (Cerrejon Coal)

Control Action	Predicted NOx (vppm)	Predicted CO (vppm)	State	Suggested Secondary Airflow Rate (m^3/h)
1	622.98	116.44	7	155
2	609.33	113.25	7	145
3	568.60	121.25	4	135
4	429.08	259.70	1	130
5	406.10	283.03	1	130
6	383.17	314.91	2	130
7	426.87	281.33	1	127.5
8	410.61	311.25	2	127.5

Note: The colour coding is presented as follows: - (a) Magenta – High, (b) Yellow – Average and, (c) Green – Optimum, at Indicating Emissions Concentrations inside the Burner.

6.2.2 Control Experiment 2 – Daw Mill Coal

The same procedure as in control experiment 1 was applied to control experiment 2 firing Daw Mill coal. The objective was to examine the adaptability of the FMCS under different coal conditions. The burner was initially set to a high secondary airflow rate of 160 m^3/h. The lower bands for NOx and CO were 500 and 350 ppm (Figure 6.7) and their respective upper bands were 550 and 500 ppm. Daw Mill has a lower nitrogen content than Cerrejon and should therefore emit less NOx. However as Cerrejon has higher calorific value it was fired at a lower feed rate and so NOx was lower. In addition, the lower volatility of the Daw Mill coal may have led to more char nitrogen retention, which was later converted into molecular nitrogen [IEA, 2000].

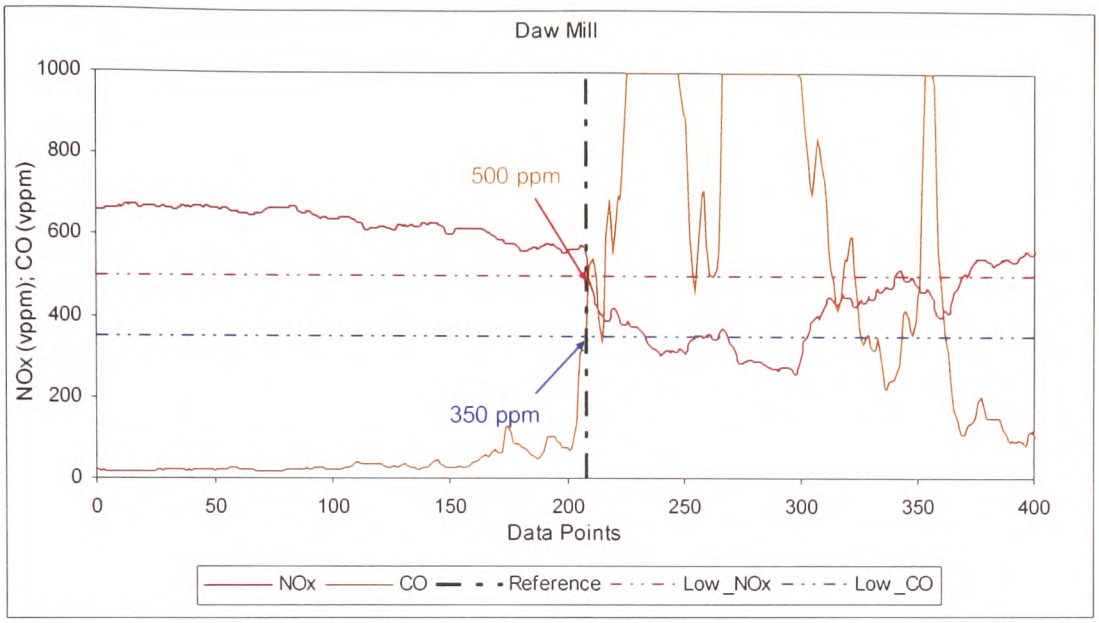

Figure 6.7 Data for (a) Determining System Target Band Settings and (b) Gaseous Models Training – Daw Mill Coal

It was fortunate that the solutions for conditions of Table 6.1 have proven successful in control experiment 1. The same set of settings was also applied to Control Experiment 2. Figures 6.8 (a), (b) and (c) indicate the results for NOx, CO and O_2 obtained as the experiment proceeded. The predictions were in good agreement with the measured gases. The NOx reduced as the secondary air increased and the percentage errors for the prediction of the NOx and CO were 20 % and 62 % respectively. An improved prediction of CO has been observed with the NOx error remaining almost the same (Figures 6.8 (a) and (b)). Furthermore, because neural network tends to predict noise in addition to the underlying signal as well as the network responded to the region close to zero thus yielded negative predictions.

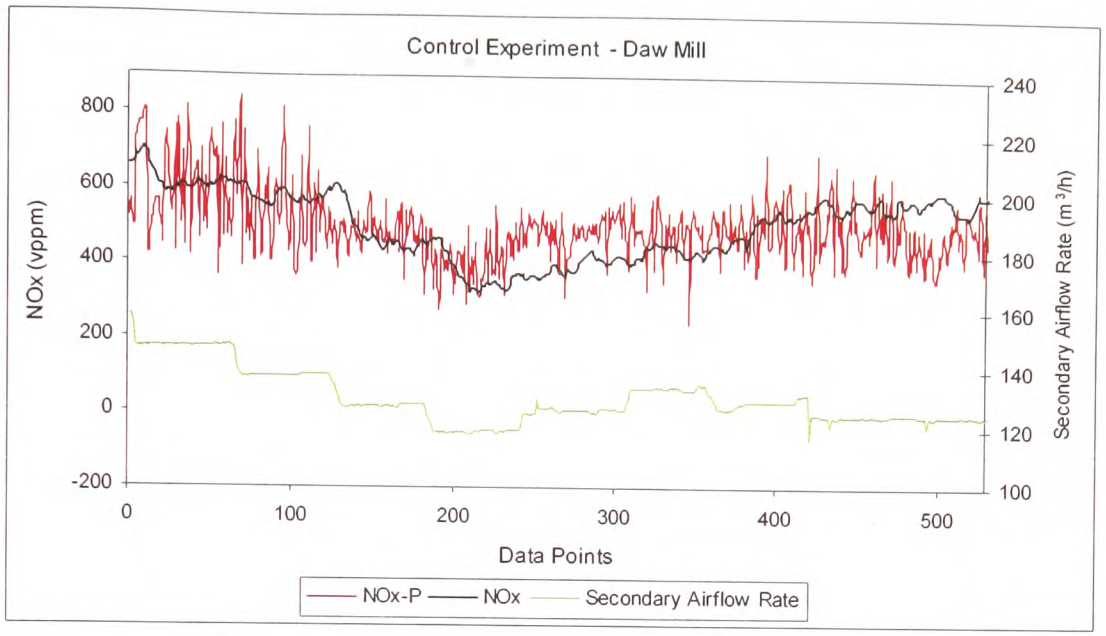

Figure 6.8 (a) Control Experiment – Predicted NOx

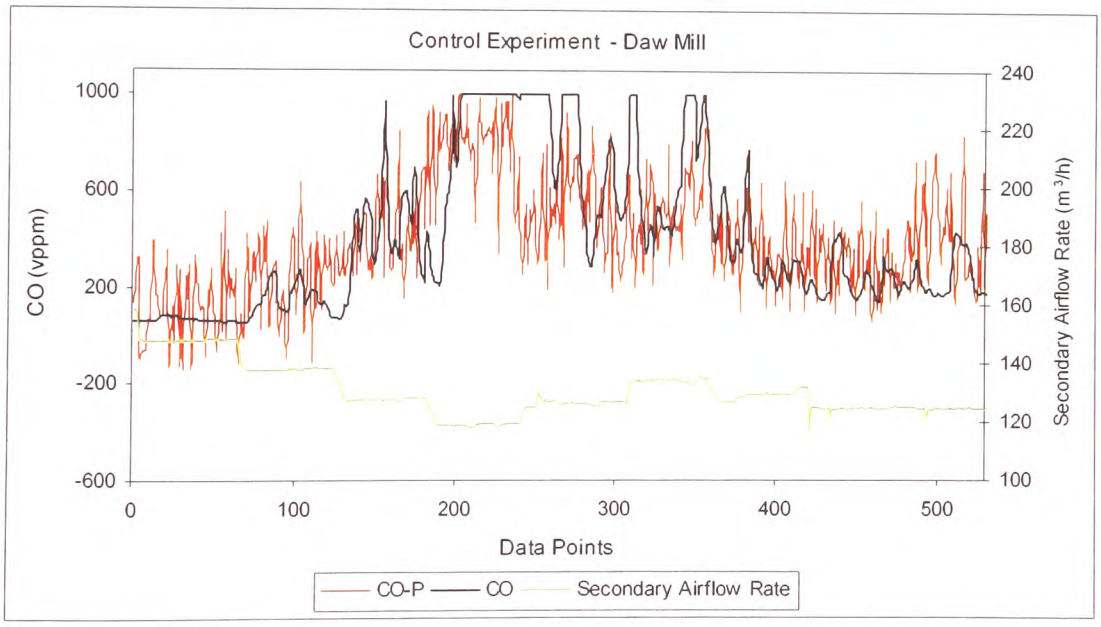

Figure 6.8 (b) Control Experiment – Predicted CO

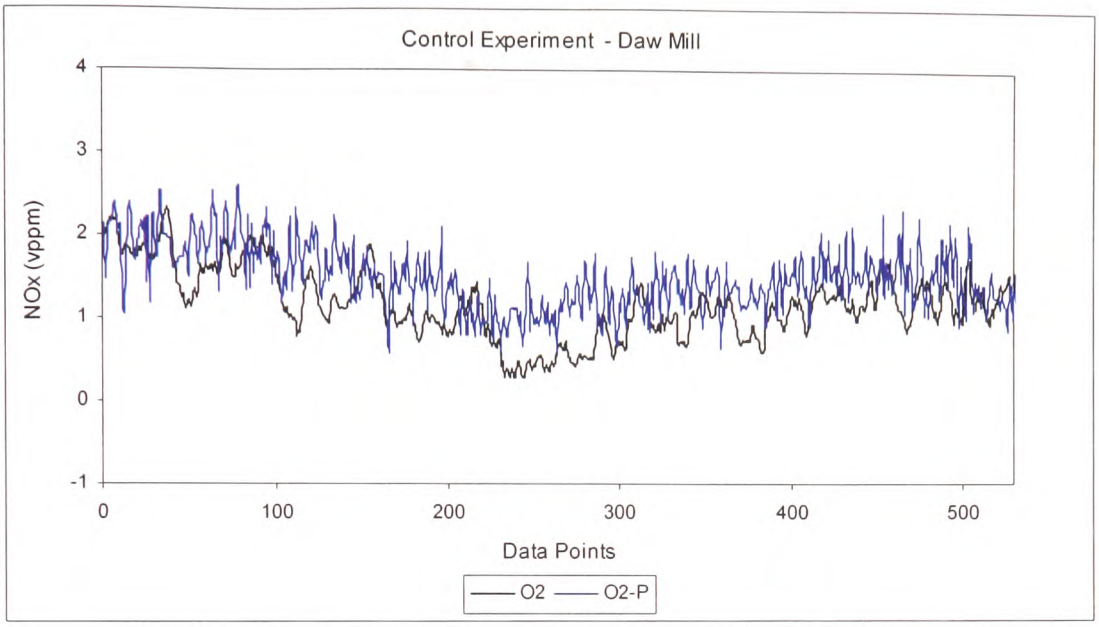

Figure 6.8 (c) Control Experiment – Predicted O_2

The control result is presented in Figures 6.9 (a) and (b). As before, the green (optimal) and red (sub-optimal) arrows are included to highlight the burner conditions. It was found that the system achieved good combustion after the 3rd adjustment of the secondary airflow rate, so a further reduction of 10 m^3/h was introduced manually at the 4th control interval with the intention of examining the reaction of the controller towards air deficient conditions. Subsequently, the FMCS drove the burner out from the highly unburned carbon situation and settled in the optimal combustion condition at control interval 8. The summary of this experiment is presented in Table 6.3.

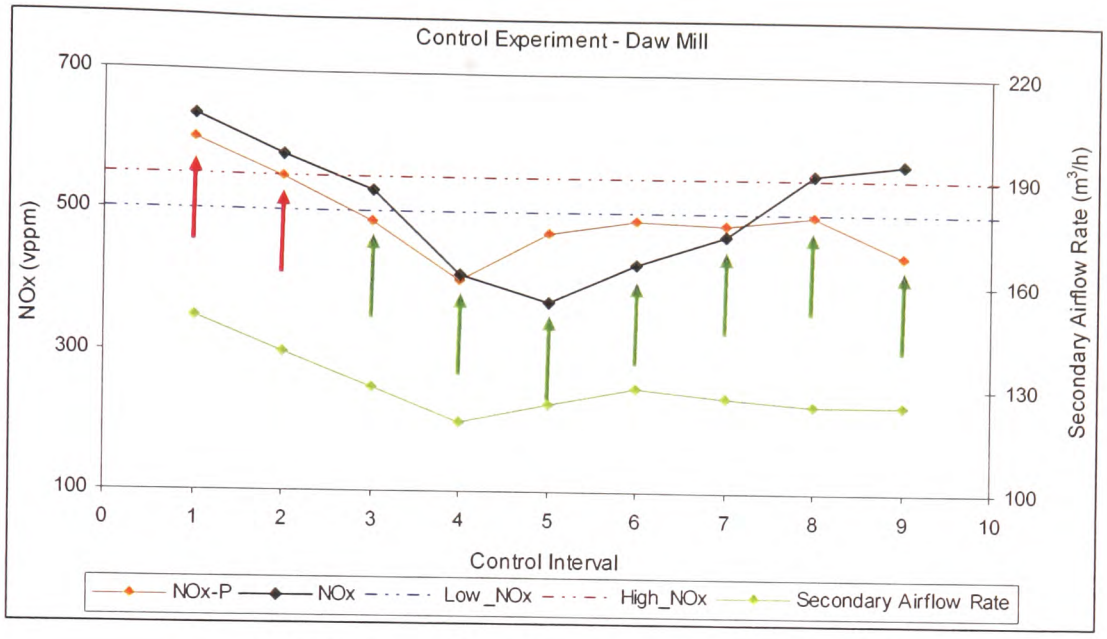

Figure 6.9 (a) Control Experiment – Average Predicted NOx

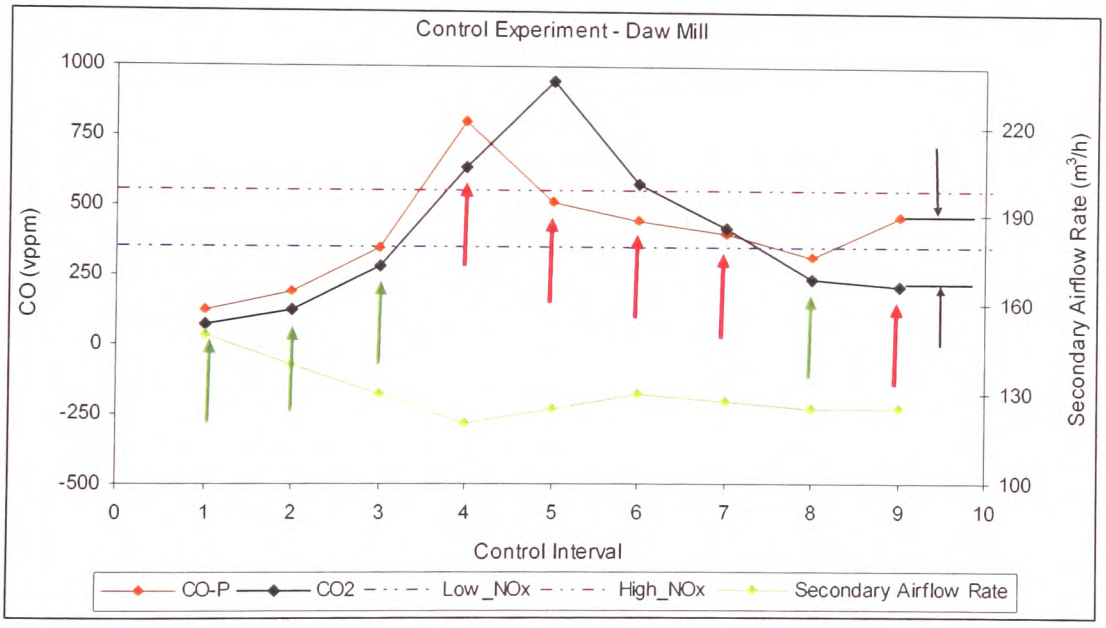

Figure 6.9 (b) Control Experiment – Average Predicted CO

Table 6.3 The Summary of Control Experiment 2 (Daw Mill Coal)

Control Action	Predicted NOx (vppm)	Predicted CO (vppm)	State	Suggested Secondary Airflow Rate (m^3/h)
1	602.42	124.32	7	150
2	550.50	190.65	7	140
3	486.87	348.16	1	130
4	404.50	803.71	3	120
5	470.95	510.38	3	125
6	491.37	449.00	2	130
7	484.47	398.38	2	127.5
8	498.85	313.78	1	125
9	440.07	458.71	2	125

Note: The colour coding is presented as follows: - (a) Magenta – High, (b) Yellow – Average and, (c) Green – Optimum, at Indicating Emissions Concentrations inside the Burner.

6.3 Summary of Chapter 6

This section summarises the development of the Flame Monitoring and Controller System (FMCS). The successful proof-of-concept has offered a low cost Flame Monitoring and Control System specifically for a PF system.

One can design a good controller if the scheme is governed by sound knowledge concerning the process itself. Artificial Neural Networks (ANNs) are highly capable of modelling system input-output relationships when there is an understanding of the system dynamics, this makes them very lucrative especially for highly complex nonlinear processes. In theory, there are many neural network model based controller schemes, which claim to be highly adaptable to system changes. Nevertheless, they are not parsimonious when dealing with the updating of a very large number of weights [Krishnapura, 1999]. A rule-base was found to be suitable for handling the ambiguity of a process based on "crisp" algorithms. The integration of the salient features of both the ANN set of rules solved the problems more elegantly and naturally [Palakal *et al.*, 1995].

The IR, Microphone and AE signals were all capable of representing the gaseous emissions. A recursive network with one input and one output layer and with 10 hidden neurons was employed. ANNs were used as a "software sensor" to predict gas readings with the predicted values being ensemble averaged before being used through a set of rules to control the burner.

The Flame Monitoring and Controller Scheme (FMCS) builds on existing boiler system knowledge, models the process, and controls the combustion and achieves improved levels of performance while staying within predetermined operational constraints. The system has been successfully tested on the 150 kW combustion rig based at Casella CRE Ltd., U.K. with two sets of control experiments indicating that the FMCS is able to cope with the different coal types. The experiments also suggested that the flame based monitor has a better response than a gas analyser and hence achieves better control performance.

Chapter 7 Wavelet Analysis, ANN based *k*-step Predictions, and Self-Organising Map as System, Novelty Detector

In this chapter three sections will be discussed, that is (a) Wavelet Analysis (WA), (b) an Artificial Neural Network (ANN) *k*-step ahead prediction model, and (c) Self Organising Map (SOM) neural network. Despite traditional signal processing techniques such as the statistical description of data and the Fast Fourier Transform (FFT) algorithm, another area that has recently gained a great deal of attention from scientists and engineers is known as Wavelet Signal Analysis. Other techniques such as the use of a *k*-step ANN predictor that can improve the system time response, and the adoption of a SOM neural network as a system fault detector is also discussed.

7.1 Discrete Wavelet Transform

Earlier chapters demonstrated the successful implementation of signal processing based on the statistical description of data and the Fast Fourier Transform. However, a disadvantage of the Fast Fourier Transform is that the time information is lost when the signal is converted from the time to the frequency domain. This situation may not be so important to a stationary signal but as most signals contain numerous non-stationary or transitory characteristics such as, drift, trends, and abrupt changes, the FFT that uses a fixed time window for all frequencies was found to be lacking.

Many signals require a more flexible approach where the window size has to be varied, for example, a discontinuity in a sinusoidal signal will not be shown using a purely frequency-based FFT analysis, whereas the exact location in time of the discontinuity will be revealed in the wavelet coefficients [Wavelet Tool Box - for use with Matlab™]. The Discrete Wavelet Transform (DWT) is capable of capturing an instantaneous impulse that spreads over all frequencies. The DWT uses long time intervals where low frequency information is highly important and vice versa for high frequency information. In general, the low frequency content is the most important part and yields the signal identity. In the filtering process of the DWT, one often speaks of approximations and details (Figure 7.1) of the signal.

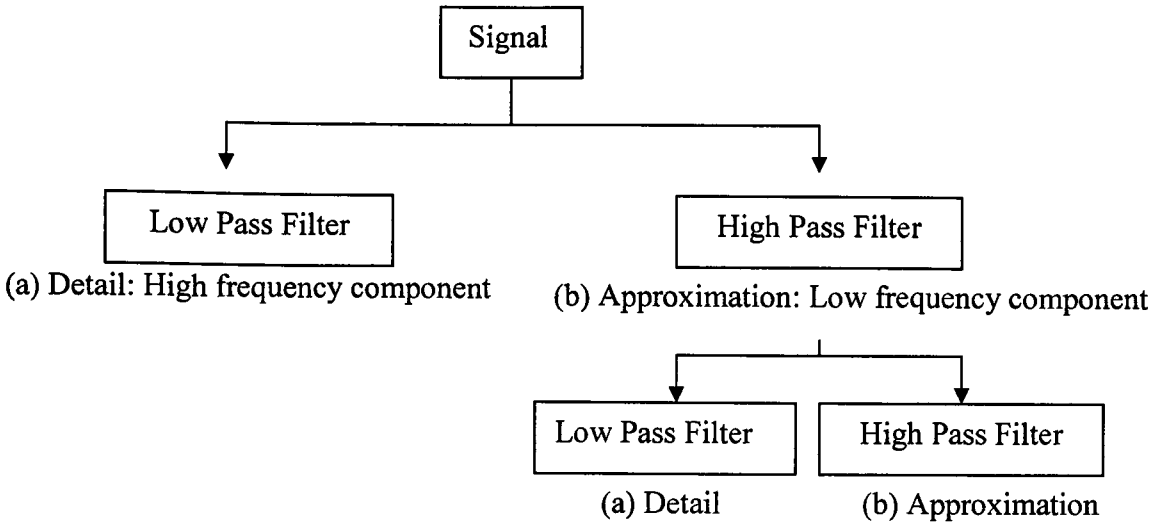

Figure 7.1 Wavelet Decomposition Tree

As can be seen in Figure 7.1 the decomposition process can be iterated, with successive approximations being decomposed in turn, so that one signal can be broken down into many lower resolution components. This is known as the wavelet decomposition tree. The advantage of using WA is that it is a time scale version where both time and frequency interaction of a signal is well preserved.

7.1.1 Wavelet Analysis of Combustion Signals

The widespread use of WA in research and engineering is motivated by the following two reasons: -

1. WA is capable of revealing aspects of data that other signal analysis techniques miss, such as, breakdown points, discontinuities in higher derivatives, and self-similarity.

2. WA compresses, or de-noises signals without appreciable degradation.

Suh (1999) claimed that WA is suitable for monitoring vibration signals. He demonstrated that the decomposed Wavelet Coefficients (WCs) were highly

correlated to the events corresponding to the degradation of bearings in a gear box and later reported that the WCs can provide good estimation when combined with classification using ANN approaches. In another example, Zheng (1999) used WA to decompose a series of financial data for future time-series predictions. Both Suh and Zheng concluded that the predictions made by the decomposed WCs constantly outperformed the predictions made by the original data set. In combustion, the DWT was used to analyse the sensor signals that correspond to the burner conditions. The WCs were compared with existing features and gaseous readings followed by ANN predictions using the same network. Obviously, the objective is to make a direct comparison of both the WA and statistical, or FFT based systems.

Data corresponding to the Daw Mill coal, swirl number 0.8 of Control Experiment 2 were used for the comparison. The number of WCs generated was determined by the level of decomposition. The IR signal was decomposed to the 5^{th} level (i.e., 32 WCs) using a 4^{th} order Daubechies wavelet. Multi-resolution Analysis (MRA) [Zheng *et al.*, (1998)], was used to observe WCs from each node in the decomposition tree and separate those that look similar to the gas signals. Figures 7.2 (a) and (b) show the results from a selection of features, WCs, and the gases NOx, CO and O_2.

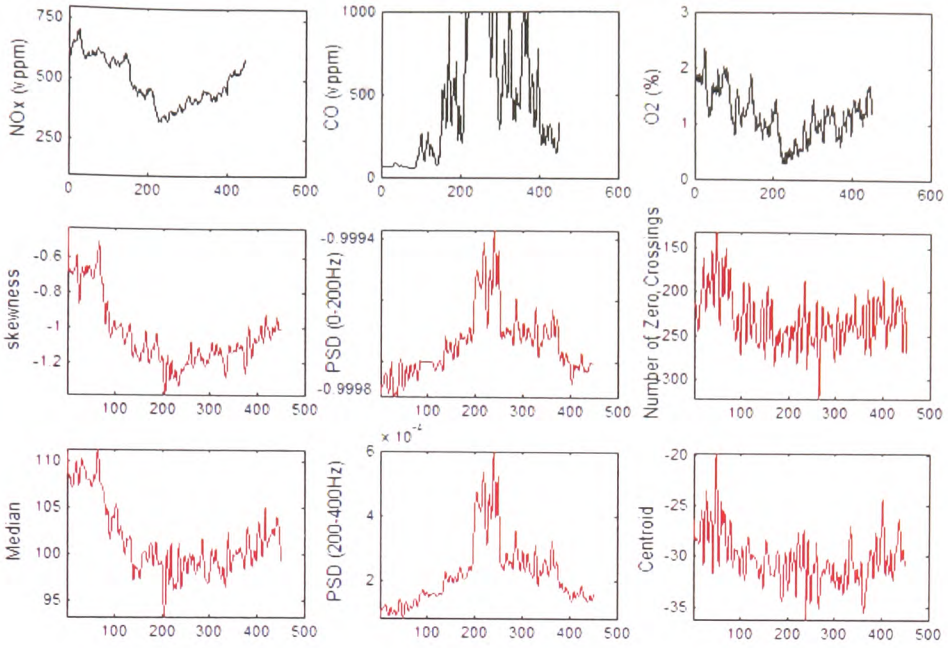

Figure 7.2 (a) Gases, Statistical based Features and PSDs at different Frequency Bands

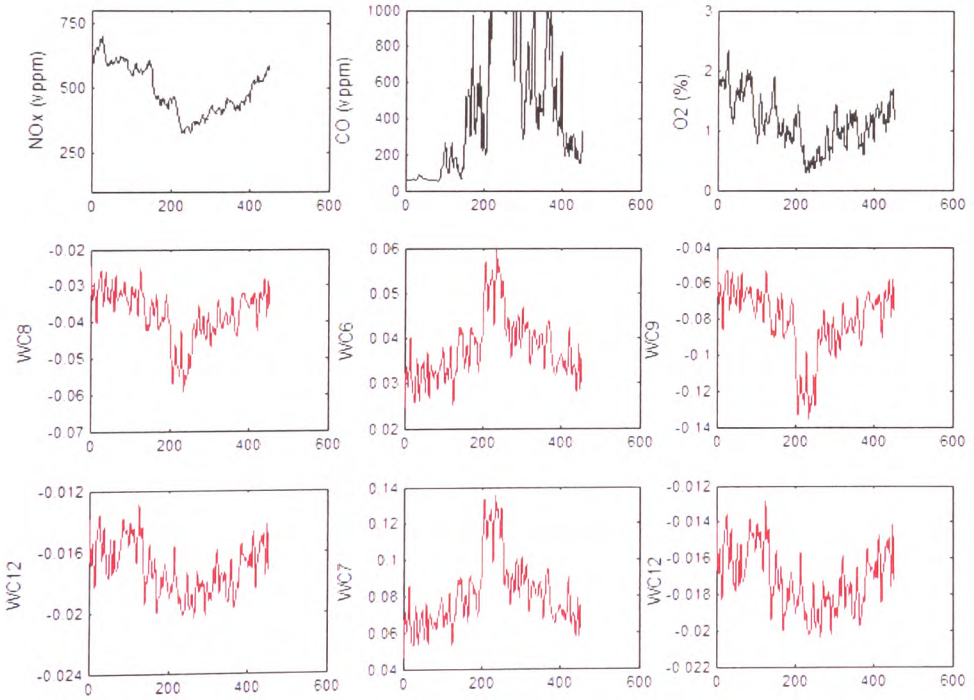

Figure 7.2 (b) Gases and Wavelet Coefficients

A recursive neural network with one hidden layer of 12 neurons with hyperbolic tangent activation function and an output layer with a neuron of linear activation transfer function was used in the prediction of NOx. The inputs were chosen to be those variables, which are known to be strongly influenced by that particular output. As a result the ANN was simulated using only the 3 most highly correlated features, and WCs. The same procedures were repeated for the prediction of CO and O_2. The results are plotted in Figures 7.3 (a), (b) and (c) respectively.

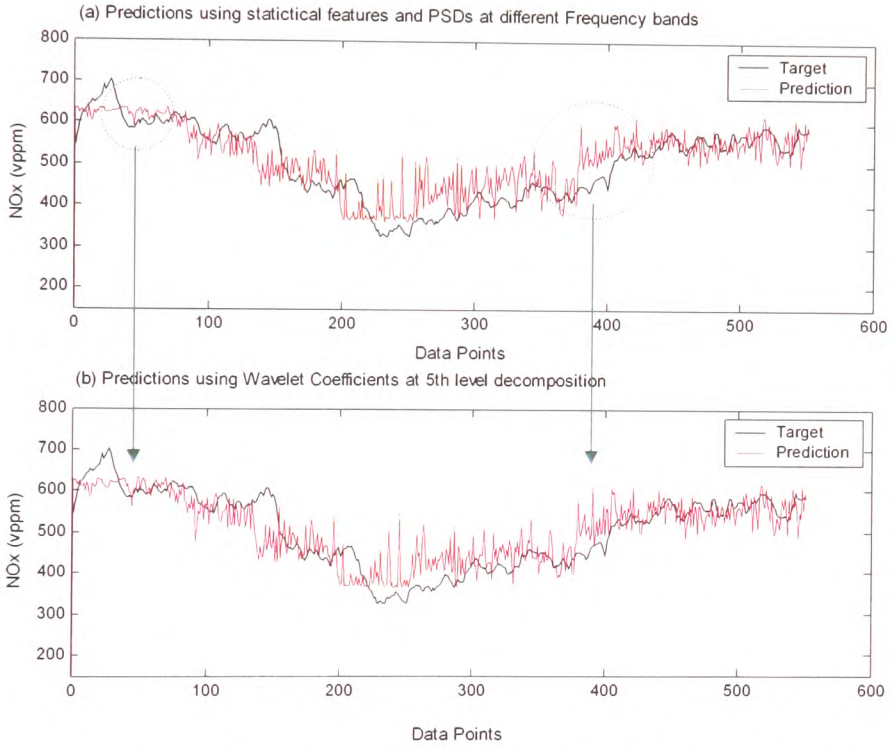

Figures 7.3 (a) Prediction of NOx using (a) Statistical Features and PSDs at different Frequency Bands, and (b) Wavelet Coefficients

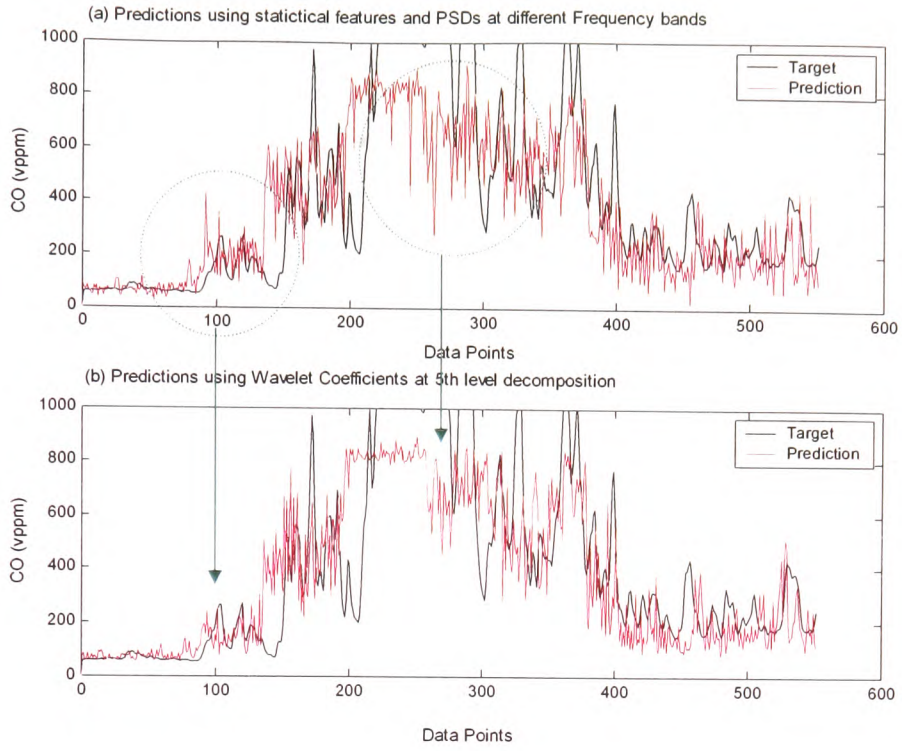

Figures 7.3 (b) Prediction of CO using (a) Statistical Features and PSDs at different Frequency Bands, and (b) Wavelet Coefficients

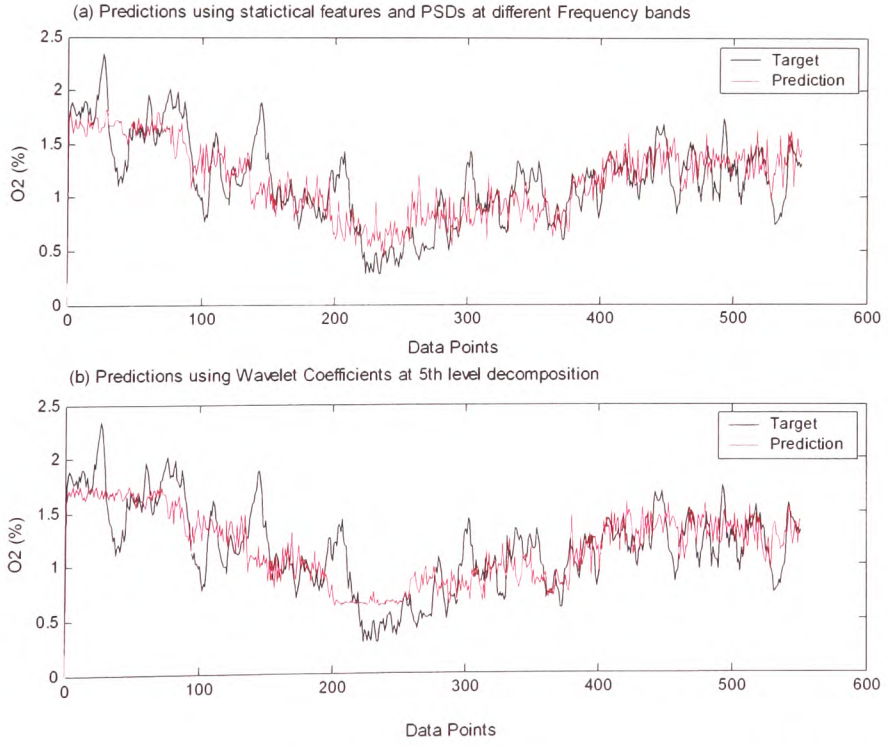

Figures 7.3 (c) Prediction of O_2 using (a) Statistical Features and PSDs at different Frequency Bands, and (b) Wavelet Coefficients

It was established from the graphical presentations that both features and WCs were sufficiently capable of estimating all three gases. However, there are detailed signals indicating that simulations based on WCs produced more accurate and less noisy predictions (as highlighted in Figures 7.3 (a) and (b)). Further to this, the calculated percentage errors in Table 7.1 suggest that WCs were slightly better features.

Table 7.1 The Percentage Errors in correspond to the Predictions of NOx, CO and O_2 for both Features, and Wavelet Coefficients

Target Gases	**Prediction using Statistical Features and PSDs of the data**	**Prediction Using Wavelet Coefficients**
NOx (% Error)	10	10
CO (% Error)	46	43
O_2 (% Error)	24	23

7.2 Artificial Neural Network based *k*-step Ahead Prediction Model

Another area of ANN research that has already attracted a great deal of attention to the control community is future prediction models. The *k*-step prediction is concerned with forecasting the process output over a certain horizon into the future, based on a model describing the process evolution and the available information. Generally, there are two types, that is (a) recursive and (b) non-recursive predictors [Tan *et al.*, 1999]. Ironically, a *k*-step prediction model can be created externally through incorporating a regressor vectors (i.e., ARX and ARMA) to any static models. This type of arrangement is also known as the "externally recursive network" [Russell *et al.*, 1997].

ANNs are very useful for nonlinear system modelling. As time goes by, the theory has now been extended to perform nonlinear *k*-step predictions into the future. The predictor employs past measurements of the process output, and past as well as future values of the manipulated input, to forecast the future output of the process over a rather long horizon. The schematic of a recursive *k*-step predictor can be found in

Figure 5.40. The process can be described by the following nonlinear discrete time equation: -

$$\hat{y}(t+1) = f[y(t).....y(t-n_a+1), u(t-n_k+1).....u(t-n_k-n_b+1), \theta] \qquad [7.1]$$

Where n_a and n_b are the orders of $\{y(t)\}$ and $\{u(t)\}$, n_k is the number of delay, $\hat{y}$ is the output of the model, θ is the parameter matrix, and f is the nonlinear input-output mapping. Based on this model, substitute $t = t + 1$ into Equation 7.1 yields: -

$$\hat{y}(t+2) = f[y(t+1).....y(t-n_a+1), u(t-n_k+2).....u(t-n_k-n_b+2), \theta] \qquad [7.2]$$

In order to demonstrate the performance of *k*-step predictions, IR features from the Daw Mill coal at a swirl number of 0.8 for Control Experiment 2 were used for offline simulations. The input-output variables of the system were configured in agreement to Equations [7.1] and [7.2]. The n_a, n_b and n_k were 3, 1, 1 respectively. The MLP network had one hidden layer of 10 neurons of hyperbolic tangent activation function, and an output layer of a neuron with a linear activation transfer function. The first 300 data points were used for the training with the rest for validation. For comparability, the target signals were moved *k*-steps forward to ensure that the targets coincided with the predicted values. Figure 7.4 presents four results corresponding to 1, 5 10 and 20 step future predictions.

It is clear that the prediction errors increased as the number of steps into the future increased. This is because in the iteration procedure, any errors in the ANN output are fed back into the network causing an accumulation of errors that degrade the network's prediction accuracy especially when the prediction horizon is larger [Tan *et al.*, 1999].

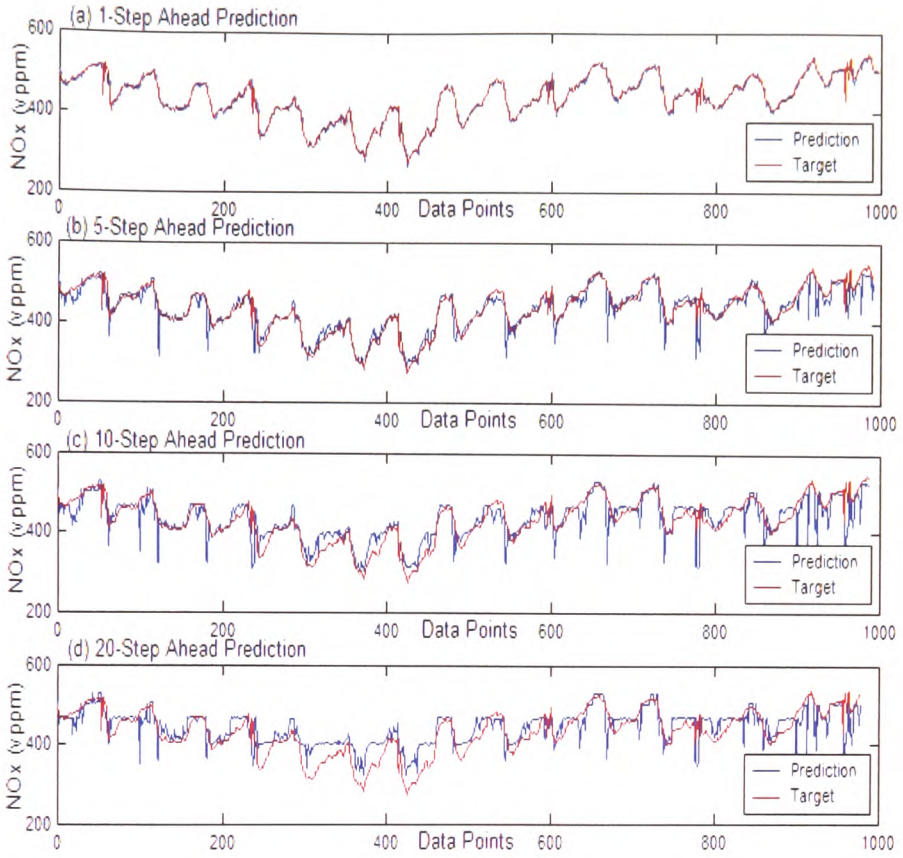

Figure 7.4 (a) 1-Step, (b) 5-Step, (c) 10-Step, and (d) 20-Step, ahead Predictions using Recursive ANN Predictor

Another way to perform k-step predictions is by the use of the non-recursive predictor. In the training process, the regressor vectors were pre-arranged by shifting the target signal a few time steps in front of the current inputs (Equation 2.3). Non-recursive k-step predictors do not depend upon the recursive technique in that it predicts $t + k$ steps of the process based on the available information until that time.

In a similar way to the plotting of results when simulating recursive predictors, Figure 7.5 shows the result of the predictions made by the non-recursive k-step predictor. The network dimensions and parameters remained unchanged. The regressor vectors were configured in agreement to Equation 2.3. One may observe in Figure 7.5 that the predictions are somewhat lag behind the target NOx, especially at larger k-step predictions. Unlike the recursive predictor where the intermediate predictions served

to provide adequate information for the model to estimate the final value, the lack of intrinsic feedback signals prevented accurate predictions to be made and as a result, a non-recursive predictor is only suitable to 1-step ahead predictions.

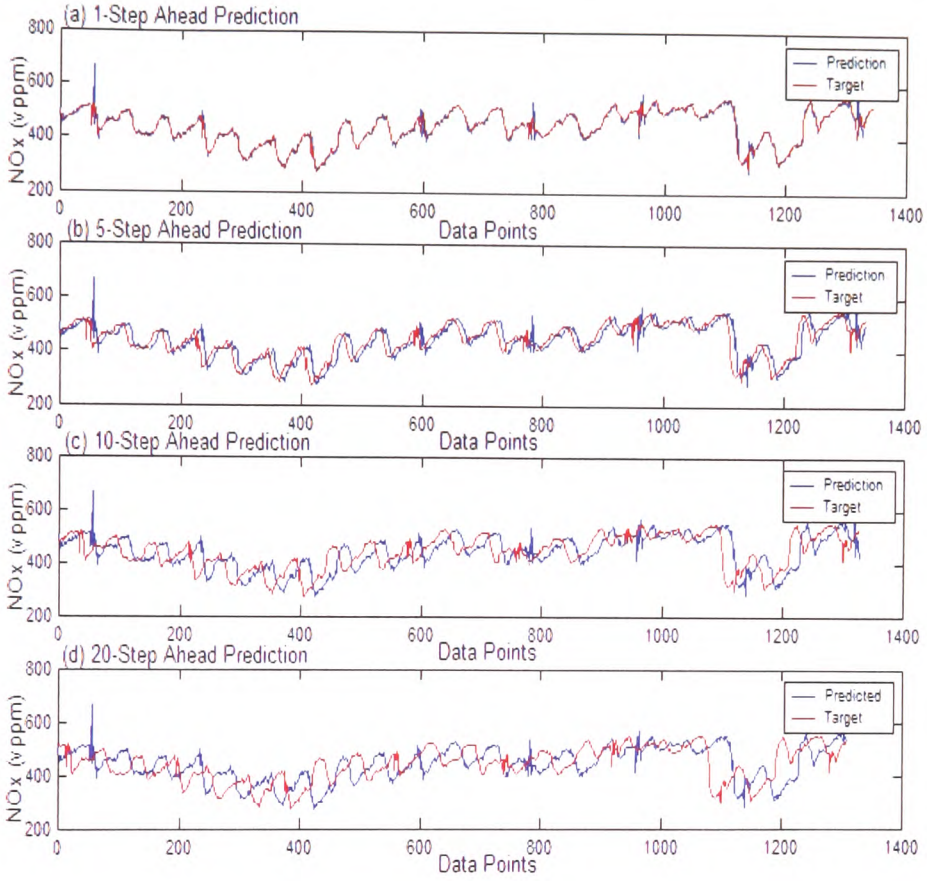

Figure 7.5 (a) 1-Step (b) 5-Step, (c) 10-Step, and (d) 20-Step, Ahead Predictions using Non-Recursive ANN Predictor

The exploration of ANN future predictive models serves to provide a general overview of how these networks could be used to improve the overall response time of a controller system. As in Chapter 6, the FMCS averaged the predictions over a sufficient length of time (i.e., 5-minute) so that this time-delay within the system had elapsed before an adjustment was made. If an accurate *k*-step predictive model could be devised the control decision could be made based on a set predictive values obtained consequently better controller response time.

7.3 Online Model Adaptation

The application of ANNs in modelling technical processes requires not only their abilities to classify process states but also the possibility of monitoring changes of process variables over time in order to predict developing dangerous states. This, of course, is highly idealised in that the real plant or process is subject to disturbances and changing situations. For this reason, it is worth noting that in the development of the FMCS, the ANN modules are incorporated statically and because of that, the time-varying nature of the burner/boiler has not yet been addressed.

A common misconception about optimisation is that by developing accurate models from historical data, the optimum will be contained within the range of that model. However, that is seldom true when dealing with complex processes such as in PF systems [Eakle *et al.*, 1998]. To discover improvements and move toward a region of optimal performance requires a method that can extrapolate the settings beyond the range of the historical data used to create the model. In this context, it is necessary to retrain a new ANN model for the gases. One of the innovative aspects of the current project is to integrate different ANN schemes for different purposes. A Self - Organising Map (SOM) neural network is proposed as a tool for validating the sensor signals before they are fed to the ANN for predictions. In other words, the predictions corresponding to different flame states with respect to time, are only valid if the models can be updated.

The integration of ANNs in a modular architecture is common in modern applications. Esteves (2002) used SOM networks to classify the incoming data before passing them to the most suitable trained ANN controller in a combined anaerobic and aerobic treatment process for textile industrial effluents. Also, Valentine *et al.* (2001) used different ANNs to validate the sensor measurements performed at a survey station so as to provide reliable inputs to the automatic coagulation control system for a water treatment plant. In the present work, an SOM can be used as a separated module for validating sensor signals in order that the inputs are always within the trained data boundaries that were used to create the model.

The change in dynamics of a combustion system occurs due to factors such as ageing of the boiler, varying coal quality (i.e. surface moisture and size distribution), changes in ambient conditions, feed system variations, and building of an "eyebrow" that alters the near burner flow pattern. Man made mistakes such as plant maintenance and visual inspection can result in changes in the flame position and incursion of air respectively. Furthermore, low NOx burners are typically more sensitive to changes in operating parameters than conventional burners and therefore the change of the burner condition is important [Timothy, 2003]. For long-term benefit, an adaptive scheme needs to make the model of the controller change automatically to match those of the plant or process being monitored.

One major concern in PF fired burners is slag formation. Hanson *et al.* (1998) suggested that slag formation might take a couple of hours, or even days to become significant. In fact, every system can be made adaptable to changes in its environment if these changes can be measured, or predicted. The slow changes affecting a PF burner allows sufficient data to be collected for model retraining but the question lies as to how to identify the change as compared to the previous sample. The Self-Organising Map (SOM) neural network is suggested as a system novelty detector (Figure 7.6).

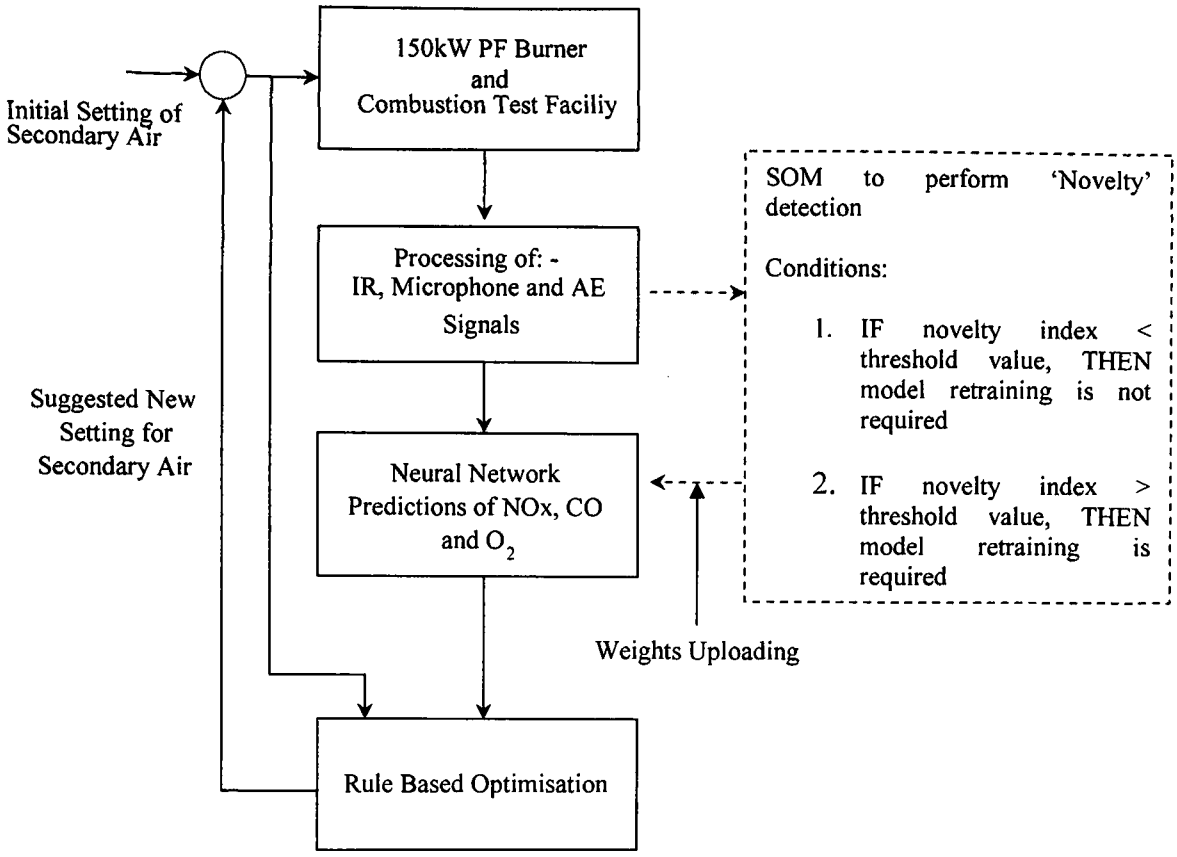

Figure 7.6 Dynamics Optimisation

7.3.1 Self-Organising Map

The Self-Organising Map (SOM) belongs to another class of neural networks that learn in an unsupervised manner. It requires no target value for learning and is particularly useful for data clustering and visualisation. The prototype vectors are positioned on a low-dimensional grid of neurons in an ordered fashion. Each neuron is represented by a d-dimension weight vector (e.g., prototype vector, codebook[1] vector) $m = [m_i .....m_d]$ where d is equal to the dimension of the input vectors. The neurons are connected to adjacent neurons by a neighbourhood relation, which dictates the topology, or structure, of the map. In SOM learning, both the best-matching weight vector and its topological neighbours on the map are updated. The region around the best matching vector is stretched towards the presented training sample. The end result is that the neurons on the grid become ordered, neighbouring

[1] The main component of Vector Quantisation is a codebook, which maps k-dimensional space to reproduction vectors called Codebook vectors. The mapping is done on the basis the distance measure between the feature vector to be quantised and code book vectors.

neurons having similar weight vectors. Upon presenting a new data vector, the closest prototype vector, or Best Matching Unit (BMU) will be identified. The interpretation of new data can be obtained by naming its prototype vector, whose type (e.g., class) is known through direct inspection of the weight vectors and clusters on the map. The trajectory of the location on the map can be used to form a display of the operational states (i.e., current and past history). This allows efficient tracking of the process dynamics to be studied visually. In conclusion, an SOM facilitates understanding of processes so that several variables and their interactions may be inspected simultaneously [Vesanto, 1999].

Figure 7.7 (a) presents the simulation of an SOM, which was created to identify signals that belong to two different coal types – Cerrejon and Daw Mill coals. The inputs to the network were NOx, CO, CO_2, O_2, secondary airflow rate and coal feed rate. For the simple visual presentation, the high-dimensional features space has been viewed in 3 principal planes using a Principal Component Projection algorithm with only 2-dimensions being plotted. As can be observed, both coals are scattered in two regions with slight overlapping.

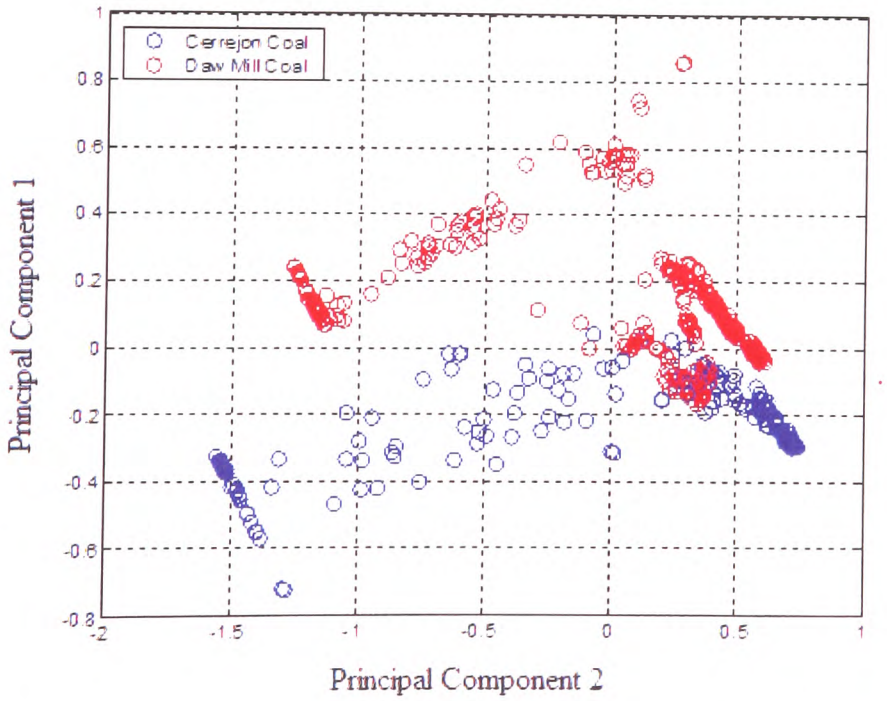

Figure 7.7 (a) SOM based Data Clustering – Two Different Clusters Represent Different Coal Types

A more comprehensive example of the application of a SOM was to classify experiment data corresponding to secondary airflow rates (Figure 7.7 (b)). Please also note that the quantisation vectors are also included.

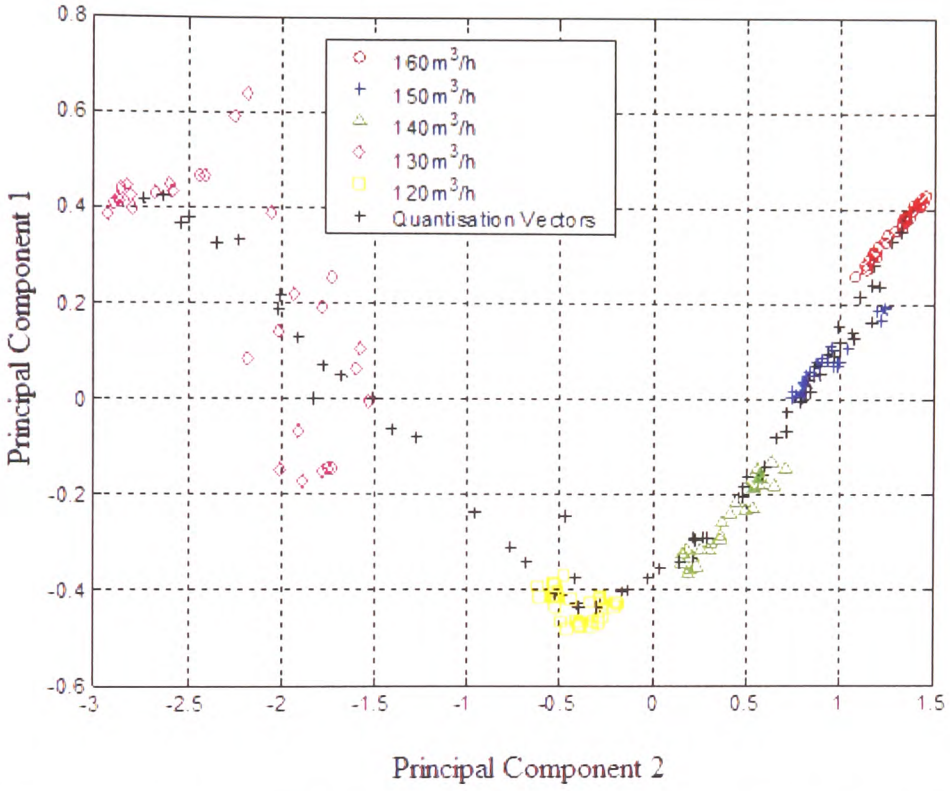

Figure 7.7 (b) SOM based Data Clustering – Five Distinctive Clusters with their corresponding Prototype Vectors ('+') of individual Secondary Airflow Rates

7.3.2 Self-Organising Map as System Novelty Detector

In a SOM, once a model is trained, the Euclidean distance of the new input to their closest prototype vector can be calculated. This is a measure of dissimilarity as the error is expected to increase with respect to time for the burner. For a simple model, abnormality can be identified if the new variables are identified as lying outside training range – extrapolation [Simula *et al.*, 1996]. However, coal combustion requires the search of a complex dimensional space and so the SOM is perhaps a better option.

Figure 7.8 graphically presents the concept of a SOM being used as a Novelty detector. $B \cup C$ is the original data space in which the SOM model was trained. As time passes, the burner operation extends to $A \cup B$. If newly presented data appears in the top left corner of the region A, the Euclidean distance of this data to its Best Matching Unit (BMU) will be extremely large. This is realised as a novel state of change for the system.

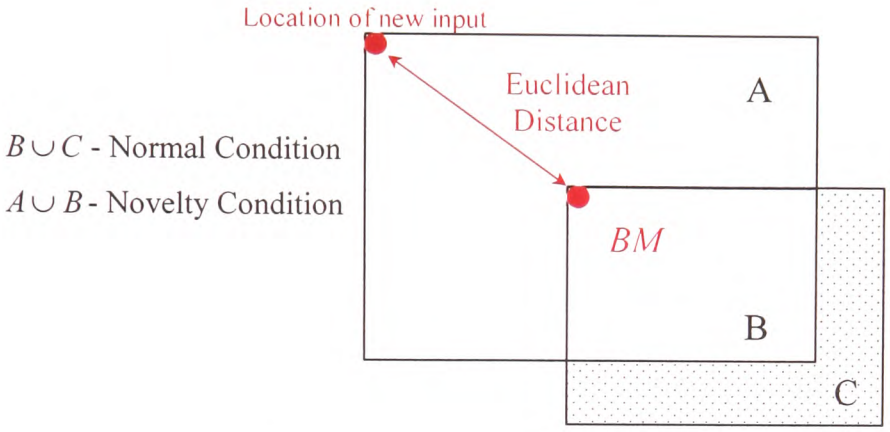

Figure 7.8 Normal and Novelty Model

7.3.3 Novelty Detection Simulated Result – Coal Type

Both Cerrejon and Daw Mill coal information at a swirl number of 0.8 were selected for the demonstration of identifying novel conditions for the burner. Daw Mill was used for training and Cerrejon for testing. The magnitude of error defined by its Euclidean distance to its BMU, was being presented as the novelty index. A threshold value was required and Ko (2002) suggested that the threshold should be set 4 times higher than average quantisation error. Figure 7.9 (a) shows a different magnitude in the novel index between the training and simulation based on gaseous information, also, Figure 7.9 (b) was simulated with the sensor features.

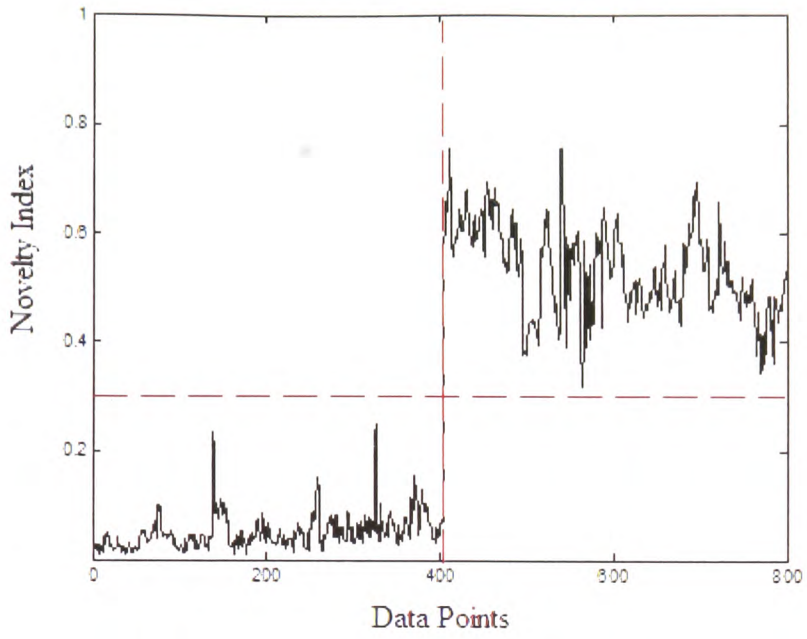

Figure 7.9 (a) The Detection for the Change of Burner dynamics Based on the Gaseous Information of Two Different Coal Types

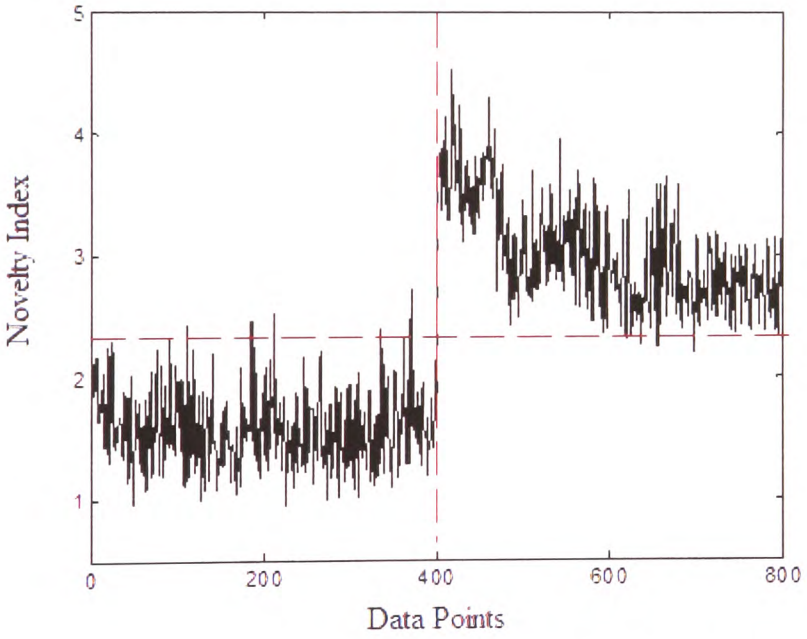

Figure 7.9 (b) The Detection for the Change in Burner Based on the Sensors Features that belong to Two Different Coal Types

One limitation encountered when using a SOM is that the prediction values are merely an indication of the change in the signal. For example, the simulation in Figure 7.10 shows a SOM trained with gaseous information corresponding to a secondary airflow rate of 120 m^3/h, followed by validating the trained SOM model

with the gaseous information of 130 m^3/h, 140 m^3/h, 150 m^3/h and 160 m^3/h. In this situation, the data vectors corresponding to 160 m^3/h, were not found to attain the highest novelty index, which implies that there is no sense of magnitude in the network, something perhaps not to be expected.

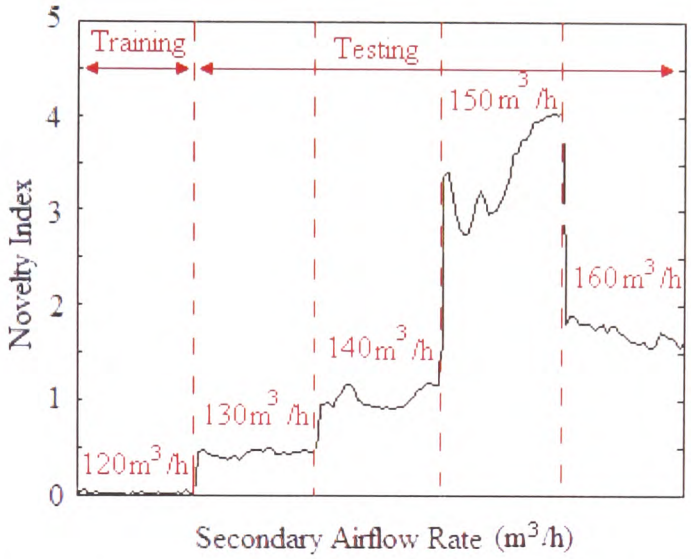

Figure 7.10 The Detection for the Change in Burner based on the Sensors Features of Different Secondary Airflow Rates

Although the simulation results of the SOM in Section 7.3 and onwards were only for illustration, a SOM can be trained with data sets representing well distinguishable states of the process. The network structure formed in this way can then be sensitised successively by presenting the different states. Such sensitised networks are able to separate even very similar states that "normal" trained networks cannot classify and therefore, they form an improved supporting classification and alarming module.

7.4 Summary of Chapter 7

Unlike the ordinary FFT, Wavelet Analysis uses a variable sized window technique, which is claimed to provide more precise interpretation of a complex signal. WA breaks up a signal into a shifted and scaled version of the original wavelet through multiple-level decomposition into many lower resolution components (WCs). This technique is particularly useful for the signal with an inherent instantaneous impulse

and that exhibits a transient (non-stationary[2]) nature. In addition, WA is a software filter. WA has the ability to separate out the noise from the actual signal, and so WCs can yield good prediction results.

If a process has a time-delay, one must wait until the time-delay has elapsed before seeing any effect of a control action and for this reason a time-delay has a significant influence on the degree of difficulty of control. One useful method to overcome the effect of a time-delay is to use a prediction approach where future predictions are based on past and current plant variables and on a set of future control actions [Tan *et al.,* 1998]. However, the results showed that the errors increased with respect to the number of predictions into the future. The difference in error for both recursive and non-recursive simulation tests was also recorded. One must also bear in mind that the nonlinear *k*-step prediction strategies can be implemented in practice only because the ANNs are such powerful tools.

In general, a SOM is used to cluster data on the map and examine the relationship between variables [SOM Toolbox for Matlab™, 2000]. In this project, the idea of encoding a SOM within the main control system to deal with long-term factors or time-varying characteristics, such as boiler fouling was presented. From the experiments, the SOM has been found to be useful to identify changes in the burner. It is clear that the combination for both the controller and a SOM with an expert system could deliver "self-checking" abilities.

[2] The definition of non-stationary signal components can be described as one of the three categories: - (a) impulsive (abrupt amplitude change with time), (b) varying wide-band (wide-band signals, with spectral composition changing with time) and (c) varying harmonic (signal composed of harmonic terms of frequency changing with time). All non-stationary signals are composed of a combination of all categories, but in special cases, a single category may dominate

Chapter 8 Conclusions and Further Recommendations

This chapter seeks to draw conclusions based on the objectives set out in Chapter 1. The first of these set out to establish whether it was possible to use low cost sensors to monitor the PF flame and in conjunction with neural networks to estimate the gaseous emissions. The second objective was to determine a strategy that used the neural network predictions of the gaseous emissions to control the burner to ensure optimal combustion.

8.1 Monitoring and Control of the PF Flame using Low Cost Sensors

The investigation of the gaseous response to different burner settings, namely, (a) swirl number, and (b) secondary airflow rate, was undertaken. The analyses show the NOx reduced as the CO increased, and the NOx and CO were functions of the secondary airflow rate. In addition, the results show no consistent reduction of CO as the swirl number increased. This implies that unlike the NOx, there was not direct correlation between CO and the swirl number. However, the burner achieved lowest NOx and CO simultaneously when the burner was operated at a swirl number 0.8 and secondary airflow rate of 130 m^3/h. Since different burner designs result in different gaseous emission profiles, therefore it is necessary to understand them individually. The search for best burner performance was, however, obtained through the scoping trials. These results were particularly useful in the process of formulating adequate solutions for conditions when dealing with the controller design.

The large amount of sampled sensor data was reduced by calculating a set of features that included; statistics such as *mean, rms,* and *Kurtosis*, and in the frequency domain, the *Average Energy* of the Power Spectral Density (PSD) in different frequency bands. As a result, the sensor signals were transformed into a series of features, which were assessed to determine their relationship with the gaseous readings. The results confirmed that these sensors were capable of discriminating the changes in the flame signals that corresponded to varying settings.

These signal features were then used to train ANNs that were used as software sensors to predict the combustion gases. This had the advantage of the prediction being based solely on the flame state that will not be disturbed by other unexpected changes such as the incursion of air.

It is believed that the corroboration of useful information from diverse sensors features helped to improve modelling accuracy. Feature-level data fusion allowed data at the feature's level to be combined before prediction and it was found that features sought by assessing the correlation coefficient gave the lowest prediction error. In addition, the search for the best ANNs and their parameter settings, which were motivated by Decision-level data fusion scheme, was undertaken. The analyses concluded that the recursive network outperformed the ordinary MLP. In addition, a model trained with the early stopping regularisation technique allowed better control of the network parameters and thus ensured the best network dimension whilst avoiding over-fitting. Other system identification techniques, namely, NNARX were investigated with outstanding performance, however, the NNARX was not used because it required past sensor readings, which were not available in this situation. As a result, the recursive networks were incorporated into the controller structure for real-time predictions in the control experiments.

The final control experiment results have marked the success of using the FMCS to control the PF system. The system recognised the high excess air condition and the controller brought the burner towards good combustion conditions and continuously assessed the burner. The responses of the controller were governed by the target emission bands, rate of change and to increase or decrease the airflow rate, which were carefully decided and amended as a set of rules

Other novel aspects such as the use of (a) Discrete Wavelet Transform technique, (b) *k*-step predictive model, and (c) SOM to deal with the time varying nature of the burner were discussed. DWT serves to provide an alternative route to statistical and FFT based signal analysis of combustion signals. The neural network *k*-step predictive model was

found to be useful for situations where the time-delay of the process dynamics is of great concern. Since a boiler is continually subjected to fouling and plant ageing a SOM network could be incorporated to indicate the signal changes thus suggesting when ANN model is required to retrain.

8.2 Further Recommendations

The search for advanced flame monitoring and control systems for coal utility boilers is an on-going effort on the global scale. The methodology used to yield flame information in this work was via flame radiation intensity and frequency. Other areas, which might yield interesting information, is by the use of a vision system.

Until recently, to install a video camera for monitoring a flame would have been difficult as there was limited computer processing power and data storage. However, with the ever-increasing processing speed of modern PCs and data storage, application of vision systems has become easier and more cost effective. The motivation behind the use of flame imaging is that combustion parameters such as load and gaseous emissions are well correlated to the flame image (i.e., size, shape, brightness, and luminosity) [Ozanyan, 2000 and Lu *et al.*, 2000]. Rolla and Bethlehem (2000) used a flame image system that consisted of video cameras with advanced image analysis and pattern recognition techniques to identify flame features. Both authors concluded that the flame images are highly correlated with combustion parameters such as the air-fuel ratio, level of nitrogen oxide emissions and flame temperature. This implies that both video images and Artificial Intelligence techniques could derive information for optimal control of coal-fired furnaces.

Despite the potential of the flame imaging technique, one must bear in mind that the use of video cameras poses problems such as: -

1. Using a video camera requires a sufficiently large aperture for viewing.

2. Low operating temperature.

3. High setup cost as it would usually be retrofitted.

Nevertheless, through the use of optical fibers, the signals can now be transmitted reliably to the signal processing system, meters away, thus lowering the temperature the sensor or the system is exposed to. It is envisaged that modern fibre-optic based sensing technology could have the following features: -

1. It can detect the flame of each burner.

2. It utilises remote sensing by optical fibre cable.

3. The flame signals correlate well with the burner parameters.

Since optical fibres are particularly useful for remote sensing, they have been widely used in nuclear reactors and chemical vats. As such, it is thought to be the best approach to the application of traditional methods of monitoring flames to achieve maximum burnout and fuel efficiency of the plant.

Each flame has its own characteristic type of spectrum, which correlates with the chemical species that are present in the flame. The radiation from the reaction zone (flame-front region) contains free radicals and combustion intermediate species such as OH, CH, CN, and C_2 [EPRI, 1986]. Both Gaydon (1957) and Clausen (1995) suggested those strong bands of CO and CO_2 appear at 4.50 μm, and 2.88 μm, and 2.7, 4.3 and 15 μm respectively. Also, strong bands for the NO, NO_2 and O_2, were found at approximately 0.22, 0.48 and 0.18 μm respectively. Otherwise, it is possible to determine CN and NH bands, which can be used as the early indicators of NOx [Leipertz, 1996]. It

is obvious that more specific signals can be acquired by using a narrow band optical filters in a spectroscopy system thus yielding better signal definitions.

A correct way to combine features ensures good model predictions hence better control decisions. Commonly, the method used in the search for connected features for modelling is based on correlation analysis, which is fundamentally a linear model. Another computational search method to obtain a best-combined feature set is the use of Genetic Algorithm (GA). GA is a search algorithm that is modelled on evolution and can provide a robust approach in situations where there is little or no *a priori* knowledge about the process to be controlled.

Figure 8.1 outlines how the approach could be applied to the current work where the search starts by randomly initialising the input features. The objective function is then evaluated based on the ANN with the selected features and the first generation is produced. If the optimization criteria are not met, the creation of a new generation starts (Figure 8.1). The cycle is continuous until the best-combined feature set is reached. It was learned that GA has become a popular tool in the search for the "fit" of variables over large data dimensions in modelling.

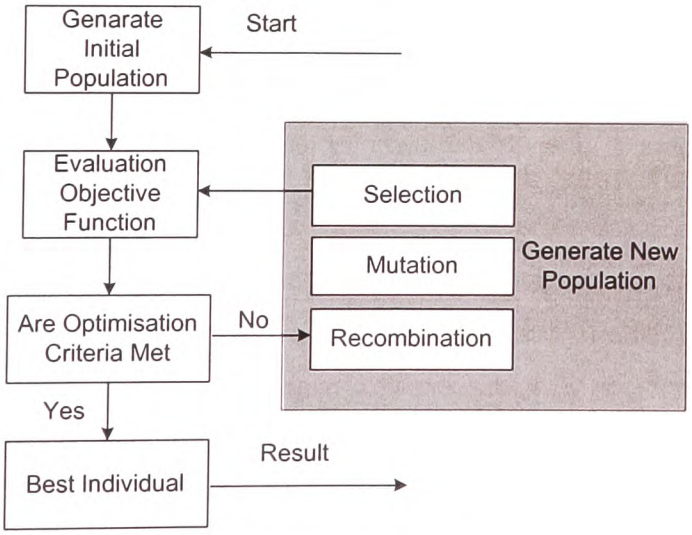

Figure 8.1 Structure of a Single Population Evolutionary Algorithm

References

Abugov D. (1980) Generation and Amplification of Acoustic Waves by Thermal Process. *Soviet Aeronautics*. 23(3):1-5

Abugov D. and Obrezkov O. (1978) Acoustic Noise in Turbulent Flames. *Combustion Explos Shock Waves*. 14(5):63-71

Abugov D. and Obrezkov O. (1982) Interaction between the Combustion Process and Acoustic Vibrations. *Combustion, Explosion and Shockwaves*. 17:387-393

Afgan N. and Carvalho M. (1995) Knowledge-Based Expert system for Fouling Assestment of Industrial Heat Exchangers. *Applied Thermal Engineering*. 16(3):203-208

Ahmed M. (1999) Neural Net Based MRAC for a Class of Nonlinear Plants. *Neural Networks*.13:111-124

Atieza, F., Alzamora, N., Velasco J., Dreiseitl S., and Ohno-Machado L. (2003). *Risk Stratification in Heart Failure Using Artificial Neural Networks. Valencia, Spain.*

Allison S., Slatsky M., Sorge J., Mayes I., Menzies B., Brown T., and Stallings J. (1996) GNOCIS™ – Continuous Combustion Optimisation for Utility Boilers. *First Joint Power and Fuel Systems Contractors Conference, US Department of Energy, Pittsburgh, USA.*

Ballard D. (1984) Retrofit of Flame Monitoring Instrument and Control. *IEE*.1-3

Bendisciol P., Francesconi F., Malcovati P., Maloberti F., Poletti M., and Valacca R. (1988) A CMOS Intergrated Infrared Radiation Detector for Flame Monitoring. *IEEE*. 6:625-628

Bhasker C. (2002) Numerical Simulation of Turbulent Flow in Complex Geometries used in Power Plants. *Advances in Engineering Software*. 33(2):71-83

Bing G., Shen Y., Li D. and Zhao F. (1997) Modelling Coal Gasification with a Hybrid Neural Network. *Fuel*. 76(2):1159-1164

Bishop C. (1995) Neural Networks for Pattern Recognition. *Oxford University Press.*

Bittanti S. and Piroddi L. (1997) Nonlinear Identification and Control of a Heat Exchanger: A Neural Network Approach. *The Franklin Institute*. 334B(1):135-153

Booth, R. and Roland W. (1998) Neural Network Based Combustion Optimisation Reduces NOx Emissions while Improving Performance. *Proceedings of the American Power Conference*. 2:667-672

Borman G. and Ragland K. (1998) Combustion Engineering. *McGraw-Hill.*

Borse G. (1997) Numerical methods with Matlab: A Resource for Scientists and Engineers. *International Thomson Publishing.*

Bryant J. (1980) Updated your Flame-Monitoring Know-How. *Power.* 124(8):21-25

Cao Z., Wang B., Wang K., Lin H. and Yu R. (1998) Chemical Acoustic Emissions from Gas Evolution Processes Recorded by a Piezoelectric Transducer. *Sensors and Actuators.* 50:27-37

Chong A. (1999) The Monitoring and Control of Stoker-Fired Boiler Plant by Neural Network. *Ph.D Thesis, University of Glamorgan.*

Chung C. and Kumar V. (1993) Knowledge Acquisition using a Neural Network for a Weather Forecasting Knowledge-based System. *Neural Computing and Applications.*1:215-223

Chung C. and Saini, D. (2000) The total energy and the total entropy of force signals – new parameters for monitoring oblique turning operations. *International Journal of Machine Tools & Manufacture.* 40(13):1879-1897

Clausen S. (1995) Infrared Combustion Diagnostics in Fluctuating Flames. *Proceedings of SPIE - The International Society for Optical Engineering.* 2506:30-44

Cobourn G. and Dolcine L., (2000) Frence M. and Hubbard M. Comparisor of Non-linear Regression and Neural Network Models for Level Ozone Forecasting. *Journal of Air & Waste Management Association.* 50:1999-2009

Daw C. & Finney C. (2002) Real-time Monitoring of Dynamical State Changes in Staged Combustion. *International Mechanical Engineering Congress & Explosition, ASME, USA.* 17-22

Dimla E (1996) Sensor Signals for Tool-Wear Monitoring in Metal Cutting Operations. *International Journal of Machine Tools & Manufacture.* 40:1073-1098

Doherty T. and Froud D. (1994) Characteristics of a Power Station Boiler. *Journal of Power and Energy, Proceedings of Institute Mechanical Engineers.* 208:89-102

DTI (2003) Instrumenet and Control for Conventional Coal-fired Power Plant. *CB003*

Durbin M., Vangsness M., Ballal D. and Katta V.(1996) Study of Flame Stability in a Step Swirl Combustor (1996) *Journal of Engineering for Gas Turbines and Power.* 118:309-315

Dwight F. (1995) Random Signal Processing. *Prentice Hall Press.*

Eakle D., Patterson P.(1998) Optimising Combustion to Reduce NOx and Improve Boiler Efficiency using Constrained Empirical Optimisation based on Bayesian Models. *Proceeding of Internal Combustion Engine ASME.* 30(1):87-92

Electric Power Research Institute (EPRI) Report (1986) Spectral Flame Analyzer for Burner Control in Fossil Fuel Boilers. *Research Project 1681-2.*

Esteves S. (2002) Monitoring and Control of Biological Textile Wastewater Treatment Using Artificial Neural Networks. *PH.D Thesis. University of Glamorgan*

Elghamry M., Brown E., Ferguson I., Gill J., Rueben R., Steel J. and Middelton S. (1998) Gaseous Air-Fuel Quality Identification for a Spark Ignition Gas Engine Using Acoustic Emission Analysis. *International Journal of Comadem.* 235-244

Faller C., Dvorakova R. and Horacek P. (2000) Short-term Load Forecasting Based On a Multi-Model. *Conference of IFAC Power Plants and Power Systems Control, Brussels, Belgium.*

Fog T., Hansen, L., Larsen J., Hansen, H., Madsen, L., Sorensen P., Hansen E. and Pedersen P.(1999) On Condition Monitoring of Exhaust Valves in Marine Diesel Engines. *Neural Networks for Signal Processing; Proceedings of the IEEE.* 554-564

Fossil Fuel Power Generation within the European Research Area (2003) *PowerClean R, D&D Thematic Network Report.*

Gabor J., Pakulski D., Swirski K. and Domanski P.(2000) Close Loop NOx Control and Optimisation using Neural Networks. *IFAC Power Plants and power Systems Control.*141-146

Gaydon A. (1957) The Spectroscopy of Flames. *Chapman and Hall.*

Gaydon A., and Wolfhard H. (1978) Flames - Their Structure, Radiation and Temperature. *Chapman and Hall.*

Gencay R. and Liu T. (1997) Non-linear Modelling and Prediction with Feedforward and Recurrent Networks. *Physica D.* 108:119-134

Giammar R. and. (1970) Combustion Roar of Turbulent Diffusion Flames. *Journal of Engineering for Power.* 1(1): 157-165

Glasheen W. and Grassi M (1998) UV Flame Sensor for Industrial Combustion Control. *International Gas Research Conference, San Diego, California., USA.* 462-468

Grant J. (1980) Boiler Flue Gas - Its Analysis and use in Burner management and Combustion Control in Oil Fired Power Plant. *Combustion.* 52:10-15

Grant, J.(1980) Boiler Flue Gas - Its Analysis and Use in Burner Management and Combustion Control in Oil Fired Power Plant. *Combustion.* 52:10-15

Greaves K. (1999) Monitoring Techniques Improves Reburn Efficiencies by Balancing NOx/CO. *Conference on Reburning for NOx Control - NETL Publication.*

Hall D. and Llinas J. (2001) Handbook of Multisensor Data Fusion. *CRC Press.*

Hanson, Simon P. and Abbott, Murray F. (1998) Furnace Water-wall Slag Deposition Testing in a 0.5 MW_t Combustion Pilot Plant. *Progress in Energy and Combustion Science.* 24(6):503-511

Hashimoto H., Miyamae S., and Makino K. (1992) Development of Flame Diagnostic System for a Coal-Firing Boiler. *International Power Generation Conference, ASME.* 1-8

Hou R., Hunt A. and Williams R. (1998) Acoustic Monitoring of Hydro-cyclone Performance. *Minerals Engineering.* 11(11): 1047-1059

Huang Y., Yan Y., Lu G., and Reed A. (1999) On-line Flicker Measurement of Gaseous Flames by Image Processing and Spectral Analysis. Measurement Science and Technology. 10 (8):726-733

IEA Coal Research (1997) Coal Information - International Energy Agency Statistics.

IEA Coal Research (1997) Continuous Emissions Monitoring for Coal-fired Power Stations. *IEACR/94*

IEA Coal Research (1997) Experience with Low NOx Burner. *IEACR/99*

IEA Coal Research (2000) NOx Modelling and Prediction. *CCC/31.*

IEA Coal Research (2000) Prevention of Particulate Emission. *CCC/40.*

IEA Coal Research (2002) World Energy Outlook

Irwin G., Warwick K. and Hunt K. (1995); Neural Network Application In Control. *The Institute of Electrical Engineer - Control Engineering, Series 53.*

Jackson P. and Bulger J. (1987) Enhancing Techniques for Flame Monitoring Control and Instrumentation. *Control and Instrumentation.* 19(9):73-75

Jain L. (1999) Intelligent Adaptive Control - Industrial Applications. International Series on Computational Intelligence. *CRC Press*

Jaques R. and Feldman E. (1998) Identification and Control of NOx Emissions using Neural Networks. *Journal of Air and Waste Management Association.* 48:408-417

Jarmulak J., Spronck P. and Kerckhoffs E. (1997) Neural Networks in Process Control: Model Based and Reinforcement Trained Controllers. *Computers and Electronics in Agriculture.* 18(2):149-166

Jiaa C. and Dornfeld D. (1988) Experimental Structure of Sliding Friction and Wear via Acoustic Emission Signal Analysis. *Wear.* 139:403-424

Kalyanasundaram P., Kasiviswanathan K., Jayakumar T. and Murthy C (1992) Leak Detection in Pressure Tubes of a Pressurised Heavy Water Reactor by Acoustic Emission Technique. *British Journal of Non-Destructive Testing.* 34 (11):539-543
Kay J. (1994) Monitoring - Equipment and Methods. *Energy world.* 223:6-10

Kenneth F and Ling B. (1994) Neural Networks for NOx Control. *American Power Conference.* 354-359

Khesin, M. and Strohecker, B. (1997) Application of a New Burner Diagnostic System for Coal-fired Utility Boiler. *Proceedings of Instrumentation, Control, and Automation in the Power Industry.* 40: 127-136

Kidin N. and Librovich V.(1984) On Sound Sources in Turbulent Combustion. *Progress in Astronautics and Aeronautics.* 95:345-355

Kiyan, T., and Yildirim, T. (2003) Breast Cancer Diagnosis Using Statistical Neural Networks. *International XII. Turkish Symposium on Artificial Intelligence and Neural Networks. University Besiktas, Istanbul, Turkey*

Ko J., Sun Z., and Ni Y. (2002) Multi-stage Identification Scheme for Detecting Damage in Cable-Stayed Kap Shui Mun Bridge. *Engineering Structures* 24(7):857-868

Kondakov I., Shaposhnikov V. and Lobojko B. (1992) Exhibition of acoustic emission at ignition and combustion of explosive materials. *Fizika Goreniya i Vzryva.* 28(6):39-42

Krishnapura, G. and Jutan A. (2000) Neural adaptive controller. *Chemical Engineering Science.* 55(18):3803-3812

Kyrtatos N. Dimopoulos G. Theotokatos E., Tzanos E., Xiros N., (2003) NOx-BOX: A Software Sensor for Real-Time Exhaust Emission Estimation in Marine Engines. *13th ISCSS, Florida, USA.* 1-7

Larrimore L, Sorge J. (1997) Evaluation of Online Carbon-in-Ash Measurement Technologies. *The 3rd Annual Conference on Unburned Carbon on Utility Fly Ash.*

Lee D and Park J. (1999) Neural Network Modelling for on-line estimation of nutrient dynamics in a sequentially operated batch reactor. *Journal of Biotechnology.* 75(2):229-239

Lendasse A., Lee J., Wertz V. and Verleysen M (2001). Forecasting Electricity Consumption Using Non-linear Projection and Self-Organising Maps. *Neurocomputing.* 48:299-311

Leipertz A., Hoffman D. and Munch, K. (1996) Two-dimensional Temperature Determination in Sooting Flames by Filtered Rayleigh Scattering. *Optics.* 21(7):525

Lizarraga, 1998 Real-Time Adaptive Neural Control of a Class of Nonlinear Systems. *Engineering Application of Artificial Intelligence.* 12:3-19

Lu G., Yan Y. and Ward D. (2000) Advanced Monitoring - Characterisation and Evaluation of Gas-fired Flames in an Utility Boiler. *Journal of the Institute of Energy.* 73:43-49

Lu G., Yan Y., Huang Y. and Reed A. (1999) An Intelligent Vision System for Monitoring and Control of Combustion Flames. Measurement and Control. 32:164-168

Lu. S.and Hogg B.(2000) Dynamical Non-linear Modelling of Power plant by Physical Principles and Neural Networks. *Electrical Power and Energy Systems.* 22:67-78

Luh G. and Wu C. (2000) Inversion Control of Non-linear Systems with an Inverse NARX model Identified using Genetic Algorithms. *Proceeding of Institute of Mechanical Engineers.* 241(1): 259-269

Lynn P. (1989) An Introduction to the Analysis and Processing of Signals. *Macmillan Education.*

MacIntyre J., Tait J., Kendal S., Harris T., Brason A. and Smith P. (1996) Neural Networks Applications in Condition Monitoring. *Applications of Artificial Intelligence in Engineering.* 37-48

Martin P. (1993) The Actual State of Technology of Flame Monitoring and Valuation. *Professor and Doctor of Engineering Science.* 93(321):751-771

Martin P. (1993) Actual State Of Technology of Flame Monitoring and Advances in Instrumentation and Control. *International Conference and Exhibition.* 48(2):751-772

Michel J. B., Champinot C. and Jacques D. (2001) State of the Art on Emerging Combutsion Control Sensors. *6th International Conference on Technologies and Combustion for a Clean Environment. Portugal.*

Masri S.,.Chassiakos A. and Caughey T. (1992) Structure Structure-unknown Non-linear Dynamic Systems Identification Through Neural Networks. *Smart Materials and Structures.* 1(1) 45-54

Mistiti M., Mistiti Y., Opppenheim G. and Poggi J (1997) Wavelet Toolbox: For the Use with MatLab™

Mitchell J. and Tarbell J.(1982) A Kinetic Model of Nitric Oxide Formation during Pulverised Coal Combutsion. *AIChE Journel.* 28:302-311

Neill G., Rueben R., Sandford P., Brown E. and Steel J. (1997) Detection of Incipient Cavitation in Pumps using Acoustic Emission. *Proceedings of Institute of Mechanical Engineers.* 211:267-277

Neural Network Tool Box - Matlab™ (1998)

Niksa S. (1996). Forecasting Coal Quality Impacts on Utility Furnace Performance: Foundations of Accurate Emissions Predictions. *Proceedings of International Symposium on Advanced Energy Technology, Sapporo, Japan.* 95-102.

Noørgard M., (2000) Neural Network Based system Identification Toolbox - Technical report [00-E-891], *Technical University of Denmark, Version 2.*

O'Connor M (1999) The Effects of Coal Quality on NOx Emissions and Carbon Burn out in Pulverised Coal-fired Utility Boilers. *COAL R 153, Harwell, Energy Technology Support Unit.*

Ozanyan K., Carey S., Hindle F., McCann H., Winterbone Young S. and Black J. (2000) *IEE Electronic and Communication Seminar.* 8:1-4

Pacheco-Vega, Rodney L., and McClain (2000) Analysis of Fin-tube Evaporator Performance with limited Experimental Data using Artificial Neural Network. *Proceedings of the ASME Heat Transfer Division ASME.* 3:95-100

Palakal J.and Hudli V.(1995) Augmenting parallel reasoning mechanisms with learning networks in expert systems. *Engineering Applications of Artificial Intelligence.* 8(5): 515-525

Pastor J., Garcia J. and Molina S. (2000) Analysis Methodology of Diesel Spray and Flame by means of In-cylinder Endoscopic Imaging. *IEE Control, Electronic and Communication Seminar.* 13:1-4

Patino H. and Liu D. Neural Network-Based Model Reference Adaptive Control System (2000) *IEEE Transaction on System, Man and Cybernatics.* 30(1):199-204

Pham D. and Oh S. (1999) Identification of Plant Inverse Dynamics using Neural Networks. *Artificial Intelligence in Engineering.*13:309-320

Pinder T. and Atreya A. (2004) An Experimental Investigation of the Effect of Fuel Concentration and Velocity Fluctuations on Nonpremixed Jet Flames. *Proceedings of the 2004 Technical Meeting of the Central States Section of The Combustion Institute.*

Premier G., R. Dinsdale R., Guwy A., Hawkes R., Hawkes D. and Wilcox S. (1999) A Comparison of the Ability of Black Box and Neural Network Models of ARX structure to represent a Fluidised Bed Anaerobic Digestion Process. *Water Research.* 33(4): 1027-1037

Refenes A., Azema-Barac M., Chen L. and Karoussos S. (1992) Currency Exchange Rate Prediction and Neural Network Design Strategies. *Neural Computing and Applications.* 1:46-58

Reifman J.and Feldman E. (1998) Identification and Control of NOx Emissions Using Neural Network. *Journal of Air and Waste Management Association.* 48:408-417

Reinschmidt K. and Ling Bo.(1994) Neural Networks for NOx Control. *American Power Conference Boston USA.* 354-359

Ringe J., Graves D. and Reeb J. (1998) Woodwaste Biomass Cofiring with High Sulphur Coal for Power Generation in Kentucky. *Forest Products Journal.* 48(4):88-93

Reuben R. (1998) The Role of Acoustic Emission in Industrial Condition Monitoring. *International Journal of Comadem.* 1(4)35-46

Rodriquez F., Enrique T., Cortes V. and Canadas L. (2001) Opticom: Advanced Automatic Monitoring System of Local Combustion Conditions for Improving Boiler Performance in PC Power Plant. *Fuel.* (81) 637-645

Russell N., Bakker H. (1997) Modular Modelling of an Evaporator for Long-range Prediction (1997) *Artificial Intelligence in Engineering* 11:347-355

Saha P, Shoib M., Kamruzzaman J. Development of a Neural Network Based Integrated Control System of 120 ton/h Capacity Boiler (1998) *Computers & Electrical Engineering.* 24:423-440

Salehfar H. and Benson S.(1998) Electric Utility Coal Quality Analysis using Artificial Neural Network Techniques. *Neurocomputing.* 23(1-3):195-206

Sankar K. and Pradip K (1996). Neurocomputing- Motivation, Models, and Hybridisation. *IEEE Computational Science and Engineering.* 24-28

Shepard W., Cook, R., Zongxun S., Xu Y., and Zixiang, J. (1993) Advanced Optical Diagnostics for Controlling a Coal-Fired MHD Retrofit Power Plant. *Proceedings of the Intersociety Energy Conversion Engineering Conference.* 2:455-461

Shimoda M., Sugano A. and Watanabe Y. Prediction Method of Unburnt Carbon for Coal-fired Utility Boiler using Image Processing Technique of Combustion Flame (1990) *IEEE Transactions on Energy Conversion.* 5(4):640-645

Simula O., Alhoniemi E., Hollmen, J. and Vesanto J. (1996) Monitoring and modelling of Complex Processes using Hierarchical Self-Organizing Maps (1996) *Proceedings of IEEE International Symposium on Circuits and Systems,v Suppl, Circuits and Systems Connecting the World.* 73-76

Singer J. (1981) Combustion - Fossil Power Systems, Combustion Engineering, Inc. Volume 1.

Skarkey A., Sharkey N., and Chandroth G. (1996) Diverse Neural Net Solutions to a Fault Diagnosis Problem (1996) *Neural Computing & Application.* 4:218-227

Smart J. and Nakamura T. (1997) NOx Emission and Burnout from a Swirl Stabilised Burner Firing Pulverised Coal: The effects of firing Coal Blends. *Journal of the Institute of Energy.* 66(467): 99-196.

Smith, T. and Kilham J. (1963) Noise generation by Open Turbulent Flame. *Journal of the Acoustical Society of America,* 35(5): 715-724.

SOM Toolbox for Matlab™ 5 (2000) Report A57

Stanmore B. and Visona S. (2000) Prediction of NO emissions from a number of Coal-fired Power Station Boilers. *Journal of Fuel Processing Technology.* 64(1):25-46

Stevens D. and Sclader D.(1984) Acoutic Leak Detection in Fossil Boilers. *Joint Power Generation Conference, ASME, New York USA.* 1-7

Stowe H. (1996) SO_2 and NOx compliance at New England Electric System. *Proceeding Fof International Joint Power Generation Conference, Houston.* 535-540

Suh J., Kumara S. and Mysore S. (1999) Machinery Fault Diagnosis and Prognosis: Application of Advanced Signal Processing techniques. *Annals of the CIRP.* 48(1): 317-321

Susan L., Luopa. J. and Zhu Y. (1996) Neural Networks as 'Software Sensors' in Enzyme Production. *Journal of Biotechnology.* 52:257-266

Swanston D., Kambhampati C., Manchanda S., Tham M. and Warwick K (1995) Relative Order Defines a Topology for Recurrent Networks. *IEE Conference Publication 409 - Artificial Neural Networks.* 256-261

Tan C.K. (2003) The Monitoring of Burner Slag Formation. *PhD Thesis, University of Glamorgan.*

Tan Y. and Cauwenberghe A. (1999) Neural-Network d-ahead Predictors for Nonlinear Systems with Time Delay. *Engineering Applications of Artificial Intelligence.* 12:21-35

Tang L., Zheng H., Wang W., Zhang Y. and Zhang Z.(1999) Features Analysis About Vibration Signals on the Gearbox in a Vehicle. *Proceedings of the International symposium in Test and Measurement.* 688-692.

Timothy A., Thomas J., Flynn & Ralph T., Bailey C., Daw S and Charles E.A. (2003). Field Experience with the Flame Doctor™ System. *Combined Power Plant Air Pollutant Control Mega Symposium Washington, DC, USA.*

Timothy, A. and Thomas, J. (1996) Enhancing Burner Diagnostics and Control with Chaos-based Signal Analysis Techniques. *Proceeding of the ASME Heat Transfer Division.* 4:281-291.

Tretnikov N. (1987) Determining the Noise Characteristics of Boilers on Thermal Power Stations. *Soviet Energy Technology.* 3:69-73

Turner P., Montague G., and Morris J. (1996) Dynamical Neural Networks in Non-linear Predictive Control (An Industrial Application). *European Synposium on Computer Aided Process Engineering.* 20: 937-942

Tzanakou, E. (1999) Supervised and Unsupervised Pattern Recognition – Feature Extraction and Computational Intelligence. Industrial Electronic Series, *CRC Press.*

Valentin N. and Denoeux T. (2001) Neural Network-Based Software Sensor for Coagulation Control in a Water Treatment Plant. *Intelligent Data Analysis.* (5) 1-11 IOS Press

Van C., Te B., Hellinga C., Krijgsman A., Verbruggen H., Luyben K. and Heijnen J. (1995) Design and Real Time Testing of a Neural Model Predictive Controller for a Nonlinear System. *Chemical Engineering Science.* 50(15):2419-2430

Vesanto J. (2000) Clustering of the Self-organizing Map. *IEEE Transactions on Neural Networks.* 11(3):586-600

Visona S and Stanmore B (1995) Prediction of Nitric Formation in a Turbulent Premixed Pulverised Coal Flame. *2nd International Conference on Combustion and Emission Control, Institute of Energy.* 199-208

Wang F., Wang Z., Ma J., Yan Y., Chi C., Ni M. and Cen K., (2002) The Research on the Estimation for the NOx Emission Concentration of the Pulverised Coal Boiler by the Flame Image Processing Technique. *Fuel.* 82:2113-2120

Wang S. (1996) Neural Networks in Genaralising Expert Knowledge. *Computers Industrial Engineering.* 32(1):67-76

Warren C. (1978) Combustion Noise. *Progress in Energy and Combustion Science.* 4:157-176

Wildman D., Ekmann, J., and Smouse S.M. (1994) Prediction of Pilot-Scale Coal Ash Deposition: Comparison of Neural Network and Multiple Linear Regression Techniques. *The Impact of Ash Deposition on Coal Fired Plants.* 62:231-246

William H. (1992) Optimising Combustion With Integrated Neural Networks and AI Technology (AI Ware Inc). *Control Engineering.* 38-40

Willson P. and Chappell T. (1985) Pulverised Fuel Flame Monitoring in Utility Boilers. *Journal of the Institute of Energy.* 58(434): 12-19

Wilson T., Roberts G, Scruggs D. and Stapper E. (2002) Application of a Neural Network Based, Closed-Loop Control Optimization System to a Load-Following Utility Boiler. *POWER-GEN International 2000, FL, USA.*

Wojcik, 2003, Golec T., komada P., Przyluckia S., Smolarza, A., Surtel A. and Duk M. Concept of Application of Signals from Fiber-Optic system for Flame Monitoring to Control separate Pulverised Coal Burner. *Optoelectronic and Electronic Sensors; Proceedings of SPIE.* 5124:291-298

Xu Y., Liu Y., Jun Tang X., Yang H. and Gu. Y (1997) Study on Properties of Acoustic Emissions in the Coal Fired Fluidised Bed. *Processing of the International Symposium.* 2:88-93

Yan Y., Lu, G. and Colechin, M. (2002) Monitoring and Characterisation of Pulverised Coal Flames using Digital Imaging Techniques. *Fuel.* 81(5): 647-656

Yin C., Luo Z., Ni M., and Cen K. (1998) Prediction Coal Ash Fusion Temperature with a Backpropagation Neural Network Model. *Fuel.* 15:1777-1782

Zadirake A. (1986) Advanced Sensors and Control Requirements for Multi-Burner Pulverised Coal-Fired Boilers. *ISA Cleveland Symposium, Ohio, USA.*

Zheng G., Starck J., Campbell J. and Murtagh F. (1999) The Wavelet Transform for Filtering Financial Data Streams. *http://strule.cs.qub.ac.uk/~gzheng/financial-engineering/;* Last Accessed: 15 April 2005

Zhou H., Cen K. and Fan J. (2004) Modelling and Optimisation of the NOx Emissions Characteristics of a Tangentially Fired Boiler with Artificial Neural Network. *Energy.* 29:167-183

Zhu Q., Jones J., Williams A. and Thomas K. (1999) The Predictions of Coal/Char Combustion Rate Using an Artificial Neural Network Approach. *Fuel* 78:1755-1762

Zukowski W. (1999) Acoustic Effects During the Combustion of Gaseous Fuels in a Bubbling Fluidised Bed. *Combustion and Flame.* 117(3):629-635

Appendix A – Reaction of Gas Phase Nitrogen

The following describes the mechanism for the evolution of coal-bound nitrogen. During the primary de-volatilisation of coal, nitrogen is released as HCN, NH_3, and N_2 or is contained in aromatic compounds present in the tar. As the pyrolysis temperature increases, non-nitrogenous volatiles are released thus increasing the content of nitrogen in the tar. The evolution of nitrogen from tar is governed by a much slower reaction than the initial de-volatilisation.

The major forms of gas phase nitrogen released are HCN and NH_3, and can be formed from three nitrogen sources via the following mechanisms: -

1. *Thermal NO*x oxygen atoms formed from the dissociation of O_2 react with nitrogen molecules at temperatures greater than 1573 K (with an almost exponential with increases in the peak flame temperature). The following reaction mechanism was identified as "Zeldovich Mechanism" as shown in the Equations A1 and A2.

$$N_2 + O \leftrightarrow NO + N \qquad [A1]$$

$$N + O_2 \leftrightarrow NO + O \qquad [A2]$$

Under fuel-rich conditions, OH and H radicals also take part in the oxidation reactions during combustion: -

$$N + OH \leftrightarrow NO + H \qquad [A3]$$

$$H + N_2 \leftrightarrow N_2H \qquad [A4]$$

$$N_2H + O \leftrightarrow NO + NH \qquad [A5]$$

2. *Fuel NO*x coal-bound nitrogen is the major contributor to NO formation in PF combustion. During de-volatilisation, nitrogen is liberated in the primary combustion zone into a tar of heavy aromatic compounds, before being converted primarily to HCN and NH_3 through oxidative pyrolysis, which may be secondary products from the pyrolysis of primary tar. Under fuel-lean conditions, HCN reacts with oxygen atoms to form oxy-cyanogens and amine intermediates, which are later oxidised to form NO. Under fuel-rich conditions, Nx formation is more favourable due to the reaction of additional hydrogenated amine species and NO. At the same time, NO is destroyed by hydrocarbon radicals, producing more HCN to continue the cycle. Theses products enter a series of homogeneous gas phase reactions as follows: -

Reactions between amine intermediates, hydrocarbon radicals and NO: -

$$NH_2 + NO \rightarrow N_2 + H_2O \qquad [A6]$$

$$CH. + NO \rightarrow HCN + O \qquad [A7]$$

Nitric oxide formed may be reduced by HCN to molecular nitrogen as follows:

$$HCN + O \rightarrow NCO + H \qquad [A8]$$

$$NCO + OH \rightarrow NO + CO + H \qquad [A9]$$

$$NCO + NO \rightarrow N_2O + CO \qquad [A10]$$

$$NO+NH_2 \rightarrow N_2 + H_2O \qquad [A11]$$

$$N_2O + H \rightarrow N_2 + OH \qquad [A12]$$

3. *Prompt NOx* Occurs in fuel-rich environments whereby hydrocarbon radicals (mostly CH) react with atmospheric nitrogen. The conversion of prompt NOx can be found in the equations A13, A14 and A15. The concentration of CH radicals is fewer and their formation may be more concentrated in "hot spots". Its significance to NO formation however, is minuscule in comparison to the influences of thermal and fuel NO.

$$CH + N_2 \leftrightarrow HCN + N \qquad [A13]$$

$$HCN + NH \leftrightarrow CO \qquad [A14]$$

$$NH + O \leftrightarrow NO + H \qquad [A15]$$

Relatively little information exists on the conversion of char nitrogen into NO. Furthermore, a simplified reaction scheme for the production of NO from chars is yet to be developed. Goel *et al* (1996) discovered that char nitrogen conversion in the absence of oxygen, is independent of de-volatilisation times. Goel also concluded that NO produced from the combustion of char nitrogen is not formed via the oxidation reactions of HCN. Most experiments carried out to date have been under slow heating rates and relatively low temperatures, conditions that do not apply in PF combustion. Consequently, it is difficult to use this particular research considering the importance of thermal history to char reactivity.

Appendix B – Combustion Air Calculations

The ultimate analysis of coal is used to calculate the total stoichiometric combustion air. The ultimate analysis of the coals on the "as received" basis and the total stoichiometric, which determined by the chemical balance based upon the combustible constituents of the coal are presented in Table A1 and A2 accordingly.

Table A1 Ultimate Analyses of the Coals (% by Weight)

Element	**Molecular Weight (kg/mole)**	**"As Received" basis**	
		Cerrejon	**Daw Mill**
Carbon	12	67.9	65.2
Hydrogen	2	4.2	3.6
Nitrogen	28	1.3	1.1
Sulphur	32	6.9	1.5
Oxygen	32	3.6	4.8
Moisture	-	4.9	5.1
Ash	-	11.2	18.7

Table A2 Combustion Air Calculations

Coal Constituent	**Cerrejon Coal**		**Daw Mill Coal**	
	Mass per kg of coal	**The required stoichiometric O_2 (kg/kg of coal)**	**Mass per kg of coal**	**The required stoichiometric O_2 (kg/kg of coal)**
Carbon	0.679	1.810	0.652	1.740
Hydrogen	0.042	0.336	0.036	0.288
Nitrogen	0.013	Nil	0.011	Nil
Sulphur	0.069	0.069	0.015	0.015
Oxygen	0.036	-0.036	0.048	-0.048
Moisture	0.049	Nil	0.051	Nil
Ash	0.112	Nil	0.187	Nil
Total	1	2.251	1	1.995

In combustion calculation2 it is common to consider air to consist of (by weight) 77% nitrogen and the remaining 23% as oxygen with the density of air at atmospheric pressure of 1.225 kg/m^3. Hence, the total stoichiometric air for Cerrejon and Daw Mill coals are (2.251/0.23/1.225) = 7.98 m^3 and (1.995/0.23/1.225) = 7.08 m^3 respectively per every kg of coal.

The percentage of excess oxygen is given as: -

$$\left(\frac{\text{Actual secondary air} + \text{Primary air} - \text{Total stoishiometric air}}{\text{Total stoichiometric air} - \text{Primary air}}\right) \times 100\% \qquad [A16]$$

The primary air, which was entrained into the burner, can be calculated from the following empirical formula, where the rotameter flow is measured in litre/min: -

$$\text{Primary air} = (60/1000) \times [(4.6 \times \text{rotameter flow}) - 119] \text{ m}^3/\text{h} \qquad [A17]$$

Since the rotameter flow was maintained at 120 litre/min throughout the experiments, the primary combustion air supply was 26 m^3/h. The required total stoichiometric combustion air at the given coal-feed rate are 7.83 x 19.3 = 151 m^3/hr, and 6.94 x 21.6 = 150 m^3/h for the Daw Mill and Cerrajon coals respectively.

Table A3 Percent Excess Secondary Combustion Air

	Cerrejon		**Daw Mill**	
Secondary Air (m^3/h)	**Total stoichiometric combustion air (m^3/h)**	**% Excess secondary air**	**Total Stoichiometric combustion air (m^3/h)**	**% Excess secondary air**
130	151	4.0	150	4.8
140		12.0		12.9
150		20.0		21.0
160		28.0		29.0

Appendix C – Matlab™ Code for Neural Network Training

% Introduction - Programme for training and testing of ANN in Matlab™

```
clear;
home;

% load file
data=xls2mat('D:\MyDocuments\ohtan_control\101002\day8_101002.xls:sheet11','r4c3:r
500c62');
kstep=1; % # of steps required for the ANN to predict into the future

% data de-noised
[b,a]=butter(5,0.5);
ip=filtfilt(b,a,ip);
op=filtfilt(b,a,op);

% data normalisation
ip=ip';
op=op';
[ipn,meanip,stdip,opn,meanop,stdop]=prestd(ip,op)
[ipn,meanip,stdip]=prestd(ip)

% constructs a regressor vector
na=3; nb=[1 1 1 1 1 1]; nk=[1 1 1 1 1 1]; kstep=1;
[ipregn,opregn]=regvec(ipn,opn,na,nb,nk,kstep);

M=400;
N=401;

p=ipn(:,1:M);
t=opn(:,1:M);
pv=ipn(:,N:end);
tv=opn(:,N:end);

% training data
p=ipn(:,1:M);
t=opn(:,1:M);

% validation data
pv=ipn(:,N:end);
tv=opn(:,N:end)
```

```
test.P=pv;
test.T=tv;

% network parameters
S1=15; S2=1;  % # of hidden and output neurons

% create a feedforward network structure
net=newff(minmax(p),[S1,S2],{'tansig','purelin'},'trainbr');
net.trainParam.show=1;
net.performFcn='mse';
net.trainParam.epochs=2000;
net.trainParam.goal=0.01;
net=init(net);
[net,tr]=train(net,p,t,[],[],[],test); % network training

inpt=[p pv];
Yn=sim(net,inpt); % network simulation
Y=poststd(Yn,meanop,stdop);  %  de-normalised data (trained data)
NOx=Y(1,:);
target=poststd(opn,meanop,stdop); % de-normalised data (validation set)
NOxt=target(1,:);

error=(NOx-NOxt); % error prediction

% plot predictions
subplot(2,1,1); plot(1:length(NOxt),NOxt,'b',1:length(NOx),NOx,'r--');
txt=strcat('output(solid) and  ',num2str(kstep),'-step ahead prediction(dashed)');
title(txt);
xlabel('time (samples)');
ylabel('Emissions (ppm)');

subplot(2,1,2); plot(1:length(error),error);
title('% prediction error');
xlabel('time (samples)');
ylabel('error - NOx');

% standard deviation and mean-square error
stdev_NOx=std(error4);
txt=strcat('STDV(Va)=',num2str(stdev_NOx));
text(52,5,txt);
MSE_NOx=mse(error4);
txt=strcat('MSE(Va)=',num2str(MSE_NOx));
text(52,5,txt)

% saves variables to excel
range1=strcat('r3c2:r',num2str(length(target)),'c2');
```

```
mat2xls(K,target',range1);
range2=strcat('r3c3:r',num2str(length(Y)),'c3');
mat2xls(K,Y',range2);

% saves model weight and network structure
save NOx_MODEL1 mat meanip meanop stdip stdop net na nb nk
```

Appendix D – Matlab™ Code for Self-Organising Map (SOM) Neural Network

% Introduction - Programme of SOM in Matlab™

```
clear;
home;

% load file
data=xls2mat('D:\My Documents\PHD Thesis\Chapter6
1st\book1.xls:sheet3','r2c10:r151c14');

% data normalisation
[pn,minp,maxp] = premnmx(data'); %p must be transposed before normalisation

% create labels
Tc=[1*ones(30,1); 2*ones(30,1); 3*ones(30,1); 4*ones(30,1); 5*ones(30,1)];

% divides data (training and validation)
ptr = pn(:,1:405)';
pts = pn(:,406:end)';
ttr = Tc(1:405,:);
tts = Tc(406:end,:);

% labelling
sD_tr = som_data_struct(pn');
for i=1:length(sD_tr.data)
   sD_tr.labels{i} = num2str(Tc(i));
end

% SOM training
sM=som_make(sD_tr);
sM = som_make(sD_tr,'msize',[15 15]);
sM=som_autolabel(sM,sD_tr,'vote');

% computes and plots 3 principal component planes
[Pd,V,me] = pcaproj(sD_tr,3);
 Ps= pcaproj(sM.codebook, V, me);
som_grid(sM,'Coord',pcaproj(sM,V,me),'marker','none','label',sD.labels,
'labelcolor','r','linecolor',[0.7 0.7 0.7]);

% label predictions corresponding to clusters
c1 = Pd(find(str2num(char(sD_tr.labels))==11),:);
c2 = Pd(find(str2num(char(sD_tr.labels))==12),:);
```

```
c3 = Pd(find(str2num(char(sD_tr.labels))==13),:);
c4 = Pd(find(str2num(char(sD_tr.labels))==14),:);
c5 = Pd(find(str2num(char(sD_tr.labels))==15),:);
c6 = Pd(find(str2num(char(sD_tr.labels))==21),:);
c7 = Pd(find(str2num(char(sD_tr.labels))==22),:);
c8 = Pd(find(str2num(char(sD_tr.labels))==23),:);
c9 = Pd(find(str2num(char(sD_tr.labels))==24),:);
c10 = Pd(find(str2num(char(sD_tr.labels))==25),:);

% examine predictions using Unit Distance Matrix
som_show(sM,'subplots',[2 2],'empty','','footnote','');
som_show_add('label',sM,'subplot',1,'textsize',10);colormap(1-gray);
figure

% plot results
subplot(1,2,2)
plot3(c1(:,1),c1(:,2),c1(:,3),'ob','markersize',10);
hold on
plot3(c2(:,1),c2(:,2),c2(:,3),'+r','markersize',10);
plot3(c3(:,1),c3(:,2),c3(:,3),'^g','markersize',10);
plot3(c4(:,1),c4(:,2),c4(:,3),'sy','markersize',10);
plot3(c5(:,1),c5(:,2),c5(:,3),'dk','markersize',10);
plot3(c6(:,1),c6(:,2),c6(:,3),'or','markersize',5);
plot3(c7(:,1),c7(:,2),c7(:,3),'+r','markersize',5);
plot3(c8(:,1),c8(:,2),c8(:,3),'^r','markersize',5);
plot3(c9(:,1),c9(:,2),c9(:,3),'sr','markersize',5);
plot3(c10(:,1),c10(:,2),c10(:,3),'dr','markersize',5);

box on
view(2)
xlabel('Principal Component 1','fontsize',10); ylabel('Principal Component
2','fontsize',10);

% save model weight and network structure
save cess5irsom.mat sM sD_tr sD_ts minp maxp

% plot prototype vectors
plot3(Pd(1:30,1),Pd(1:30,2),Pd(1:30,3),'ro',Pd(31:60,1),pd(31:60,2),Pd(31:60,3),'yo',Pd(
1:90,1),Pd(61:90,2),Pd(61:90,3),'go',Pd(91:120,1),Pd(91:120,2),Pd(11:120,3),'bo',Pd(121
150,1),Pd(121:150,2),Pd(121:150,3),'mo')
```

Appendix E – Matlab™ Codes for Wavelet Analysis

%Introduction - Programme of Wavelet Analysis in Matlab™

```
clear;
home;

% create file path
paths = {'D:\My Documents\ohtan_control\test44\rawae\'};
for m=1:length(paths)
spath = paths{m};

% load files
DirInfo = dir(spath); %return directory info of spath
fname = {DirInfo(3:end).name}; %return cell array of filenames contained in spath
fpath = strcat(spath,fname); %return cell array of full filepath
fpath = char(fpath); %convert to rows of character array
row = size(fpath,1); %number of files in the current directory

% empty matrix
E = zeros(row,32);  % expected band energy
oindx = 1;

% main programme
for i=1:row
fprintf('File %i of %i\n',[i,row]);
[fid,message] = fopen(fpath(i,:),'r');
if isempty(message)==0
error(message);
else

% matlab workspace variable is of "Double" by default
data = fread(fid,32768,'int16');
fclose(fid); % file closed
end

if length(data)= =32768


% data normalisation
data = (data - mean(data))./std(data);
N = 5; % # of layers to discompose

 [T,D] = wpdec(data,N,'db2','shannon');
for k=1:(2^N)
wc = wpcoef(T,D,[N k-1]);
```

```
E(i,k) = sqrt(mean(wc.*wc));
end
else

outlier{m}(oindx) = i;  % return indices of outlier
oindx = oindx +1;

end
end
end

% plot results
for j=1:k
subplot(4,8,j)
plot(E(:,j));
end
```

Appendix F – Matlab™ Codes for the Controller

```
% Introduction - Programme of signal processing and control in Matlab™

home
clear

% controller settings – emission targets
NOx_low=550;    % Low level of NOx
NOx_high=575;   % High Level of NOx
CO_low=300;     % Low level of CO
CO_high=350;    % High level of CO


% signal processing
m=1;
Z=2000;          % length of control period
P=round(Z/3);
Q=60;            % control time (60 seconds)
% empty matrices (storage)
mtx=zeros(Z,54);
pred=zeros(Z,3);
FGA=zeros(P,4);
SEC=zeros(Z,1);
SES=zeros(P,1);


% create file paths
paths ={'d:\ohtan_control\test51\ir\'
        'd:\ohtan_control\test51\mic\'
        'd:\ohtan_control\test51\rawae\'};

% create statement
SE_init=input('Enter Initial Secondary  Air = ');

% main programme
for k=1:Z

% read secondary air input
RR=strcat('r',num2str(k),'c1:r',num2str(k),'c1');
dat=xls2mat('D:\ohtan\book2.xls:sheet5',RR);
SEI(k,1)=dat;

% logged time
start_time=clock;
tt=round(start_time(1,4:6));
```

```
T=tt;
T1=T(1,1);
T2=T(1,2);
T3=T(1,3);
Time=strcat(num2str(T1),':',num2str(T2),':',num2str(T3));

% save logged time and # steps in control in excel
Ra=strcat('r',num2str(k+1),'c1:r',num2str(k+1),'c1');
mat2xls('D:\book1.xls:sheet1',Time,Ra);

Rb=strcat('r',num2str(k+1),'c2:r',num2str(k+1),'c2');
mat2xls('D:\book1.xls:sheet1',k,Rb);

if k>=3;
k

% empty matrix for secondary airflow rate
if k<=Q;
SI=SE_init;
SEC(k,1)=SI;
else
SI=SE_Cur;
SEC(k,1)=SI;
end

% plot secondary airflow rate
SEC(1:k,1);
subplot(2,4,4);
plot(SEC(1:k,:),'k');
title('Current Air');
ylabel('m3/h');
xlabel('# sample');


% save secondary airflow rate in excel
Rc=strcat('r',num2str(k+1),'c6:r',num2str(k+1),'c6');
mat2xls('D:\book1.xls',SI,Rc);

% empty matrix for secondary airflow rate information
SES(1:m,1);

% plot suggested secondary airflow rate
if m>=2
subplot(2,4,8);
plot(SES(1:m-1,:),'k');
title('Suggested Air');
```

```
ylabel('m3/h');
xlabel('# sample');
end

% load files as in binary from directories
for i=1:length(paths);
DirInfo = dir(paths{i});
fname = {DirInfo(1:end).name}; % return cell array of filenames contained in spath
warning on

while (k-length(fname))>0
warning('Still Wait for latest files from LabView');
warning off
DirInfo = dir(paths{i});
fname = {DirInfo(1:end).name};
pause(1)

end

fname = fname(end);
fpath = strcat(paths{i},fname); % return cell array of full filepath
fpath = char(fpath); %convert to rows of character array
 [fid,message] = fopen(fpath,'r');

if isempty(message)==0
error(message);

 else data = fread(fid,32768,'int16'); %matlab workspace variable is of double by
default
 fclose(fid); % close file
 end

% signal processing
% time analysis
Me = mean(data);
Med = Median(data);

% data normalisation
data = detrend(data,'constant');
data = premnmx(data);

St = std(data);
vars = var(data);
zcrs = mcross(data);
Rms = rms(data);
Ku = kurtosis(data);
```

```
Sk = skewness(data);

% frequency analysis of IR signals
if i==1
[U,f] = pwelch(data,1024,[],[],8192);
findx = find(f<=1000); f = f(findx); U = U(findx);
PUf = U./sum(U); %probability of U(f)
S = sum(PUf.*log(1./PUf));
fcg = U'*f./sum(U);
SF = std(U,1)./mean(U);
f1 = find(f<=200); f2 = find(f>200&f<=400); f3 = find(f>400&f<=600); f4 =
find(f>600&f<=800);
f5 = find(f>800&f<=1000);
E = [sum(PUf(f1)) sum(PUf(f2)) sum(PUf(f3)) sum(PUf(f4)) sum(PUf(f5))];
f_vectors = [Me vars St zcrs fcg SF S Rms Ku Sk Med E];
IR=f_vectors;

FV_IR = [k f_vectors]; %Total data with time & #step
xlsname=strcat('d:\book1.xls\sheet',num2str(i+1));
Rd=strcat('r',num2str(k+1),'c2:r',num2str(k+1),'c29');
mat2xls(xlsname,FV_IR,Rd);
mat2xls(xlsname,Time,Ra);


% frequency analysis of microphone signals
elseif i==2
[U,f] = pwelch(data,1024,[],[],8192);
findx = find(f<=1000); f = f(findx); U = U(findx);
PUf = U./sum(U); %probability of U(f)
S = sum(PUf.*log(1./PUf));
fcg = U'*f./sum(U);
SF = std(U,1)./mean(U);
f1 = find(f<=200); f2 = find(f>200&f<=400); f3 = find(f>400&f<=600); f4 =
find(f>600&f<=800);
f5 = find(f>800&f<=1000);
E = [sum(PUf(f1)) sum(PUf(f2)) sum(PUf(f3)) sum(PUf(f4)) sum(PUf(f5))];
f_vectors = [Me vars St zcrs fcg SF S Rms Ku Sk Med E];
MIC=f_vectors;

FV_MIC = [k f_vectors]; %Total data with time & #step
xlsname=strcat('d:\book1.xls\sheet',num2str(i+1));
mat2xls(xlsname,FV_MIC,Rd);
mat2xls(xlsname,Time,Ra);

% frequency analysis of AE signals
else
```

```
[U,f] = pwelch(data,1024,[],[],5000000);
findx = find(f>=100000&f<=1200000); f = f(findx); U = U(findx);
PUf = U./sum(U); %probability of U(f)
S = sum(PUf.*log(1./PUf));
fcg = U'*f./sum(U);
SF = std(U,1)./mean(U);
f1 = find(f>=100000&f<=200000); f2 = find(f>200000&f<=300000); f3 =
find(f>300000&f<=400000); f4 = find(f>400000&f<=500000);
f5 = find(f>500000&f<=600000);f6 = find(f>600000&f<=700000);f7 =
find(f>700000&f<=800000);f8 = find(f>800000&f<=900000);f9 =
find(f>900000&f<=1000000);
f10 = find(f>1000000&f<=1100000);f11 = find(f>1100000&f<=1200000);
E = [sum(PUf(f1)), sum(PUf(f2)), sum(PUf(f3)), sum(PUf(f4)), sum(PUf(f5)),
sum(PUf(f6)), sum(PUf(f7)), sum(PUf(f8)), sum(PUf(f9)), sum(PUf(f10)),
sum(PUf(f11))];
f_vectors = [Me vars St zcrs fcg SF S Rms Ku Sk Med E];
AE=f_vectors;


FV_AE = [k f_vectors]; %Total data with time & #step
xlsname=strcat('d:\book1.xls\sheet',num2str(i+1));
mat2xls(xlsname,FV_AE,Rd);
mat2xls(xlsname,Time,Ra);
end
end

% empty matrices for storing features
Tol=[IR MIC AE];
mtx(k,:)=Tol;


% ANN model predictions
f=4;
if k>=f
ip=mtx(3:k,1:54);


% feature sets use for predictions
FV_IR=[mtx(3:k,2:3) mtx(3:k,6:10) mtx(3:k,12:16)];
FV_MIC=[mtx(3:k,20:21) mtx(3:k,28:29)];
%FV_AE=[mtx(3:k,45) mtx(3:k,47:48) mtx(3:k,53)];
ip=[FV_IR FV_MIC];

% load weight for NOx predictions
load ASTON.mat meanip meanop stdip stdop net
```

```
% data normalisation
pnew=trastd(ip,meanip,stdip);

% NOx predictions
Yn=sim(net,pnew);
Y=poststd(Yn,meanop,stdop);
Y=Y';
n=k-2;
Y_NOx=Y(n,1);
Y_NOx

if Y_NOx<=100
Pr_NOx=pred(k-3,1);
elseif Y_NOx>900
Pr_NOx=pred(k-3,1);
else
Pr_NOx=Y_NOx;
end

% load weight for CO predictions
load BMW.mat meanip meanop stdip stdop net

% data normalisation
pnew=trastd(ip,meanip,stdip);

% CO predictions
Yn=sim(net,pnew);
Y=poststd(Yn,meanop,stdop);
Y=Y';
Y_CO=Y(n,1);
Y_CO

if Y_CO<=-1000
Pr_CO=pred(k-3,2);
elseif Y_CO>1000
Pr_CO=pred(k-3,2);
else
Pr_CO=Y_CO;
end

% load weight for O2 predictions
load CIVIC1.mat meanip meanop stdip stdop net

% data normalisation
pnew=trastd(ip,meanip,stdip);
```

```
% O2 predictions
Yn=sim(net,pnew);
Y=poststd(Yn,meanop,stdop);
Y=Y';
Y_O2=Y(n,1);
Y_O2
if Y_O2<=0.5
Pr_O2=pred(k-3,3);
elseif Y_O2>5
Pr_O2=pred(k-3,3);
else
Pr_O2=Y_O2;
end

% form new vectors for predictions information
prediction=[Pr_NOx Pr_CO Pr_O2];
xlsname='d:\book1.xls:sheet1';
Re=strcat('r',num2str(k+1),'c3:r',num2str(k+1),'c5');
mat2xls(xlsname,prediction,Re);
pred(k,:)=prediction;

pNOx=pred(f:k,1);
pCO=pred(f:k,2);
pO2=pred(f:k,3);

% create NOx & CO targets for plotting
LLNOx(1:Z,1)=NOx_low;
LNOx=LLNOx(f:k,1);
HHNOx(1:Z,1)=NOx_high;
HNOx=HHNOx(f:k,1);

LLCO(1:Z,1)=CO_low;
LCO=LLCO(f:k,1);
HHCO(1:Z,1)=CO_high;
HCO=HHCO(f:k,1);

% plot results
subplot(2,4,1);
plot(f:k,pNOx,'r',f:k,LNOx,'g--',f:k,HNOx,'g--');
title('NOx Emission');
ylabel('vppm')
xlabel('# sample')

subplot(2,4,2);
plot(f:k,pCO,'b',f:k,LCO,'g--',f:k,HCO,'g--');
title('CO Emission');
```

```
ylabel('vppm')
xlabel('# sample')

subplot(2,4,3);
plot(pO2,'m');
title('O2 Emission');
ylabel('%')
xlabel('# sample')
end


% data averaging
% input variable - average over 30 points (5 minutes) of predictions

FG=pred(1:k,:);
if k==m*Q


% initial secondary airflow rate
SE_Cur=input('Enter Current Secondary  Air = ');

L=k-(Q-20);
L

  NOxb=FG(L:k,1);  %Carbon Monoxide
  COb=FG(L:k,2);   %Oxygen
  O2b=FG(L:k,3);   %Nitrogen Oxides


% average
NOxa=mean(NOxb);
COa=mean(COb);
O2a=mean(O2b);

FGT=[k NOxa COa O2a];
FGA(m,:)=FGT;


% plot averaged NOx & CO targets
LNOx=LLNOx(1:m,1);
HNOx=HHNOx(1:m,1);
LCO=LLCO(1:m,1);
HCO=HHCO(1:m,1);

% transfer values of averaged NOx & CO to excel
xlsname='D:\book1:sheet1';
Rf=strcat('r',num2str(m+1),'c7:r',num2str(m+1),'c10');
```

```
mat2xls(xlsname,FGT,Rf);

% plot results - averaged NOx & CO
NOx=FGA(1:m,2);
CO=FGA(1:m,3);
O2=FGA(1:m,4);

subplot(2,4,5);
plot(1:m,NOx,'r',1:m,LNOx,'g--',1:m,HNOx,'g--');
title('Average NOx Emission');
ylabel('vppm')
xlabel('# sample')

subplot(2,4,6);
plot(1:m,CO,'b',1:m,LCO,'g--',1:m,HCO,'g--');
title('Average CO Emission');
ylabel('vppm')
xlabel('# sample')

subplot(2,4,7);
plot(O2,'m');
title('Average O2 Emission');
ylabel('%')
xlabel('# sample')


% controller
% CV - calorific value %Frate - Load(kW)  %CoalFeed Rate[kg/h] =
Load[kW]*3600./CV [kJ/kG]

NOxf=FGA(m,2);
COf=FGA(m,3);
O2f=FGA(m,4);

Rg=strcat('r',num2str(m+1),'c12:r',num2str(m+1),'c12');
Rh=strcat('r',num2str(m+1),'c11:r',num2str(m+1),'c11');

% NOx & CO tuning loop
% status 1
if NOxf<=NOx_low & COf<=CO_low;

disp('Status 1');
disp('Optimal Setting - Low NOx & CO');
disp('No Air Adjustment Required');

SEI_new=SE_Cur
```

```
W='1';

Y='Balance';

SES(m,1)=SEI_new;

mat2xls(xlsname,W,Rg);
mat2xls(xlsname,Y,Rh);

% status 2
elseif NOxf<=NOx_low & CO_low<COf & COf<=CO_high;
disp('Status 2');
disp('O2 Tuning - Increase Air Slightly ');

Rate=2.5;

SEP=SE_Cur;
SEI=round(SEP);

SEI_new=SEI+Rate;
SES(m,1)=SEI_new;
fprintf('%s %.2f','Suggest Air =',SEI_new)
W='2';

mat2xls(xlsname,W,Rg);
mat2xls(xlsname,SEI_new,Rh);

% status 3
elseif NOxf<=NOx_low & CO_high<COf;

disp('Status 3')  %Status 3 - Refer to the statement 3
disp('O2 Tuning - High CO, Increase Air'); % High CO. Increase air to reduce CO

Rate=5;

SEP=SE_Cur;
SEI=round(SEP);

SEI_new=SEI+Rate;
SES(m,1)=SEI_new;
fprintf('%s %.2f','Suggest Air =',SEI_new);

W='3';

mat2xls(xlsname,W,Rg);
mat2xls(xlsname,SEI_new,Rh);
```

```
% status 4
elseif NOx_low<NOxf & NOxf<=NOx_high & COf<=CO_low;
disp('Status 4')
disp('O2 Tuning - Reduce Air slightly');

Rate=5;
SEP=SE_Cur;
SEI=round(SEP);
SEI_new=SEI-Rate;
SES(m,1)=SEI_new;
fprintf('%s %.2f','Suggest Air =',SEI_new);

W='4';

mat2xls(xlsname,W,Rg);
mat2xls(xlsname,SEI_new,Rh);

% status 5
elseif NOx_low<NOxf & NOxf<=NOx_high & CO_low<COf &COf<=CO_high;
disp('Status 5')
disp('O2 Tuning - Reduce Air Slighty');

Rate=2.5;
SEP=SE_Cur;
SEI=round(SEP);

SEI_new=SEI-Rate;
SES(m,1)=SEI_new;
fprintf('%s %.2f','Suggest Air =',SEI_new);
W='5';

mat2xls(xlsname,W,Rg);
mat2xls(xlsname,SEI_new,Rh);

% status 6
elseif NOx_low<NOxf & NOxf<=NOx_high & COf>CO_high;
disp('Status 6')
disp('O2 Tuning - High CO, Increase Air');

Rate=2.5;
SEP=SE_Cur;
SEI=round(SEP)
SEI_new=SEI+Rate;
SES(m,1)=SEI_new;
```

```
fprintf('%s %.2f','Sugget Air =',SEI_new);
W='6';

mat2xls(xlsname,W,Rg);
mat2xls(xlsname,SEI_new,Rh);

% status 7
elseif NOx_high<NOxf & COf<=CO_low;
disp('Status 7');
disp('O2 Tuning - NOx high, Reduce Air');

Rate=10;
SEP=SE_Cur;
SEI=round(SEP);

SEI_new=SEI-Rate;
SES(m,1)=SEI_new;

 fprintf('%s %.2f','Sugget Air =',SEI_new);
W='7';

mat2xls(xlsname,W,Rg);
mat2xls(xlsname,SEI_new,Rh);

% status 8
elseif NOx_high<NOxf & COf<=CO_high & COf>CO_low;
disp('Status 8');
disp('O2 Tuning - NOx high, Reduce Air');

Rate=5;

SEP=SE_Cur;
SEI=round(SEP);
SEI_new=SEI-Rate;

SES(m,1)=SEI_new;
fprintf('%s %.2f','Sugget Air =',SEI_new);
W='8';

mat2xls(xlsname,W,Rg);
mat2xls(xlsname,SEI_new,Rh);


% status 9
else
disp('Status 9');
```

```
disp('O2 Tuning - Both NOx & CO high. Increase Air ');

Rate=5;
SEP=SE_Cur;
SEI=round(SEP);

SEI_new=SEI+Rate;

SES(m,1)=SEI_new;
fprintf('%s %.2f','Sugget Air =',SEI_new);
W='9';

mat2xls(xlsname,W,Rg);
mat2xls(xlsname,SEI_new,Rh);
end

m=m+1;
end
end
end
```

Publications

1. O.H. Tan, S.J. Wilcox, J. Ward and M. Lewitt (2003) The Development of a Monitoring and Control System for Pulverised Coal Flames Using Neural Networks *Proceedings of ASME International Congress, Washington D.C. USA.* Nov. 2003 pp15-21.

2. O.H. Tan, S.J. Wilcox, J. Ward and M. Lewitt (2003), A Neural Network Based Monitoring System for Control of Pulverised Coal Flames. *A Sustainable Energy Supply for Industry, IFRF conference,* May 11-12, Netherlands.

3. Ward, J., Wilcox, S.J, Tan O.H., Tan, C.K, Payne, R.J. and Garwood, D.R. (2001) Simulation of a Range of Thermal System by Artificial Neural Networks. *Proceedings of 2001 ASME International Mechanical Engineering Congress and Exposition,* Nov 11–16, 2001, New York, NY, USA, Paper HTD-24824, 7 pages.

4. Wilcox, S.J., Ward, J., Tan, C.K., Tan O.H. and Payne, R.J. (2001) The Application of Neural Networks in a Range of Combustion Systems. *Proceedings of the 6th European Conference on Industrial Furnaces and Boilers, April 02-05, Estoril-Lisboa, Portugal.* Vol. 4, pp 203-214.